Perfluorocarbon Nanodroplets for Oxygen Delivery for Bone Repair

Kirsten Emma O'Brien

Supervised by Prof Nick Evans, Dr Dario Carugo, Dr Robin Rumney, Prof Eleanor Stride

School of Engineering

Faculty of Engineering and Physical Sciences

University of Southampton

June, 2025

A thesis submitted in partial fulfilment of the requirements for the degree of PhD in Bioengineering.

Abstract

Around 2-10% of bone fractures result in delayed or non-union fractures. These typically require surgery, which can be painful and carry a risk of infection. There is, therefore, a critical need for minimally invasive treatment methods. Many bone diseases linked to unsuccessful fracture healing, like osteoporosis and osteonecrosis, are associated with hypoxia. Perfluorocarbons are inert and have very high oxygen solubilities. They can be stabilised in aqueous solutions to form nanodroplets. These perfluorocarbon nanodroplets have previously been shown to successfully increase the oxygen tension in tumours. This study tested the hypothesis that perfluorocarbon nanodroplets relieve the effects of hypoxia on cells of osteoblastic and osteoclastic lineage in a manner that aids bone repair.

Perfluoropentane (PFP) nanodroplets with a 1,2-distearoyl-sn-glycero-3-phosphocholine (DSPC) and polyoxyethylene (40) strearate (PEG(40)s) shell were fabricated using sonication. Temperature, PFP concentration, sonicator tip height, total sonication time, sonication amplitude and post-processing techniques were varied to evaluate their effect on nanodroplet characteristics through nanoparticle tracking analysis. The optimised formulation was investigated for cytotoxicity on cells of both osteoblastic (MC3T3E1, Saos-2 and BMSC) and osteoclastic (PBMC) lineages using Alamar blue, Picogreen and cell counting. Alkaline phosphatase enzyme and calcification served as osteogenic markers in BMSCs exposed to the nanodroplets in normoxia and hypoxia, while osteoclastic activity was measured by manually assessing osteoclast number and size in peripheral blood mononuclear cells (PBMCs). Hypoxic stress was measured by quantifying HIF-1 protein expression in Saos-2s by western blotting and VEGF secretion by ELISA.

Nanodroplets exhibit low cytotoxicity on osteoblastic cells but significantly reduce osteoclast numbers. Treatment with 0.1% v/v nanodroplets led to a marked increase in calcification. Osteoclast number and size were evaluated manually after long-term nanodroplet treatment. A decrease in osteoclast number and size when treated long-term occurred in both normoxia and hypoxia, while short-term treatment reduced osteoclast numbers in normoxia but increased them in hypoxia. Microscope examination showed a preferential association of nanodroplets with phagocytic cells over other cell types.

This work demonstrated that precise control over sonication parameters enables better control over nanodroplet size and repeatability. The resulting nanodroplets were capable of significantly increasing mineralisation and decreasing hypoxic stress in osteoblastic cells, as well as relieving hypoxia-induced apoptosis in osteoclastic cells. Overall, nanodroplets present a promising new oxygen delivery method for relieving hypoxic stress in bone cells.

Contents

List of Tables

List of Figures

Declaration of Authorship

I declare that this thesis and the work presented in it is my own and has been generated by me as the result of my own original research.
I confirm that:

1. This work was done wholly or mainly while in candidature for a research degree at this University;
2. Where any part of this thesis has previously been submitted for a degree or any other qualification at this University or any other institution, this has been clearly stated;
3. Where I have consulted the published work of others, this is always clearly attributed;
4. Where I have quoted from the work of others, the source is always given. With the exception of such quotations, this thesis is entirely my own work;
5. I have acknowledged all main sources of help;
6. Where the thesis is based on work done by myself jointly with others, I have made clear exactly what was done by others and what I have contributed myself;
7. Parts of this work have been published as:

Faculty/Institute/Centre/School	Faculty of Engineering and Physical Sciences
Degree	PhD in Bioengineering
Candidate (Id.)	Kirsten Emma O'Brien (32522672)

Signature of Student	_____
Date	June 2, 2025

Acknowledgements

I would like to express my heartfelt gratitude to all those who have supported and contributed to the completion of this project.

First and foremost, I would like to extend my deepest appreciation to my supervisor, Prof. Nick Evans, for his unwavering guidance, encouragement, and expertise throughout this research. His mentorship and thoughtful feedback were invaluable in shaping the direction of my work and in navigating the many challenges that arose along the way.

I also wish to thank my co-supervisors, Dr Dario Carugo, Dr Robin Rumney and Prof Eleanor Stride, for their invaluable support, insightful suggestions, and constructive advice. Their expertise significantly enriched the quality of this project and broadened my understanding of the field. I am also grateful to Helen Knowles and Hannah Smith, whose unceasing technical assistance made a lot of this work possible.

Special thanks to the members of the Bone and Joint research group for their collaboration, technical assistance, and encouragement. In particular, I would like to acknowledge Christopher Campbell and Dariusz Kosk for their extraordinary amount of help with nanodroplet manufacturing optimisation and design. The sheer volume of experiments we performed to achieve that would simply not have been possible without your agreement, dedication and friendship. I would also like to thank Sam Sloan for both his technical and emotional support, without which this thesis would be nowhere near the achievement it is today. Additionally, Alex Clarke for always saying exactly what I needed to hear when I needed to hear it and Aya Ben Issa for her advice and constantly lending me her ear. I would also like to recognise Maria Stagno Navarra. Sharing the thesis writing months with you significantly brightened the experience.

I would like to acknowledge the financial support from Orthopaedic Research UK, which made this research possible.

Finally, I would like to express my deepest gratitude to my family and friends, especially my parents, brother and grandmother, for their constant love, support, and patience. Their encouragement has been a constant source of strength throughout my academic journey and all aspects of my life.

List of Abbreviations

ADV acoustic droplet vaporisation

AFM atomic force microscopy

ALP alkaline phosphatase

BMP bone morphogenetic protein

BMSC bone marrow stromal cells

BSA bovine serum albumin

CATK cathepsin-K

DAPI 4′,6-diamidino-2-phenylindole

DLS dynamic light scattering

DMEM Dulbecco's modified Eagle's medium

DMOG dimethyloxalylglycine

DOX doxorubicin

DSPC 1,2-distearoyl-sn-glycero-3-phosphocholine

EDTA ethylenediaminetetraacetic acid

EDX energy dispersive X-ray analysis

ELISA enzyme-linked immunosorbent assay

FBS foetal bovine serum

FDA Federal Drug Agency

FTLA finite tracking length analysis

GMFI geometric mean fluorescence intensity

HBOC haemoglobin-based oxygen carrier

HIF hypoxia inducible factor

HOLLT hyperbaric oxygen in lower limb trauma

HRP horseradish peroxidase

MCSF macrophage colony stimulating factor

mRNA messenger ribonucleic acid

MSC mesenchymal stromal cell

NADH nicotinamide adenine dinucleotide

NHS National Health Service

NTA nanoparticle tracking analysis

OPG osteoprotegerin

PBMC peripheral blood mononuclear cell

PBS phosphate buffer solution

PEG(40)s polyoxyethylene (40) strearate

PFA paraformaldehyde

PFC perfluorocarbon

PFP perfluoropentane

PFTBA perfluorotributylamine

RANKL receptor activator of nuclear factor-β ligand

ROS reactive oxygen species

RUNX2 runt-related transcription factor 2

SEM scanning electron microscopy

TEM transmission electron microscopy

TNF tumour necrosis factor

TRAP tartrate resistant acid phosphotase

VEGF vascular endothelial growth factor

List of Symbols

C	concentration	$mol\ m^{-3}$
D	diffusion coefficient	$m^2\ s^{-1}$
d	particle diameter	m
H	Henry's constant	$mol\ m^{-3}\ Pa{-}1$
I	light intensity	$-$
J	concentration flux	$mol\ m^{-2}\ s{-}1$
k_B	Boltzmann constant	$J\ K^{-1}$
k_p	permeability coefficient	Pa
N	number	$-$
P	pressure	Pa
R	hydrodynamic radius	m
r	radius of particle	m
T	temperature	K
t	time	s
x	distance	m
η	viscosity	$N\ s\ m^{-2}$
σ	surface tension	$N\ m^{-1}$

"How wonderful it is that nobody need wait a single moment before starting to improve the world"

Anne Frank.

1

Introduction

The aim of this thesis was to explore the development of perfluorocarbon nanodroplets as a novel agent for oxygen delivery to bone tissue to enhance the repair process. While perfluorocarbon nanodroplets have previously been studied for oxygen delivery, such as blood substitutes and oxygen delivery to tumours, they have not been explored for bone repair or targeted delivery of oxygen to bone. This research aims to address that gap, providing insights into the efficacy of perfluorocarbon nanodroplets as potential oxygen-delivering therapeutics through *in vitro* investigation. Therefore, an initial review focused on non-union fractures, the influence of hypoxia on bone repair and perfluorocarbon nanodroplets as oxygen-delivering therapeutics is warranted.

1.1 | The Clinical Problem of Bone Fracture

Bone fractures are a common cause of hospital admission. Between 2004 – 2014, over 2.4 million people were admitted to hospital with a bone fracture in England (Jennison, Brinsden, 2019). Around 2-10 % of bone fractures result in non-union (Cunningham et al., 2017; Giannoudis et al., 2007; Mills et al., 2017; Stewart, 2019). A non-union fracture is one which does not heal without clinical intervention. Practically speaking, this is often defined as a fracture that has shown no signs of healing for at least three months and has not healed at all after 9 months (Cunningham et al., 2017). Some liberty may be taken with this definition as aspects such as which bone is broken or gender may influence the likelihood of a non-union occurring (Mills et al., 2017). The

severity of the fracture may also lead to immediate intervention, as it may be clear that the fracture will lead to non-union.

The consequences of non-union fractures are far-reaching. Not only is there a significant socioeconomic burden, with an estimated cost of £7000-£79000 spent per non-union fracture, but patients have to endure chronic pain and have difficulties going about daily activities (Ekegren et al., 2018; Mills et al., 2017).

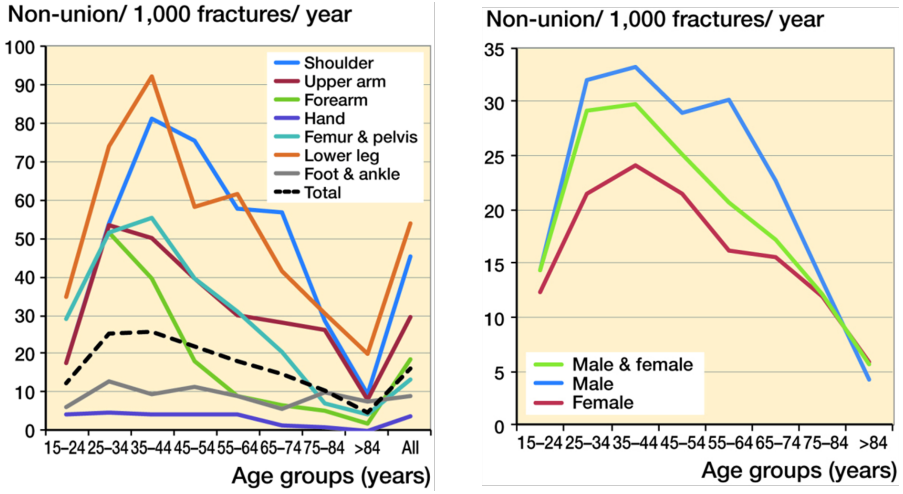

Figure 1.1: Prevalence of non-union fractures. (Mills et al., 2017)

Non-unions often result as a consequence of comorbidities such as diabetes, osteoporosis or osteonecrosis. Additionally, aspects such as age, gender and location of fracture can affect the likelihood of a non-union as seen in Figure 1.1 (Ekegren et al., 2018; Mills et al., 2017; Vanderkarr et al., 2023). As a result, each case is patient-specific, and a blanket treatment may not be possible.

1.2 | Current Interventions for Non-Union Fracture Repair

Most current interventions for non-union fractures require invasive surgery. The current gold standard is an autologous bone graft (Sen, Miclau, 2007). However, there is momentum towards using minimally invasive techniques such as bone stimulators (Zura et al., 2015). This trend is driven by the need for procedures that result in less

pain, less bleeding, and reduced likelihood of other risks associated with surgery, such as pulmonary embolism and infection.

1.2.1 | Bone Grafts

The reason autologous bone grafts, also known as autografts, remain the gold standard in terms of efficacy in the treatment of non-union fractures is their osteoinductive and osteoconductive nature (Schmidt, 2021; Sen, Miclau, 2007); that is they promote *de novo* bone formation and bone growth and are absorbed into the surrounding bone environment. Typically, trabecular bone is harvested from elsewhere in the patient, usually the iliac crest or reamings from the femoral medullary canal (Sakkas et al., 2017; Schmidt, 2021; Sen, Miclau, 2007), and implanted where it is needed. The fundamental reason that bone grafts are successful is that they contain an optimal mixture of cells as well as growth factors involved in the repair process (Waddington, Sloan, 2016). A major limitation of this approach is the ability to harvest enough material which limits their practical usage. Additional disadvantages include donor site morbidity as well as the need for major surgery at both the donor and the non-union sites (Bray et al., 2017; Waddington, Sloan, 2016). Allografts, where tissue has been donated (usually from a cadaver), address the issue of insufficient supply and donor site morbidity but do not adequately address the need for major surgery. Additionally, they introduce potential immune response complications as well as reduced osteoinduction as a result of the preparation processes (Roberts, Rosenbaum, 2012; Waddington, Sloan, 2016). Biomimetic bone grafts offer an artificial solution to many of the problems posed by autografts, such as the limited supply, but share a lot of the same difficulties with allografts, such as immune response and osteoinduction problems. They also carry their own difficulties, such as the suitability of the mechanical properties (such as strength to density ratio) (Sohn, Oh, 2019). It is possible that, for synthetic bone grafts to be completely successful, other strategies must work synergistically with them, such as the inclusion of mesenchymal stromal cell (MSC)s, growth factors such as bone morphogenetic protein (BMP)s and oxygen delivery methods (Farris et al., 2022; Kim et al., 2024; Marshall et al., 2024).

1.2.2 | Bone Fixation

Bone grafts alone are often not sufficient to promote healing in a non-union fracture. This is because bone grafts, especially trabecular bone grafts, do not provide the required stability for the fracture to heal (Sen, Miclau, 2007). Fixation is also essential for hypertrophic non-union repair where the fracture site has the required cells and growth factors for repair but not the required stability (Roberts, Rosenbaum, 2012; Sen, Miclau, 2007). As a result, artificial fixation may sometimes be needed. There are two types of fixator: internal and external. Internal fixators include nails and compression plates. Of these internal fixation methods, compression plates are the most successful with over 90 % of fractures resulting in union (Kumar, Sadiq, 2002; Padhye et al., 2013). However, surgery is very invasive as large amounts of tissue dissection is required and cortical screws are required (Padhye et al., 2013). These devices will either require additional surgery to remove or they will permanently remain to support the bone. This is a particular problem for metal implants as metal particles can be released as a result of wear, which can result in inflammation and tissue deterioration (Torgersen et al., 1995; Voggenreiter et al., 2003). Research into non-metal and resorbable polymer-based implants is ongoing, with many already in use (Pina, Ferreira, 2012). External fixation avoids this issue and can be useful where the bone surrounding the fracture is osteoporotic or infected and, therefore, does not possess the required strength to support an internal fixator (Padhye et al., 2013). The main disadvantages of external fixation are that the equipment is bulky and uncomfortable for the patient, and that they pose a greater risk of internal rotation (Fernando et al., 2021; Padhye et al., 2013).

1.2.3 | Bone Stimulators

Bone stimulators are external devices that attempt to stimulate bone formation through low-intensity pulsed ultrasound or electrical stimulation (Bhavsar et al., 2019; Victoria et al., 2009; Zura et al., 2015). It is believed, following *in vivo* experiments by Yang *et al.*, that ultrasound stimulation increases the chondrocyte (cartilage producing cells) population, allowing for the formation of a soft callus (Victoria et al., 2009; Yang et al., 1996). *In vitro* studies have also found that exposing osteoblasts to electromagnetic fields stimulates growth factors known to participate in bone repair (Hannouche et al., 2001). One such stimulator that is approved for use in the NHS is Exogen (National Institute for Health and Care Excellence (NICE), 2013). Exogen is a low-intensity

pulsed ultrasound stimulator. Patients are able to self-administer the treatment for 20 continuous minutes a day (Zura et al., 2015). Despite it being approved for use, a lack of untreated controls and the fact that participants had undergone an average of 3.1 prior surgeries make the results of the clinical trials difficult to interpret (Dijkman et al., 2009; Zura et al., 2015). Additionally, there is reported to be resistance from surgeons to using such a device due to conflicting results (Bhavsar et al., 2019).

1.3 | Bone Repair and Oxygen Tension

Oxygen is essential for all eukaryotic organisms. In particular, it is important for the production of ATP. Whilst cells are able to produce ATP through anaerobic glycolysis, this process is not as efficient, producing 2 ATP molecules per glucose molecule compared to the usual 30-36, and has serious side effects such as reducing the pH of the cell. It has been observed that conditions that lead to reduced oxygen tension, such as sleep apnoea (Terzi, Yılmaz, 2016) and anaemia (Valderrábano et al., 2017), lead to poor bone density. It can, therefore, be inferred that low oxygen tension and poor bone mineralisation may be linked. Recent studies have since found that oxygen tension plays a key role in bone repair. Studies have shown that hypoxia has a negative impact on bone regeneration, prolonging the fracture healing time or preventing the fracture from healing completely (Kim et al., 2016; Lu et al., 2013; Utting et al., 2006). There is, however, evidence to suggest that during haematoma formation, localised hypoxia is actually beneficial as it promotes angiogenesis and immune cell recruitment (Grosso et al., 2017). Hyperoxia, high blood oxygen tension, has also been shown to have a negative effect on bone regeneration due to reactive oxygen species formation (Lu et al., 2013; Yamasaki et al., 2009). The one exception to this is under ischaemic conditions where hyperoxia has been shown to be initially beneficial by stimulating angiogenesis (Lu et al., 2013). Hypoxia is also associated with many common bone diseases and complications such as osteoporosis, osteonecrosis and non-union fractures (Yellowley, Genetos, 2019). Therefore, controlled and targeted delivery of oxygen is essential.

1.3.1 | Bone Regeneration

Bone regeneration is a natural process that occurs continuously throughout adult life in the form of bone remodelling (the replacement of old bone with new bone). Bone regeneration is also immensely important for bone repair. There are two types of bone development processes that occur in the body during fracture healing: intramembranous ossification and endochondral ossification (Giannoudis et al., 2007; Phillips, 2005). Intramembranous ossification is the less predominant of the two as it requires the fracture to be small enough that osteoblasts in the cortical bone may be recruited directly to the fracture site as well as almost complete immobility (Giannoudis et al., 2007; Little et al., 2011; Phillips, 2005). This, therefore, occurs mostly in the skull, mandible and clavicle in adults (Little et al., 2011). The ability for the skull to heal through intramembranous ossification occurs as a result of the bone cell lineage from the neural crest rather than from the mesoderm, like in the rest of the body (Gilbert, 2000). Bone repair involving endochondral ossification is much more common, occurring in the rest of the body in bone fracture repair. Endochondral ossification can be split into four temporal phases: inflammation, soft callus formation, hard callus formation and bone remodelling. Inflammation occurs immediately after the fracture due to the rupture of the surrounding blood vessels, forming a haematoma (Sheen, Garla, 2022). This inflammation results in the secretion of pro-inflammatory growth factors and cytokines including tumour necrosis factor (TNF), BMP and interleukins including IL-1β, IL-6, IL-17F and IL-23. TNF and IL-6, in particular, have been shown to be essential for tissue regeneration, and bone repair has been shown to be significantly delayed by their absence (Einhorn, Gerstenfeld, 2015; Glass et al., 2011; Yang et al., 2007). For example, these cytokines are essential to attract cells such as macrophages that remove necrotic tissue present as a result of the fracture (Einhorn, Gerstenfeld, 2015; Little et al., 2011; Phillips, 2005). Additionally, osteoclasts will themselves accumulate to remove any old bone fragments. This is followed by the recruitment and differentiation (prompted by BMP) of stem cells that form vascular and skeletal tissue (Einhorn, Gerstenfeld, 2015; Sheen, Garla, 2022). Chondrocytes then start to form a soft callus made of cartilage adjacent to the fracture. Through this method, the bone is supported by the soft callus (Schindeler et al., 2008). This occurs alongside a suppression of the immune system within the forming fracture callus due to induced T regulatory cells (Al-Sebaei et al., 2014). This protects the

developing tissue. Alongside the formation of the cartilaginous soft callus, the release of vascular endothelial growth factor (VEGF) leads to nascent blood vessel cells differentiating in the surrounding tissue, resulting in angiogenesis. Angiogenesis provides a source of nutrients, oxygen and osteochondral progenitor cells (Schipani et al., 2009; Wang et al., 2007). It is at this point that the hard callus starts to form. The periosteum swells, and the cartilage extracellular matrix is mineralised by osteoblasts. This mineralisation gradually replaces the soft callus with hard callus of woven bone (Schindeler et al., 2008). As woven bone formation is initiated, the cartilage is resorbed and chondrocyte (cartilage forming cells) apoptosis occurs. This callus of woven bone is then remodelled by first resorbing the bone before it is replaced by lamellar bone structures (Schindeler et al., 2008). The bone is remodelled continuously, resulting in a bone structure resembling the original bone structure (McKinley, 2003).

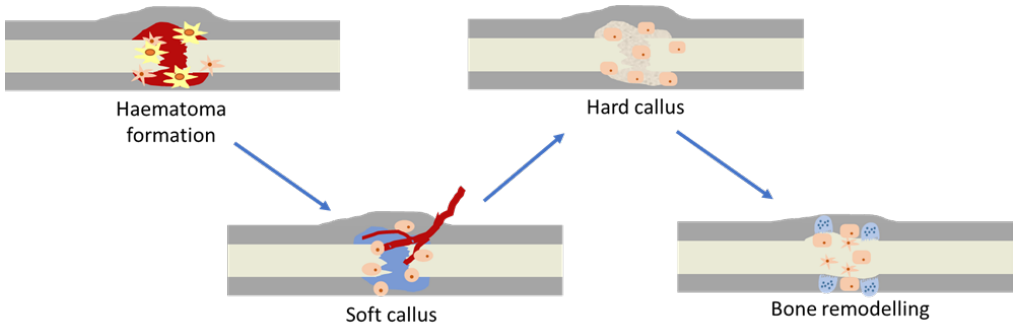

Figure 1.2: Bone repair during endochondral ossification. The haematoma formation allows for the recruitment of inflammatory cells and initiates angiogenesis. The soft callus provides support to the fracture site, allowing woven bone formation to take place. Finally, bone remodelling reshapes the bone so that it is almost identical to the original, unbroken bone.

A multitude of cells, cytokines and signalling pathways are involved in this process. The cells most instrumental in bone formation are osteoblasts and osteoclasts. The balance between these two cell types is paramount as osteoclasts resorb old bone and osteoblasts lay down new bone material.

1.3.1.1 | Osteoblasts

Osteoblasts are responsible for the synthesis of new bone material by depositing collagen and mineralisation of the collagen scaffold to generate bone. Osteoblasts appear to derive from numerous sources such as the bone marrow or the periosteum (Mizoguchi, Ono, 2021). For bone regeneration in severe fractures in adults, the majority of osteoblasts are believed to originate from bone marrow stromal cells and periosteal cells (Colnot, 2009). These cells, sometimes referred to as mesenchymal stem cells or MSCs, are multipotent cells capable of differentiating into myoblasts, osteoblasts, chondrocytes or adipocytes depending on the transcriptional regulators present (MyoD, Runx2, Sox9 and PRAPγ respectively) (De Bari et al., 2006; Rutkovskiy et al., 2016).

The intracellular expression of the runt-related transcription factor 2 (RUNX2) is necessary for osteoblastogenesis (Valenti et al., 2016). RUNX2 itself is regulated by Wnt and Notch signalling. Wnt signalling is an essential process for embryonic development, and it is also essential in adults for tissue regeneration. In bone regeneration, canonical Wnt signalling occurs: Wnt binds with the surface membrane receptor complex of the cell, starting a cascade of events, which ultimately leads to the blocking of the binding complex that captures β-catenin for degradation. This allows β-catenin to accumulate in the cell and eventually enter the nucleus, allowing for transcription of certain genes, including the genes necessary for RUNX2 production (Barker, 2008; Deregowski et al., 2006). In contrast to this, Notch suppresses Wnt/β-catenin signalling (Deregowski et al., 2006). It is important to note that while RUNX2 is necessary for osteoblast differentiation, a reduction in RUNX2 expression and an escalation of osterix expression production is required for mature osteoblast formation and therefore calcification of the bone matrix (Komori, 2006). Additionally, RUNX2 inhibits osteoblasts becoming osteocytes (Komori, 2006). Osteocytes are terminally differentiated osteoblasts that are entrapped within the calcified bone matrix (Bonewald, 2010).

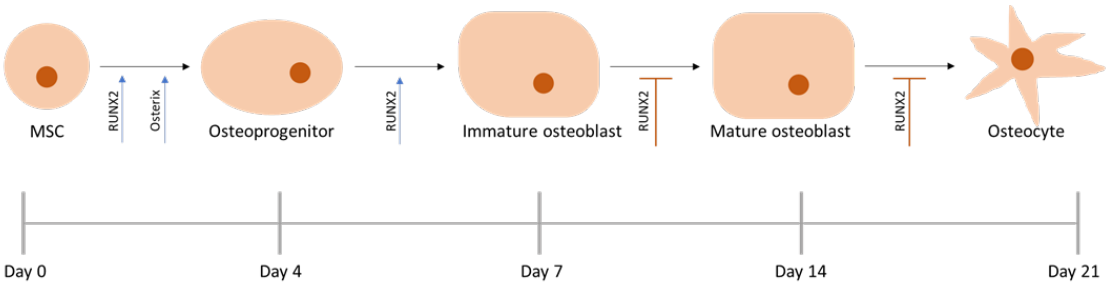

Figure 1.3: Differentiation pathway for osteoblasts. Blue arrows indicate a stimulatory effect, while the orange lines indicate an inhibitory effect. The osteoblasts originate from the marrow stromal cells, which differentiate into osteoblasts in the presence of osterix and RUNX2. The RUNX2 expression needs to be downregulated for mature osteoblast and osteocyte formation.

1.3.1.2 | Osteoclasts

Osteoclasts are a multinucleated cells of haematopoietic lineage, responsible for bone resorption. An imbalance between osteoblasts and osteoclasts can therefore be problematic, as is the case with many bone diseases such as osteoporosis, rheumatoid arthritis and periodontal disease (Boyle et al., 2003). Osteoclasts "digest" bone by attaching to the bone surface, secreting hydrochloric acid to dissolve the inorganic phase of bone, and secreting two enzymes known as cathepsin-K (CATK) and TRAP. The products of this degradation are endocytosed by the osteoclast and transported to the cell's antiresorptive surface (Teitelbaum, 2000).

It has been shown that for osteoclast differentiation to take place, two cytokines are required. Macrophage colony stimulating factor (MCSF), which is produced in the bone marrow (Mak, Saunders, 2006), is necessary but not sufficient for osteoclast differentiation. In the presence of MCSF, the resulting monocyte is still capable of becoming a macrophage; however, receptor activator of nuclear factor-β ligand (RANKL) sets the cell on the path of osteoclast specific differentiation (Boyle et al., 2003). Given osteoblasts and osteoclasts work together to maintain bone, it is no surprise that there is interaction between the two. RANKL is expressed by osteoblasts and osteocytes, which then binds with the cell surface receptor RANK expressed by the osteoclast precursors, stimulating osteoclastogenesis (Hannah et al., 2021; Katagiri, Takahashi, 2002). This activates and differentiates the cells into a mature osteoclast (Boyle et al., 2003; Li et al., 2000; Teitelbaum, 2000), the point at which it is capable of resorbing bone.

Another protein that plays a key role in osteoclastogenesis is osteoprotegerin (OPG). OPG is a decoy receptor for RANKL, neutralising it and therefore its presence down-regulates osteoclastogenesis.(Udagawa et al., 2000).

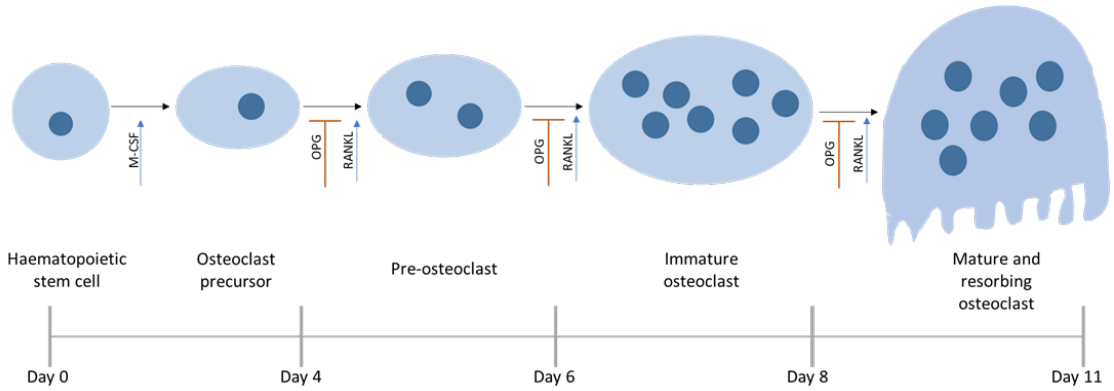

Figure 1.4: Differentiation pathway for osteoclasts. Blue arrows indicate a stimulatory effect, while the orange lines indicate an inhibitory effect.

1.3.1.3 | Osteocytes

As mentioned in section 1.3.1.1, osteocytes are terminally differentiated cells of osteoblastic lineage. These cells reside within the bone matrix and have been found to be integral for controlling osteoblast and osteoclast differentiation and function (Bonewald, 2011; Dallas et al., 2013). Their location embedded within the bone matrix makes them difficult to study; for this reason, their importance for bone repair and maintenance is only just beginning to be properly understood. Osteocytes do not directly contribute to new bone formation or resorption but they are capable of expressing signalling molecules such as sclerostin, an agonist to the Wnt pathway, osteopontin and RANKL in response to mechanical and chemical stimuli (Baron, Kneissel, 2013; Nakashima et al., 2011; Raheja et al., 2008). Through these signalling mechanisms, osteocytes are possibly one of the most important cells involved in bone repair.

1.3.2 | Bone's Cellular Response to Hypoxia

The literature regarding bone's cellular response to hypoxia is conflicting and somewhat complicated. This may be due, in part, to an inconsistency in what is considered hypoxic conditions with oxygen levels described as "hypoxic" varying between 0.1-8% in the literature (Knowles, Athanasou, 2009; Ren et al., 2006; Utting et al., 2006). It is difficult to ascertain exactly what is meant by normoxic and hypoxic physiologically, as the body does not consist of one singular oxygen concentration value throughout (Wenger et al., 2015). Some attempts have been made to measure physiological oxygen concentrations in bone with Maurer *et al*. measuring 8.6% in healthy mandibular bone and 3.9–1.6% in diseased mandibular bone using a polarographic fine needle probe (Maurer et al., 2006). However, it is worth noting that these measurements were only possible in disrupted tissue, as the method is invasive, and accurate measurement of normal healthy bone remains elusive. What is clear from the literature is that there is a temporal effect that needs to be taken into consideration. As illustrated earlier in this introduction there are essentially four stages of bone repair: inflammation (prompted by HIF signalling discussed later in this review), soft callus formation (which only occurs in endochondral ossification), hard callus formation (where the cartilage is replaced by bone) and bone remodelling (the final "corrections" stage) (Schindeler et al., 2008). For the former two stages, hypoxia has generally been shown to be stimulatory (Grosso et al., 2017; McGarry et al., 2018; Schipani et al., 2001). The latter two stages of this process are when new bone formation is taking place, and also when any intervention is most likely to occur. It has largely been shown that hypoxia is inhibitory during these two stages (Hannah et al., 2021). *In vitro*, low oxygen tension has been shown to increase proliferation in MSCs (Lu et al., 2013). A high number of MSCs is essential for increased bone repair; even so, it has been shown that hypoxia decreases the MSCs ability to differentiate into osteoblasts (Berniakovich, Giorgio, 2013; Nicolaije et al., 2012), inhibiting bone production. Utting et al. not only found that 2% oxygen, hypoxia resulted in a 10-fold decrease in bone nodule formation compared to 20% oxygen, normoxia, but that the collagen fibril deposition was affected. Fibrils formed under normoxic conditions were dense, regular and parallel, but under hypoxia they were found to be more sparse and erratic (Utting et al., 2006). Reduced collagen deposition is likely due to reduced hydroxylated proline resulting in collagen instability and under-hydroxylated procollagen being stored intracellularly (Utting et al., 2006). It

has been suggested that this reduced bone formation is a result of RUNX2 expression being inhibited, resulting in reduced differentiation of MSCs to osteoblasts (Ontiveros et al., 2004; Salim et al., 2004). Moreover, bone mineralisation has been shown to be significantly reduced due to the reduction in ALP production (Nicolaije et al., 2012; Utting et al., 2006).

In contrast, there appears to be an increase in differentiation and activity of osteoclasts in the presence of hypoxia (Arnett et al., 2003; Knowles, Athanasou, 2009; Utting et al., 2006). *In vitro* mouse cultures have demonstrated a 21-fold increase in osteoclast activity (Arnett et al., 2003). It has been demonstrated *in vitro* that hypoxia results in a suppression of OPG (Shirakura et al., 2010; Yu et al., 2015). As OPG is a decoy receptor for RANKL, the protein responsible for osteoclast differentiation, it is logical that a decrease in OPG will result in an increase in osteoclast differentiation. However, there is literature to suggest that continuous hypoxia actually causes an increase in osteoclast apoptosis (Gorissen et al., 2019; Knowles, Athanasou, 2009; Muzylak et al., 2006). It has, therefore, been suggested that a careful balance between increased differentiation and increased apoptosis is achieved and increased osteoclastogenesis is observed (Knowles, Athanasou, 2009). It has been suggested that this can be achieved through reoxygenation following short hypoxic exposure, where the hypoxia induces osteoclastogenesis and the reoxygenation "rescues" the cells from cell death (Knowles, Athanasou, 2009). The effects of reoxygenation may also be related to increased production of reactive oxygen species (ROS), which is discussed in more depth in section 1.3.4. Overall, the decrease in osteoblasts and increase in osteoclasts could lead to an imbalance that results in net bone resorption.

Given the ability of osteocytes to sense chemical stimuli, it is no surprise that they are capable of sensing and responding to hypoxic conditions. *In vitro* hypoxic osteocyte-conditioned media have been shown to upregulate osteopontin expression and cell migration in mesenchymal stromal cells (Raheja et al., 2008). Conversely, osteocyte cell death has been shown to be induced by hypoxia (Montesi et al., 2016). Osteocyte cell death has been shown to release osteoclast inducing factors that promote resorption (Zhao et al., 2025).

1.3.3 | HIF Signalling and Bone repair

A key protein involved in oxygen detection in the body is hypoxia inducible factor (HIF). There are three members of the HIF family: HIF-1, HIF-2 and HIF-3 (Rankin et al., 2007; Tanaka et al., 2009; Ziello et al., 2007). HIFs are heterodimers made of two subunits: HIF-α subunits and HIF-β subunits (Yellowley, Genetos, 2019). This introduction will mainly focus on HIF-1. The ability of HIF-1 to detect hypoxia stems from the HIF-1α subunit. While HIF-1β remains stable, HIF-1α's stability is dependent on oxygen tension. The presence of oxygen results in prolyl hydroxylation which essentially "tags" it for degradation by the proteosome (Jaakkola et al., 2001). Under hypoxic conditions, this degradation is suppressed, allowing for HIF-α's translocation to the nucleus and dimerisation with HIF-β to form a HIF-1 complex. This, in turn, binds with the hypoxic response elements of the promoter region of certain genes such as *VEGF* (Drager et al., 2015). VEGF is necessary for angiogenesis to occur, which is in turn necessary for the initial stages of bone regeneration, in that it allows for the appropriate inflammatory response and osteoclast recruitment (Grosso et al., 2017). To this extent, hypoxia is essential for immediate bone fracture healing. Interestingly, a loss of HIF-1α expression in osteoblasts has shown a decrease in endochondral bone volume in mice (Wan et al., 2010; Wang et al., 2007). This contrasts with *in vitro* work with osteoblasts and osteoclasts. It is, however, likely to be due to the lack of vascularisation rather than a direct effect on the osteoblast and osteoclast population as there was no significant change in cell proliferation in either case (Wang et al., 2007). However, there has been some suggestion that overexpression of HIF-1α may lead to an increase in glycolytic activity, leading to an increase in osteoblast activity (Rankin et al., 2007). Despite this, HIF-2α has been shown to inhibit osteoblastogenesis and a deficit of HIF-2α leads to increased bone mass (Lee et al., 2019). It is important to note that these experiments were performed in post-natal mice and investigated bone development rather than bone repair. It is, therefore, not necessarily an accurate model for late-stage non-union fractures where there is existing vasculature (Menger et al., 2022). In contrast to this behaviour observed in osteoblasts, it has been suggested that HIF-1α increases osteoclast activity (Knowles, Athanasou, 2009). This is consistent with the observations that hypoxia stimulates osteoclastic activity discussed previously in this chapter. In osteocytes, enhanced HIF-1α signalling caused by the deletion of prolyl hydroxylase 2 (PHD2), decrease the expression of the Wnt agonist sclerostin. This was

further reflected *in vivo* where bone mass increased with increased HIF-1α signalling.

1.3.4 | Reactive Oxygen Species Production

Another aspect of hypoxia worth considering is ROS production. It has been suggested that ROS are produced under hypoxic conditions as a result of inefficiencies in the mitochondrial electron transport chain (Clanton, 2007; Møller et al., 2001; Srinivasan, Avadhani, 2007; Srinivasan et al., 2010). These inefficiencies arise due to a shift towards increased glycolytic activity resulting in increased nicotinamide adenine dinucleotide (NADH) production. This causes an over-reduction of the electron transport chain, producing superoxide radicals (Clanton, 2007; Srinivasan et al., 2010). This effect is demonstrated in Figure 1.5. ROS production has been associated with reduced osteoblast differentiation by disrupting the relevant signalling pathways (Bai et al., 2004) and osteoclast activity has also been reported to be stimulated by ROS generation (Fraser et al., 1996; Garrett et al., 1990). ROS may also have a direct effect on bone resorption since TRAP generates ROS during the resorption process, which break down the type I collagen present in bone (Halleen et al., 2003). ROS produced under hypoxic conditions may also contribute to this process (Hannah et al., 2021).

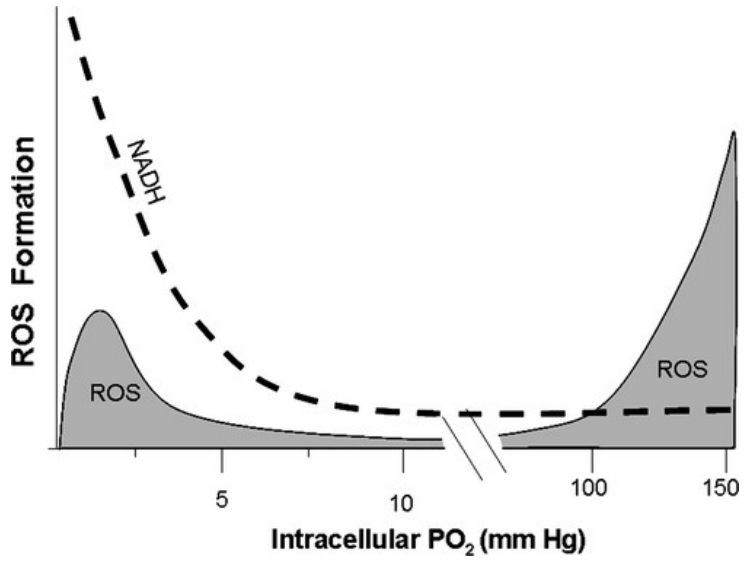

Figure 1.5: ROS production with respect to intracellular oxygen tension (Clanton, 2007).

1.3.5 | The Effect of Hyperoxia

Figure 1.5 demonstrates how ROS is theorised to vary with oxygen tension. Whilst it demonstrates that there is an increase in ROS with hypoxia, this effect is far more pronounced in hyperoxia (Clanton, 2007). It stands to reason that increasing the number of oxygen molecules available increases the possibility of ROS being formed. As mentioned in section 1.3, some research has shown that over prolonged periods of time, hyperoxia may, in fact, induce ROS production (Garrett et al., 1990) and increase osteoclast production (Yamasaki et al., 2009). Consequently, when evaluating oxygen delivery as a potential intervention for non-union fractures, it is imperative to consider the quantity of oxygen administered as well as the temporal dynamics of such delivery. Increasing the oxygen tension in a fracture that is failing to heal may also have damaging effects if it is raised too much. This effect, caused by hyperoxic conditions, is particularly important to keep in mind when considering *in vitro* experiments, as many experiments refer to 20% oxygen as "normoxia". This is likely much higher than physiological normoxia in bone and so 20% oxygen may actually be considered hyperoxic (Mamalis, Cochran, 2011).

In an *in vivo* context, bone fractures will result in the disruption of the local blood vessels, resulting in insufficient blood supply or ischaemia. This will result in a very hypoxic environment and metabolic stress within the cells. As the vasculature is restored, reperfusion occurs and the sudden influx of oxygen into an environment that has adapted to hypoxia. This can result in the rapid production of ROS, which can be detrimental to bone repair, although there is limited research into the direct effects this has on bone repair (Kalogeris et al., 2012).

1.4 | Current and Emerging Technologies in Oxygen Delivery

Hypoxic environments are not unique to bone fractures. As such, a great deal of research has previously been conducted into artificially increasing the oxygen tension within the body. This is typically done through two routes: increasing the oxygen tension circulating through the whole body or locally changing the oxygen concentration at the required location.

1.4.1 | Altering Inspired Oxygen

One method of increasing oxygen tension is by increasing the amount of inspired oxygen. This is usually achieved by breathing 100% oxygen or carbogen (a carbon dioxide and oxygen mixture) at increased pressures (Menendi et al., 2022). *In vivo* experiments in rats found that hyperbaric oxygen therapy led to accelerated bone healing as well as increased Runx2 expression (Rocha et al., 2015). Increased oxygen tension has been investigated with respect to bone with clinical trials in the form of hyperbaric oxygen in lower limb trauma (HOLLT) (Millar et al., 2015). Recently published results of the clinical trials found that patients that underwent hyperbaric oxygen therapy following surgery for severe bone fractures, had reduced incidence of soft tissue necrosis and infection as well as increased incidence of wound healing (Millar et al., 2022). However, HOLLT does not offer the ability to deliver oxygen to the fracture site only at the time it is needed. This lack of specificity could result in more side effects due to systemic hyperoxia such as temporary myopia, pulmonary oedema and hyperglycemia (Heyboer et al., 2017; Shykoff, Lee, 2019).

1.4.2 | Haemaglobin-Based Oxygen Carriers

Haemoglobin-based oxygen carriers (HBOCs) mimic red blood cells by using purified haemoglobin to capture and release oxygen. However, free haemoglobin is toxic as it leads to the generation of superoxide radicals and potentially renal failure (Cao et al., 2021). It also has a high oxygen and nitric oxide affinity compared to haemoglobin sequestered within red blood cells and limited stability (Alayash, 1999; Jahr et al., 2002). To overcome these problems, haemoglobin-based oxygen carriers are often genetically or chemically modified through methods such as cross-linking, conjugation, encapsulation or being bound within a polymer matrix (Alayash, 1999; Jahr et al., 2021; Olson et al., 2004). Despite these advances, to date, no haemoglobin-based oxygen carrier has been approved for use in the UK, EU or USA. Phase III clinical trials elsewhere in the world have reported a lack of significant improvement from saline controls and/or significant adverse effects such as anaemia, neurotoxicity, jaundice and fever. Despite this, one formulation, Hemopure, is approved for use in South Africa for emergency situations in which safe blood alternatives are not available (Alayash, 2014; Chen et al., 2009; Jahr et al., 2021).

1.4.3 | Perfluorocarbon-Based Emulsions

Perfluorocarbon (PFC)-based emulsions have been used in a wide range of industries, including medicine, agriculture, food and cosmetics (Jafari, McClements, 2018). For example, in agriculture, they are used for delivering pesticides (Feng et al., 2016); in cosmetics, to deliver ceramides to combat dry skin (Yilmaz, Borchert, 2006) and in food for delivering nutrients and enhancing flavours (Chen et al., 2016). This review will focus specifically on how PFC nanodroplets have been used in medicine. The three main areas in which PFC nanodroplets are being investigated are cancer therapies, biomedical imaging and blood substitutes. Figure 1.6 lists some of the main examples of perfluorocarbon nanodroplets under active research.

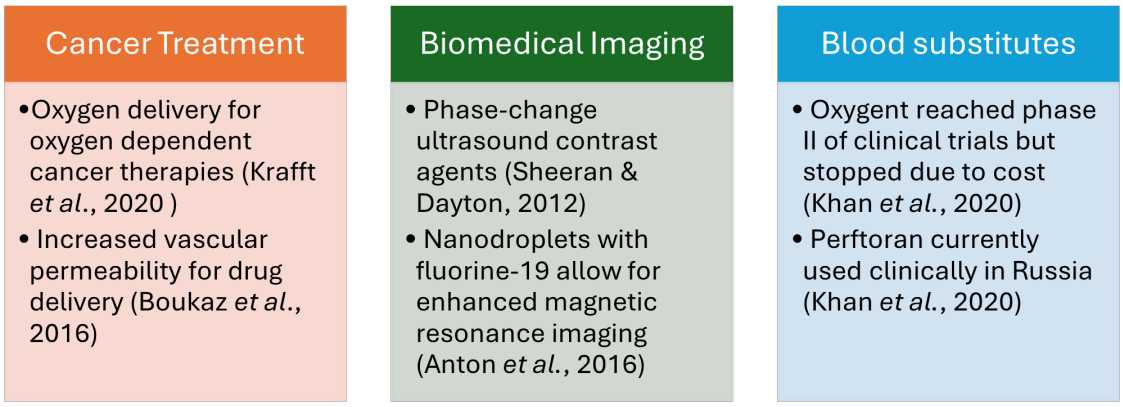

Figure 1.6: Diagram listing the areas of current research of PFC nanodroplets (Anton et al., 2016; Bouakaz et al., 2016; Khan et al., 2020; Krafft, Riess, 2021; Sheeran, Dayton, 2012).

1.4.3.1 | Perfluorocarbon-Based Oxygen Carriers

Of the above examples, blood substitutes and oxygen delivery in tumours are of particular interest as they use perfluorocarbon (PFC) nanodroplets as oxygen carriers. Perfluorocarbons have the advantage of having high oxygen solubility, capable of dissolving approximately 20 times the volume of oxygen that water is capable of dissolving (Wesseler et al., 1977). Given this property, perfluorocarbons have been studied as potential blood substitutes for decades. Previous studies into perfluorocarbon nanodroplets, e.g., Oxygent, Fluosol and Perftoran, have proceeded to clinical trials, investigating areas such as decompression sickness, blood loss due to surgery and treating

haemorrhagic shock. PFC nanodroplets are useful when treating hypoxia caused by the narrowing of blood vessels or in smaller capillaries because of their smaller size (Jägers et al., 2020). One clinical trial for perfluorocarbon-based oxygen carriers is Oxygent. Phase II trials demonstrated that patients that had received Oxygent were able to tolerate more preoperative autologous blood harvesting and allogenic blood transfusions were reduced or not required (Rapoport, 2016). This illustrates that PFC nanodroplets are successful in delivering oxygen (Krafft, Riess, 2021). However, phase III trials were voluntarily postponed due to neurological problems that were later shown to be linked to poor compliance with clinical protocol. Due to a shortage of funding, trials were not resumed (Castro, Briceno, 2010). Two PFC nanodroplets have been approved for clinical use. Perftoran (Vidaphor in the United States (Latson, 2019)) is approved for use in case of haemorrhagic shock and perfusion of organs in Russia, Brazil, Kazakhstan and Mexico; however there are concerns over the short shelf life of 1 month (Castro, Briceno, 2010) and lack of compliance with good manufacturing practice (GMP) (Latson, 2019). Another formulation, Fluosol, was approved by the US Food and Drug Administration (FDA) but has since been removed from the market due to difficulties with storage and questions over long-term side effects such as anaemia, leukocytosis or chemical pneumonitis (Castro, Briceno, 2010).

Perfluorocarbon-based microbubbles are very similar to nanodroplets in composition, but they have a gas core and are significantly larger. They typically are 1-2 µm in size (Unger et al., 2004). They have also been investigated for oxygen delivery (Dauba et al., 2020; Gerber et al., 2009; Swanson et al., 2010) but they are typically less stable, have short circulation times and are unable to reach the smaller capillaries or extravasate due to their larger size (Kim et al., 2020; Mannaris et al., 2019).

1.5 | Perfluorocarbon Nanodroplets

The carbon and fluorine atoms in perfluorocarbons form a very strong bond resulting in a molecule that is inert and very stable. Fluorine is the most electronegative element in the periodic table. As a result, the electron cloud is firmly pulled towards the fluorine atoms, making it difficult to induce a temporary dipole, resulting in very weak Van der Waals forces.

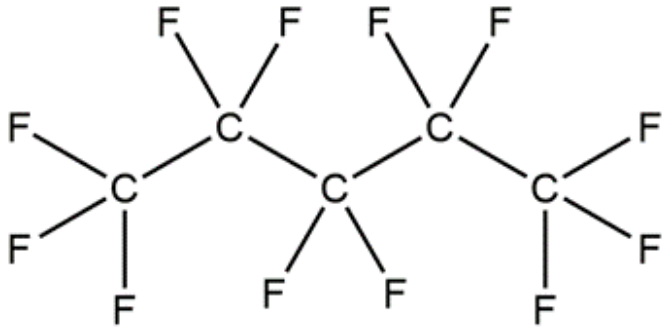

Figure 1.7: Structural formula showing the molecular structure of perfluoropentane (PFP), a straight chained perfluoroalkane

.

The symmetry of straight-chained perfluoroalkane molecules also results in these very weak Van der Waals forces being the only intermolecular forces that arise as the carbon-fluorine dipoles balance each other out. The weak intermolecular forces result in a low boiling point relative to the PFCs equivalent hydrocarbon, e.g., perfluoropentane has a boiling point of 29^{o}C but pentane has a boiling point of 36^{o}C (Johnstone, 2007). The weak intermolecular interaction also results in less tight packing, which allows molecules with similarly weak intermolecular forces (e.g., O_2 and CO_2) to move between the PFC molecules and dissolve unobstructed (Riess, 2005). This results in gases such as oxygen being highly soluble in PFCs. The weak intermolecular forces also result in PFCs being both hydrophobic and lipophobic. The low polarisability means the perfluorocarbon molecules are at a lower energy state mixed with themselves than lipids or water.

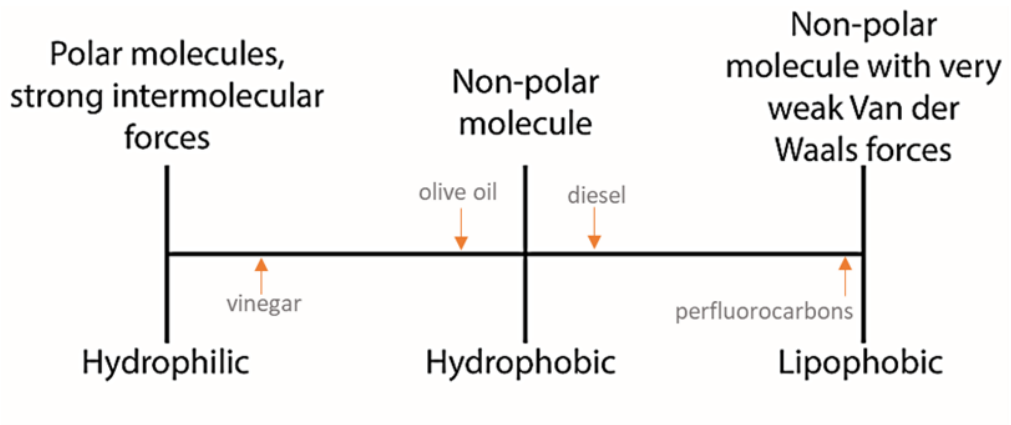

Figure 1.8: Comparison of the lipophobic nature of perfluorocarbons with other common substances (not to scale).

Due to their hydrophobicity, PFCs will not disperse in an aqueous solution. PFCs can, however, be encapsulated in a phospholipid monolayer known as PFC nanoemulsions or nanodroplets, as the phospholipid acts as a surfactant. This has the benefit of creating a barrier for gas diffusion, but more importantly, inhibiting particle coalescence and Ostwald ripening, thereby stabilising the PFC droplet in aqueous solution (Mountford, Borden, 2016). Phospholipids occur naturally in the body and are therefore biocompatible as well as soluble in blood. This means that phospholipid-coated droplets can be injected into the bloodstream (Krafft, Riess, 2021).

Phospholipid molecules have two principal regions: a hydrophilic head and a hydrophobic tail. The phospholipid will align itself so that it is in its lowest energy state, and so the hydrophobic tails will align themselves away from the polar solution on the outside and towards the PFC, whereas the hydrophilic heads will do the opposite. Despite the PFC being classed as lipophobic, it is in a lower energy state next to the hydrophobic tails than in the hydrophilic heads or surrounding aqueous solution and therefore preferentially associate. This creates an aqueous dispersion of perfluorocarbon nanodroplets, also known as a nanoemulsion.

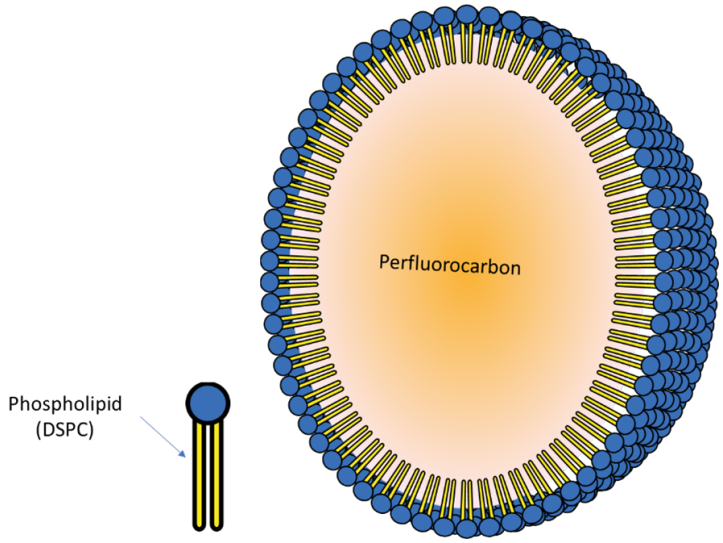

Figure 1.9: Schematic diagram showing the basic structure of a nanodroplet (not to scale). Typical nanodroplet diameters range from 100-500 nm.

It is important to note that the pressure inside a nanodroplet is greater than that outside due to surface tension (equation 1.1). This, in turn, results in the boiling point of the perfluorocarbon increasing when contained within the nanodroplet compared to bulk perfluorocarbon (Krafft, Riess, 2021).

$$\Delta P = \frac{2\sigma}{r} \tag{1.1}$$

Where ΔP is the pressure increase (the Laplace pressure) as a result of surface tension, σ is the surface tension and r is the radius of the particle. Equation 1.1 implies the smaller the nanodroplet, the greater the Laplace pressure and therefore, the greater the boiling point. The difference in pressure allows for perfluorocarbons such as perfluoropentane, which has a boiling point of 29^oC at atmospheric pressure, to remain liquid at higher temperatures, such as body temperature (37^oC) when encapsulated as a nanodroplet (Krafft, Riess, 2021). This allows the nanodroplet to undergo spontaneous vaporisation when an external stimulus is introduced, such as ultrasound (Krafft, Riess, 2021), allowing more targeted delivery of gases dissolved in the perfluorocarbon. As the stability is dependent on their size, the ability to precisely control and measure the size of the nanodroplets is very important.

It has been suggested that this phenomenon of Laplace pressure leading to superheated stability may not be entirely correct. Mountford et al. have hypothesised that the superheated stability of nanodroplets can be explained by the reduced probability of nucleation and hence a phase change (vaporisation) occurring in a very small volume of liquid (Mountford, Borden, 2016).

1.5.1 | Methods for Creating Perfluorocarbon Nanodroplets

Multiple methods have been used to produce nanodroplets each with their own advantages and disadvantages. Methods can generally be classed into four categories: homogenisation, sonication, microfluidics and condensation from microbubbles (Anton et al., 2016; Lea-banks et al., 2021). High-pressure homogenisation is already commonly used in a range of industrial processes, one key example being the homogenisation of milk. The lipid and the fluid it will encapsulate are premixed and forced through a very small orifice at high pressures. The effect of the particle hitting the side wall of the orifice causes shear forces and heating. This fragments the premixed droplets into sub-micron sized droplets. This technique is especially useful for industrial scale processes due to its ability to run continuously and produce large amounts of nanodroplets in a relatively short amount of time. However, small production scales are technically challenging and may lead to waste.

Sonication is the most commonly used technique for making nanodroplets. It is a technique much more suited for use in a laboratory setting due to its smaller size and smaller production amounts. The sonicator tip is placed in a container with both the aqueous surfactant solution and the PFC. When it is turned on at low frequency (i.e., typically 20-60 kHz), high-intensity ultrasound agitates the fluids by inducing the formation of bubbles by cavitation. These bubbles collapse, generating shear forces in the liquid. This results in the fluids both mixing and breaking up the droplets, creating progressively smaller ones until a submicrometre size is achieved. This process allows for small amounts to be made for experiments; however, the resulting size profiles are more broad than from a high-pressure homogeniser. For both homogenisation and sonication, temperature is an important consideration. For example, perfluoropentane has a boiling point of $29^{o}C$ at atmospheric pressure. As discussed previously, the vaporisation temperature of the perfluorocarbon increases once encapsulated. If the temperature gets too high, the perfluorocarbon may evaporate before being encapsulated.

Additionally, larger droplets will have lower boiling points and so larger droplets also vaporise if the temperature gets too high. Temperature is also a key consideration if thermolabile bioactive substances are to be encapsulated.

Microfluidic methods have also been explored for nanoparticle production. Microfluidic systems allow for a much more controlled environment for particle production, resulting in a much tighter size distribution. This is a significant advantage if vaporisation and potential side effects are dependent on size. However, with this comes an added degree of complexity as well as significantly slower production rates. Martz et al. demonstrated that it is possible to produce sub-micrometre nanodroplets by microfluidics (Martz et al., 2012). Perfluoropentane (PFP) and a lipid suspension were injected into two separate channels that merged into one single channel to promote mixing. The size of the resulting nanodroplets was dependent on the two input flow rates, with an increased PFP flow rate resulting in larger nanodroplets and an increased lipid flow rate resulting in smaller nanodroplets (Martz et al., 2012). The droplets produced, however, were significantly larger ($\sim$7.4µm) than those typically made using sonication and production rates were approximately 10^8 times slower. Additionally, samples produced using this microfluidic system were shown to contain a large proportion of lipid vesicles that did not encapsulate the PFC (Martz et al., 2012). Nevertheless, microfluidic devices typically reduce size dispersity (Sheeran et al., 2017). Teston *et al.* have since developed a method for producing nanodroplets that depends on the interfacial tension between the lipid and the perfluorocarbon using an approach known as microchannel emulsification. Put simply, the lipid suspension flows continuously in one direction through one channel and the perfluorocarbon solution alternates between flowing parallel and anti-parallel. The two channels are connected by orthogonal channels and the pressures are controlled so that the perfluorocarbon travels to the lipid suspension. This resulted in an approximately four fold increase in production rate and droplets of half the size compared with previous attempts at microfluidic systems (Teston et al., 2018); although both the production rate and droplet size were still inferior to those that can be achieved using other methods.

Condensation methods require microbubbles to be created first (e.g. using agitation, microfluidics or sonication). The microbubbles are then placed in a cool and high-pressure environment to condense them. Sheeran *et al.* used a temperature of -5^oC and pressure of 600-750 kPa to make lipid nanodroplets containing perfluorobutane

(Sheeran et al., 2011a). However, this method can result in a mixture of droplets and bubbles if condensation is incomplete, which is undesirable for *in vivo* use (Krafft, Riess, 2021). Additionally, the method is less convenient for perfluorocarbons with boiling points above room temperature at atmospheric pressure, as the microbubbles cannot be made under standard conditions. It is also a difficult method for drug encapsulation in the core (Sheeran et al., 2017).

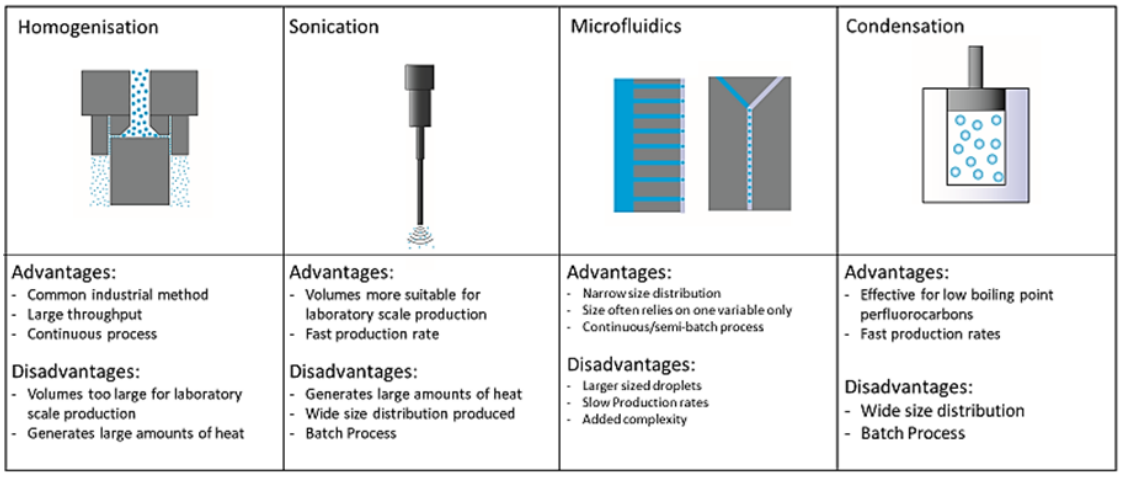

Figure 1.10: Diagram outlining the different nanodroplet production methods.

1.5.2 | Methods for Characterising Nanodroplets

Once made, it is important to be able to characterise nanodroplets in order to improve understanding of their function and reproducibility. Whilst microbubbles (generally 1-10 μm) may be characterised by studying them with a light microscope, nanodroplets ($\sim$10-500 nm) are too small to resolve optically and so other techniques are required. Techniques such as transmission electron microscopy (TEM), scanning electron microscopy (SEM) (Klang et al., 2012) and atomic force microscopy (AFM) (Silva et al., 2011) can be used to observe stable nanodroplets. These techniques offer valuable information with regards to size and shape. However, they are often costly and time-intensive due to the fact that they require a lot of energy and expensive equipment and many measurements must be made in order to make them statistically viable. These techniques are therefore not suitable for batch analysis. Additionally, preparation techniques may alter the sample structure (Jafari, McClements, 2018), especially for nanodroplets designed for acoustic droplet vaporisation, as energy input during prepara-

tion or observation techniques will be enough to stimulate vaporisation. As a result of these drawbacks, more indirect methods of characterising nanodroplets are often used to ensure the size and polydispersity index (a measure of particle size dispersity) are as expected.

When reviewing the literature for nanodroplet emulsions, dynamic light scattering (DLS) is the most common method used to determine the nanodroplets' size. It operates by relating the scattered light intensity fluctuations due to Brownian motion to the particle diameter by using the Stokes-Einstein equation.

$$D = \frac{k_B T}{6\pi\eta R} \tag{1.2}$$

Where D is the translational diffusion coefficient, k_B is the Boltzmann constant, T is the temperature, η is the viscosity of the solvent and R is the hydrodynamic radius of the particle. However, the intensity of the light scattered by the particles is also related to the size and is given by equation number 1.3.

$$\%I_a = \frac{100 N_a d_a^6}{\Sigma_i^k N_i d_i^6} \tag{1.3}$$

Where $\%I_a$ is the intensity distribution for a given particle size d_a, and N_i is the number of molecules of diameter d_i (Stetefeld et al., 2016). This relationship is very sensitive to size due to the intensity being proportional to the diameter to the sixth power (Stetefeld et al., 2016). This gives DLS a bias towards larger particles, which can especially be a problem when the suspension has a high size dispersity (Filipe et al., 2010).

NTA, another technique for measuring particle size, also uses Brownian motion and the Stokes-Einstein equation. The NTA uses a camera to capture the scattered light from the nanodroplets. As individual particles are measured rather than a bulk solution, there is less bias towards larger particles. The minimum size detection limit is, however, determined by the particle's ability to scatter light. The diffusion coefficient can be calculated from the movement due to Brownian motion as shown in equation 1.4.

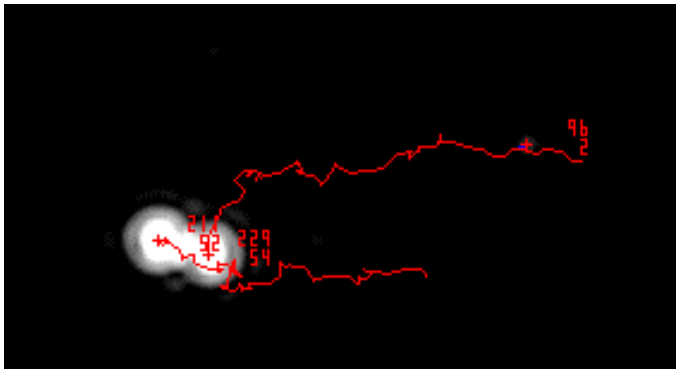

Figure 1.11: Screenshot of nanoparticle analysis software (Nanosight, Malvern) tracking the particles moving through PBS.

$$D = \frac{\overline{(<x, y>^2)}}{4t} \tag{1.4}$$

Where D is the diffusion coefficient, $\overline{(<x, y>^2)}$ is the mean-squared displacement of the particle, and t is the time interval over which it is measured. This relationship can be used in combination with the Stokes-Einstein equation (equation 1.2) to find the diameter of the particle.

1.5.3 | Oxygen Delivery

As mentioned above, the weak intermolecular interactions in PFCs allow for high oxygen solubility. Wesseler et al. demonstrated that solubility of oxygen in perfluorohexane is 488 ml_{O_2}/L at 25^oC (Wesseler et al., 1977) and atmospheric pressure. To put this into context, water is about 10 ml_{O_2}/L and blood is 200 ml_{O_2}/L (Jägers et al., 2020). Oxygen solubility in PFCs obeys Henry's law as seen in equation 1.5.

$$C_{O_2} = Hp \tag{1.5}$$

Where C_{O_2} is the concentration of oxygen in the aqueous phase, H is Henry's constant and p is the partial pressure of the gas phase. This implies the concentration of oxygen is directly proportional to the partial pressure of the gas phase oxygen, a phenomenon not shared with haemoglobin (Riess, 2005), which chemically binds to the oxygen with a polydentate ligand. As a consequence, oxygen delivered by PFCs is

more readily available than oxygen delivered using haemoglobin. This may be a disadvantage in some cases, as some of the oxygen may be lost before reaching the target site.

Oxygen diffusion from the nanodroplets obeys Fick's first law of diffusion. This can be approximated by the equation below.

$$J = -k_p D \frac{C_i - C_o}{r_o - r_i} \tag{1.6}$$

Where J is the oxygen flux $(molm^{-2}s^{-1})$, k_p is the permeability coefficient, D is the diffusion coefficient, $(C_i - C_o)$ is the difference between the oxygen concentration inside and outside the droplet and $(r_o - r_i)$ is the thickness of the membrane. The derivation and assumptions for this equation can be found in the appendices.

From Fick's law, it can be seen that the partial pressure (directly proportional to the concentration) gradient is the main driving force for diffusion. The partial pressure will decrease as the oxygen diffuses out until the nanodroplet is in equilibrium with the surrounding environment, when the diffusion stops. This can help with delivering oxygen to localised hypoxic environments, such as in haemorrhagic shock, as the nanodroplet will have more oxygen than its surrounding environment when entering hypoxic regions.

It is important to note that the phospholipid monolayer is very thin (∼2.5nm for pure DSPC (Yamaoka et al., 1998)). As such, it offers very little resistance to oxygen diffusion with equilibrium likely occurring within minutes if not seconds. This means any oxygen within the nanodroplet is readily available.

Nanodroplet oxygen delivery has been previously studied *in vivo* for treating hypoxia in tumours. Oxygen is often required for tumour therapies to be effective. Huang et al. studied oxygen delivery using doxorubicin (DOX) hydrochloride and perfluorotributylamine (PFTBA) containing nanodroplets for chemosonodynamic therapy. It was found that HIF-1α was significantly decreased in the group treated with nanodroplets containing perfluorotributylamine (PFTBA) and DOX compared with the group treated with nanodroplets containing DOX only (Huang et al., 2020). Given that the presence of HIF-1α is indicative of hypoxia, a decrease in its expression provides evidence for the perfluorocarbon being responsible for introducing oxygen

to the tumour. Similar results were reported by Zeng *et al.* when studying the use of nanodroplets loaded with perfluorohexane for sonodynamic therapy. A 10-fold decrease in pimonidazole immunofluorescent staining (a hypoxic marker in tumours) was observed in the vesicles containing perfluorohexane compared to those without. Interestingly, there was no observable difference in the perfluorohexane droplets that had been preloaded with oxygen and the perfluorohexane nanodroplets that had not (Zeng et al., 2020). This is a significant observation as it suggests that the nanodroplets are assisting in delivering oxygen to the tumour but not necessarily by delivering the oxygen with which they were originally loaded. This is consistent with the fact that the amount of oxygen the nanodroplets are capable of encapsulating is very small compared with that carried by healthy red blood cells (see Table 1.1).

Table 1.1: Estimations of oxygen delivered assuming all perfluorocarbon was encapsulated and assuming 100% saturation of the nanodroplet at atmospheric temperature and pressure. Perfluorocarbon oxygen solubility values were obtained from Wesseler *et al.* (Wesseler et al., 1977)

Perfluorocarbon	**Approx. volume of PFC injected (μl)**	**PFC oxygen solubility**	**Estimated volume of oxygen delivered (μl)**	**Reference**
Perfluorotributylamine	0.4	38.4	0.16	Huang et al. (2020)
Perfluorohexane	1.2	48.8	0.59	Zeng et al. (2020)
Perfluoro-15-crown-5-ether	15	39.7	6	Song et al. (2016)

Table 1.1 shows estimated values of oxygen delivered by perfluorocarbon nanodroplets used to relieve hypoxia in tumours. These are optimistic estimates assuming perfect conditions for making the nanodroplets, loading the nanodroplets and subsequently retaining the oxygen prior to injection. As a result, the real values are likely to be significantly less. It can be seen, however, even with these optimistic values, that the amount of oxygen the nanodroplets are capable of introducing to the body is negligible. For context, blood is typically capable of storing 20.5 mL of oxygen per 100 mL

of blood (Pittman, 2011). Therefore, the particles must be enhancing oxygen delivery in some other way.

1.5.3.1 | Increased Diffusion Hypothesis

One proposed solution to this problem is the increased diffusion hypothesis. Perevedentsiva *et al.* proposed the idea that the nanodroplets actually increase oxygen transport from the erythrocytes to the tissue (Perevedentseva et al., 2009). Under flow, the nanodroplets will be suspended in the blood, filling the gap between the erythrocytes and the endothelium (Spiess, 2010). The perfluorocarbons have approximately 50 times higher oxygen solubility compared to plasma (Jägers et al., 2020; Wesseler et al., 1977), resulting in more rapid diffusion from the erythrocytes to endothelium (Perevedentseva et al., 2009; Spiess, 2010). It has also been suggested that the phospholipid membrane of the nanodroplets adsorbs onto the surface of the erythrocytes. The interaction of the polar head on both nanodroplet and erythrocyte membrane results in a reduction in charge in the membrane, increasing the non-specific oxygen permeability of the erythrocyte membrane (Perevedentseva et al., 2009). There has also been a suggestion that stable nanodroplets unaffected by ultrasound have the ability to recirculate around the body and be oxygenated by the lung, which would also increase oxygen supply (Song et al., 2021).

1.5.3.2 | Increased Perfusion Hypothesis

It has been suggested that perfluorocarbon nanodroplets increase oxygen transport through the increased perfusion hypothesis. There are instances where erythrocytes are incapable of reaching a desired location despite vascularisation, for example, in smaller capillaries or where vasoconstriction has occurred (Castro, Briceno, 2010). In these cases, oxygen is transported by the plasma only, and the diffusion gradient is no longer constant. Nanodroplets are small enough that they are able to perfuse these areas. The high oxygen solubility of the perfluorocarbon results in an increased capacity of the blood medium. This ability to perfuse has been shown to be enhanced by the presence of ultrasound, where they have been able to penetrate deeper out of the vasculature into the tissue (Song et al., 2016).

1.5.4 | Ultrasound Stimulation of Nanodroplets

In the oxygen delivery experiments performed by Huang *et al.* and Zeng *et al.*, ultrasound was used with the nanodroplets. The aim of the ultrasound exposure was to vaporise the nanodroplets to create pores through which the oxygen could be delivered. Both studies found evidence that hypoxia was significantly decreased by the presence of their respective perfluorocarbon nanodroplets (Huang et al., 2020; Zeng et al., 2020). Song *et al.* found that this significant decrease in hypoxia markers, both pimonidazole and HIF-1α, was not as great without the presence of ultrasound (Song et al., 2016). This suggests the ultrasound has a significant effect on the nanodroplets' ability to deliver oxygen. It has been suggested that this might be due to a "burst-like" release of the oxygen (Song et al., 2016). However, this is not consistent with the small volume of oxygen available within the droplets, as discussed previously.

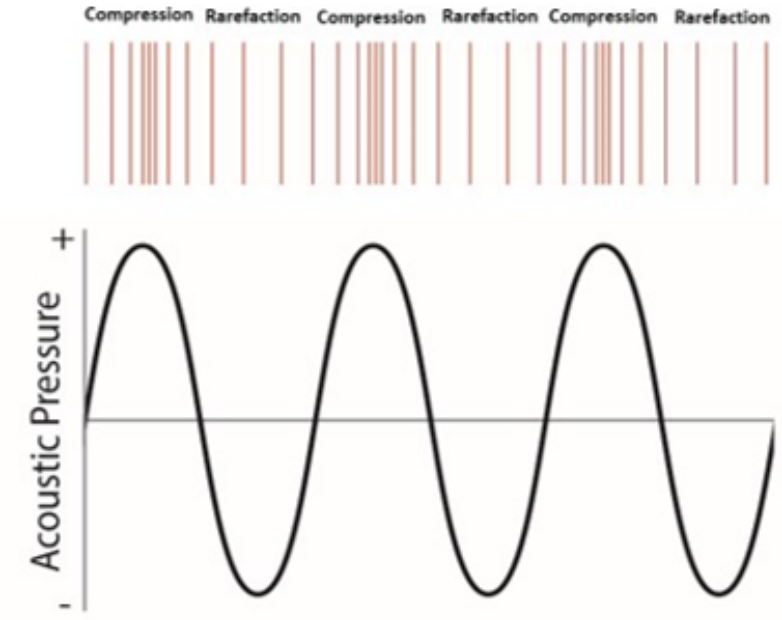

Figure 1.12: An illustration of the change in pressure in a sound wave. The areas of compression result in increased pressure, and the areas of rarefaction lead to decreased pressure.

It has been shown that the superheated stability of nanodroplets enables them to undergo acoustic droplet vaporisation (ADV). ADV occurs due to an applied ultrasonic sound wave. Sound waves occur due to changes in pressure in the surround-

ing media. Areas of increased pressure occur as a result of the particles being compressed together (compressions). Areas of decreased pressure occur due to the particles spreading further apart (rarefactions).

Rarefaction results in a decrease in pressure across the nanodroplet. If the pressure drop is enough, then the required vaporisation temperature will reduce to below the surrounding temperature, allowing the nanodroplet to vaporise into a microbubble of diameter roughly 2.5-3.5 times the diameter (Zhou, 2015). If the peak negative pressure is large enough, the resulting microbubble is able to undergo a violent collapse due to the inertia of the surrounding fluid greatly exceeding the gas pressure inside the bubble (Figure 1.13). This collapse and the mechanical effects on the bubble's immediate environment can facilitate both tissue permeabilisation and release and transport of any encapsulated drugs (Wu et al., 2021) by either increasing "leakage" from the microbubble or increasing permeability through the endothelium. It is important to note that the pressure generated by the transducer for acoustic droplet vaporisation is significantly larger than that used during the production of nanodroplets.

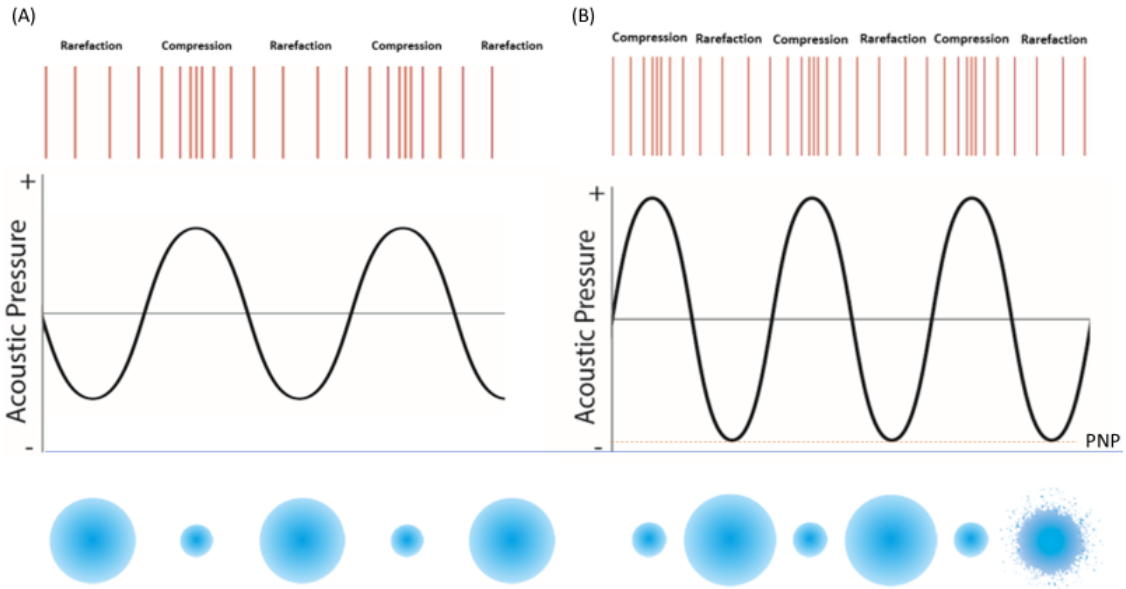

Figure 1.13: A diagram demonstrating how the microbubbles behave under the influence of ultrasound, where (A) the peak negative pressure (PNP) is not large enough to induce inertial cavitation, and (B) where the PNP is large enough to induce inertial cavitation.

One potential drawback of this mechanism is that haemolysis and platelet aggregation have been observed *in vitro* as a result of microbubble-ultrasound interaction; however, the severity of these effects can be controlled by tailoring the exposure time, pulse length, pressure and acoustic frequency (Mannaris et al., 2019).

1.5.5 | Targeted Drug Delivery Alongside Oxygen Delivery

Whilst not specifically addressed in the experiments described within this thesis, oxygen delivery may sometimes be used to enhance other therapies. For example, many chemotherapy and radiotherapy treatments rely on the production of ROS. However, tumours are hypoxic environments and so the efficacy of the therapy is limited by the oxygen availability (Muz et al., 2015). Nanodroplets have been investigated to help combat this limitation by delivering oxygen alongside the cancer therapy (Krafft, 2020). In the context of bone, delivering oxygen alongside MSCs may be beneficial in order to prevent them from dying before proper vascularisation can take place but also to encourage their differentiation into osteoblasts (Kim et al., 2019).

1.6 | Summary

Nanodroplets have been extensively studied for their potential use as oxygen carriers for oxygen delivery to tumours and for use as a blood substitute but not for use in bone. Whilst the exact mechanism of oxygen delivery is not fully understood, there have been successful attempts to reoxygenate tissue *in vivo* using nanodroplets. This shows promise for the use of nanodroplets to deliver oxygen to bone fractures, where it has been shown that hypoxic conditions can be detrimental to bone healing. The exact effect of hypoxia on individual bone cells has also been extensively investigated, with hypoxia resulting in an increase in apoptosis in both cell types but a decrease in osteoblast differentiation and activity and an increase in osteoclast differentiation and activity.

1.7 | Research Aims & Objectives

This thesis investigates perfluorocarbon nanodroplets as a possible method for delivering oxygen to bone fractures with the aim of aiding fracture healing. Despite significant progress in understanding how hypoxia diminishes bone healing capacity, little work has been done to attempt to reverse the effects. Nanodroplets are well studied in terms of their ability to deliver oxygen to tumours. To the best of the author's knowledge, however, their ability to deliver oxygen to bone has not been investigated previously. This project looks at the effect of treating bone cells, namely those of an osteoblastic and osteoclastic lineage, *in vitro* with an optimised nanodroplet formulation in order to reverse these effects of hypoxia.

The overarching aim of the work reported in this thesis is to test the hypothesis that nanodroplets are capable of relieving the effects of hypoxia on osteoblastic and osteoclastic cells *in vitro*. In order to achieve this aim, the research in this project will specifically evaluate skeletal stromal cells and their osteoblastic derivatives which are essential for laying new bone material, as well as peripheral blood mononuclear cells and their osteoclast derivative, which remove old bone material. Additionally, the research aimed to optimise nanodroplet formulation through sonication by minimising nanodroplet size (larger nanodroplets are less stable and more susceptable to immune response) and increasing reproducability. The specific objectives include:

1. To optimise nanodroplet formulation for size and manufacturing repeatability and oxygen loading by testing the hypothesis that:

   - Variation in formulation parameters, such as sonication temperature, PFP concentration, immersion depth of the sonicator tip, sonication amplitude and total sonication time, significantly affects nanodroplet size and concentraion;

   - Storage temperature and gas-loading techniques affect nanodroplet size and stability;

   - Post-processing techniques such as filtration and centrifugation reduce nanodroplet size dispersity.

2. To evaluate the cytotoxic effects of oxygen-loaded nanodroplets on bone cells *in vitro* by testing the hypothesis that:

- Nanodroplets do not affect bone cell metabolism;

- Nanodroplets do not reduce bone cell proliferation and osteoclast fusion;

- Gas-loaded nanodroplets do not reduce bone cell metabolism;

- Nanodroplets do not affect osteoblastic activity, namely mineralisation and ALP enzymatic activity.

3. To verify whether oxygen tension influences bone cell differentiation and activity and whether nanodroplets relieve this effect *in vitro* by testing the hypothesis that:

- Hypoxia decreases osteoblastic activity but yo a lesser extent in the presence of nanodroplets;

- Hypoxia increases osteoclast number and size but this is reduced in the presence of nanodroplets;

- Hypoxia increases HIF-1α concentration but this is mitigated by the presence of nanodroplets;

- Primary osteoblastic and osteoclastic cells' metabolism and proliferation decrease in hypoxic conditions but not in the presence of nanodroplets.

2

General Methods

A full list of materials, their suppliers and catalogue numbers can be found in Appendix B table S2.

2.1 | PFC Nanodroplet Preparation

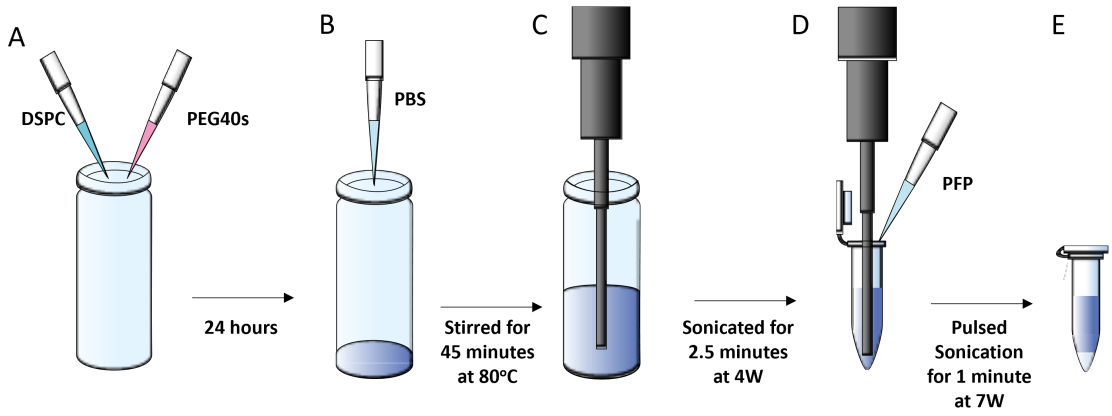

Figure 2.1: Schematic diagram showing the sonication process for creating the nanodroplet emulsions. (A) DSPC and PEG(40)s dissolved in chloroform were added with a 9:1 molar ratio, respectively, and left overnight to allow the chloroform to evaporate and a lipid film to form. (B) the lipid film is rehydrated using PBS and then (C) homogenised using the sonicator. (D) PFP is added, and the solution is sonicated to create the droplets. (E) the nanodroplets can be spun in a centrifuge to speed up the settling process.

The nanodroplet formulation was initially performed using parameters as set out by Ferri et al. (Ferri et al., 2021). To create the nanodroplets, first, a lipid film was made. 1,2-distearoyl-sn-glycero-3-phosphocholine (DSPC, Avanti Polar Lipids, Alabaster, Alabama, USA) and polyoxyethylene (40) stearate (PEG(40)s, Sigma-Aldrich, Saint Louis, Missouri, USA) solutions were made up to 31.6 mM and 4.89 mM concentrations respectively by dissolving the lipids in chloroform (Fisher Scientific, Basingstoke, UK). For fluorescent droplets, DiO (Thermofisher, UK) was added from a stock solution (1 mg/ml) to final molar ratio of 90:10:1 (615 μL of DSPC:442 μL of PEG(40)s: 191 μL of DiO). The resulting mixture was left open to the air overnight in a fume hood to allow the chloroform to evaporate, leaving a thin lipid film (Figure 2.1A). DSPC is a common phospholipid that has been used in a wide range of biomedical situations from tumour therapy (Abdalkader et al., 2020) to the Pfizer-BioNTech and Moderna mRNA SARS-Cov-2 vaccines. The PEG(40)s is used to increase the stability of the nanodroplets as well as cell uptake and reduce size (Blume, Cevc, 1990; Parhizkar et al., 2015; Talu et al., 2006; Yarmoska et al., 2019).

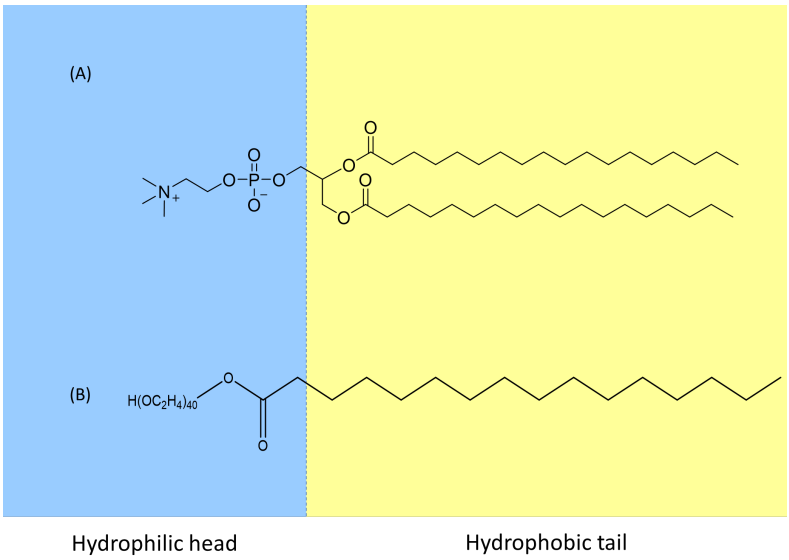

Figure 2.2: Structural formula of (A) DSPC and (B) PEG(40)s. The long hydrocarbon chains form the hydrophobic tails, with the rest of the molecule forming the hydrophilic head.

The lipid film was rehydrated in a class II sterile hood (Safelab, UK) using 5 mL of phosphate buffered saline (PBS, Lonza Group, Basel, Switzerland) at 90 ^{o}C, stirred at

500 rpm for 45 minutes to create a final lipid concentration of 4 mg/mL (Figure 2.1B). The high temperature was chosen so that the lipids were above their phase transition temperature (DSPC: 55^{o}C, PEG(40)s: 41^{o}C). The resulting solution was then homogenised by sonicating it continuously for 2.5 minutes at the 40% amplitude setting (Figure 2.1C) using a Model 120 Sonic Dismembrator (Fisher Scientific, Basingstoke, UK) with a 3.22 mm diameter sonicator tip.

The solution was then placed on ice for 10 minutes to cool. 800 μL of the lipid solution was placed in an Eppendorf tube with 40 μL of perfluoro-n-pentane (PFP, STREM Chemicals UK Ltd., Cambridge, UK). Next, the Eppendorf was placed in an ice-saline or ice-water bath to keep it cool as the PFP has a boiling point of 29^{o}C and the sonication will increase the temperature to above this. The solution in the Eppendorf is sonicated for a total of 60s with 15-second intervals between each 2-second pulse unless otherwise specified. This second sonication is performed at 60% on the amplitude setting (Figure 2.1D). For all experiments, nanodroplets were stored on ice and used within an hour of production.

Where nanodroplets were processed post-production, either centrifugation or filtration were used. For centrifugation the Eppendorf was placed in a Sorvall Legend Micro 17 Microcentrifuge (ThermoScientific, Basingstoke, UK) for 5 minutes at 500 x g to separate out the droplets from the PBS. For filtration, a 0.2 μm or 0.45 μm syringe filter was used.

2.2 | Sonicator Setup

Sonication was utilised for emulsifying perfluorocarbon nanodroplets. The setup for the sonicator was modified to enhance control over the sonication parameters and improve user-friendliness. An ice-water bath was used to manage the temperature during sonication. Alongside Dariusz Kosk and Christopher Campbell from the Bone and Joint research group at the University of Southampton, three containers were designed. Key design factors included: ensuring the containers were waterproof, consistently fitting into the same position to limit sonicator position variability, stabilising the sonicator in the ice-water bath during sonication, and permitting temperature monitoring of the ice-water bath throughout the sonication. A micrometre stage (Thorlabs, UK) was used to precisely adjust the sonicator tip's height.

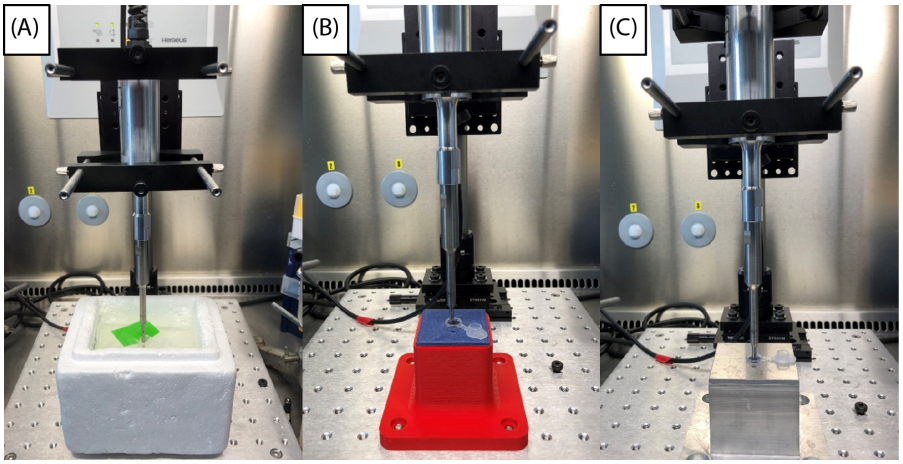

Figure 2.3: Pictures of the three ice-water baths used during the sonication process. (A) has a polystyrene container with a lid cut out from plastic. (B) has a 3D printed plastic container with holes to hold the container in place. (C) has an aluminium container with holes to hold the bath in place.

2.3 | Sonication Parameter Optimisation

Four main variables were identified during the second sonication step: PFP concentration, the height of the sonicator tip in the solution, total sonication time and sonication amplitude. For these experiments, the 3D-printed plastic container was used. First, the concentration of PFP used was investigated by keeping a constant volume of lipid solution (2 ml) with different volumes of PFP (200 μl, 100 μl, 50 μl, 25 μl, 12 μl, 0 μl). Nanodroplets were created as described in section 3.1 with the volume of PFP and lipid solution altered accordingly. Given the PFP is more dense than the lipid solution, the height of the tip and the volume of PFP are variables that will affect each other. As such, each PFP condition was tested against each tip height condition. This experiment was performed using 800 μl of lipid solution with 80 μl, 40 μl, 20 μl, 10 μl and 0 μl of PFP at tip heights of 2 mm, 5 mm, 8 mm, 10 mm and 12 mm from the bottom of the Eppendorf tube.

The same approach was taken for sonication amplitude and total sonication time as both will contribute towards the energy output. As the depth against PFP concentration experiment had been performed first, this experiment was performed with 800 μl of lipid solution and 40 μl of PFP. The tip height was 12 mm from the bottom of the Eppendorf. Amplitude was investigated at 20 %, 40 %, 60 %, 80 % and 100% and a total

sonication time of 15 s, 30 s, 45 s 60 s, 75 s, 90 s, 105 s and 120 s.

2.4 | Gas Loading

Once made, the nanodroplets were loaded with oxygen or nitrogen by gently sparging the solution with the relevant gas. This was done by placing a needle at the bottom of an Eppendorf tube for 2 minutes in 840 μL of freshly made nanodroplet solution in a 1.5 mL eppendorf with either oxygen or nitrogen on ice. The exact flowrate was not controlled but the gas cylinder regulator was opened by the smallest amount required for any gas flow to visibly occur.

2.5 | Nanodroplet Size Characterisation

The resulting nanodropets were characterised by measuring their size and concentration. Measurements were initially performed using DLS with a Malvern Zetasizer Ultra (Malvern Panalytical, Malvern, UK). 1.5 mL of particle dispersion at a dilution of 1:750 was placed in a cuvette. However, as mentioned previously in section 1.5.2, the intensity of the signal is proportional to the sixth power of the diameter (Stetefeld et al., 2016). This created a bias towards the larger particles creating an inaccurate representation of the particle distribution.

As a result, NTA was performed using a Nanosight NS300 (Malvern Panalytical, Malvern, UK) as NTA is less susceptible to scatter intensity bias. The Nanosight NS300 was configured with a 488 nm laser, a 500 nm long-pass filter for fluorescent detection where needed and a high sensitivity sCMOS camera system with a syringe-pump. Samples were diluted 1:5000 by volume in PBS and flowed through the low volume flow cell at syringe pump speed 50 (syringe pump uses arbitrary units) for all measurements except fluorescence measurements which were run at syringe pump speed 200 to avoid photobleaching of the sample. Particles were captured at 25 frames per second with five 90 second videos. The mean and median hydrodynamic diameter and standard deviation were then calculated using the NTA software as well as an approximate particle concentration. NTA measurements were always taken the same day the nanodroplets were made unless otherwise specified. The particle distribution curve was provided in 1 nm width bin centres that ranged from 0.5-999.5 nm.

On occasion, the nanodroplets were diluted 1:100 and viewed under a Zeiss axiovert microscope with a 40× lens to check for particles larger than the NTA upper threshold (1 μm).

2.6 | Oxygen Release Profiles

A TOVIAL20 optical oxygen and temperature sensor connected to a Firesting-PRO optical meter (Pyroscience) was used to measure oxygen concentration and temperature in water. Experiments were performed in the cold room to control the temperature and to prevent evaporation of the PFP. The vial was filled with 18 mL of water and the lid screwed tightly on. The vial was placed at a 45^o angle with the sensor stripes on top so that the PFP would not interact directly with the sensor stripes because the PFP was found to dissolve them. 2 mL of PFP or water was injected into the vial through the septum so that it gently sank to the bottom of the vial. PFP and water are practically immiscible so a phase boundary formed. Oxygen concentration and temperature data was logged from the moment all of the liquid was injected. PFP was oxygenated by sparging the solution with oxygen in the same way as described for the nanodroplets.

2.7 | Temperature Measurement

2.7.1 | Evaluating Temperature and Pulse Sonication

PFP has a boiling point of 29^oC and the lipid suspension freezes at approximately 0^oC. As a result, temperature was thought to have a significant impact on the sonication process. The temperature before, and after sonication were measured using a RS PRO RS42 K thermocouple thermometer. The thermocouple was placed in the Eppendorf tube (placed in an ice-water bath) prior to the second sonication and the temperature recorded. The thermocouple was then removed and the second sonication started immediately. For the final measurement, the thermocouple was immediately reinserted in the Eppendorf as soon as the final sonication pulse took place. The timing of the temperature measurements was key because the solution cooled very quickly. This was all repeated 3 times.

For measurements during sonication, a type K thermocouple with a data logger

was used. Four lipid/PFP solutions were prepared from the same lipid film but the sonication times for each were varied as shown in Table 2.1. The thermocouple was carefully placed in the Eppendorf (placed in either an ice-water or ice-saline bath) to avoid it touching the tip of the sonicator. The second sonication was only performed once the solution temperature reached 0^{o}C.

Table 2.1: Pulse settings for second sonication for temperature experiments

Sample	Pulse on duration / s	Pulse off duration
1	2	5
2	2	8
3	2	10
4	2	12
5	2	15

2.7.2 | Characterising the Sonicator Power Output

The sonicator power output was controlled by controlling the amplitude of the displacement of the sonicator tip. This was given as a percentage of the maximum amplitude of the tip (180 μm). In order to better understand the sonication process, the temperature rise in a 20 mL volume of water in an insulated 30 mL universal container (Starlab, UK) was measured using a thermocouple data logger (RS component, UK). The power output to the solution was characterised using the calorimetric power output as measured by this temperature rise. Sonication amplitudes of 20, 40, 60, 80 and 100% were tested over a total sonication time of 120 s. A 110 s linear section from the sonication time was used to calculate the rate of temperature increase. This was also performed on 0.8 mL samples in a 1.5 mL Eppendorf tube on PBS, lipid suspension and lipid suspension with PFP, in order to simulate the conditions during the nanodroplet formulation process.

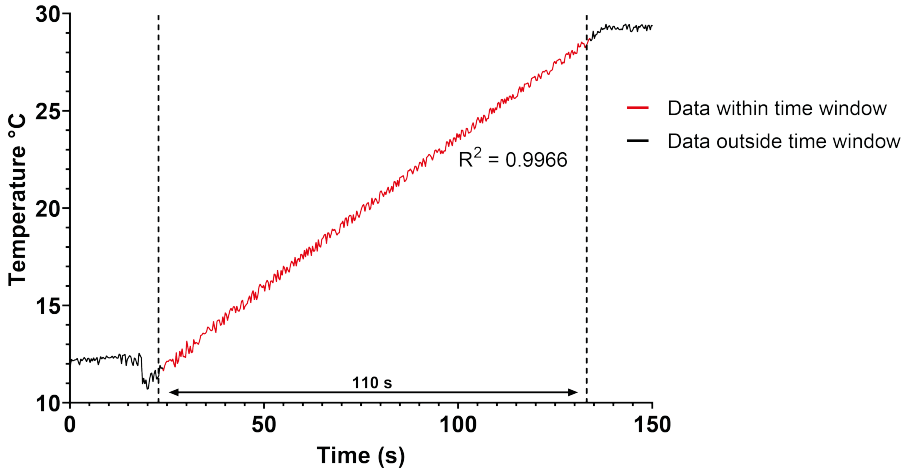

Figure 2.4: Graph showing the data recorded by the data logger

2.8 | Cell Isolation and Culture

2.8.1 | Media Composition

Different media compositions were required for different experiments. A full list of media compositions are listed below in Table 2.2. Any media used subsequently in this report use the names listed below.

Table 2.2: Media compositions for cell culture experiments (suppliers and catalogue numbers provided in the appendix)

Media	Composition
Plain α-mem	α-mem only
Complete α-mem	α-mem, 10% FBS, 1% Penicillin/streptomycin[a]
Complete DMEM	DMEM, 10% FBS, 1% Penicillin/streptomycin[a], 1% L-glutamine[b]
Basal media	Phenol red free DMEM, 0.5% FBS, 1% Penicillin/streptomycin[a], 1% L-glutamine[b]
Osteogenic media	Phenol red free DMEM, 0.5% FBS, 1% Penicillin/streptomycin[a], 1% L-glutamine[b], 50 μM Ascorbic acid 2-phosphate, 10 mM Dexamethasone, 2 mM β-Glycerophosphate
Monocyte media	α-mem, 10% FBS, 1% Penicillin/streptomycin[a], 1% L-glutamine[b], 2.7 μM MCSF
Osteoclast media	α-mem, 10% FBS, 1% Penicillin/streptomycin[a], 1% L-glutamine[b], 2.7 μM MCSF, 1.6 μM RankL

[a] 100 U/mL penicillin and 100 μg/mL streptomycin, [b] 200 mM L-glutamine in PBS

2.8.2 | Bone Marrow Stromal Cell Isolation

Primary human BMSC were isolated from patients undergoing hip replacement surgery at Southampton General Hospital and Spire Southampton Hospital with sex (male (M) or female (F)) and age as the only identifiers. All isolations were performed with patients' written informed consent and approval of the national research ethics committee (National REC REF: 18/NW/0231 North West -Greater Manchester East Research Ethics Committee University of Southampton ERGO: 31875). Bone marrow was collected aseptically by surgeons and placed in a universal container. The bone marrow was washed in plain α-mem at least 5 times by centrifuging at 400xg for 5 minutes and resuspending to remove the fat, bone fragments and other contaminants. Following the second centrifugation, the solution was poured through a 0.6 μm cell strainer to remove any remaining bone fragments. The remaining cells were incubated at 37^{o}C in complete α-mem in a T-175 flask for one week before being washed with PBS and complete media to remove the non-adherent cells.

2.8.3 | Peripheral Blood Mononuclear Cell Isolation

CD14+ PBMCs were isolated from leukocyte cones from NHS blood and transplant (NHSBT) platelet apheresis donors who have provided general research consent. The contents of the leukocyte cone were made up to 50 mL with 2 mM EDTA containing phosphate buffer solution (PBS) solution before being carefully layered on top of 12.5 mL of a density gradient separation solution (Lymphoprep) in a 2:1 ratio (v/v) across two falcon tubes. The solution was centrifuged at 800xg for 20 minutes at 25^{o}C with the brake setting switched off. The monocytes were collected from the interphase of the resulting solution and washed 4 times in cold 2 mM EDTA-PBS solution by centrifugation at 400xg and resuspension. The number of cells was counted by diluting 50 μL of the cell suspension in 450 μL of 20 mM acetic acid to lyse red blood cells and then staining the resulting mixture with trypan blue in a 1:1 ratio. The remaining cells were resuspended with 800 μL of selection buffer (2 mM EDTA containing PBS solution with 0.5 w/v% BSA) and 200 μL CD14 human microbeads per 10^8 cells and incubated at 4^{o}C for 15 minutes. The solution was centrifuged at 400xg for 10 minutes then resuspended in 500 μL of selection buffer per 10^8 cells. The CD14+ cells were then selected using an LS column (Miltenyi) with magnetic-activated cell sorting (MACS). The cells were resuspended in complete α-mem and seeded at 7.8×10^5 cells/cm^2

in a 96 well plate. For flow cytometry experiments the cells were seeded at 2.1×10^5 cells/cm^2 in a 6 well plate.

2.8.4 | Cell Culture

MC3T3E1 and Saos-2 cells were cultured in complete Dulbecco's modified Eagle's medium (DMEM) in T75 flasks before use in experiments. Both were used up to passage 25. BMSCs were cultured with complete α-mem in T175 flasks and were used up to passage 3. In all three cases, cells were passaged by first aspirating the media, washing three times with PBS. A 1:1 trypsin/EDTA solution was then added (2 mL for a T75 and 5 ml for a T175) and the cells were incubated at 37^oC for 5 minutes. Complete media was then added to the cells to inactivate the trypsin (5 mL for a T75 and 10 mL for a T175) and the cell suspension was transferred to a falcon tube before being centrifuged at 400×g for 5 minutes. The supernatant was aspirated and the pellet resuspended with 10 mL of complete media. The necessary proportion of the cell suspension was added to the cell culture flask with the required amount of complte media to achieve the desired volume (T75: 12 mL, T175: 25 mL). PBMCs were not passaged and were seeded directly after isolation for experimentation.

2.8.5 | Cell Counting

All cells were counted using an Invitrogen Countess Cell Counter. Following the resuspension of the cell pellet, 20 μL of the sample was mixed with 20 muL of Trypan blue. 10 μL of the mixture was pipetted into either side of a reusable Countess slide. Both sides were counted using the cell counter with the Trypan blue dilution preprogrammed and an average of both counts was used. For the PBMCs only, the red blood cells were lysed by diluting the cell suspension 1:5 in 20 mM acetic acid. The resulting solution was then mixed 1:1 with Trypan blue and the normal protocol resumed.

2.9 | Cell Viability

2.9.1 | Cell Metabolism

An Alamar blue assay was performed on MC3T3E1 (a preosteoblastic murine cell line) and SAOS-2 (human osteosarcoma cell line) cell lines as well as primary BMSCs and

PBMCs. The MC3T3E1s were seeded at a density of 1.6×10^4 cells/cm^2. The SAOS-2s were seeded at 5.2×10^4 cells/cm^2. The BMSCs were seeded at 2.5×10^4 cells/cm^2. The PBMCs were seeded at 7.8×10^5 cells/cm^2. Seeding densities were chosen so that cells were at approximately 80% confluent at the point the assay was performed. All were seeded in a 96 well plate with 200 μL of media (MC3T3E1, SAOS-2: complete DMEM; BMSC: complete α-mem; PBMC: monocyte or osteoclast media as specified). The cells were then left in the incubator for 24 hours to allow the cells to adhere to the plate. The media was then replaced with 90 μL of new media with 10 μL of PBS containing a given volume percentage of nanodroplets (0, 0.01, 0.1 or 1% v/v) or the relevant controls (DSPC:PEG(40)s lipid solution, DSPC only or PEG(40)s only). The solution was then left in the incubator for 24 hours unless otherwise stated. Cell metabolism was then measured using Alamar blue, a cell viability reagent with resazurin as its active ingredient which is reduced to the fluorescent compound resorufin in the presence of aerobic metabolism. The Alamar blue was diluted 1:10 in complete media and 100 μL was added to each well and left in the incubator for 2 hours for MC3T3E1 and SAOS-2 and 4 hours for BMSCs and PBMCs before the fluorescence was read using a glomax plate reader (Promega, Southampton, UK).

2.9.2 | Cell Proliferation

2.9.2.1 | Counting Nuclei through DAPI Staining

MC3T3E1s were seeded at a seeding density of 1.56×10^4 cells/cm^2 and SAOS2s were seeded at a seeding density of 3×10^3 cells/cm^2 in a 24 well plate with 600 μL of complete DMEM. The cells were then placed in the incubator for 24 hours. The media was then replaced with 540 μL of new media with 60 μL of PBS containing a given volume percentage of nanodroplets. One set of cells were then fixed using a 1:1 acetone-methanol solution. This was repeated every 24 hours for 96 hours. The cells were then stained using DAPI (1:1000 dilution of 1 mg/mL DAPI in PBS), where images were taken using an inverted microscope with a DAPI filter set (excitation: 357nm, emission: 417-477nm). The nuclei in the images were then thresholded and counted using an ImageJ macro (found in the appendix).

2.9.2.2 | DNA Concentration Quantification through PicoGreen Assays

To quantify the DNA concentration, a PicoGreen (Sigma-Aldrich) assay was performed in line with the manufacturer's protocol with eleven 2000-0 ng/mL DNA standards prepared using a 1:2 serial dilution and performed in duplicate (Herring sperm DNA diluted in 1x Tris/EDTA buffer). 50 μL of samples were made up to 100 μL using 1x TE (Tris/EDTA) buffer. Next, 100 μL of diluted PicoGreen solution (1:200 dilution in 1x TE buffer) was added. The plate was incubated at room temperature in the dark for 5 minutes before the fluorescence was read (excitation: 480 nm, emission 520 nm).

2.10 | HIF-1α Expression Using Western Blotting

HIF-1α is a protein that degrades in the presence of oxygen. As such, its concentration can be used as an indicator of hypoxic stress in cells. SAOS-2 cells were grown in complete DMEM in a T175 until confluent. The cells were then seeded evenly across five 100$\times$15 mm cell culture dishes (Thermo Fisher, US). The dishes were incubated overnight at 37^{o}C before the media was changed with the experimental supplements. Two culture dishes were placed in a hypoxic incubator (1% O_2), one with complete DMEM and one with complete DMEM containing 0.1% v/v nanodroplets. The remaining three dishes were placed in a normoxic incubator, one with complete DMEM, one with complete DMEM with 0.1% v/v nanodroplets and one with complete DMEM with 1 mM dimethyloxalylglycine (DMOG) as a positive control. After 24 hours, the cells were washed in cold PBS and lysed in 500 μL of urea-based lysis buffer and homogenised by a Model 120 Sonic Dismembrator (Fisher Scientific, UK) for 10 seconds. The samples were then frozen at -20^{o}C overnight. The protein concentration was determined using a Bio-rad protein assay with a bovine serum albumin (BSA) standard following the manufacturer's instructions. 50 μg of protein solution was added to the well of a 10% acrylamide gel. The gel was run for 1 hour at 150 V and transferred to a PVDF membrane using a power blotter (Invitrogen, US). HIF-1α (BD biosciences, UK) and β-actin primary mouse anti-human antibodies were used. Immunoreactivity was visualised using HRP secondary antibody sheep anti-mouse and chemiluminescence (membrane washed with SuperSignal West Pico PLUS substrate) measured and quantified using an iBright imager and its associated software (Invitrogen, US).

2.11 | VEGF ELISA

VEGF is a hypoxic marker downstream of HIF-1α. A VEGF ELISA (human VEGF Quantikine ELISA kit, R&D systems, US) was performed as per the manufacturer's instructions. Eight standards of concentrations 1000 - 0 pg/mL were prepared using a 1:2 serial diultion. The supernatant from each of the cell culture dishes used in the HIF-1α experiment was collected into LoBind tubes (Fisher, UK) and stored at -20^{o}C and thawed completely before use. 50 μL of assay diluent was added to each well with 200 μL standard, control or sample. The plate was then covered with an adhesive strip and incubated at room temperature for 2 hours. Each well was emptied by inversion and then washed thrice with 400 μL of wash buffer. The plate was finally inverted and blotted against a paper towel to ensure it is dry. 200 μL of human VEGF conjugate was added to each well before the plate was again covered with an adhesive strip and incubated for 2 hours at room temperature. The plate was again washed and emptied as before. 200 μL of substrate solution was added to each well before a 20 minute incubation with foil covering the plate to protect it from light. At the end of the incubation, 50 μL of stop solution was added. The plate was gently tapped against the workbench until a uniform colour was observed to ensure adequate mixing. The absorbance at both 450 nm and 560 nm was measured using a Glomax and the latter values were subtracted from the former to provide a value corrected for any optical imperfections in the plate. The resulting VEGF concentration was interpreted from the standard curve.

2.12 | Osteoblast Activity

BMSCs were seeded at 2.5×10^4 cells/cm^2 in a 24-well plate in complete α-mem and grown to confluence. The media was then changed to osteogenic media or basal media unless otherwise stated. This media change represents day 0 in all subsequent protocols.

2.12.1 | Alkaline Phosphatase (ALP) Assay

ALP is an early-stage marker for osteogenic activity. An enzymatic quantification assay was performed to measure ALP expression in BMSC, both treated and untreated,

with nanodroplets in both normoxia and hypoxia. Normoxic measurements were measured on days 0, 4, 7 and 14. Hypoxic measurements were performed at day 14 only. A control where cells were grown in basal media instead of osteogenic media was also performed at day 14 only. The growth medium was removed and the cells gently washed once with PBS. 300 μL of cellytic M lysis reagent was added to the wells and incubated on a shaker for 15 minutes. Each well was scraped using a pipette tip and the lysate transferred to a 1.5mL Eppendorf tube. The samples were centrifuged at 15000xg to pellet any cellular debris and the supernatant transferred to a new 1.5 mL eppendorf tube. The samples were frozen at -20^{o}C until the assay was ready to be performed. Each sample was tested in triplicate with 10 μL of sample made up to 100 μL of a chromogenic substrate solution (1.3 mg/mL phosphatase subtrate, 0.5M Alkaline buffer solution). Eight standards of 400 nmol/mL to 0 nmol/mL p-nitrophenol from a 10 mM stock solution were diluted in an assay buffer (0.5M alkaine buffer solution containing 31.8 mg/mL Igepal CA-630) and were prepared using a 1:2 serial dilution in the same assay buffer and were also tested in triplicate. The well plates were incubated for 30 minutes before the reaction was terminated using sodium hydroxide. The absorbance was then measured using a Glomax plate reader at a wavelength of 410 nm. Supernatant for each ALP assay was also used for picogreen assays as described in section 2.9.2.2 in order to normalise the ALP enzyme quantity to DNA concentration to account for any variation in cell number between groups.

2.12.2 | Alizarin Red

To assess bone cell mineralisation, an Alizarin red S solution was prepared by adding 3.4226 g of Alizarin red S powder to 150 mL of deionized water, mixing the solution for at least 3 hours prior to use. 0.5% ammonium hydroxide and distilled water were added gradually until a 250 mL solution of pH 4.1-4.3 was achieved. The solution was then filtered through filter paper before use. BMSCs were cultured until day 21. The cells were washed twice in 500 μL PBS before being fixed in 300 μL of 4% w/v paraformaldehyde (PFA) solution for 15 minutes. Next, the cells were washed with 500 μL of distilled water and incubated at room temperature with 200 μL of 40 mM Alizarin red S solution (pH 4.1) for an hour. All wells were subsequently washed five times with 800 μL of distilled water. Three images of each well was taken with a Zeiss axiovert microscope with a 10$\times$ objective lens with a colour camera. The intensity of

the alizarin red stain was then quantified using CellProfiler (Carpenter et al., 2006). (Positive and negative control images used to program positive and off-target staining are provided in the appendix).

2.12.3 | Collagen Coating for Well-Plates

To validate that any calcium deposition was from increased activity and not through another mechanism using the nanodroplets, the Alizarin red assay was repeated on collagen-coated well plates. Type I rat tail collagen was diluted to 50 μg/mL in 20 mM acetic acid. 190 μL of the solution was added to each well for a final coating concentration of 5 $\mu g/cm^2$. The plates were then incubated at room temperature for 1 hour before the solution was carefully aspirated and the wells washed three times with PBS to remove any remaining acid. The well plates were then incubated for 21 days with 450 μL of either osteogenic media or cell-conditioned media with 50 μL of the appropriate dilution of nanodroplets or lipid suspension and the media was changed every three days until day 21 before undergoing Alizarin red staining as above. Cell-conditioned media was osteogenic media that was used to culture BMSCs in a T175 before being collected and used for the well-plates. The BMSCs in the T175 were seeded on day 0 of the experiment and were never above passage 3.

2.13 | Osteoclast Culture

Osteoclasts were cultured from PBMCs seeded at 7.8×10^5 cells/cm^2 in a 96 well plate. The cells were incubated at 37^oC for 24 hours in in complete α-mem. The first media change was considered day 0. Osteoclasts were cultured in osteoclast media for a total of 12 days in 180 μL of osteoclast media (see table 2.2) and 20 μL of PBS containing the appropriate dilution during treatment and 200 μL of osteoclast media at all other times. The timing of each treatment regimen is discussed in detail in section 2.13.2. Cells were cultured with seven different treatment groups in total: three different concentrations of nanodoplets (0.01, 0.1, and 1% v/v), as well as 0.1% v/v PEG(40)s, DSPC, DSPC:PEG(40)s (9:1) lipid mixture and a no treatment control.

2.13.1 | TRAP Staining

At day 12 osteoclast cultures were washed twice with cold PBS, fixed using 100 μL of 4% PFA and washed before undergoing TRAP (tartrate-resistant acid phosphatase) staining. The TRAP staining solutions were made according to a protocol by the Center for Musculoskeletal Research, University of Rochester (Center for Musculoskeletal Research, 2020). Fixed cells were incubated for 30 minutes at 37^{o}C with the TRAP staining solution described in Table 2.3 then washed with PBS. The stained cultures were then imaged using a 10$\times$ objective lens with a colour camera. The number and average size of osteoclasts per image were quantified by manually drawing around each osteoclast in ImageJ.

Table 2.3: Components of the TRAP staining solution adapted from (Center for Musculoskeletal Research, 2020). Components were mixed in the order specified below unless otherwise stated. (Suppliers and catalogue numbers provided in the appendix)

TRAP staining solution	
Sodium Acetate Anhydrous	2 g
L-(+) Tartaric Acid	2.4 g
Glacial Acetic Acid	0.6 mL
Distilled water	200 mL
Napthol AS-MX Phosphate	20 mg
Ethylene Glycol Monoethyl Ether	1 mL
Fast Red Violet LB Salt	120 mg

2.13.2 | Hypoxia and Nanodroplet Treatment Regimens

Three different treatment regimens were used for the osteoclast experiments. Firstly, to investigate the effect on osteoclast differentiation and fusion, the cells were grown in hypoxia for their entire 12-day culture (2% or 5% O_2). Secondly, to investigate the effect on mature osteoclasts, the cells were cultured in normoxia for 9 days until mature osteoclasts formed the majority of the culture before they were moved to hypoxia (2% O_2) for the final 3 days of culture. Finally, to test if intermittent hypoxic exposure affects osteoclast apoptosis and fusion, the cells were grown for 7 days under normoxic conditions and then moved to hypoxia (2% O_2) for 2 days before being returned to normoxia for the final 3 days of culture. In each case, where nanodroplets were investigated, the nanodroplets were added only when the osteoclasts were exposed to hypoxia.

2.14 | Macrophage Flow Cytometry

To investigate whether nanodroplets affect macrophage activity, PBMCs were cultured with monocyte media for a total of 7 days in 6 well plates with 0.1% nanodroplets, 0.1% lipid suspension and a no treatment control. 48 hours before the cells were collected, M1 and M2 polarised controls were induced by treating them with the relevant cytokines (M1: 5 μg/mL LPS, 2 ng/mL interferon-γ; M2: 10 ng/mL IL-4, 10 ng/mL IL-13). Cells were detached from the well plate by scraping with 2 mL of cold PBS with 2mM ethylenediaminetetraacetic acid (EDTA) with a cell scraper and transferred to 15 mL tubes. The samples were incubated at 4^{o}C for 15 minutes before being centrifuged for 15 minutes at 300xg for 5 minutes and resuspended in 0.3 mL PBS. Each sample was split equally into three test tubes: one for panel 1, one for panel 2 and one for no stain controls. 5 μL of each surface marker was mixed with the markers in the same panel before being added to the relevant test tube. All samples were incubated in the dark for 15 minutes. Following incubation, samples were washed in PBS 3 times and resuspended in 500 μL of fixation medium (ThermoFisher) for 30 minutes. The cells were then washed in 10x permeabilisation medium (ThermoFisher) and resuspended in 100 μL PBS containing any intracellular markers in the relevant panels (if no intracellular markers in panel then PBS only). Samples were then incubated for 30 minutes in the dark. After incubation, the samples were centrifuged and resuspended in 500 μL of FACS buffer (1x PBS, 5 μg/mL BSA and 0.1%v/v Azide) and analysed by flow cytometry (Becton Dickinson, US, FACS Canto II).

Table 2.4: Table of Panels used for markers used for macrophage flow cytometry. Markers are surface markers unless otherwise stated (*denotes intracellular marker).

Panel 1	Panel 2	Fluorescent Dye
CD14 (M0)	CD86 (M1)	APC
CD163 (M2)	CD11b (M2)	PerCPCy5.5
HLA-DR (M0)		PB
CD38 (M1)	CD206 (M2)	PE
CD40 (M1)		PECy7
	CD68* (M0)	FITC

Compensation controls were used to correct for spectral overlap between different fluorophores. UltraComp eBeads (Thermofisher) were stained using the membrane antibodies listed in Table 2.4.

2.15 | Cell Association Experiments

To test the hypothesis that nanodroplets associate with the cells, fluorescent DiO-labelled nanodroplets were made as described in section 2.1. Mature osteoclasts (Day 10 PBMCs cultured in osteoclast media) and BMSCs were treated with 0.1% v/v fluorescent nanodroplets for 48 hours. The resulting cultures were then fixed in 4% PFA. Osteoclasts were TRAP stained as described in section 2.13.1 and the BMSC were stained using cellTracker deep red. The nuclei of both were then stained using DAPI. The cells were imaged using a Leica TCS-SP8 Laser Scanning confocal microscope at the wavelengths described in Table 2.5.

Table 2.5: Table of excitation and emission wavelengths used for cell association experiments.

Stain	Excitation (nm)	Emission (nm)
Cell tracker Deep Red	630	655
TRAP	633	647
DAPI	357	447
DiO	490	507

2.16 | Statistical Analysis

Statistical analysis was performed using GraphPad Prism version 9.2 software. Where the significance of two groups only was tested, a Mann-Whitney test was performed for unpaired data and a Wilcoxon matched-pairs signed rank test was used for paired data. Where the significance of three or more groups was tested, an ANOVA was performed with multiple comparisons (Tukey for comparing all groups, Dunnett for comparing with control only). Statistical significance was defined as *$p<0.05$, **$p<0.01$, ***$p<0.001$, ****$p<0.0001$ and non significant (n.s.) $p>0.05$. Experimental repeats are depicted by N and technical repeats by n.

3

Optimisation of Nanodroplet Formulation

3.1 | Introduction

There are multiple methods for nanodroplet production, including sonication, condensation of microbubbles, homogenisation and microfluidics (Anton et al., 2016; Leabanks et al., 2021; Martz et al., 2012; Sheeran et al., 2011a). The advantages and disadvantages of each method are discussed in depth in section 1.5.2. However, sonication is the most common laboratory process for making nanodroplets with perfluorocarbons heavier than perfluorobutane (Ferri et al., 2021). This is primarily due to the small batch sizes and the relatively small particle size. Despite its benefits, the sonication process is very stochastic. This can result in reduced repeatability and predictability. The diameter of the nanodroplets affects many of the nanodroplets' characteristics, from the peak negative pressure required for acoustic droplet vaporisation to their ability to be detected by the immune system (Krafft, Riess, 2021; Mountford, Borden, 2016; Sheeran et al., 2011b). Optimising the repeatability of the sonication process is, therefore, integral. Understanding how production parameters affect nanodroplet size distribution is also crucial for developing nanodroplets optimised for their required function. For developing nanodroplets with the end goal of use within the body, smaller sizes (median < 200 nm, largest nanodroplet < 400nm) are preferable to reduce interaction with the reticuloendothelial system and to increase perfusion.

Before the sonication process can be optimised, the sonicator output must be characterised to allow for comparison between different sonicators in different laboratories. In addition to the sonicator type, variables that may affect the sonication process include temperature, the placement of the tip within the liquid to be sonicated, lipid to perfluorocarbon ratio, the amplitude of the sonicator tip oscillation and the time of the pulse.

In the case of PFP nanodroplet production, the temperature is likely to have a very significant effect due to PFP having a boiling point of 29^oC (Johnstone, 2007). Before the sonication takes place, the PFP is not stabilised in the nanodroplets, and so the PFP may evaporate if the temperature is too high. Equally, if the temperature is too low, the aqueous lipid mixture may freeze at roughly 0^oC. The power input from the sonicator also leads to the solution being heated. The narrow window of acceptable temperature makes the temperature during the sonication the highest priority. This was investigated by changing both the method of cooling, as well as the sonicator pulse regimen.

The PFP to lipid ratio affects the height of the PFP to lipid boundary and, therefore, its position in relation to the tip height. As a result, the PFP concentration and tip height were evaluated together by measuring the average nanodroplet size for each PFP concentration investigated at each tip height. The same was true for the sonicator amplitude and the total sonication times, as they both contribute to the overall energy output of the sonicator.

The main objective of this chapter was to identify the variables that have a significant effect on the outcome of the sonication process and optimise the reproducibility and size of the nanodroplets. The fact that some variables may interact with each other has been taken into consideration by changing multiple variables at once in a factorial design experiment.

An inherent complexity that arises when optimising the nanodroplet formulation is establishing a method for quantifying reproducibility, size and size dispersity. Due to their small size and relative instability, finding a method to characterise the nanodroplets becomes difficult. This report, therefore, endeavours to produce an appropriate means of understanding the nature of the nanodroplets produced.

In addition to establishing appropriate formulation parameters, understanding the behaviour of the nanodroplets when exposed to different temperatures and gases

for loading is vital for understanding their limitations and uses. Nanodroplets must have limited stability so that they may be converted to microbubbles using ultrasound which allows their use in targeted drug delivery. If the nanodroplets are formulated to be too stable, they will not be able to undergo acoustic droplet vaporisation, meaning any drug loaded in the shell or core may not be released (Sheeran et al., 2011b). Shelf life has been a recurring problem with nanodroplet and nanoemulsion use (Krafft, Riess, 2021). However, with an appropriate understanding of the formulation process and the nanodroplet stability, it could be possible to make the nanodroplets at the point of care.

With this in mind, this chapter can be split into the following hypotheses:

- The NTA is the preferred method of nanodroplet characterisation for yielding consistent and accurate measurements of nanodroplet diameter across independent trials;
- Modifying formulation parameters (such as PFP concentration, sonication time, tip immersion depth and sonication amplitude) significantly reduces nanodroplet diameter and improves batch-to-batch repeatability;
- Storage temperature and gas loading techniques significantly influence the stability (e.g., size and concentration) of nanodroplets over time;
- Post-processing methods, such as filtering and centrifugation, improve nanodroplet characteristics by reducing size dispersity and eliminating oversized particles;
- Oxygen diffuses from PFP to surrounding media when and oxygen gradient is present.

In addition to this, the sonicator was characterised to allow for better comparisons between different labaoratories where different brands of sonicator may be used.

3.2 | Methodology

The research in this chapter primarily focused on the optimisation of the nandroplet formulation process as detailed in section 2.1 using the sonicator setup detailed in section 2.2. First, an appropriate nanodroplet characterisation method needed to be established so that differences in nanodroplet size distributions could be quantified and understood. NTA, DLS and light microscopy methods detailed in section 2.5 were examined for use for measuring nanodroplet size distributions. NTA and light microscopy were established as the best characterisation methods when used together and were used for all nanodroplet size distributions. The sonicator was then characterised using calorimetry (section 2.7.2) to allow better comparison between sonicators of different brands that are used in different laboratories. Following this, the formulation process parameters were investigated. First the effect of temperature during sonication was explored by altering the cooling bath composition and pulse parameters as detailed in section 2.7.1. After this, the effect of PFP concentration, sonicator tip height, sonicator amplitude and total sonication duration were investigated using the method detailed in section 2.3. With an optimised nanodroplet formulation process, storage methods post-processing techniques such as filtration, centrifugation and gas-loading (sections 2.1 & 2.4) were investigated for any potential improvements in nanodroplet characteristics. Finally, the oxygen dissolving ability of PFP was verified using an oxygen sensor (section 2.6).

3.3 | Results

3.3.1 | Variability Between Nanodroplet Samples

In order to compare nanodroplet samples, size distributions were acquired. Nanodroplet size distributions were highly variable despite identical methods of sonication. Figure 3.1 demonstrates the issue of repeatability during the sonication process. The particle distributions produced by the NTA have been fitted using finite tracking length analysis (FTLA), a technique that attempts to fit the data into a log-normal (a common distribution for particles) and residuals distribution.

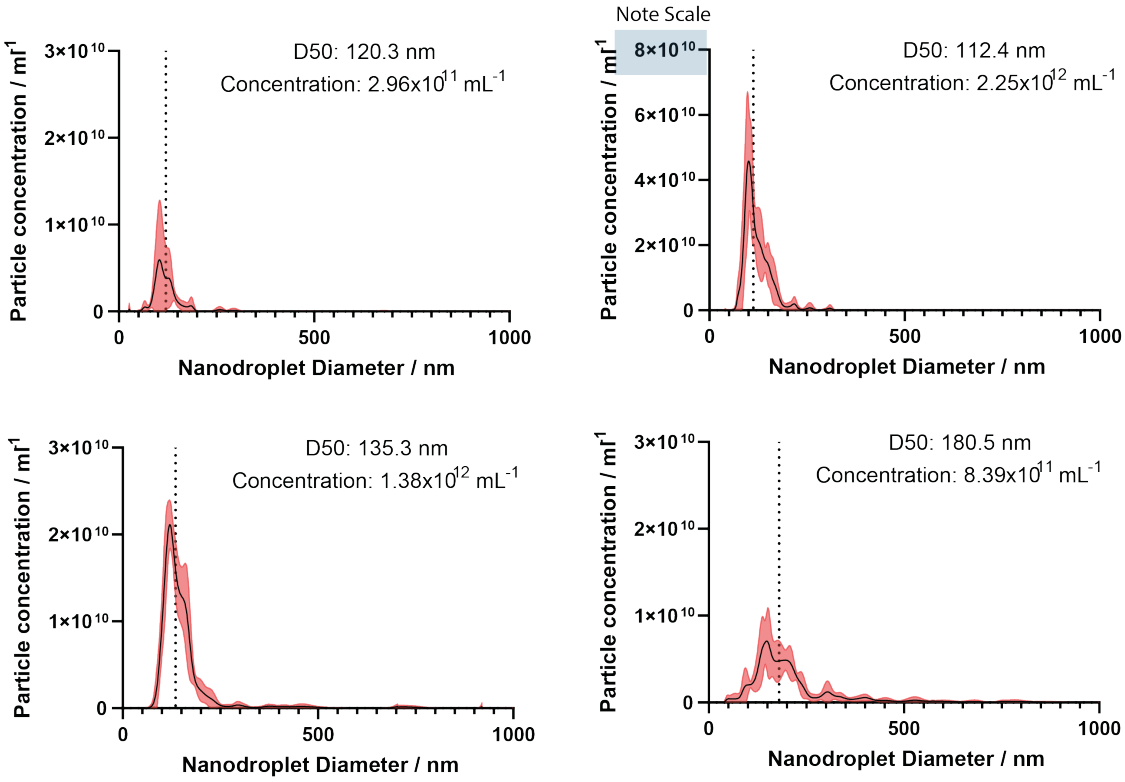

Figure 3.1: Naodroplet size distributions can vary drastically between samples. Size distributions for nanodroplets measured using NTA with the means and standard deviations calculated using the Nanosight software. All four distributions come from four separate samples of nanodroplets made from the same lipid solution, the same sonication parameters and on the same day. Each distribution is a mean distribution of five videos. The red shaded are is the standard deviation for that bin centre.

3.3.2 | NTA and DLS Measurement Comparison

Two common methods for characterising nanodroplet size are NTA and DLS. Figure 3.2 has particle size distributions from NTA and DLS. The distributions are from nanodroplets from the same sample. Despite this, the distributions are clearly different, the most unexpected feature being the DLS distribution forming two very separate peaks. The particle concentration given by the DLS was found to be lower, but the median size was larger. All measurements from here were performed using NTA as it was found to be more accurate. N=4, n=5.

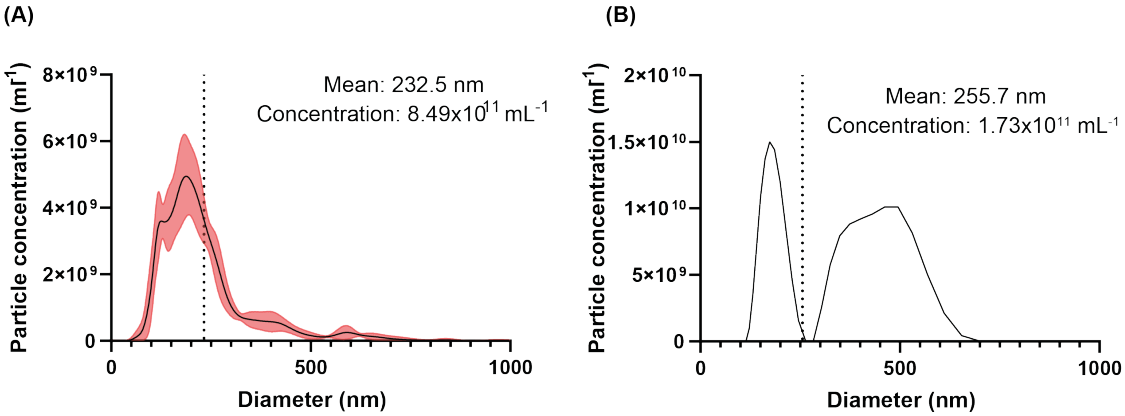

Figure 3.2: NTA provided more reliable measurement of the nanodroplet distributions that DLS. Representative size distributions of the same nanodroplet sample as measured by (A) NTA (n=5) and (B) DLS (n=1) with the mean diameter and concentrations as given by each machine. The dashed line represents the mean in each case. The red shaded area represents the standard deviation of five separate videos.

3.3.3 | NTA Limitations

As NTA relies on tracking the Brownian motion of the particles, the NTA becomes less sensitive as the particles get larger because the Brownian motion decreases. To test this sensitivity, the particles were observed under a light microscope to see if any particles were not detected using NTA. Figure 3.3A shows a particle size distribution from NTA for a sample produced at 60% amplitude, 60s total sonication time, 2 mm tip height and 10% PFP. Figure 3.3B shows the same sample under a light microscope. Many of the particles observed in the light microscopy image are not present in the particle size distribution produced using NTA as they are so large that Brownian motion is limited.

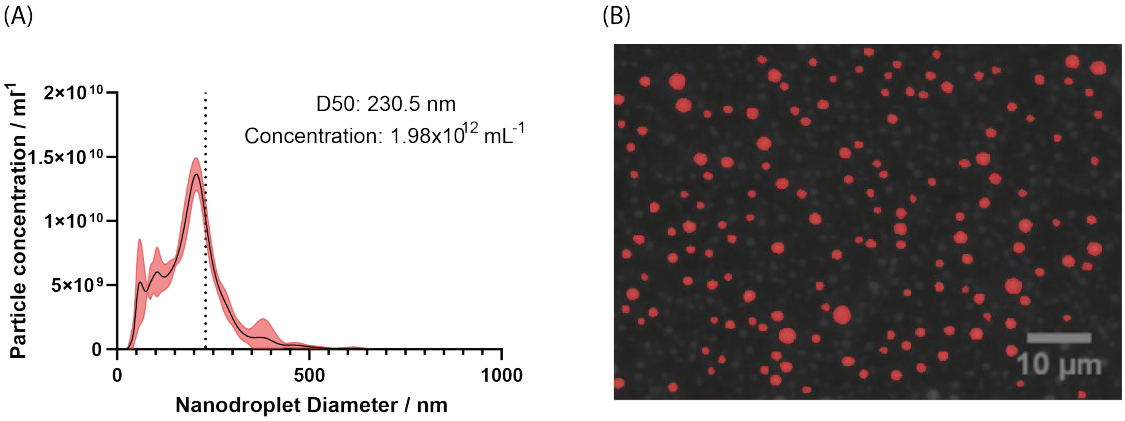

Figure 3.3: Microscopy was necessary alongside NTA measurements to verify whether larger particles are present.(A) Particle size distribution as measured using NTA displaying the mean of five separate videos and the standard deviation given by the shaded red area (n=5) and (B) phase contrast image of the same sample (60% amplitude, 60s total sonication time, 2 mm tip height and 10% PFP) with particles larger than 1μm in diameter are highlighted in red. These particles will not be detected using the NTA.

3.3.4 | Characterisation of the Sonicator

In order to compare production methods between labs, the sonicator was first calibrated. The amplitude was given as a percentage of the maximum possible displacement of the tip (120 μm as given by the manufacturer). The power output of the sonicator into the solution was characterised using calorimetry. Figure 3.4 shows the percentage amplitude was proportional to the square root of the calorimetric power.

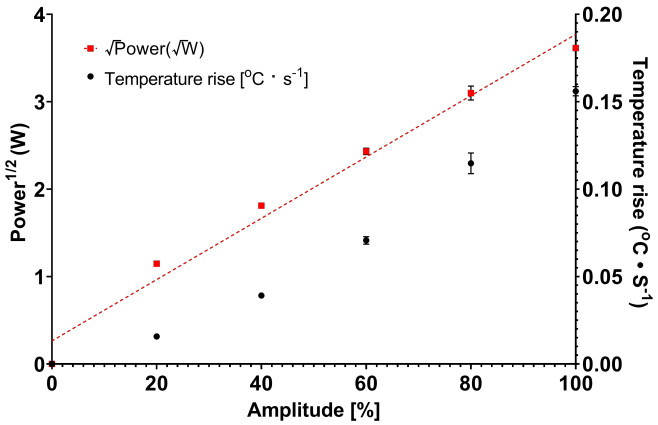

Figure 3.4: Calorimetric power output is proportional to the square of the sonicator amplitude. Square root of calculated calorimetric power output (left) of the sonicator with assumed specific heat capacity of 4184 $Jkg^{-1}K^{-1}$ at different sonication amplitudes (R^2 = 0.9818). The mean temperature rise (right) from which the power was calculated has also been presented.

In order to more closely simulate the conditions during the sonication process, calorimetry was performed on 0.8 mL solutions in a 1.5 mL tube. The effect of the presence of the lipids and the PFP was quantified.The presence of PFP in the formulation led to a significant increase in temperature within the experiment (Figure 3.5).

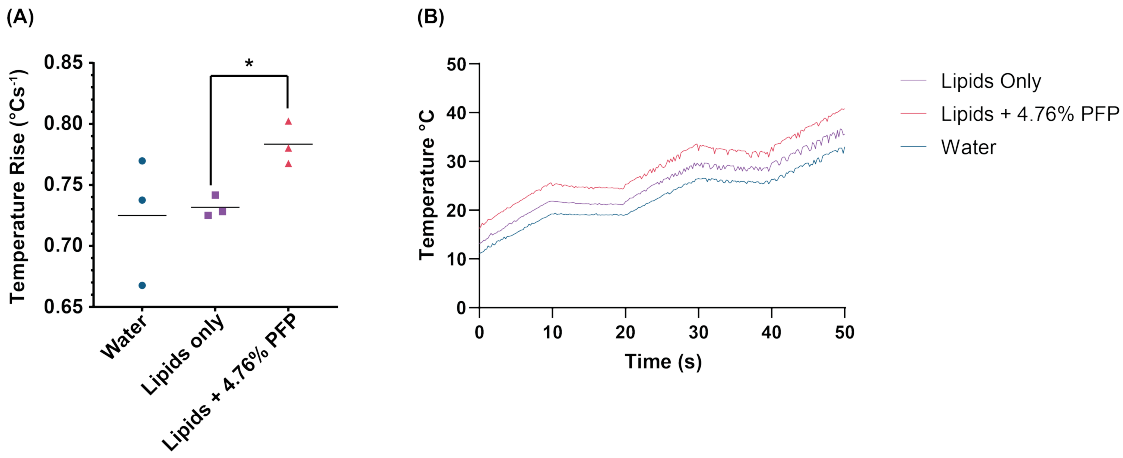

Figure 3.5: Mean temperature rise in water (0.8 mL), lipids suspension (0.8 mL) and lipids with 4.76% v/v PFP (40μL) in a 1.5 mL Eppendorf tube insulated in polystyrene. Lipids only and lipids with 4.76% v/v PFP showed a significant difference with p*=0.0103, N=3. (B) Representative temperature traces for samples sonicated at 60 % amplitude for 60 s with a 10 s on, 10 s off pulse regimen were used to calculate the temperature rise of the sample.

3.3.5 | Cooling Method has a Significant Impact on the Sonication Process

Temperature during sonication is an important consideration for the nanodroplet manufacturing process. Figure 3.6A demonstrates the foaming that occurred when the cooling during the sonication was inadequate. In order to avoid this excessive foaming, different cooling methods were investigated using the sonicator setup described in section 2.2. In Figure 3.6B, an ice-water bath and ice-saline bath were compared. The ice-saline bath was more effective at cooling but occasionally froze the solution before the sonication took place. The ice-water did manage to keep the temperature below the boiling point of PFP but its proximity to the boiling point was still a concern. Figure 3.6C demonstrates that increasing the time between pulses decreases the maximum temperature during sonication. From this, a 2s on and 15s off pulse regimen was used in all following experiments. To ensure this was a sufficient cooling method for further planned experiments, the temperature was measured at 60% amplitude and 100% amplitude to validate that it will stay below PFP's boiling point, as seen in Figure 3.6D.

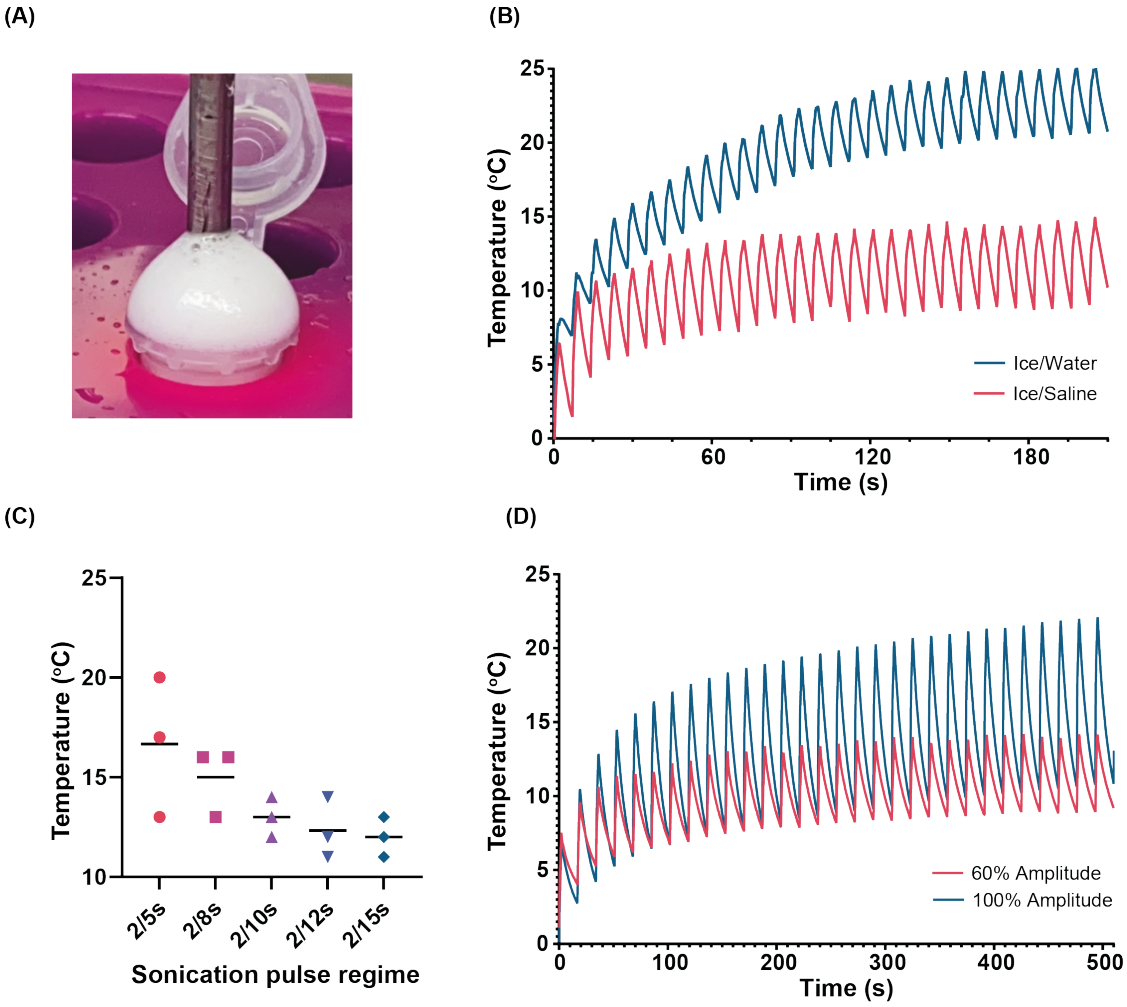

Figure 3.6: Temperature control is important during nanodroplet production. Excessive foaming (A) occurs when the temperature within the solution gets too high. Initially, a 2 s on 5 s off pulse regimen was used with an ice/water and ice/saline bath (B). Various pulse regimens were studied in relation to the maximum temperature during sonication (C) in an ice/water bath (N=3). The resulting 2 s on, 15 s off pulse regimen was validated to ensure the solution would not go above $25^{o}C$ when cooled in an ice/water bath even at 100% amplitude (D).

The temperature at the end of the second sonication was also measured, and the particle size distributions' mean diameter and standard deviation were noted. After statistical analysis using a Pearson test, it was found the correlation between the mean diameter and temperature was significant (P=0.0465) with an R^2 value of 0.3138, but the correlation between the distribution standard deviation and the temperature was

found not to be statistically significant (P=0.1332, R^2=0.1929).

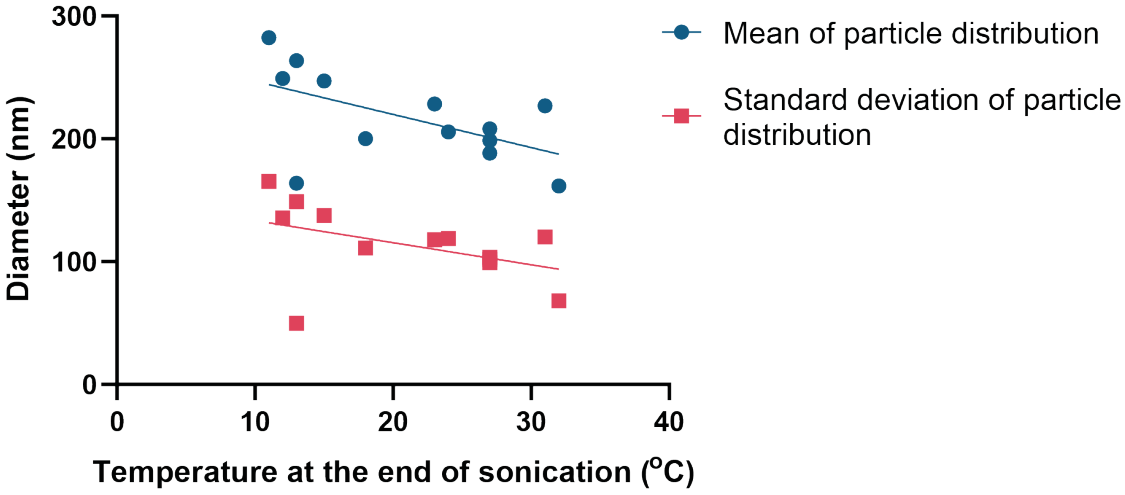

Figure 3.7: Temperature of the solution before the end of the second sonication against the mean of the resulting particle distribution and the standard deviation of the resulting particle distribution to demonstrate the change in dispersity (N=12, Mean: P=0.0465, R^2=0.3138; Standard deviation: P=0.1332, R^2=0.1929).

3.3.6 | PFP Concentration Experiments

Figure 3.8 demonstrates that the ratio of PFP to lipid solution (lipid volume was kept constant at 2 mL) had a significant effect on not only the mean diameter of the resulting nanodroplets but also the standard deviation of the particle size distribution as it also increased with size. It was found that the Pearson correlation coefficient of the PFP volume against the resulting nanodroplet size had a value of R^2 = 0.9321 and a correlation significance of P = 0.0018, suggesting a very strong relationship between the two variables. The images from the light microscope show particles too large to be detected by the NTA. There were very few of these particles observed at lower PFP concentrations (25 μL, 12 μL and no PFP). Contaminants were observed both visually, by presenting as a grey solution rather than white (see supplementary material) and under the microscope, where dark particles were observed. This contamination was investigated using energy dispersive X-ray analysis (EDX) analysis. The qualitative results can be found in the supplementary material. The key difference that can be noted between the nanodroplet samples and the contaminant-only sample is the presence

of the titanium. This is also the element present in the contaminant that cannot be explained by the presence of the nanodroplets, the glass slide or the PBS.

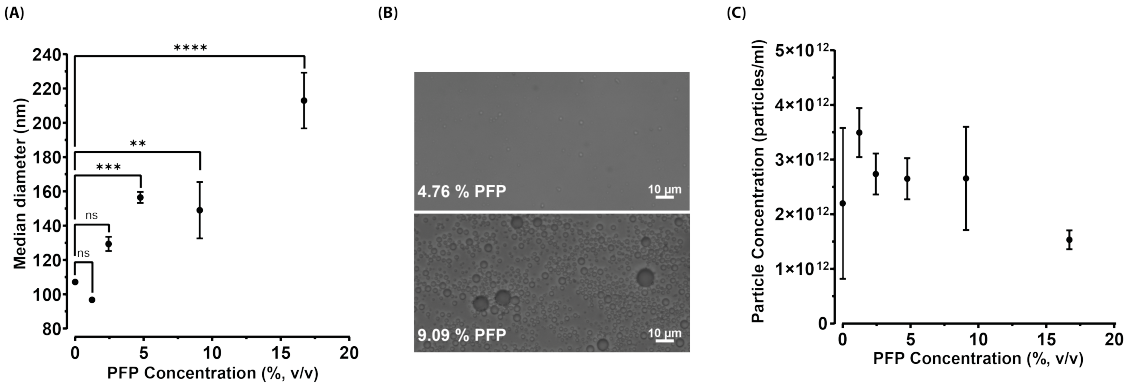

Figure 3.8: Volumetric PFP concentration significantly affected the characteristics of the resulting nanodroplets. (A) illustrates the impact of PFP concentration (0-16.7 % v/v) on median nanodroplet diameter, as measured using NTA at a tip height of 12 mm (R^2=0.9321, P=0.0018, N=3, n=5). Figure (B) shows microscopy images of nanodroplets made at 12 mm tip height with a PFP concentration of 4.76 and 9.09 % v/v under a 40× objective lens. (C) displays the concentration of the nanodroplets measured using NTA also at a tip height of 12 mm (N=3, n=5). Error bars represent the standard deviation.

3.3.7 | Effect of Sonicator Tip Height and PFP Concentration on Nanodroplet Size

The PFP concentration appears to have a more significant influence on the median and standard deviation of the particle size distribution. Both the tip height and the PFP concentration were found to have a significant contribution using a 2-way ANOVA (P<0.0001). The median was used in this case due to the distributions being right-skewed. Below 5 % vol, there is no clear difference between the median or the standard deviation values. In general, a greater tip height led to a lower median and standard deviation. The value of the median and standard deviation for 2 mm tip height at 20 % vol PFP were taken as anomalous due to the PFP and the lipid solution visibly not mixing (see Figure S4 in the supplementary material).

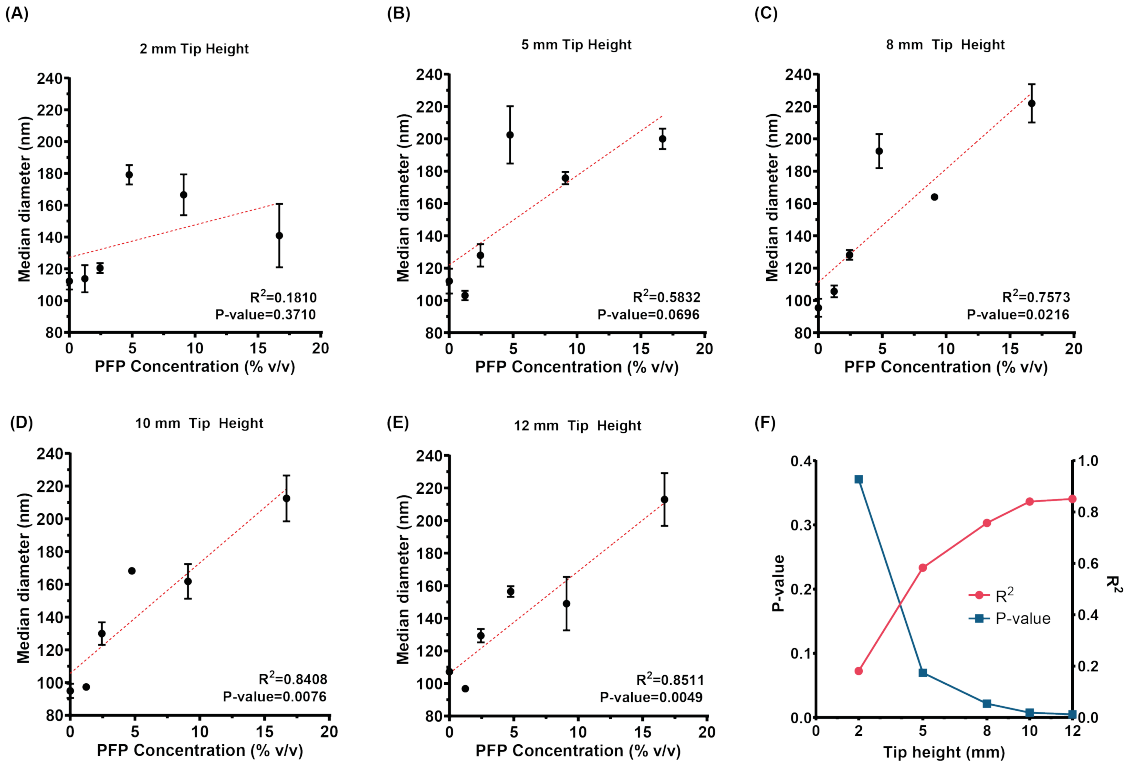

Figure 3.9: Tip height affects the strength of the relationship between PFP concentration and median nanodroplet diameter. The PFP was plotted against the median diameter at each tip height from the bottom of the Eppendorf (A-E). The strength of the relationship between the PFP concentration and the median nanodroplet diameter is shown to increase with tip height, with the R^2 increasing with tip height and the associated P-value decreasing (F). (Error bars represent the standard deviation, N=3, n=5)

3.3.8 | Total Sonication Time

There is no observable trend between nanodroplet diameter or concentration and total sonication time; however, the 90-second sonication time consistently yields the smallest nanodroplet diameter.

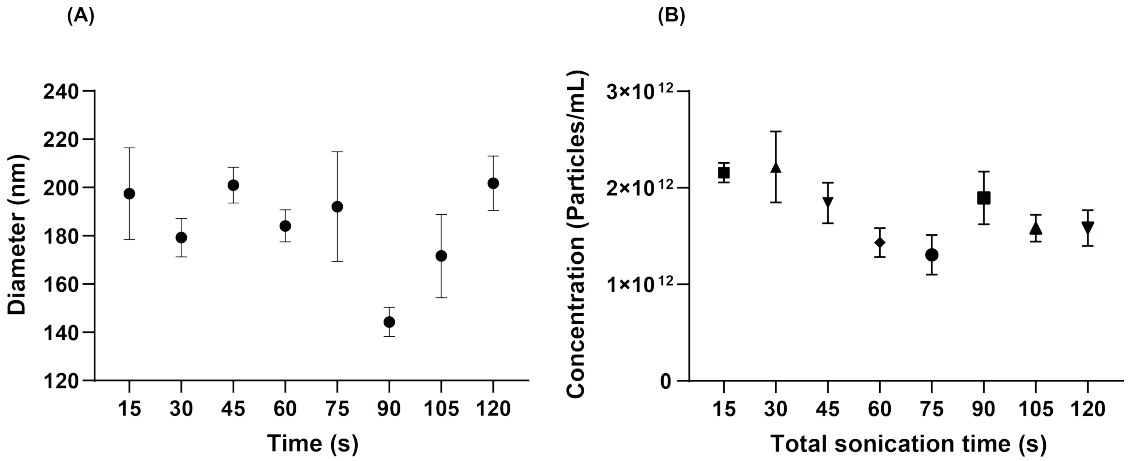

Figure 3.10: Sonication time had little effect on nanodroplet characteristics. Total sonication time was varied (15-120 s) with nanodroplets made at 12 mm tip height and 4.76% v/v PFP. (A) shows the resulting nanodroplet diameter and (B) the nanodroplet concentration at 60% amplitude (N=3, n=5).

3.3.9 | Sonication Amplitude

Sonication amplitude is likely to affect the intensity of the mixing. It can be seen in Figure 3.11A that 20% and 40% amplitude are not sufficient to enable the mixing of the PFP and lipid phases. This was observed visually in Figure 3.12. Larger amplitudes do not appear to have an effect on the nanodroplet size as measured by NTA (Figure 3.11), but larger amplitudes did lead to more foaming (Figure 3.12). Figure 3.11B suggests that the amplitude does affect the nanodroplet concentration, with larger amplitudes leading to larger concentrations.

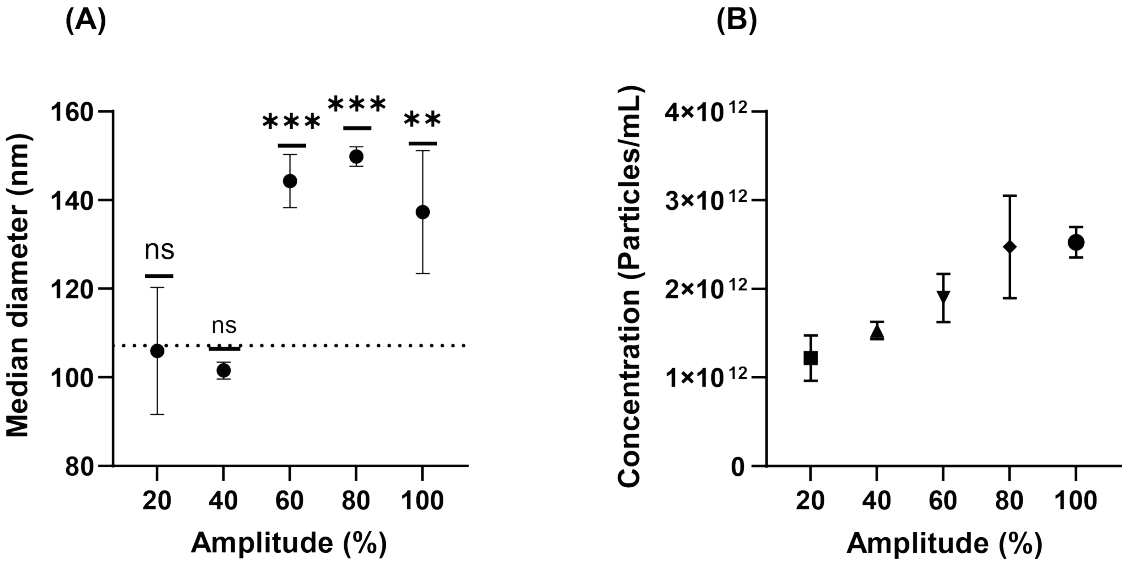

Figure 3.11: Nanodroplet characteristics are significantly affected by sonication amplitude. The results of median nanodroplet diameter (A) and concentration (B) measured using NTA when nanodroplets are made at varying sonication amplitudes (20-100%) at 90 s total sonication time, a 12 mm tip-height and 4.76% v/v PFP. The dashed line at 107 nm represents the average particle size in a PFP-free control. Each value is the mean of N=3, n=5 values.

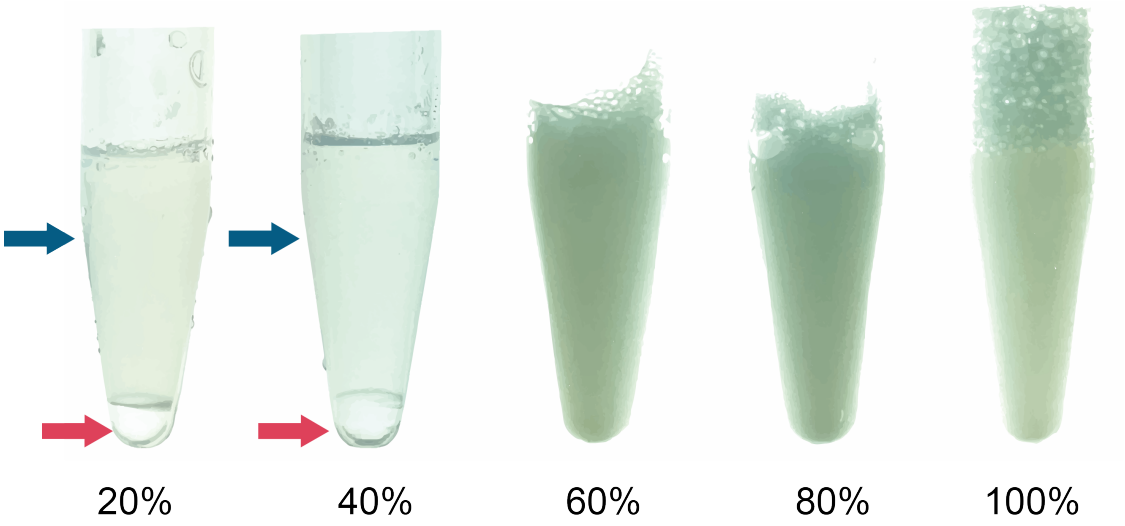

Figure 3.12: Images showing the resulting nanodroplet solutions following sonication for 90 s at a 12 mm tip-height and 4.76% v/v at various sonication amplitudes. There is an observed lack of mixing observed at lower sonication amplitudes with a phase separation between the PFP (pink arrow) and the lipid suspension (blue arrow) observed at 20% and 40% amplitude as well as the excessive foaming observed at 100% .

3.3.10 | Storage Temperature and Stability

By itself, under normal atmospheric conditions, PFP has a boiling point of 29^oC. This has potential implications for the storage stability of the nanodroplets. Nanodroplets were stored at 0.1% v/v in PBS for 24 hours at 4^oC (in fridge), room temperature and 37^oC (in incubator). Following the 24 hours, the particle distribution can clearly be seen to be less smooth.

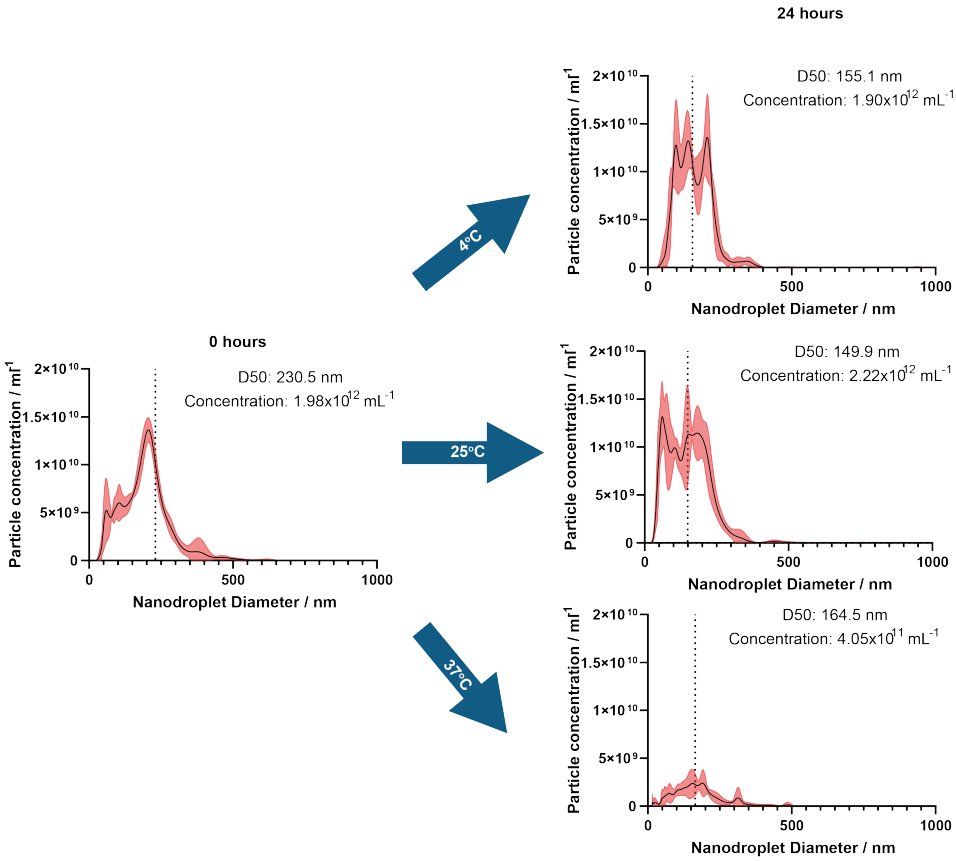

Figure 3.13: Nanodroplet size distributions before and after storage at 4^oC, room temperature and 37^oC. The dotted lines represent the median of each distribution. The median and concentration of each distribution are given by the NTA as also stated. The red shaded area represents the standard deviation of n=5 videos.

Nanodroplet size and concentration decreased with each storage temperature with the most significant decrease observed at 37^oC (Figure 3.14). No significant difference were observed between groups. The only group that displayed a significant difference between the 0 hour and 24 hour concentration was 37^oC (P=0.0215). None of the size

measurements showed statistically significant changes in size.

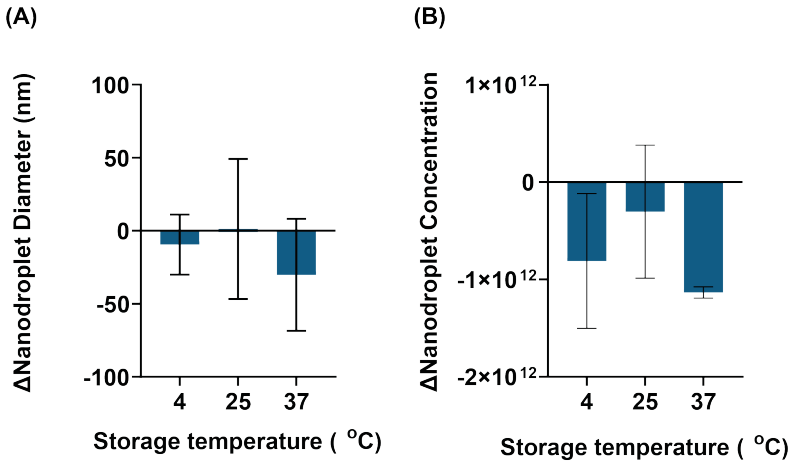

Figure 3.14: Storage temperature affects nanodroplet stability. The change in nanodroplet (A) size and (B) concentration following 24 hours of storage in 4^oC, 25^oC and $37\ ^oC$ (N=3, n=5).

3.3.11 | Post-Processing: Filter vs Centrifugation

Of the post-processing procedures, filtering the sample had a greater effect than centrifuging it. It is important to note, however, that the samples used for the filtering were larger before the post-processing. The filtering process was found to have a significant difference on the mean population diameter. However, there was no significant difference between the size of the pores. The centrifuging technique found no significant difference where the larger particles should have accumulated at the base of the pellet within the Eppendorf.

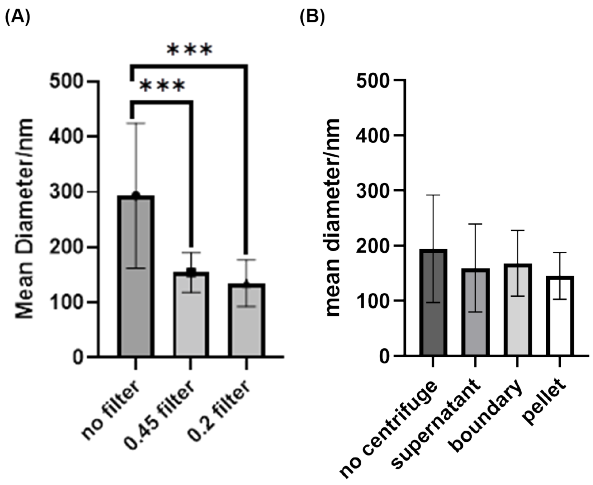

Figure 3.15: The effect of post processing techniques on nanodroplet size distribution. Nanodroplets were made through sonication (60% amplitude for 1.5 minutes at 12 mm tip height with 5% PFP) then immediately underwent post-processing using (A) a syringe filter or (B) through centrifugation. Significant differences were observed between no filter and each of the filters, 0.2 μm and 0.45 μm pore size (P=0.0004 and P=0.0003 respectively). However, this was not the case for the centrifugation methods. (N=3, n=5)

3.3.12 | Post-Processing: Gas Loading

It was hypothesised that the shear forces introduced during gas loading or the presence of the gas within the nanodroplet might affect the droplet stability. This was not observed in Figures 3.17 or 3.16 where no significant differences were observed between groups.

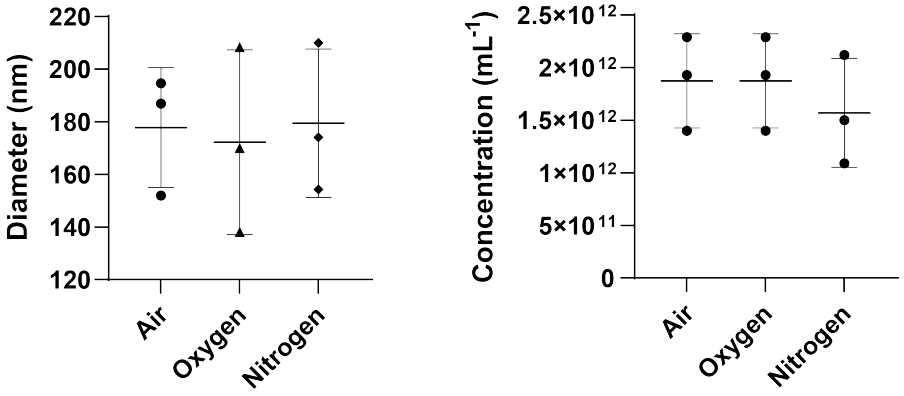

Figure 3.16: The effect of gas-loading on nanodroplet stability. The (A) median nanodroplet diameter and (B) concentration were measured using NTA following no gas-loading (air) or gas loading (oxygen or nitrogen). Middle line represents the mean and error bars represent one standard deviation (N=3, n=5).

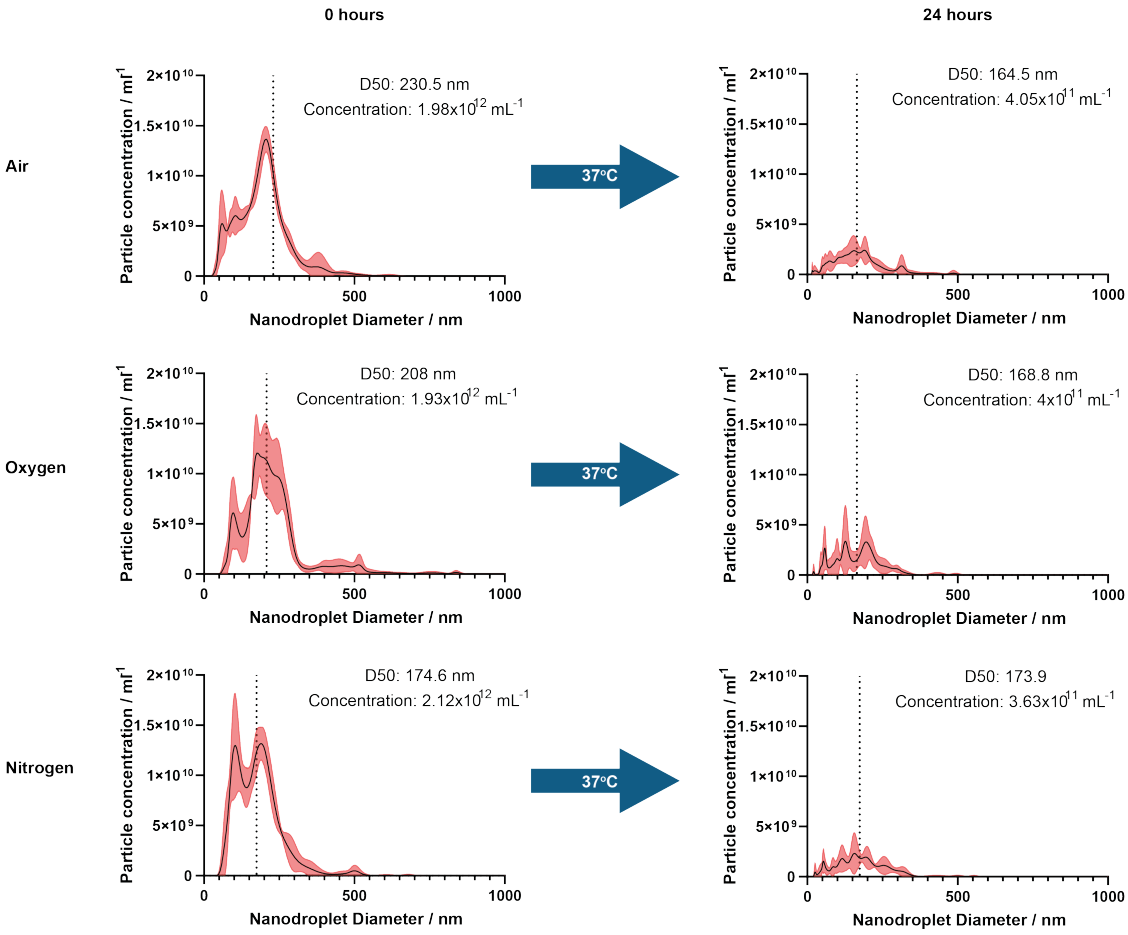

Figure 3.17: Nanodroplet size distributions before and after 24-hour storage at 37 ^{o}C after no gas loading (air-saturated) or gas loading (oxygen or nitrogen). The dashed line represents the median diameter, and the median and concentration are stated on the graphs (red shaded area represents the standard deviation, n=5).

Gas loading did not appear to have an affect on storage stability over 24 hours. No significant difference were found between groups. The only group to display a statistically significant difference between the 0 hour and 24 hour concentration was air at 37^0C (P=0.0215). No statistically significant differences were observed between 0 hours and 24 hours for median diameter in any group.

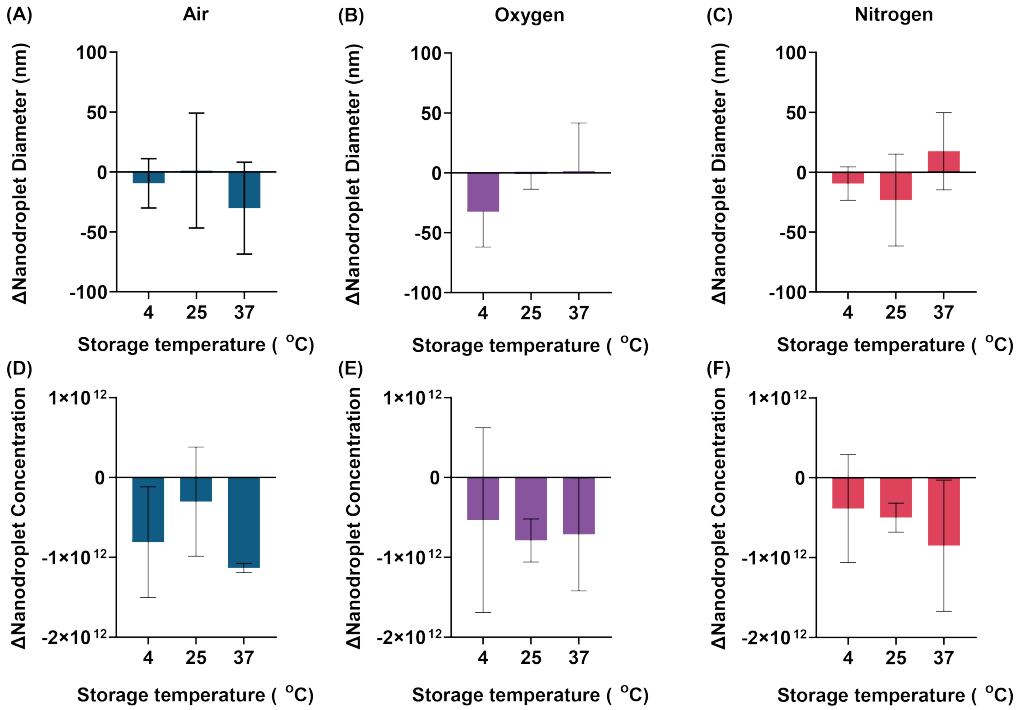

Figure 3.18: Gas loading had little effect on nanodroplet stability. Change in median nanodroplet diameter for (A) air, (B) oxygen, (C) nitrogen-loaded nanodroplets. As well as the change in nanodroplet concentration for the same samples loaded with (D) air, (E) oxygen and (F) nitrogen. (N=3, n=5)

3.3.13 | Perfluorocarbon Oxygen Release

Measuring the oxygen concentration directly in the nanodroplets or perfluorocarbon was difficult as the perfluorocarbon was found to dissolve the oxygen sensor and the nanodroplets interacted with the sensor when in suspension. Instead, the oxygen in initially air-saturated water was measured over a 2 hour period post exposure to air-saturated and oxygen-saturated PFP. It was found that air-saturated PFP led to a slight decrease in the oxygen concentration of the water (P=0.0454). However, exposure to

oxygenated PFP led to a significant increase in the concentration of oxygen concentration in the water (P<0.0001).

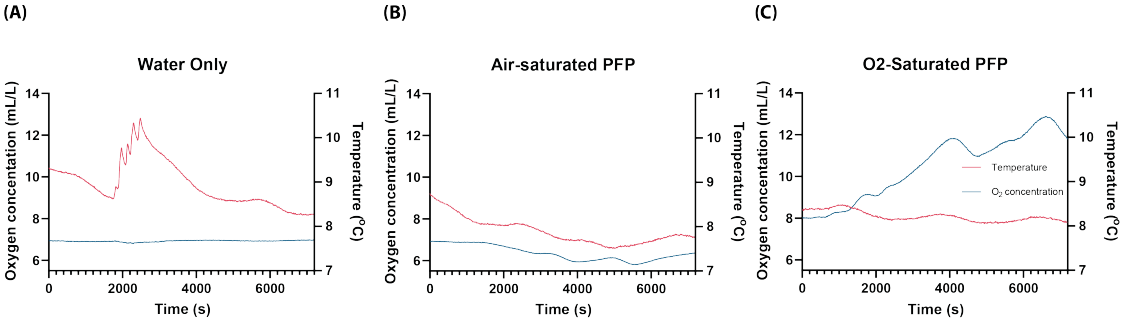

Figure 3.19: Oxygen diffuses from PFP to water when the initial concentration in the PFP is higher than the water. Oxygen concentration and temperature in water over time with (A) air-saturated water only, (B) in contact with 1 mL of air-saturated PFP and (C) in contact with 1 mL of oxygen-saturated PFP. Representative curves are shown.

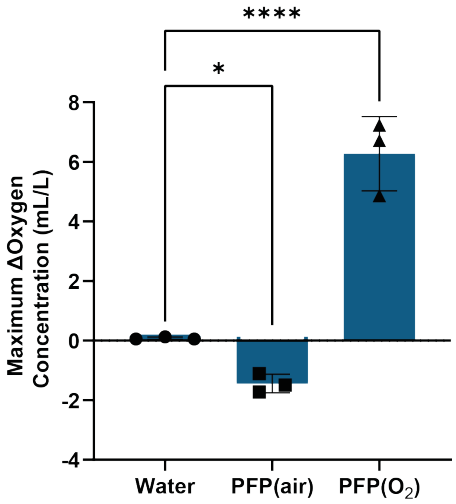

Figure 3.20: Oxygen diffused to the water from the PFP when PFP is saturated with oxygen but the opposite occurs when air-saturated PFP and water were put in contact. The maximum change in oxygen concentration in water over a two hour period when in contact with 1 ml of water, air-saturated PFP or oxygen-saturated PFP (N=3).

3.4 | Discussion

The overarching aim of this project was to develop nanodroplets capable of delivering oxygen to an area of hypoxia surrounding a bone fracture. With this in mind, it is essential that nanodroplet production is not only reproducible but nanodroplets are made small enough not to provoke an immune response and can reach areas too narrow for red blood cells to access. This chapter sought to achieve this by successfully characterising both the nanodroplets and the sonication process through which they are made. An additional aim was to understand how different sonication and post-production parameters affect the nanodroplet characteristics.

These aims were addressed by the experiments outlined in this chapter that demonstrated the following key findings:

- NTA formed the most reliable form of nanodroplet characterisation but should be supported by light microscopy images;
- Increasing sonicator amplitude increases the calorimetric power output of the sonicator into the sample;
- Sample composition has an effect on the calorimetric output of the sonicator;
- Temperature during sonication and, therefore, the method of cooling has a significant impact on nanodroplet size;
- Increasing PFP concentration increases nanodroplet size;
- The placement of the sonicator tip has an impact on the strength of the relationship between PFP concentration and nanodroplet size;
- There is a critical sonicator amplitude that needs to be achieved for adequate mixing to occur, but too high an amplitude results in vaporisation within the mixture;
- Nanodroplets are sensitive to storage temperatures;
- Filtering had a significant effect on nanodroplet size;
- Gas loading did not significantly affect nanodroplet characteristics.

3.4.1 | Nanodroplets Produced by Sonication have High Dispersity

Sonication is a standard method for nanodroplet production (Ferri et al., 2021); however, the process can be very stochastic, leading to significant variations in nanodroplets produced if not tightly controlled. The distributions in Figure 3.1 were made from the same lipid suspension and PFP with the same sonicator at 60% amplitude for 60 s (it is important to note that tip location was not precisely controlled in this case). Despite the similarities in their production, the resulting distributions are clearly very different. Sheeran et al. also demonstrated this high size dispersity using SEM on perfluorohexane nanodroplets templated with silica (Sheeran et al., 2017). This indicates that this kind of high size dispersity is not unique to this sonication system but is a significant disadvantage of all sonication methods.

Mixing during sonication occurs due to acoustic pressure leading to shear forces, cavitation events and micromixing due to turbulent flow (Bampouli et al., 2024; Sutkar, Gogate, 2009). As a result, a certain degree of randomness will always be expected, but a better understanding of the variables affecting the sonication process should allow for better control of the nanodroplet characteristics and their reproducibility. Temperature, sonication time, sonicator amplitude, tip placement, container geometry and PFP concentration are all factors for consideration (Bampouli et al., 2024; Taurozzi et al., 2012). Given this tendency to high size dispersity, the suitability of the sonication process for making nanodroplets may be brought into question. However, other methods for developing nanodroplets are not without their own complications, as discussed in section 1.5.1 of this report. Of the other production methods, microfluidics shows a promising new approach for small batch production but currently does not produce nanodroplets of the required size or concentration (Martz et al., 2012; Teston et al., 2018). It also adds complexity to the process (Zhang et al., 2022). For now, sonication lends itself the most to laboratory scale production as it is quick, easy, has a low capital cost and is most suited to small volumes, leading to reduced waste (Sheeran et al., 2017).

3.4.2 | NTA Measurement is Preferable Over DLS Measurement

Before attempting to optimise the sonication process, a reliable method should be identified for establishing nanodroplet size and concentration once they are made. As discussed in section 1.5.2, multiple methods have been used to characterise nanodroplets, including DLS, NTA, SEM, TEM and AFM. Of these techniques, DLS is the most frequently used (Ferri et al., 2021; Matsuura et al., 2009; Williams et al., 2013; Zhang, Porter, 2010). However, its bias towards larger particles and aggregates makes it an unreliable method (Filipe et al., 2010). Figure 3.2B demonstrates this bias. It shows a particle size distribution as measured using DLS. The proportion of larger particles detected compared to smaller particles is much larger than what is observed in the distribution obtained by the NTA (Figure 3.2A). This has previously been observed before by Filipe et al. where they found that NTA had significant advantages over DLS where samples with a higher size dipersity are concerned, with larger particles having little influence over the NTA results but a significant impact on DLS results.

It is important to note, however, that NTA is not without its own limitations. Figure 3.3 shows the same sample as measured quantitatively by NTA and qualitatively by light microscopy. As NTA works by using the particles' Brownian motion (as discussed in depth in 1.5.2), larger particles become increasingly more difficult to measure. This results in an upper detection limit of 1000 nm. The resolution limit of an ideal light microscope is approximately 200 nm. This makes microscopy an inappropriate method for quantitatively sizing and quantifying nanodroplets with expected diameters around this size or smaller. It can, however, confirm the presence of particles too large for NTA to detect. NTA and light microscopy were, therefore, used together when optimising nanodroplet size. As nanodroplets above 1 μm in size were considered too large for nanodroplets with the end objective of *in vivo* use, the presence of any larger particles visible was considered relevant.

3.4.3 | Sonicator Characterisation

The sonicator was calibrated using calorimetry in water. This was to enable comparisons between labs. The calorimetric power was found to increase with tip displacement amplitude. The amplitude was plotted against the square root of the calorimetric

power as this is the relationship expected for a piston-like emitter (Kinsler et al., 1982). This resulted in an R^2 value of 0.9818, strongly indicating that this model is likely.

In order to simulate the calorimetric power during the actual sonication process, the temperature rise in a 1.5 mL Eppendorf was modelled with 0.8 mL of liquid. A significant increase in the temperature rise was observed between lipids only and lipids with 4.76% PFP (P=0.0103). This suggests an increase in the calorimetric power output of the sonicator into the solution when the PFP is added. The main differences between the samples will be the sample mass, the specific heat capacity and the viscosity. Equation 3.1 predicts that a change in mass should, in fact, lead to a reduction in the temperature change, and so will not be the cause of the difference.

$$P = mc\frac{\Delta T}{t} \tag{3.1}$$

The rule of mixtures states that the specific heat capacity of a mixture is equal to the sum of the specific heat capacities of the individual components multiplied by their mass fraction. However, the mass fractions of the lipids and the PFP are so small that the specific heat capacity can be assumed to still be approximately that of water. This leaves the change in viscosity. Pal et al. modelled the viscosity of emulsions of two immiscible fluids, giving equation 3.2.

$$\eta_r \left(\frac{2\eta_r + 5K}{2 + 5K}\right)^{\frac{3}{2}} = \left(1 - \frac{\phi}{\phi_m}\right)^{-2.5\phi_m} \tag{3.2}$$

Where η_r is the viscosity of the emulsion relative to the continuous solution viscosity, K is the ratio of the viscosities of the disperse and continuous phases, respectively, ϕ is the volume fraction of the dispersed phase and ϕ_m is the maximum packing volume fraction of the particles. Equation 3.2 has been visualised in Figure 3.21 where it can be seen that the existence of an emulsion always results in the increase in viscosity, despite PFP having a lower viscosity than water.

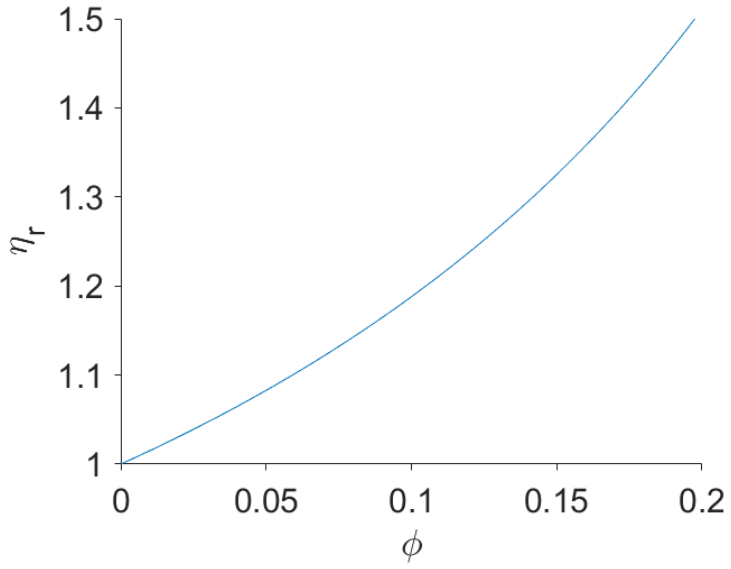

Figure 3.21: Visualisation of equation 3.2 plotted with K=0.47 and ϕ_m=0.637 (this value corresponds to the random close packing of hard spheres) for the range of volume fractions investigated in this chapter.

The sonicator tip displacement amplitude is controlled. This means more work must be done in more viscous solutions to obtain the same amplitude. This results in a larger power output for the same amplitude setting that could explain the larger temperature rise observed in the lipid and 4.76% PFP solutions.

3.4.4 | Temperature and PFP Concentration Have a Significant Effect on Nanodroplet Size

Given the innate variability of the sonication process, it is important to control as many variables of the process as possible to improve reproducibility. The solution contents and container are already constrained by the nanodroplets' desired properties and desired volume. Temperature was considered the next restricting factor due to the aqueous lipid dispersion freezing just below 0^oC and the PFP not encapsulated by the phospholipid (free PFP) boiling at 29^oC (Johnstone, 2007). This leads to a very small temperature window where the sonication can occur. Figure 3.7 demonstrates that a greater temperature after sonication leads to a smaller nanodroplet diameter. This could be due to the vaporisation of larger droplets (Sheeran et al., 2017), or it could

be a contribution from the lipid micelles being formed due to the vaporisation of the PFP, leading to less availability of the PFP for nanodroplets. Gao et al. proposed that there are critical PFP to lipid ratios above which nanodroplets can form, leading to a bimodal zone where both lipid micelles and nanodroplets may be formed. Above another critical ratio, exclusively nanodroplets are formed (Gao et al., 2008). If enough PFP vaporises due to the temperature rise during the sonication process, the contribution to the size distribution from smaller lipid particles not containing PFP will result in a smaller average size. However, this may not be due to the micellar contribution as seen in Figure 3.22. Figure 3.8A demonstrates that average nanodroplet diameter continues to increase with increasing PFP concentration. This is supported by Gao et al. and Ferri et al., who both found that increasing PFP concentration led to an increase in nanodroplet diameter even above the theorised critical ratio where nanodroplets only are created (Ferri et al., 2021; Gao et al., 2008). Smaller nanodroplets lead to a greater total surface area of all the nanodroplets combined. The greater the surface area, the greater the lipid requirement. Above this critical ratio, where nanodroplets only are formed, the lipid availability is the limiting factor, and so the total surface area of all the droplets combined cannot increase. As a result, the diameter of the nanodroplets must increase and the number decrease. Despite a rise in temperature leading to a desired reduction in particle size, it is preferable not to get close to the boiling point as vaporising the PFP leads to an unknown amount of PFP in the system, reducing reproducibility. Additionally, it could lead to the formation of microbubbles. In Figure 3.6A, the foaming that occurs in the case of excessive heating can be seen. This reinforces the idea of vaporisation occurring as it demonstrates that gas is being introduced to the solution.

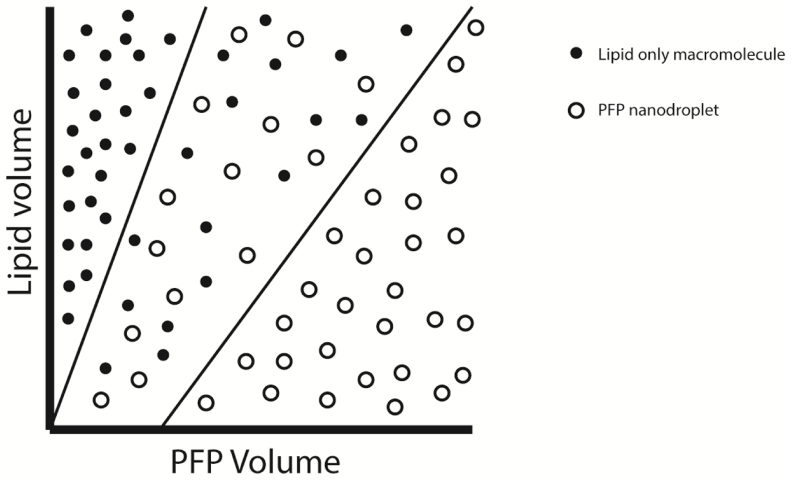

Figure 3.22: Theoretical diagram illustrating the effect of lipid-PFP ratios on the production of nanodroplets and lipid-only structures. A critical ratio is required for the lipid-only structures not to have a significant contribution to the NTA size distribution consistent with findings from Gao et al (Gao et al., 2008).

In order to avoid this excessive foaming, different cooling methods were investigated using the sonicator setup described in section 2.2. In Figure 3.6B, an ice-saline and ice-water bath were compared as a method of cooling the nanodroplet solution. It was hypothesised that the ice-saline bath would be more effective at keeping the solution cooler as it has both a higher specific heat capacity and high thermal conductivity. This was found to be the case as the ice-saline bath not only kept the solution cooler, but it reached an equilibrium temperature sooner. However, despite its effectiveness in cooling the solution during sonication, the ice-saline bath was not a viable method for cooling the solution as it would occasionally freeze the solution before sonication could take place. The ice-water bath did not have this problem, but the temperature tended to approach the boiling point of PFP. It is possible that this could be avoided by using longer pulse times. The results in Figure 3.6C support the hypothesis that longer gaps between the pulses results in a reduced solution temperature due to the solution being allowed to cool more between pulses. Eventually, a pulse time of 2 s on and 15 s off was chosen to ensure the temperature was kept well below the boiling point of PFP, no matter what amplitude was chosen (Figure 3.6D).

3.4.5 | PFP Concentration Affects Nanodroplet Characteristics

The previous section briefly discussed that increasing PFP concentration leads to increased nanodroplet diameter as seen in Figure 3.8A. A positive correlation with an R^2 value of 0.851 was found, consistent with previous results by Ferri *et al*. (Ferri et al., 2021). The relationship does not appear to be perfectly linear, with a possible change in behaviour occurring at a PFP concentration of 4.76% v/v. Samples measured below this concentration of PFP were found to not be significantly different from the no PFP control. The no PFP control contains lipids dispersed in PBS only. As a result, the particles observed in this control are likely to be lipid micelles. These lipid-only structures are indistinguishable from nanodroplets when using NTA as the technique is limited to size and concentration characterisation, except that nanodroplets are expected to be larger as they have a PFP core. As such, PFP concentrations below 4.67% v/v PFP were rejected as it was not possible to confirm the presence of nanodroplets. Of the remaining PFP concentrations, 9.09% v/v PFP appeared to yield the smallest nanodroplets when measured by NTA in Figure 3.8A. However, when observed under a light microscope, this result was not reflected, with more larger, spherical objects observed under the microscope at 9.09% v/v PFP than at 4.67% v/v. The introduction of these larger particles that are undetected by the NTA may also account for the lower nanodroplet concentrations detected at larger PFP concentrations in Figure 3.8C.

3.4.6 | Sonicator Tip Height Affects the Strength of the Relationship Between PFP Concentration and Nanodroplet Size

Due to the amount of PFP in the system affecting the location of the lipid-PFP boundary, the PFP concentration will affect the distance between the sonicator tip and the boundary. As a result, the two variables were investigated together. A two-way ANOVA was performed with Tukey's multiple comparison post-test were performed on the median size. Both the row and column factors were very significant, with a P-value of less than 0.0001. This suggests that the tip height and the PFP concentration both have an impact on the resulting nanodroplet size. However, when analysing the tip-height to median nanodroplet diameter correlation, only the correlation for 1.25% PFP was found to be significant (see Tables S2 in the supplementary Material). Interestingly, for the correlation between PFP concentration and median nanodroplet

diameter, the R^2 values increased with tip height, and associated P-values decreased (Figure 3.9F). This may suggest the solution of lipid micelles above the sonicator tip is not being treated, and the contribution from the lipid micelles is contributing to a non-linear relationship.

In the setup used in these experiments, the depth of the liquid being sonicated is 20 mm. Additionally, the sonication takes place in an Eppendorf. There is a distinct lack of literature for this geometry and depth. A report by the US National Institute of Standards and Technology recommends an immersion depth of 2-5 cm and not placing the probe any closer than 1 cm from the bottom of the container (Taurozzi et al., 2012). However, these conditions cannot be satisfied in the Eppendorf system, which is used to avoid wastage as a result of larger volumes. Note that approximately 300 µL is used for an experiment consisting of an entire 96-well plate.

Table 3.1: Approximate heights of the PFP-lipid boundary at the beginning of the sonication for each PFP concentration investigated in the tip height against PFP concentration experiment.

PFP concentration ratio/%	**Approximate height of PFP-lipid boundary/mm**
0	0
1.25	1
2.5	2
5	4
10	6
20	10

It was hypothesised that the location of the lipid-PFP boundary may affect the size of the nanodroplets. Table 3.1 gives the approximate heights of the PFP-lipid boundary for each PFP concentration to the nearest millimetre. Given these values, a closer proximity to the boundary, generally seems to result in larger droplets, with the only exception being at 2.5% PFP where the nanodroplets were smallest at 2 mm height.

3.4.7 | Total Sonication Time Does Not Effect Nanodroplet Size and Concentration

There was no clear trend in the nanodroplet diameter with respect to total sonication time. The results were, however, consistent with Ferri et al., which investigated nanodroplets made with 20, 40 and 60 s total sonication times (Ferri et al., 2021). Ferri et al. found that there was a decrease in size between 40 and 60 s which is consistent with the size decrease between 45 and 60 s. Other literature looking at the formation of nanoemulsions such as perfluorodecalin droplets stabilised using Tween 80 (Syed et al., 2021) also found that there was little relationship between nanodroplet size and sonication time, albeit on a much larger time scale.

3.4.8 | Sonication Amplitude Does Affect Nanodroplet Production

Sonicator amplitude and sonication time are both factors that will affect the total energy going into the solution. Changing the sonication time does this by changing the duration over which work is done. The sonicator amplitude changes the intensity of the work done. This appears to have a much more significant effect as nanodroplets made with sonication amplitudes of 20% and 40% failed to mix. This was seen both quantitatively in Figure 3.11, where the median diameter measured by the NTA was not significantly different from the no PFP control, but also qualitatively in Figure 3.12 where the PFP phase can still clearly be seen at the bottom of the tube, and the solution is still transparent. In these images, it can also be seen that 100% amplitude led to excessive foaming, and so should be avoided.

Interestingly, particle concentration appears to increase with amplitude. This is true even for amplitudes of 60-100%. Given that the average particle size does not really change in this range and that the chemical composition of the sample to be sonicated also remains constant, an increase in concentration may be due to contaminants such as air microbubbles.

3.4.9 | Selection of Optimised Sonication Parameters

The appropriate settings were decided using the following criteria in order:

1. The PFP concentration must result in a significant difference from the control at all tip heights;
2. The PFP and lipid solution must have no visible phase separation post-sonication;
3. The microscope images must not contain any particles larger than 1μm as these will not be measured by the NTA;
4. Of the filtered data set, the parameters resulting in the smallest nanodroplet diameter should be selected.

Exclusion criteria 1 resulted in a PFP concentration of 5% or above being selected. Criteria 2 removed 20% PFP concentration with 2 mm tip height from consideration. Microscope images demonstrated that it was possible for larger particles to remain undetected using NTA (Figure 3.8). It was deemed that any particle larger than 1μm was already too large and so any parameters resulting in samples with microscope images displaying any particles larger than 1μm were excluded according to criteria 3. The remaining filtered data set was assessed according to criteria 4 (the complete set of median nanodroplet diameters can be found in Figure S5 of the Supplementary). As a result, the 5% PFP concentration and 12 mm tip height were considered the best settings for the nanodroplet formulation.

Exclusion criteria 1 and 2 were set to ensure confidence that the nanodroplets are actually present and that the solution is not just lipid micelles and vesicles. Criteria 3 and 4 were applied to minimise possible side effects within the body and improve stability and potential ultrasound properties when using acoustic droplet vaporisation.

3.4.10 | Storage Temperature Affects Nanodroplet Stability

Nanodroplet stability is an inherent challenge for nanodroplets designed to be acoustically active. The nanodroplets rely on ultrasound stimulation to induce pressure changes that lead to microbubble formation. Unfortunately, there exists an

interdependency between pressure and temperature sensitivity. Yuan *et al*. compared nanodroplets with a perfluoropentane or perfluorohexane core and found significant fluctuations in the perfluoropentane droplet size over time when stored at 37^o where perfluorohexane remained stable. Conversely, they found that perfluorohexane nanodroplets were more resistant to undergoing phase change with an external stimulus (laser stimulated) (Yuan et al., 2019). It can be seen in Figure 3.13 that the concentration of nanodroplets stored at 37^oC was significantly less than that of the nanodroplets stored at 4^oC and room temperature. Moreover, all three distributions saw a decrease in distribution smoothness, indicating substantial alterations to nanodroplet characteristics. This is not consistent with work by Bérard *et al*. where surfactant stabilised perfluorooctyl bromide nanodroplets' size increased more significantly at 37^oC compared to 4^oC. However, these will not be directly comparable as perfluorooctyl bromide has a significantly higher boiling point of 142^oC. Increased instability at 37^oC, however, may not necessarily be an undesirable factor as it allows for increased sensitivity to ultrasound. In subsequent cell culture experiments, nanodroplets were made fresh prior to any media changes.

3.4.11 | Filtration and Centrifugation

Post-production processes were developed to remove any larger nanodroplets that may cause problems if injected. The centrifugation technique did not seem to have much impact on the nanodroplets' size. This may be because the settings that were used were not fast enough to separate any of the nanodroplets small enough to be detected by the NTA. Using Stokes' Law, it was found that the minimum particle size expected to separate into the pellet at 500 x g for 5 minutes was approximately 630 nm. There is very little agreement in the literature about centrifuging techniques with values including 10000 x g for 5 minutes, 1600 x g for 10 minutes and 200 x g for 5 minutes (Ferri et al., 2021; Lea-Banks et al., 2019; Xiang et al., 2019). This diversity of opinion in the literature is likely due to many reasons. One is the difference in production methods used, which may result in different objectives in the centrifugation process. For example, those using the sonication process may be attempting to remove larger nanodroplets or attempting to remove the lipid micelles produced in the process. For those using the condensation process, however, the aim is likely to remove the microbubbles that have not condensed into nanodroplets. Many papers simply refer to

this as a "wash" process without expanding on exactly what is being removed, and so it is difficult to ascertain which process is most suitable (Xiang et al., 2019). Additionally, there is some hesitance about using too fast or too long a centrifugation process due to their metastable nature, making it relatively easy for them to be destroyed (Sheeran et al., 2017). For this reason, centrifugation may not be the most appropriate method for separating out the larger nanodroplets. Filtering the nanodroplets is another possible method for removing any larger, unwanted nanodroplets. Two possible filters were used: a 0.45 µm pore filter and a 0.2 µm pore filter. The results showed that both filters were effective in reducing the average size of the distribution, however, surprisingly there was no significant difference observed between the two filters. This suggests that the larger droplets are mostly larger than 0.45 µm, suggesting a distinct larger group that is being formed along with the nanodroplets. Given this similarity between the 0.2 µm and 0.45 µm filters, the 0.45 µm filter is preferable as the pressure difference across the filter membrane is likely to be less and, therefore, less destructive to the nanodroplets.

3.4.12 | Gas Loading and Stability

Despite extensive research into nanodroplets for oxygen delivery for tumour and blood substitutes (Castro, Briceno, 2010; Krafft, Riess, 2021; Rapoport, 2016) there is a distinct lack of work into the effect of gas-loading on the nanodroplet stability. Gas loading did not seem to affect nanodroplet characteristics as measured using NTA in Figure 3.16 or have much of an effect on the particle distribution seen in Figure 3.17 and the associated change in median diameters and concentrations seen in Figure 3.18. This implies that gas loading does not affect the stability of the particles immediately after loading or 24 hours later.

3.4.13 | Perfluorocarbon Oxygen Release

Direct measurement of oxygen concentration in perfluoropentane or nanodroplets was not possible due to interactions with the oxygen sensor. However, measurements of the oxygen release from perfluoropentane to water was possible due to the phase separation between the two. It was found that the oxygen concentration in the water decreased with the addition of 1 mL of air-saturated PFP. It is important to note, however, that due to the significantly higher solubility of oxygen in PFP, the total oxygen

in the system will have significantly increased (Jägers et al., 2020). Upon the addition of oxygen-saturated PFP, the concentration of oxygen in the water steadily increased over a 2 hour period. As a nanodroplet, the surface area of the perfluorocarbon will be significantly increased, resulting in much faster oxygen release when moving from areas of high to low oxygen tension.

3.5 | Conclusion

In summary, precise control over the nanodroplet formulation process is necessary for reproducible nanodroplet production. Good control over the process may also allow for more precision over nanodroplet size which will affect characteristics such as acoustic vaporisation threshold or the ability to remain undetected by the immune system. The concentration of PFP was found to have the most significant effect on nanodroplet size with tip-height affecting the strength of that correlation. To the author's knowledge this is the first attempt to control and specify the immersion depth of the tip in nanodroplet production. Nanodroplet concentration was also affected by certain parameters with increasing PFP concentration leading to a decrease in nanodroplet concentration and increasing sonication amplitude leading to a decrease. Gas-loading did not have a significant effect on stability, but storage temperature did, with indications of increased instability at $37^{o}C$. However, this may be a positive outcome as it suggests the nanodroplets are more sensitive to ultrasound *in vivo*.

4

Nanodroplet Interaction with Osteoblastic Cells

4.1 | Introduction

Osteoblasts are bone-forming cells; their function and differentiation is discussed in depth in section 1.3.1.1. Breifly, their main function is laying down new bone material in the form of organic bone matrix like collagen, as well as inorganic components such as calcium phosphate in the form of hydroxyapatite. Moreover, they are implicated in the secretion of cytokines to regulate bone homeostasis (Mizoguchi, Ono, 2021). Osteoblasts are of mesenchymal lineage; whereby mesenchymal stromal cells can be isolated from the bone marrow. Osteoblasts have three probable cell fates: remaining quiescent on the bone surface, getting trapped within the bone matrix and becoming osteocytes or apoptotic (Franz-Odendaal et al., 2006). Given the necessity for osteoblastic activity in bone formation, understanding how nanodroplets interact with cells of osteoblastic lineage is key to investigating their potential use in bone repair.

Nanodroplets are generally considered biocompatible. The constituent parts of the formulation used in this research are PFP, PEG(40)s and DSPC. PFP is inert and so it is not expected to have any negative effects on the body (Riess, 2005). PEG(40)s and DSPC have been used in previously approved medicines, more recently the Covid-19 vaccines (Borgsteede et al., 2021). Previous clinical trials of perfluorocarbon nanodroplets of different chemical composition have been performed, but none currently have FDA approval due to financial and storage complications (Castro, Briceno, 2010).

There is a plethora of literature researching the cytotoxity of nanodroplets in tumour delivery systems. There is, however, a lack of literature specific to bone cells. PEG is a non-toxic, non-immunogenic, FDA approved polymer. As such, it has been investigated to improve the stability and biocompatibility of materials intended for use internally. Previous studies on microbubbles performed by Upadhyay et al. found that immunogenicity was significantly reduced in PEGylated BSA nanodroplets as opposed to non-PEGylated BSA nanodroplets (Upadhyay et al., 2017). This suggests that PEG significantly contributes to a more bioinert structure.

The overarching aim of the work presented in this chapter was to investigate whether nanodroplets are capable of promoting osteoblastic activity to aid with bone repair or at the very least are not detrimental to osteogenic activity in cells of an osteoblastic lineage.

This chapter was, therefore, composed with the following aims in mind:

- To establish a suitable range of concentrations of nanodroplets for investigating nanodroplet-osteoblast interactions;
- To elucidate the effect of nanodroplets on osteoblastic cell viability;
- To establish the impact of both gas-loaded and non-loaded nanodroplets on hypoxic markers within osteoblastic cells;
- To evaluate the effect of nanodroplets on both early and late-stage osteogenic markers;
- To explore if there is a strong physical association between nanodroplets and BMSCs.

4.2 | Methodology

The research in this chapter focused on the effect of nanodroplets on cells of an osteoblastic lineage in both normoxia and hypoxia. Details of media composition, including osteogenic and basal media, can be found in section 2.8.1. Cell culturing techniques between experiments are detailed in section 2.8.4. Following the results of the previous chapter, nanodroplets used in cell culture experiments were produced using 40 μL of PFP in 800 μL of lipid suspension with a 90s pulsed (2s on 15s off) sonication at 60% amplitude with the sonicator placed 12 mm from the bottom of the 1.5 mL Eppendorf tube. The effect of these nanodroplets and their constituent parts on the metabolic activity of the osteoblastic cells was investigated *in vitro* in both normoxia and 2% hypoxia using the Alamar blue assay detailed in section 2.9.1. To verify whether the effects observed using Alamar blue were due to a change in individual cell metabolic activity or the number of cells, the proliferation of the osteoblastic cells was also quantified using picogreen and 4',6-diamidino-2-phenylindole (DAPI) staining as detailed in sections 2.9.2.2 and 2.9.2.1, respectively. After establishing that the nanodroplets were not cytotoxic, the effect of the nanodroplet on BMSC activity and differentiation was investigated using an ALP enzymatic assay at day 14 (section 2.12.1) and Alizarin red staining at day 21 of culture (section 2.12.2). To verify whether the nanodroplets are altering hypoxic cell signally, a western blot was performed (section 2.10) to determine HIF-1α expression. The results of this were validated using a VEGF ELISA as detailed in section 2.11. Finally, any cell-nanodroplet interactions were visualised using confocal fluorescence microscopy (section 2.15).

4.3 | Results

4.3.1 | Effect of Varying Nanodroplet Concentration on Metabolism in MC3T3E1s

Before any *in vitro* experiments could be performed, a suitable range of nanodroplet concentrations to be investigated needed to be established. To establish a suitable range, the effect of a large range of nanodroplet concentrations on cell metabolism was measured using an Alamar Blue assay. For initial experiments, MC3T3E1 cells (a pre-osteoblastic murine cell line) were used for their osteoblast like properties and their ease of use. A biphasic response was observed with an increasing trend between 10^{-5} and 10^{-3} % v/v and a decreasing trend between 10^{-2} and 10^{0} % v/v. There were significant increases from the 0% nanodroplet control at 10^{-4} - 10^{-2} % v/v (Figure 4.1, P=0.0003, 0.0003 and 0.0062 respectively). Three nanodroplet concentration values, namely 0.01, 0.1 and 1 % v/v, were selected for further experimentation.

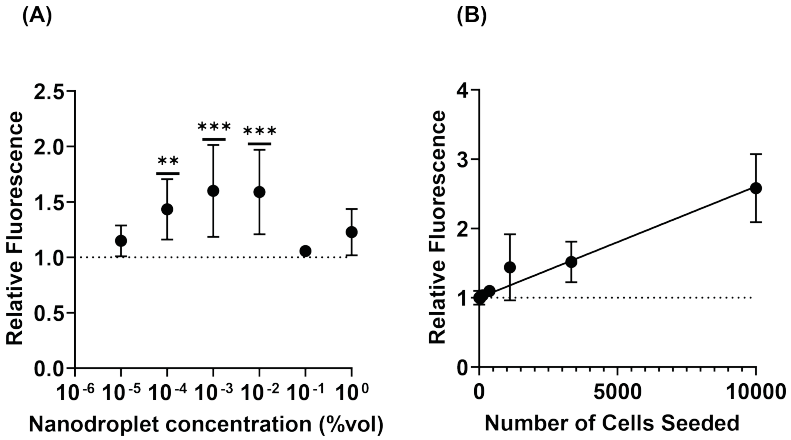

Figure 4.1: Nanodroplets had a biphasic effect on MC3T3E1 metabolic activity. Metabolic activity of MC3T3E1 as measured using Alamar Blue fluorescence following 24-hour exposure to PFP nanodroplets. The fluorescence relative to the no treatment control for (A) nanodroplet concentration up to 1 % v/v seeded with 5000 cells per well. (n=6) (B) shows the relative fluorescence for an increasing number of cells per well (R^2 = 0.9964). The control group without nanodroplets is represented by the dashed line in both graphs. Error bars represent the standard deviation.

4.3.2 | Metabolism of Different Osteoblastic Cells Treated with Nanodroplets

To determine whether the increase in metabolism observed in Figure 4.1 was specific to MC3T3E1s, the metabolism was investigated using an Alamar Blue assay in three different cell types: MC3T3E1 (a murine preosteoblastic cell line), Saos-2 (a human osteosarcoma cell line) and BMSC (primary human bone marrow stromal cells from consenting patients undergoing hip replacement surgery). It was found that nanodroplet treatment had no significant effect on cell metabolism in Saos-2s and BMSCs; however, one nanodroplet concentration, 0.01%, significantly increased the metabolism in MC3T3E1s only (Figure 4.2).

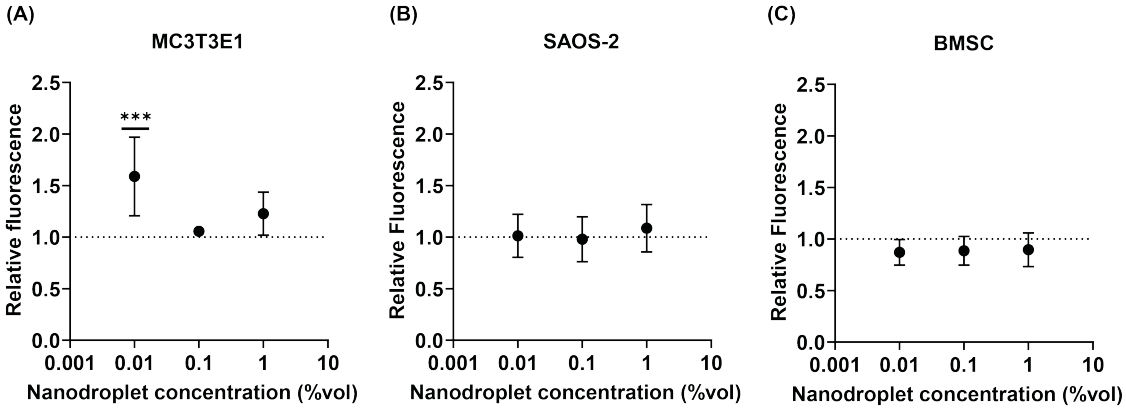

Figure 4.2: Nanodroplets only affect osteoblastic cell metabolism in MC3T3E1 cells; Saos-2 and BMSC metabolic activity was unaffected by nanodroplet treatment. Cell metabolism following a 24 hour nanodroplet exposure as measured using Alamar Blue in (A) a murine preosteoblastic cell line (MC3T3E1), (B) a human osteosarcoma cell line (Saos-2) and (C) primary human bone marrow stromal cells (BMSC) all with n=6. The 0% nanodroplet control is represented by the dashed line. Error bars represent the standard deviation.

The amount of cell metabolism measured could be a result of changes in cell number or in individual cell metabolism. To provide a more comprehensive understanding of the effect of nanodroplets on cell viability, the effect of nanodroplets on cell proliferation was measured by quantifying DNA concentration in BMSC measured using a Picogreen assay. In the samples where the higher concentrations were tested (0.1 and 1 % v/v) significantly higher DNA concentrations were observed (Figure 4.3).

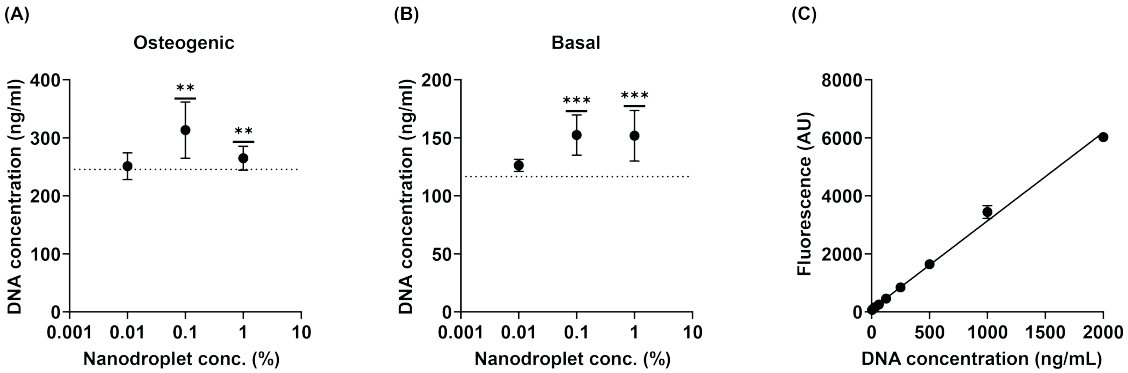

Figure 4.3: DNA concentrations in osteogenic and basal conditions increased with nanodroplet exposure. DNA concentration as measured using Picogreen fluorescence in human bone marrow stromal cells (BMSC) grown in (A) osteogenic and (B) basal media (n=3). (C) A DNA standard curve of Picogreen (R^2 = 0.9954). Dashed line represents the no treatment control. Error bars represent the standard deviation.

A more direct approach was then taken to quantify cell proliferation. Growth curves for MC3T3E1s and Saos-2s were obtained by counting the nuclei in images obtained from fixed cells at 24 hour intervals for 96 hours. To determine the effect of nanodroplets on cell proliferation, the rate of increase of the number of nuclei was considered. This was not possible in BMSCs as they proliferate much more slowly and so obtaining a suitable growth curve was difficult. In MC3T3E1s, 0.1% v/v nanodroplets were found to increase proliferation (P<0.0001 at 96 hours), while 1% v/v had the opposite effect (P<0.0001 at 96 hours; Figure 4.4A). In Saos-2s no significant differences were observed (Figure 4.4B).

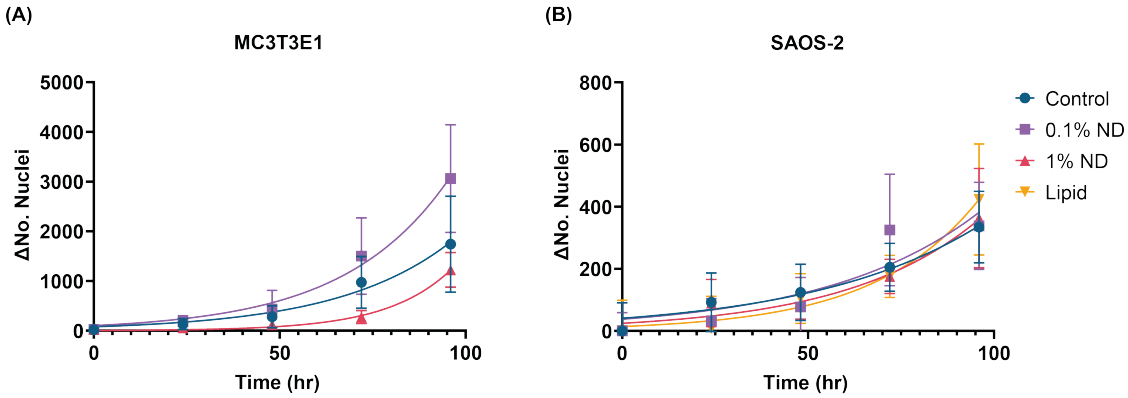

Figure 4.4: Nanodroplet treatment had a dose-dependent effect on MC3T3E1 proliferation but no effect on Saos-2 proliferation. The number of nuclei counted using DAPI staining of the nuclei in (A) MC3T3E1 cell line (n=9) and (B) Saos-2 cell line (n=4). Error bars represent the standard deviation.

To determine whether any effects were due to the nanodroplets or their individual constituents, an Alamar Blue assay was performed (Figure 4.5). There was no significant difference between the 0% nanodroplet control and any of the test groups.

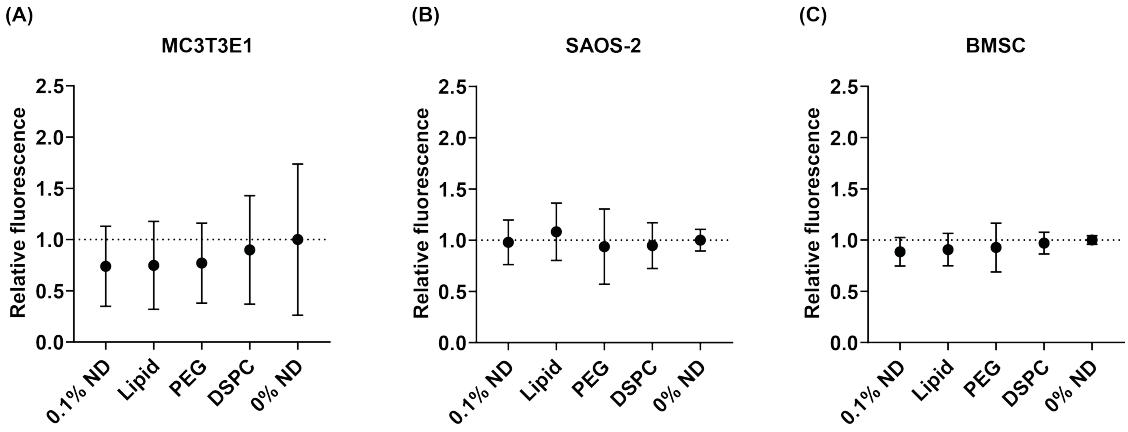

Figure 4.5: osteoblastic cell metabolism was not affected by nanodroplet treatment or their constituents. Cell metabolism as measured using Alamar Blue in (A) MC3T3E1 cell line, (B) Saos-2 cell line and (C) primary BMSC treated with nanodroplets, lipid and the lipid constituents all at 0.1% v/v concentration (n=6 for all cell types). Dashed lines represent the no treatment control. Error bars represent the standard deviation.

4.3.3 | Viability of Osteoblastic Cells in Hypoxia

To test the hypothesis that hypoxia negatively impacts viability in cells of an osteoblastic lineage, the viability of BMSC cultured in both osteogenic and basal media (to represent more differentiated and undifferentiated cells, respectively) was measured when grown in both normoxic and hypoxic conditions for 14 days. This was done by assessing the DNA concentration using a Picogreen assay (Figure 4.6). Hypoxia caused a significant decrease in DNA concentration on osteogenic BMSCs but had no effect on basal BMSCs (n=5).

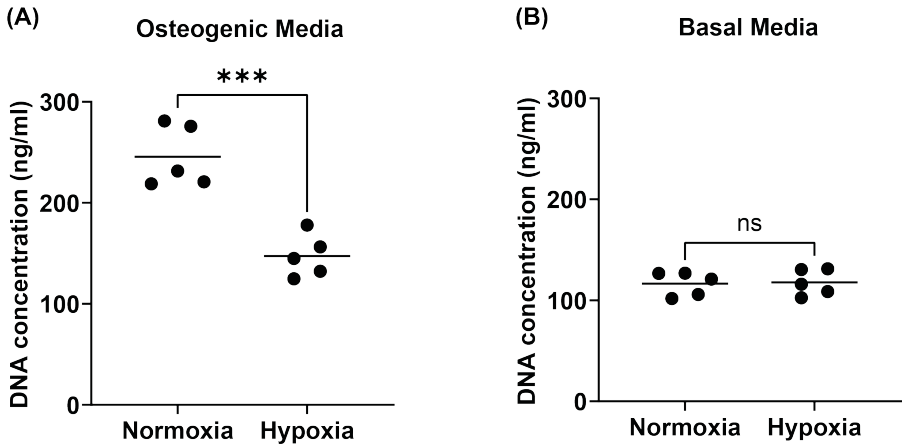

Figure 4.6: Hypoxia decreased BMSC DNA concentration in the presence of osteogenic supplements but not without. DNA concentration as measured using Picogreen (day 14) in BMSC grown in (A) osteogenic media and (B) basal media grown in normoxia and hypoxia for the duration of the experiment (n=5). ***p<0.001

To determine whether nanodroplets could relieve the effects induced by hypoxia observed in Figure 4.6, the experiments were repeated with nanodroplet treatment concurrent with hypoxic exposure. A nanodroplet concentration of 0.01% v/v was found not to have any significant effects on BMSC DNA concentration (Figure 4.7A,B). A greater nanodroplet concentration of 0.1% v/v was found to significantly increase DNA concentration in both osteogenic and basal media. The highest nanodroplet concentration tested (1% v/v) was found to decrease DNA concentration in osteogenic media only.

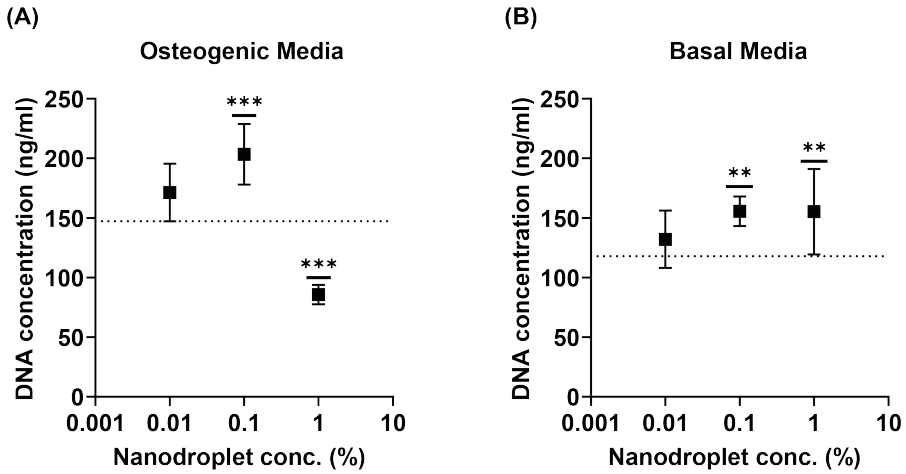

Figure 4.7: Nanodroplets had a dose-dependent effect on BMSC DNA concentration in hypoxia. DNA concentration as measured using Picogreen in hypoxic BMSCs grown in (A) osteogenic media and (B) basal media (n=5). **p<0.01, ***p<0.001. The dashed line represents the no treatment control and error bars represent the standard deviation.

To verify that short term hypoxic exposure affects metabolism in early stage BMSCs, an Alamar Blue assay was also performed on BMSCs grown in basal media to measure metabolism (Figure 4.8A) following 24 hours of hypoxic exposure. The metabolism significantly increased with hypoxic exposure. Nanodroplets were added to investigate whether they were capable of reversing this hypoxia-induce effect. Metabolism was not significantly affected in any treatment group although it is noted that there is a slight downward trend (Figure 4.8).

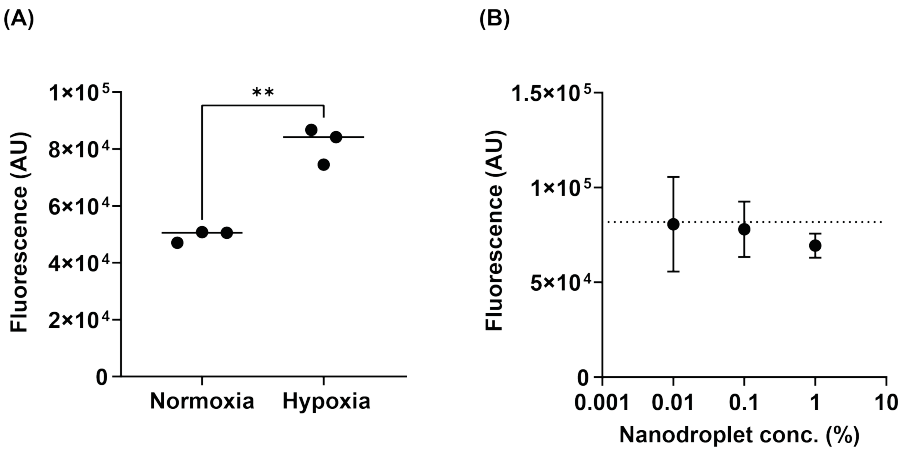

Figure 4.8: Cell metabolism increased in the presence of hypoxia which was unaffected by nanodroplet treatment. Cell metabolism measured using Alamar Blue for BMSCs cultured in (A) normoxia and hypoxia (day 3) and (B) in normoxia with different nanodroplet concentrations (N=3, n=6). Error bars represent the standard deviation and the dashed line represents the no treatment control.

To establish whether loading the nanodroplets with gas (specifically oxygen and nitrogen) affected the BMSC metabolism, an Alamar Blue assay was performed on BMSCs grown in basal media under normoxic and hypoxic conditions. There was no significant difference from the no nanodroplet control in both normoxia (Figure 4.9A) and hypoxia (Figure 4.9B).

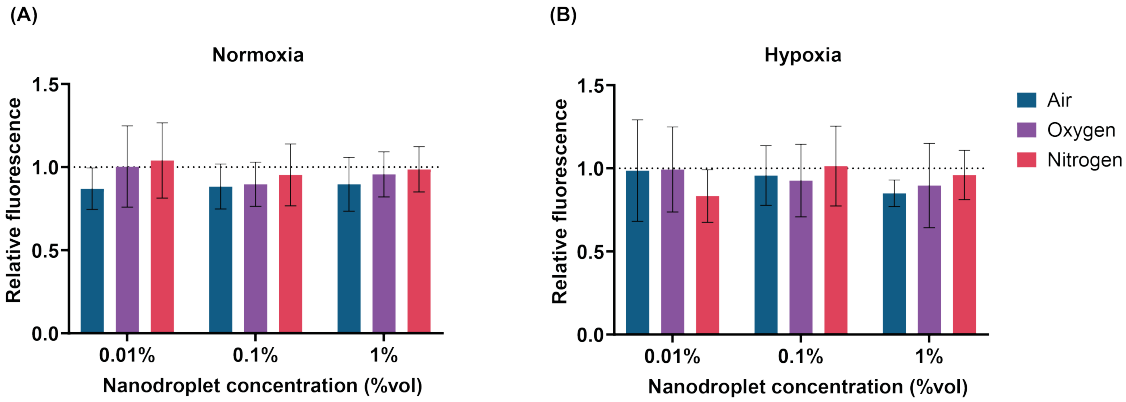

Figure 4.9: Gas-loaded nanodroplets have no significant effect on BMSC metabolism. Cell metabolism in primary human bone marrow stromal cells (BMSC) treated with nanodroplets loaded with air, oxygen and nitrogen as measured using Alamar Blue fluorescence (N=3, n=6). The 0% nanodroplet control is represented by the dashed line. Error bars represent the standard deviation.

4.3.4 | HIF-1α and VEGF Expression in Nanodroplet Treated Hypoxic Cells

HIF-1α degrades in the presence of oxygen. As such, a decrease in HIF-1α expression is indicative of an increase in oxygen tension. To test the hypothesis that nanodroplets are capable of relieving hypoxic stress, HIF-1α concentration was measured using western blotting. Figure 4.10A demonstrates a representative image of a western blot with a clear band at the DMOG positive control as well as a clear increase in HIF-1α expression in hypoxia compared to normoxia. This was quantified using densiometry in Figure 4.10C, demonstrating a decrease in HIF-1α concentration in hypoxia following nanodroplet treatment. These results were compared with VEGF expression measured using an ELISA. VEGF is further downstream to HIF-1α and so is less sensitive to hypoxia as there are more factors affecting its expression. The results of the VEGF enzyme-linked immunosorbent assay (ELISA) can be seen in Figure 4.10D. The ELISA measured no significant differences between the experimental groups with the exception of DMOG which was significantly higher than all other groups ($P<0.0001$ in all cases). Cells treated with gas-loaded nanodroplets were also investigated for HIF-1α expression (Figure 4.10B). HIF-1α expression was only found to decrease in the presence on air-saturated nanodroplets and no significant change in HIF-1α concentration was observed with oxygen and nitrogen-loaded nanodroplets.

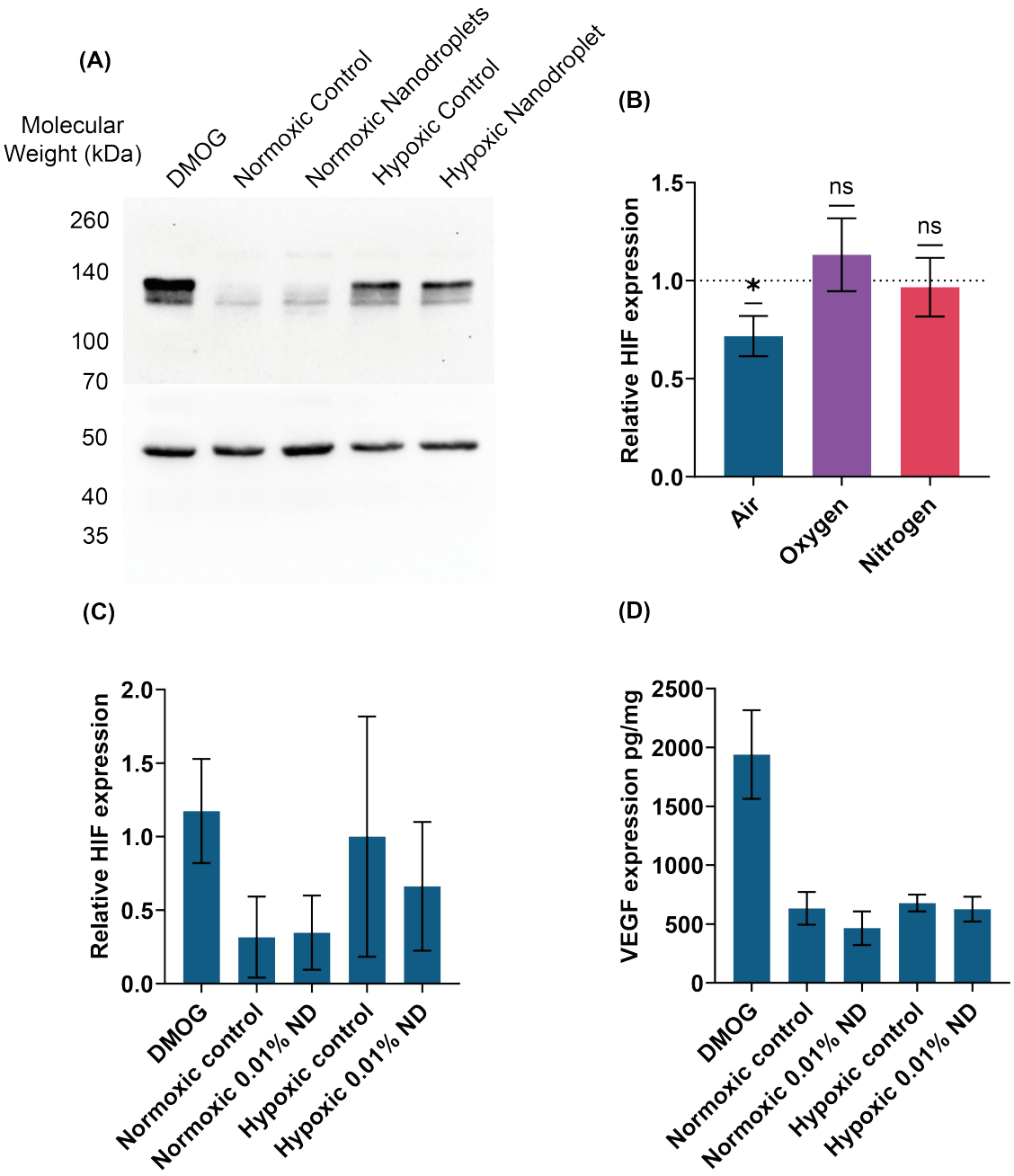

Figure 4.10: Air-saturated nanodroplets decrease HIF-1α expression in Saos-2s cultured in hypoxia. HIF-1α expression in Saos-2 cells as measured using western blotting. (A) gives a representative image of the blot with the HIF-1α band at 120 kDa and the housekeeping protein β-actin band at 42 kDa. (B) shows the HIF-1α expression in hypoxia quantified using densiometry with the no treatment hypoxic control represented by the dashed line. The individual groups for the air-loaded nanodroplets have been quantified using densiometry in (C) and supernatant from the same samples was collected and a VEGF ELISA performed (D) (N=3).Error bars represent the standard deviation, *p<0.05.

4.3.5 | Mineralisation in Bone Marrow Stromal Cells Treated with Nanodroplets

Alizarin red staining can be used to visualise calcification. It indicates that fully differentiated osteoblasts are actively producing mineralised matrix. To test the hypothesis that nanodroplets stimulate osteoblast activity, BMSCs were cultured with various concentrations of nanodroplets (0, 0.01, 0.1 and 1% v/v) or a lipid control for 21 days in both osteogenic and basal media under both normoxic and hypoxic conditions and stained with Alizarin red. Representative images of the resulting stain can be seen in Figure 4.11. Visually, it is very clear that 0.1% v/v nanodroplet treatment caused an increase in bone cell mineralisation in the presence of osteogenic supplements (Figure 4.11). This was especially the case in normoxia.

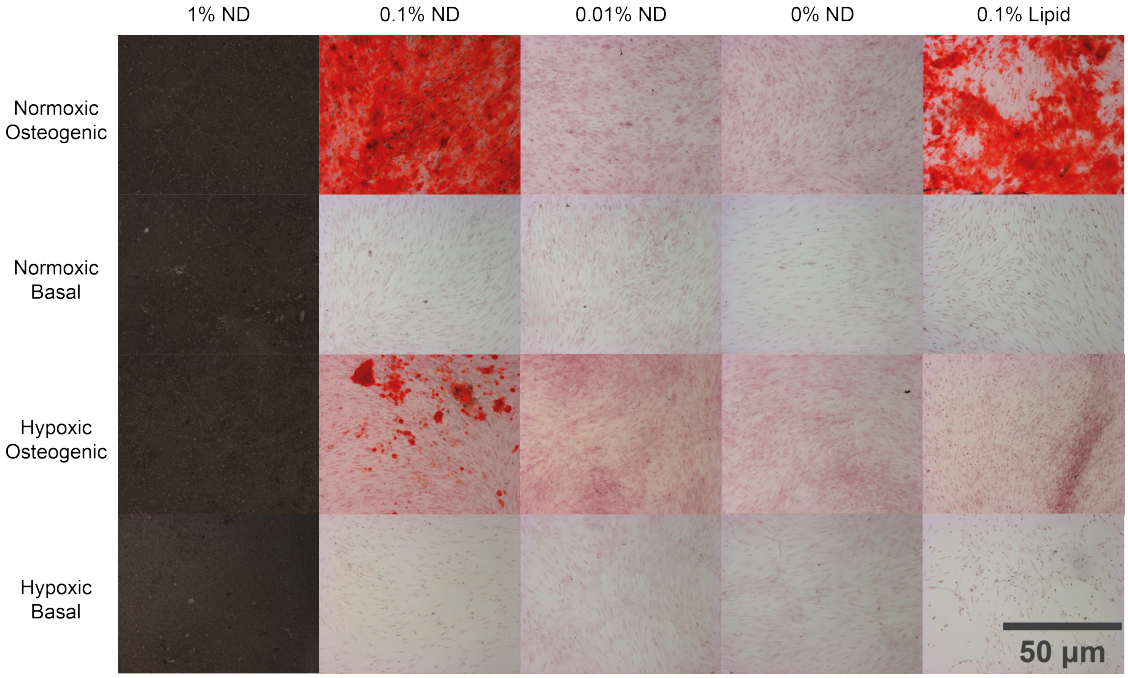

Figure 4.11: Nanodroplets cause a visible increase in mineralisation when stained using Alizarin red. Alizarin red staining representative images under a 10x objective in BMSC (Male, 77) following 21 days of culture with nanodroplets exposure and normoxic or hypoxic conditions throughout. Nanodroplets in 1% nanodroplets remained attached to the surface, obscuring the image and so were not quantified.

This was repeated in five separate patients to account for any patient-to-patient variation (F75, M77, M78, F77 and F56). The normoxic osteogenic and basal no

treatment controls can be regarded as positive and negative controls, respectively. To ensure that the Alizarin red stain had worked as expected, the intensity of the stain in these control groups was quantified using CellProfiler (Carpenter et al., 2006). Two patients (M78, F77) did not have significant differences between osteogenic and basal groups (represented by the red lines in Figure 4.12) and so were rejected for any further analysis. (F75: P<0.0001, M77: P=0.0071, M78: P=0.1741, F77: P=0.0536, F56: P=0.0035)

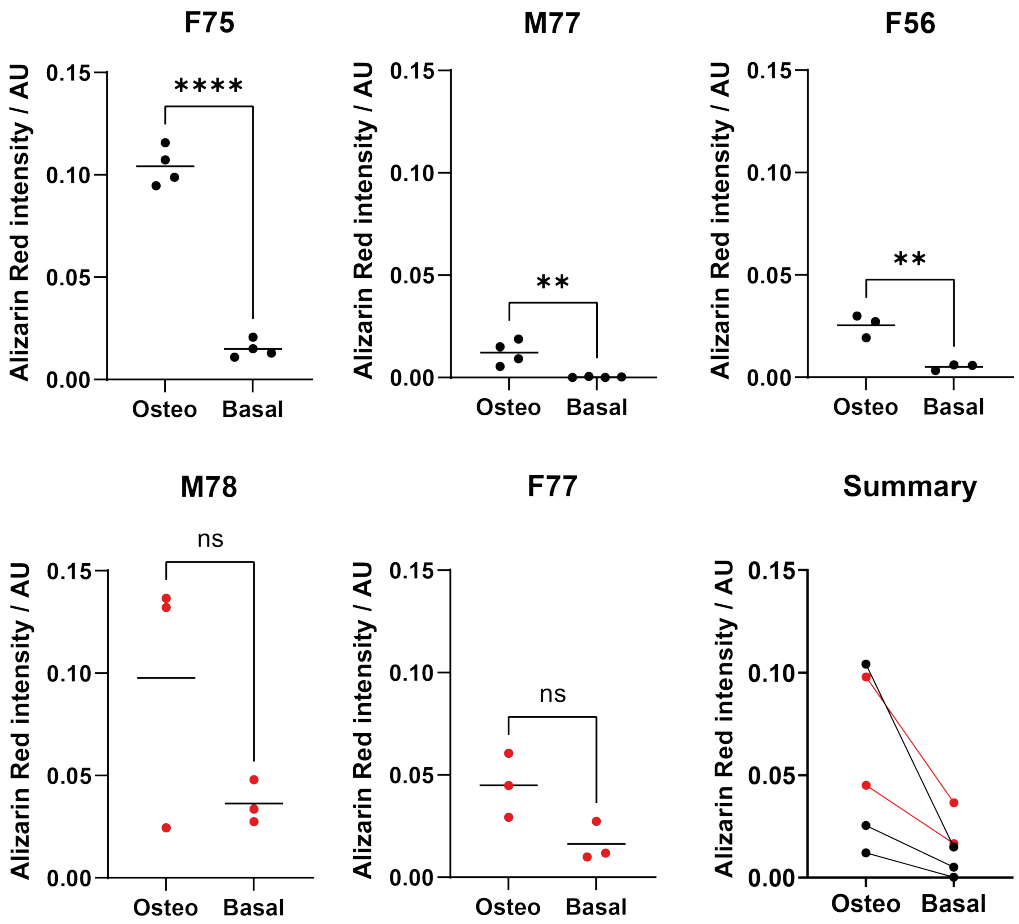

Figure 4.12: There was not a consistent increase in calcium deposition in the presence of osteogenic supplements. Results where these controls were not significantly different were rejected as anomalous. Alizarin red stain intensity in cells cultured in normoxia with both osteogenic and basal media with BMSCs isolated from five separate patients. Patients displayed in red showed non-significant differences between the positive and negative control and so were rejected from further comparisons. (N=5, n=4), **p<0.01, ****p<0.0001.

To investigate the effect that hypoxia has on the calcification of BMSCs, Alizarin red staining intensity was quantified in BMSCs grown in both osteogenic and basal media for 21 days in normoxia or hypoxia. There were no significant differences between normoxia and hypoxia in either case (Osteogenic: P= 0.9943, Basal: P=0.1205). Still, the basal group did consistently result in an increase in calcification in hypoxia compared to normoxia (Figure 4.13).

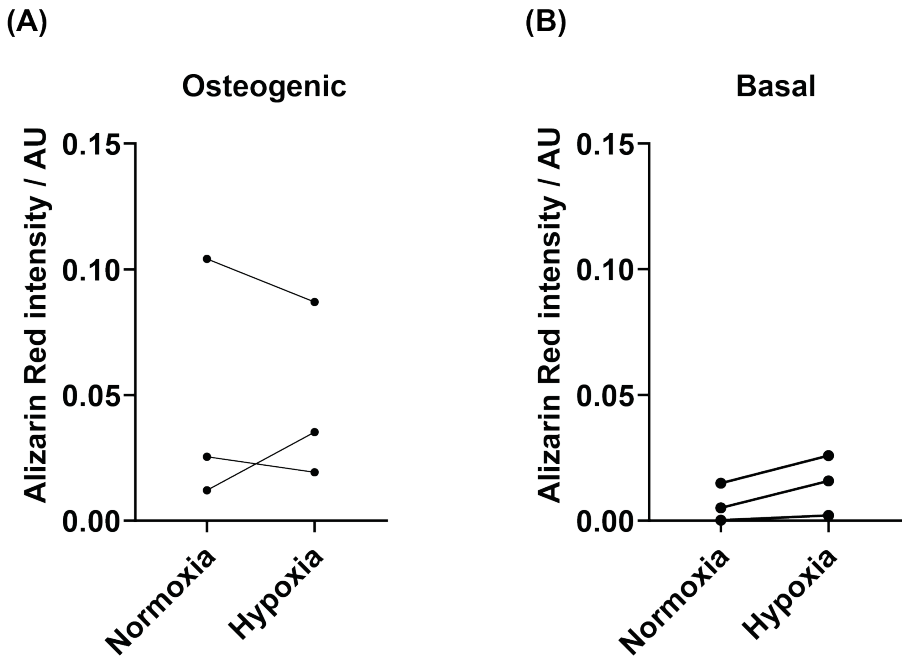

Figure 4.13: Calcium deposition was not significantly affected by hypoxia. Alizarin red staining intensity in BMSC for three patients cultured in normoxia or hypoxia for the duration of the 21 day culture. (N=3, n=4).

There was a very significant patient-to-patient variation in Alizarin red staining intensity and so patients have been plotted separately. To establish whether nanodroplets affect the osteoblastic activity, the staining intensity in the 0.1% nanodroplet treatment groups was quantified and compared with the values from the no treatment control as well as the 0.1% lipid group, to ensure any effect is from the nanodroplets and not from the lipid shell. 0.1% v/v nanodroplet treatment was found to significantly increase Alizarin red intensity in BMSCs grown in osteogenic media in two patients and an increase can be seen in the third (Figures 4.14A-C). Lipid treatment of the same concentration was also found to increase alizarin red staining intensity

significantly in the same two patients but to a lesser extent than the nanodroplet treatment. The same trend was observed in a third patient, although not statistically significant. A similar trend was also observed in BMSCs grown in basal media but to a much less significant extent (Figures 4.14D-F).

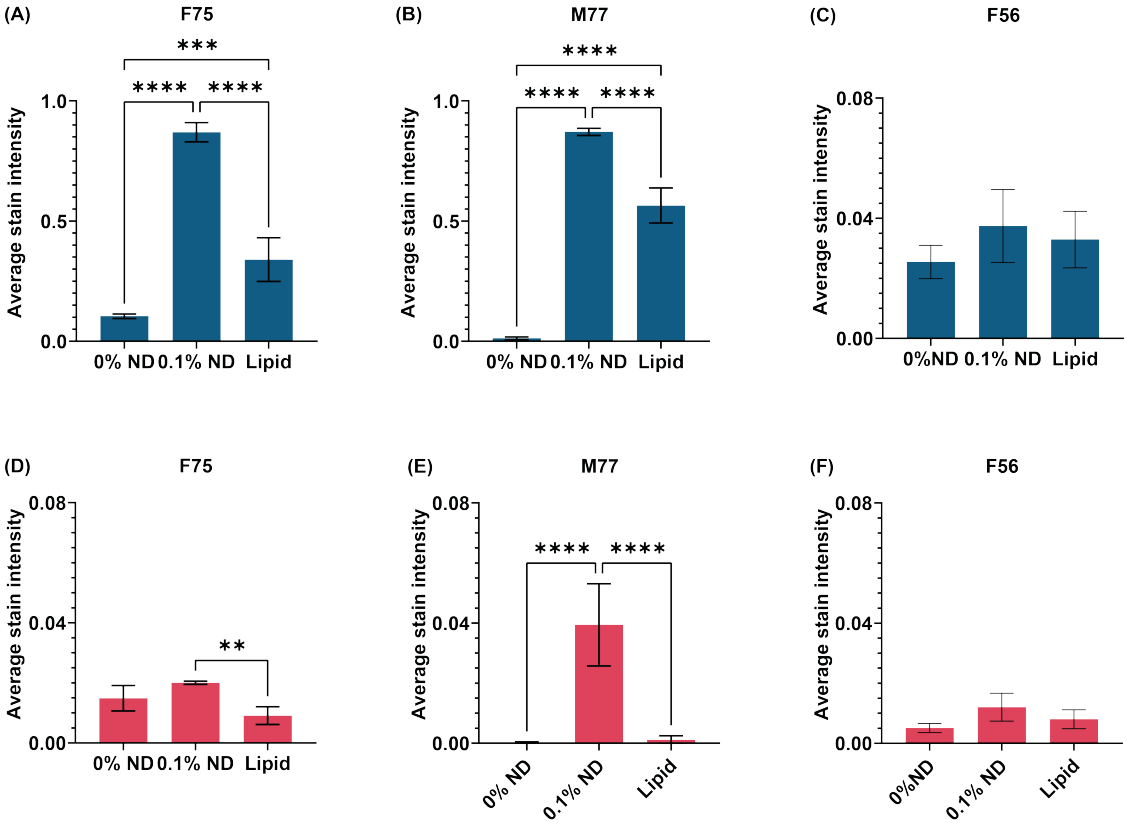

Figure 4.14: BMSC mineralisation is significantly increased by nanodroplet treatment. Alizarin red staining intensity quantified using CellProfiler in BMSC cultured at confluence for 21 days in normoxia with (A-C) osteogenic media and (D-F) basal media (N=3, n=4). Error bars represent the standard deviation, **p<0.01, ***p<0.001, ****p<0.0001.

To test the hypothesis that this increase in mineralisation occurs regardless of oxygen tension, the same experiment was repeated in hypoxia. While the results are mostly statistically non-significant, a similar although weaker trend to that seen in normoxia was observed (Figure 4.15).

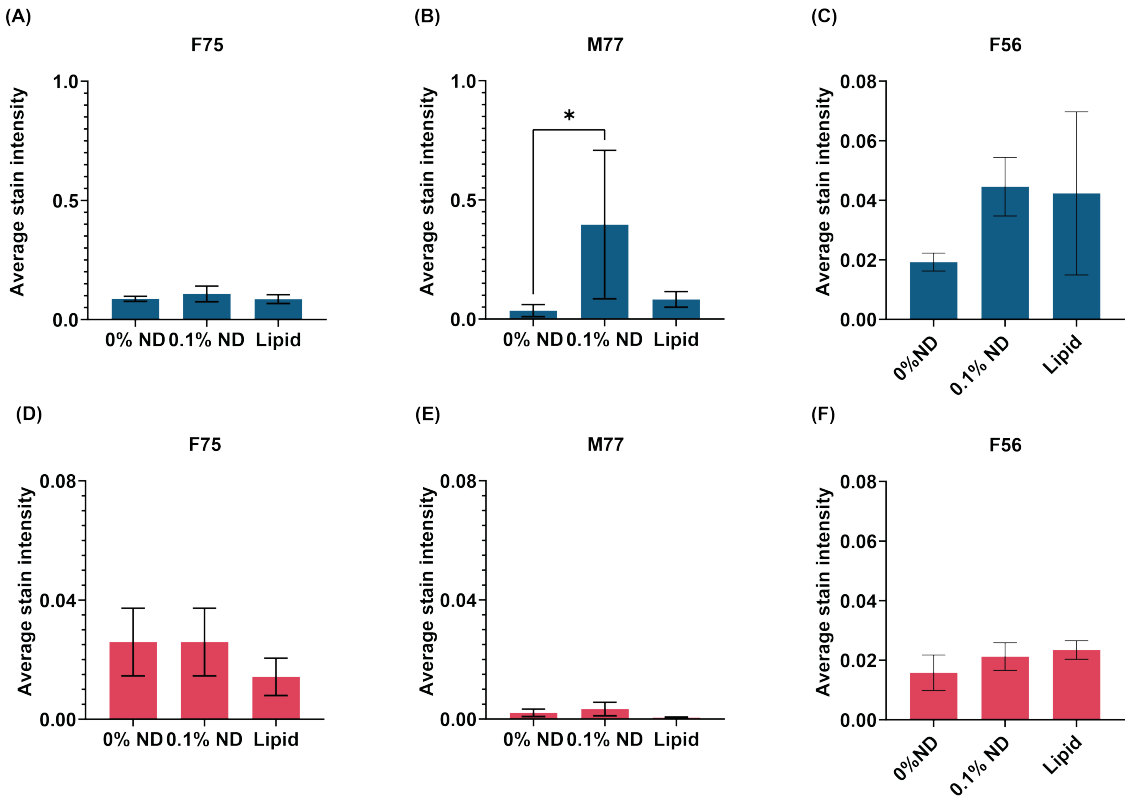

Figure 4.15: Nanodroplet treatment increased BMSC mineralisation in hypoxia but to a much lesser extent than in normoxia. Alizarin red staining intensity quantified using cellProfiler in BMSC cultured at confluence for 21 days in hypoxia with (A-C) osteogenic media and (D-F) basal media(N=3, n=4). Error bars represent the standard deviation, *p<0.05.

To test for any non-cellular effects where nanodroplets may facilitate calcium deposition through means other than stimulating osteoblasts, a 24 well plate was treated to have a collagen coating and exposed to either nanodroplets in osteogenic media or BMSC cell-conditioned ostegenic media (without any cells present) and then stained using alizarin red after 21 days. Under microscope examination, it is clear that mineralisation did not occur under these conditions (Figure 4.16).

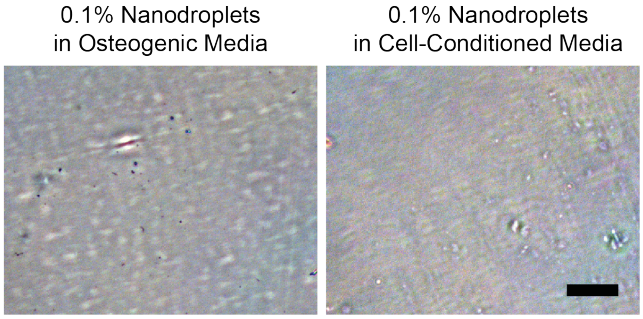

Figure 4.16: There was no evidence of nanodroplets causing indirect mineralisation. Alizarin red stained representative images under a 10x objective in collagen coated plates stained treated with 0.1% v/v nanodroplets in either normal osteogenic media (left) or cell conditioned media (right) for 14 days with the media changed every three days. Scale bar: 50 μm

4.3.6 | Alkaline Phosphatase Expression in Bone Cells Treated with Nanodroplets

Calcification is a late-stage marker for osteogenesis. Alkaline phosphatase (ALP) enzyme is indicative of immature osteoblast activity. In an enzymatic assay, a very significant difference between BMSCs cultured for 14 days in osteogenic and basal media without nanodroplet treatment was observed (Figure 4.17; P<0.0001, n=6).

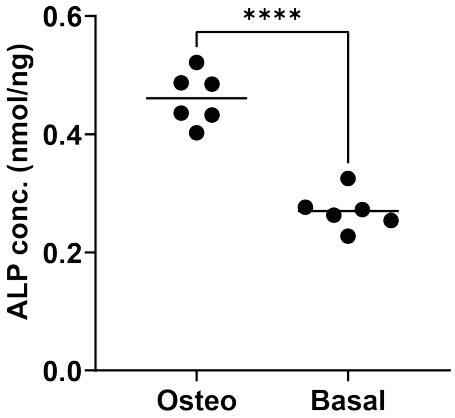

Figure 4.17: ALP expression increased in the presence of osteogenic supplements. ALP enzymatic activity in BMSC grown with osteogenic and basal media for the duration of the 14 day culture (n=6). ****p<0.0001.

ALP activity was more sensitive to hypoxia than calcification with significant decreases in ALP activity observed in both osteogenic and basal media (Figure 4.18; P<0.0001 and P= 0.3685 respectively).

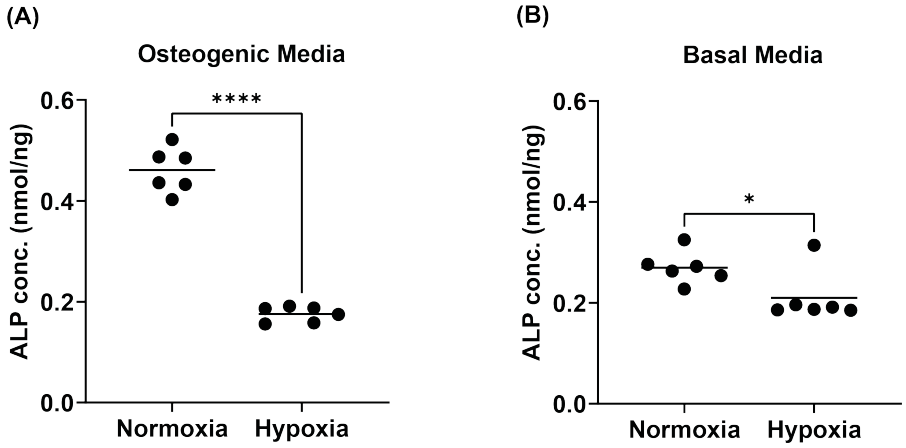

Figure 4.18: ALP enzymatic activity decreases in the presence of hypoxia. ALP expression in BMSC grown in normoxia and hypoxia for the duration of the 14 day culture with (A) osteogenic and (B) basal media (n=6). *p<0.05, ****p<0.0001.

In contrast to the findings observed with Alizarin red staining, treatment with nanodroplets and the lipid control appears to diminish ALP activity increasingly with time (Figure 4.19A), with a significant decrease by day 14 (nanodroplets: P=0.0069, lipids: P=0.0255). At day 14, 1% v/v nanodroplets significantly decreased ALP activity in all conditions compared to the no treatments control (Figure 4.19; normoxic osteogenic: P<0.0001, hypoxic osteogenic: P=0.0194, normoxic basal: P=0.0001, hypoxic basal: P<0.0001). For the 0.01 and 0.1% v/v treatment groups, a significant decrease was only observed in the normoxic osteogenic group (P=0.0005 and P=0.0002 respectively).

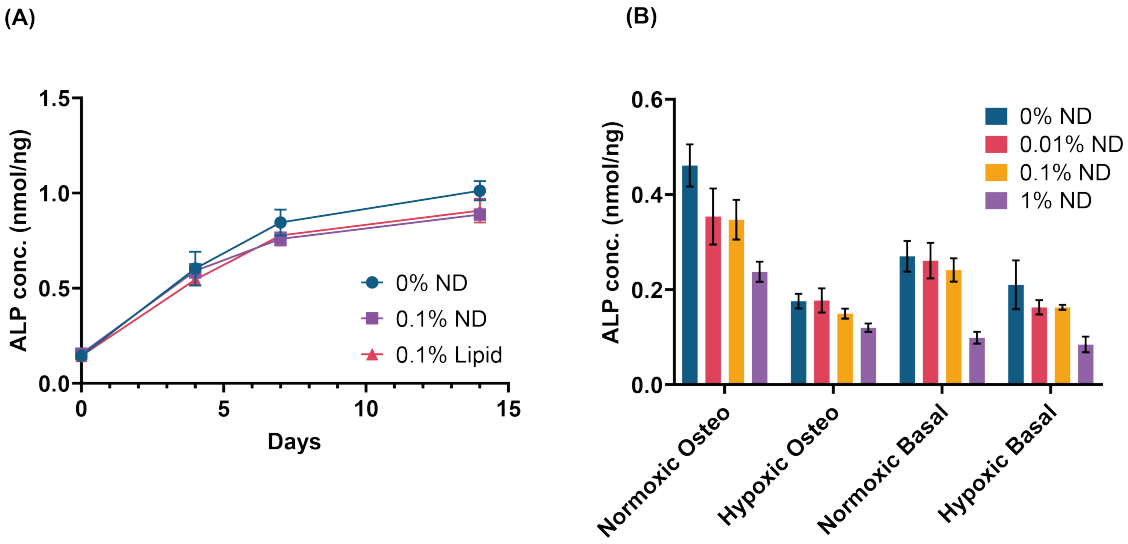

Figure 4.19: Nanodroplet treatment decreases ALP enzymatic activity in all culture conditions. ALP expression at (A) 0, 4, 7 and 14 days in BMSC and (B) nanodroplet treatment in normoxic and hypoxic conditions with and without osteogenic supplements at day 14 (n=6). Error bars represent one standard deviation.

4.3.7 | Nanodroplet Bone Marrow Stromal Cell Association

To establish whether nanodroplets associate with BMSCs, confocal microscopy was used to visualise potential interactions. Nanodroplets can be made fluorescent with the addition of DiO to the lipid film. Although nanodroplets are below the resolution of normal microscopy techniques; accumulation and agglomeration of fluorescent nanodroplets can still be observed. BMSCs were treated with 0.1% v/v fluorescent nanodroplets (green) before being fixed with PFA and the nuclei stained with DAPI and the cell membrane stained with CellTracker deep red. Nanodroplets were observed to accumulate into larger clumps but these, in general, did not seem to be associated with the BMSCs (Figure 4.20).

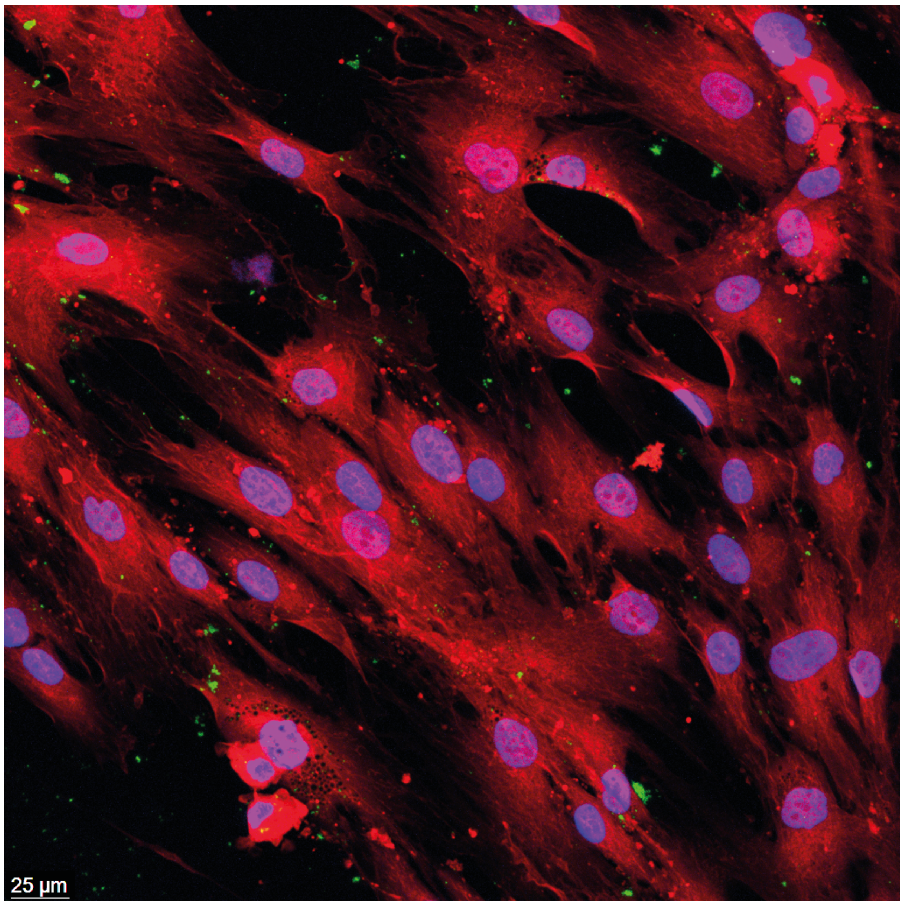

Figure 4.20: Nanodroplets do not strongly associate with BMSCs. Single, representative, maximum projection confocal image of BMSC stained with DAPI (blue; nuclei), cell tracker deep red (red: cell membrane) and nanodroplets stained with DiO (green: nanodroplets) following a 2 day nanodroplet exposure.

4.4 | Discussion

This chapter aimed to establish how nanodroplets affect cytotoxicity, osteogenic activity and expression of oxygen sensitive proteins in cells of an osteoblastic lineage. The overarching ambition of this work was to develop nanodroplets for aiding bone repair through the delivery of oxygen. As osteoblasts play a role in new bone formation, it is desirable for any potential therapeutic to be non-cytotoxic, to reduce hypoxic stress and induce osteogenic activity. As such, the suitability of nanodroplets for such a purpose was assessed on these criteria.

This was evaluated by experiments outlined in this chapter that demonstrated the following key findings:

- Nanodroplets increased MC3T3E1 metabolism and did not affect Saos-2 and BMSC metabolism as measured using Alamar Blue;
- Nanodroplets increased proliferation in BMSCs as measured by DNA concentration and had a dose dependent effect on MC3T3E1 proliferation;
- Hypoxia decreased BMSC proliferation as measured by DNA concentration in the presence of osteogenic supplements but not in basal conditions, while hypoxia increased metabolism;
- Nanodroplets had a dose-dependent ability to relieve the hypoxia induced reduction in DNA concentration without significantly affecting metabolism;
- Air-saturated nanodroplets reduced HIF-1α expression in Saos-2s cultured in hypoxia;
- Nanodroplets, and to a lesser extent, lipid dispersions significantly increased BMSC calcification;
- ALP enzymatic activity was found to decrease with nanodroplet treatment;
- Nanodroplets did not clearly associate physically with BMSCs.

4.4.1 | Selection of Nanodroplet Concentrations for Experimentation

Before examining nanodroplets as a potential treatment for bone repair, an appropriate experimental concentration must be determined. Cell viability was assessed using Alamar Blue. Alamar Blue contains resazurin, which undergoes a reduction reaction in the presence of cell metabolism (theorised to be as result of a non-specific reaction by NADH dehydrogenases) to form resorufin, a red, fluorescent compound (O'Brien et al., 2000). As a result, increased fluorescence intensity represents increased metabolism. It was hypothesized that the presence of nanodroplets would not affect the cell metabolism. In general, an increase in MC3T3E1 cell metabolism was observed with no decreases detected (Figure 4.1). Significant increases were observed between 10^{-2} and 10^{-4} % v/v. Interestingly, a biphasic pattern was observed where an increase in metabolism was observed with respect to nanodroplet concentration until a concentration of 10^{-3} where a decrease is observed. It is important to note that higher nanodroplet concentrations than those reported in this thesis were studied but led to foaming of the media and so were not considered suitable. Given the changes in cell metabolism, concentrations of 10^{-2} to 10^{0} % v/v (0.01-1 % v/v) were selected for further investigation.

4.4.2 | Nanodroplet Effect on Osteoblastic Cell Viability

One crucial aspect to consider when evaluating the biocompatibility of potential therapeutics is cytotoxicity. Cell metabolism was investigated in different cell types. It was found that the increase in cell metabolism was only observed in MC3T3E1s while no difference in metabolism was observed in Saos-2s or BMSCs compared to the no treatment control (Figure 4.2). As this is a measure of overall cell metabolism, it does not distinguish between changes in cell activity and changes in cell number. Therefore, to fully interpret the data, the cell number assays using DAPI for MC3T3E1s and Saos-2s (Figure 4.4) and using Picogreen for BMSCs (Figure 4.7) must also be taken into account. The cell proliferation at 0.1% nanodroplets was also found to increase cell number in MC3T3E1s and not affect Saos-2 cell number, consistent with the Alamar Blue assay. However, the cell number in BMSCs increased. Given the increase in cell number, it is possible that cell metabolism decreased as Alamar Blue reduction was found

not to change.

Given that PEG(40)s and DSPC are considered biocompatible, it was hypothesised that the presence of nanodroplets would not affect cell proliferation. However, in Figure 4.4 it can be seen that when 0.1 %v/v nanodroplets were added to the media the resulting proliferation was increased. As the MC3T3E1 cells are preosteoblastic, this would likely be beneficial for bone repair as osteoblasts lay down new bone material. However, when the nanodroplet concentration was increased to 1% v/v the proliferation decreased compared to the control. There is a distinct lack of literature surrounding the effect of unloaded nanodroplets on cell proliferation without ultrasound. As such it is difficult to cross-reference these findings. However, from these findings, it can be concluded that concentration is a clear factor that needs to be considered when seeking to use these nanodroplets as a potential therapy, and highlights that lower concentrations are preferable.

Of note is there was no significant difference in the groups until 72 hours ($P<0.05$). This suggests that the cell metabolism results may be independent of cell number as these experiments were performed after 24 hours of exposure to the nanodroplets.

4.4.3 | Effect of Hypoxia on Cell Viability

Given that Picogreen expression remained unchanged with hypoxia but Alamar Blue fluorescence increased, this can be attributed to an increase in cellular metabolism only. This increase is likely a consequence of anaerobic respiration being a less efficient process than aerobic respiration. Under hypoxic stress, there is insufficient oxygen for oxidative phosphorylation, i.e. the usual process through which most ATP is produced, to occur. ATP production instead relies on glycolysis only. Consequently, only 2 ATP molecules are produced per glucose molecule compared to the usual 32. Due to this reduced efficiency, the rate of glycolysis increases (Lee et al., 2020). The cells were cultured in high glucose media and so, an excess of glucose is available to allow for this increase in metabolic activity and, therefore, increased Alamar Blue reduction. A similar result was observed by Li et al. in C2C12 myoblasts where Alamar Blue reduction increased with hypoxia in high glucose environments (Li et al., 2013).

Hypoxia has previously been shown to increase proliferation in skeletal stem cells (Berniakovich, Giorgio, 2013). Basal media will ensure that MSCs maintain a more

stem-like nature than in osteogenic supplemented media. Whilst the results in Figure 4.6B do not directly support the notion that proliferation is improved in hypoxia, it is clear that these less differentiated cells are more resistant to hypoxia than their osteogenic counterparts (Figure 4.6A). The majority of literature on proliferation and cell number in BMSC reports a decrease with hypoxia, consistent with the results found in the presence of osteogenic supplements (Chung et al., 2012; Hung et al., 2007). However, one paper did report an increase in proliferation in hypoxia although 8% oxygen was used and so the hypoxia was less extreme than in previously reported studies or the 2% used in this thesis (Ren et al., 2006). Hypoxia has been shown to increase proliferation in cells yet to undergo differentiation (Di Mattia et al., 2021). The lack of a change in DNA concentration with hypoxia in basal media but a decrease in osteogenic media could be due to a balancing act between increased cell death in hypoxic conditions but an increase in proliferation in more stem-like cells. Nanodroplet treatment at 0.1% v/v led to an increase in DNA concentration in both osteogenic and basal media while 1% v/v led to a decrease in osteogenic media but an increase in basal media. These results suggests that 0.1% v/v nanodroplets is the optimum value, among those investigated herein, for a possible therapeutic agent aiming at increasing bone activity.

4.4.4 | Nanodroplet Effect on Hypoxic Markers

The aim of this study as a whole was to develop a therapeutic capable of improving bone repair through relieving hypoxia. The results in section 3.4.13 demonstrate that oxygen will transfer PFP to the surrounding liquid when loaded at a partial pressure higher than the surrounding liquid. Direct measurement of oxygen release from the nanodroplets, however, proved challenging due to their interaction with the oxygen sensors used but indirect measurement of oxygen delivery to the cells was possible through the detection of the oxygen-sensitive protein HIF-1α (Hypoxia Inducible Factor-1α). The mechanism through which HIF senses hypoxia is discussed in detail in section 1.3.3, but, to summarise, the α subunit of HIF undergoes prolyl hydroxylation in the presence of oxygen essentially "tagging" it for degradation (Jaakkola et al., 2001). As a result, lower oxygen tension should result in an increase in HIF-1α concentration as seen in Figure 4.10. When treated with air-saturated nanodroplets, the concentration of HIF-1α detected using chemiluminescence and western blotting decreased. This

indicates that the nanodroplets may have facilitated the delivery of oxygen to the cells. This result was not replicated in the VEGF ELISA. However, this was not sensitive to differences in normoxic and hypoxic incubation and so was found not to be a reliable measurement for cellular oxygen tension. Previous studies in vivo attempting to deliver oxygen to tumours using perfluorocarbon nanodroplets have found that HIF-1α concentration, as detected using immunofluorescence, decreased, consistent with the results in this chapter (Huang et al., 2020). However, this study loaded the nanodroplets with medical oxygen prior to use. Unfortunately, nanodroplets loaded with oxygen in this chapter did not appear to have an impact on HIF-1α expression (Figure 4.10). This could be due to an ineffective gas-loading process, such as affecting nanodroplet stability, and so further work should be undertaken to understand and optimise this process.

4.4.5 | Nanodroplet Effect on Osteoblastic Function

Alizarin red stains for calcium deposition, making it a useful late-stage marker for mature osteoblast activity. The enzymatic activity of ALP indicates immature osteoblastic activity due to its role in the hydrolysis and release of phosphate groups for hydroxyapatite production (Avery et al., 2020). Together, they form a useful insight into osteoblast differentiation. Hypoxia did not seem to affect mineralisation (Figure 4.13) without treatment but it did significantly decrease ALP (Figure 4.18). This is consistent with the literature which consistently reports a decrease in ALP activity with hypoxia (Nicolaije et al., 2012; Utting et al., 2006; Zhang et al., 2017). The literature regarding mineralisation in hypoxia is more conflicting. This is possibly linked to the wide range of oxygen concentrations used with decreasing Alizarin red staining usually occurring in more extreme hypoxia (Nicolaije et al., 2012; Utting et al., 2006) and increases in Alizarin red staining usually associated with less severe hypoxia, approximately 3-5% (Berniakovich, Giorgio, 2013; Kwon et al., 2017).

Exposure to 0.1% nanodroplets significantly increase Alizarin red staining in normoxic conditions (Figures 4.11 and 4.14) and a similar but non-significant trend was observed in hypoxia (Figure 4.15). 0.1% lipid significantly increased Alizarin red but to a lesser extent that the nanodroplets at the same concentration. This finding indicates that the presence of the PFP, the main distinguishing factor between the nanodroplet and lipid treatment groups, may contribute to the promotion of mineralisation (there

will also be small changes in the physical structure between the nanodroplets and the lipid micelles but unlikely to be enough to causes these observations). Given that PFP has been documented to exhibit both biological and chemical inertness (Riess, 2005), it can be inferred that the observed effect is likely attributable to enhanced oxygen availability facilitated by the presence of the nanodroplets.

In contrast to this, 0.1% nanodroplets slightly decreased ALP activity from days 0-14 (Figure 4.19). This is surprising as ALP enzyme is required for mineralisation of the bone matrix to occur. At this point, it is important to note that Alizarin red staining does not distinguish between different calcium structures (Langenbach, Handschel, 2013). As a result, it is possible that the nanodroplets are stimulating another form of calcium deposition that may result in dystrophic mineralisation. That being said, the results in Figure 4.16 show that nanodroplets on their own do not stimulate mineralisation of a collagen matrix even in the presence of cell-conditioned media implying the mineralisation observed in the Figure 4.11 is a cellular mechanism.

4.4.6 | Nanodroplet-BMSC Association

As both the nanodroplet and cell membrane are made of phospholipids, it was hypothesised that the two membranes may interact to result in a physical association or the particles may be taken up by endocytosis. No significant evidence of such physical association was observed under confocal microscopy.

4.5 | Conclusions

In summary, the perfluoropentane nanodroplets used in this chapter were not found to have significant cytotoxic effects on osteoblastic cells. Additionally, HIF-1α western blotting indicated successful delivery of oxygen and Alizarin red staining was found to increase with air-saturated nanodroplet treatment. This increase in calcium deposition, however, should be treated with caution as ALP activity was found to slightly decrease with nanodroplet treatment, indicative of reduced osteoblastogenesis.

5

Nanodroplet Interaction with Osteoclastic Cells

5.1 | Introduction

While osteoblasts are responsible for the formation of new bone tissue, osteoclasts are required for bone resorption through acid secretion and enzymatic degradation, thereby maintaining the dynamic equilibrium of bone homeostasis. During the initial stages of bone repair, osteoclasts are necessary for the resorption of damaged bone tissue. However, too many osteoclasts compared to osteoblasts will lead to reduced or reversed fracture healing (Uveges et al., 2008). Consequently, it may be the case that significantly increased osteoblast activity alongside increased osteoclast activity is detrimental for bone development. For example, in Paget's disease of bone which is characterised by an increase in both osteoblastic and osteoclastic activity (where osteoblastic activity is dominant) resulting in a rapid bone turnover producing abnormal, weak, woven bone (Tuck et al., 2017).

Osteoclasts are of the haematopoietic lineage. They form from monocytes that fuse to form multinucleated cells. These same monocytes are also capable of becoming macrophages and dendritic cells. There exists a complex interplay between monocytes, macrophages, dendritic cells and osteoclasts (Okamoto et al., 2017). It has been suggested that macrophages, osteoclasts and dendritic cells not only all differentiate from monocytes, but they are capable of converting between cell types where the need arises (Wang et al., 2020). As such, osteoclasts cannot be considered entirely in

isolation and it is vital that experiments regarding osteoclasts are performed with macrophages in mind.

The literature regarding osteoclast response to hypoxia was discussed in depth in section 1.3. The literature is somewhat conflicting with Arnett et al. finding that hypoxia induced osteoclastogenesis in mouse-derived monocytes but reduced mature osteoclast resorption in rat-derived osteoclasts. In contrast, Hulley et al. found that HIF-1α (the presence of which is increased in hypoxic conditions) had no effect on osteoclastogenesis but increased resorption in human osteoclasts (Arnett et al., 2003; Hulley et al., 2017). Knowles et al. proposed that although hypoxia may enhance osteoclast resorption, it also increases apoptosis, thus suggesting reoxygenation is essential for an increase in osteoclast activity (Knowles, Athanasou, 2009). This is by no means an exhaustive list of varying literature surrounding osteoclasts in hypoxia, but it demonstrates just some of the contradictory research. Given the complexities in the existing literature, three different oxygen regimens were investigated in this chapter. These can be seen in Figure 5.1. Knowles *et al*. investigated nanobubbles made from soybean lecithin (of which DSPC is a component) in vitro as a possible oxygen delivery mechanism demonstrating a decrease in osteoclastogenesis in normoxia and a dose-dependent effect in hypoxia. However, there were no significant decreases in HIF-1α concentration when exposed to the nanobubbles suggesting this effect was not due to the oxygen delivery (Knowles et al., 2024). Furthermore, the stability of nanobubbles is a key aspect the has been brought into question (Wang et al., 2023). Nanodroplets are more stable resulting in longer circulation times making them more suitable as a systemic therapy.

The overarching aim of this chapter was to investigate whether nanodroplets are capable of reversing the effects induced by hypoxia on osteoclasts with the end goal of decreasing osteoclastic activity to enhance bone repair. With this in mind, the experiments conducted in this chapter had the following aims:

- To elucidate the effect of nanodroplets on osteoclastic cell viability;
- To establish the effect of hypoxia on osteoclasts in vitro;
- To investigate the impact of both gas-loaded and non-loaded nanodroplets on osteoclast activity and fusion;

- To understand the impact of the nanodroplets on the osteoclast-macrophage axis;
- To explore if there is a strong association between nanodroplets and PBMCs exposed to MCSF and RANKL.

5.2 | Methodology

The research in this chapter focused on the effect of nanodroplets and hypoxia on cells of an osteoclastic lineage. Before any experiments could be performed, osteoclast differentiation was observed to determine suitable timepoints for experiments. Osteoclasts were cultured from PBMCs isolated from leukocyte cones as detailed in section 2.8.3 and cultured for 12 days with media supplemented with MCSF and RANKL (section 2.13) before being fixed and TRAP-stained (section 2.13.1). It was found that pre-osteoclasts would start to emerge around day 5 of the culture, and the most fusion of mature osteoclasts occurred on days 7-9, and an established mature osteoclast culture existed by day 12. Given this, three different hypoxia and treatment regimens were investigated in this chapter; they are discussed in depth in section 2.13.2, but a summary is provided in Figure 5.1 for ease. Note that all subsequent data in this chapter follows the same colour scheme.The nanodroplets were first investigated for any cytotoxic effects using the same nanodroplet concentrations and their constituents that were established in the previous chapter. This was investigated using Alamar Blue assays for metabolic activity (section 2.9.1) and manual cell counting (section 2.13.1). Manual cell counting also provided an average osteoclast area which could be used to infer rate of fusion. TRAP was found to fluoresce under a Cy5 channel and so fluorescent confocal microscopy was performed to visualise any nanodroplet-cell interactions (section 2.15). It was found that mononuclear cells associated strongly with the nanodroplets and so it was hypothesised that these cells were macrophages and so flow cytometry was performed of PBMC-derived macrophages to determine any cell association and if the nanodroplets cause any macrophage polarisation towards an M1 or M2 lineage (section 2.14).

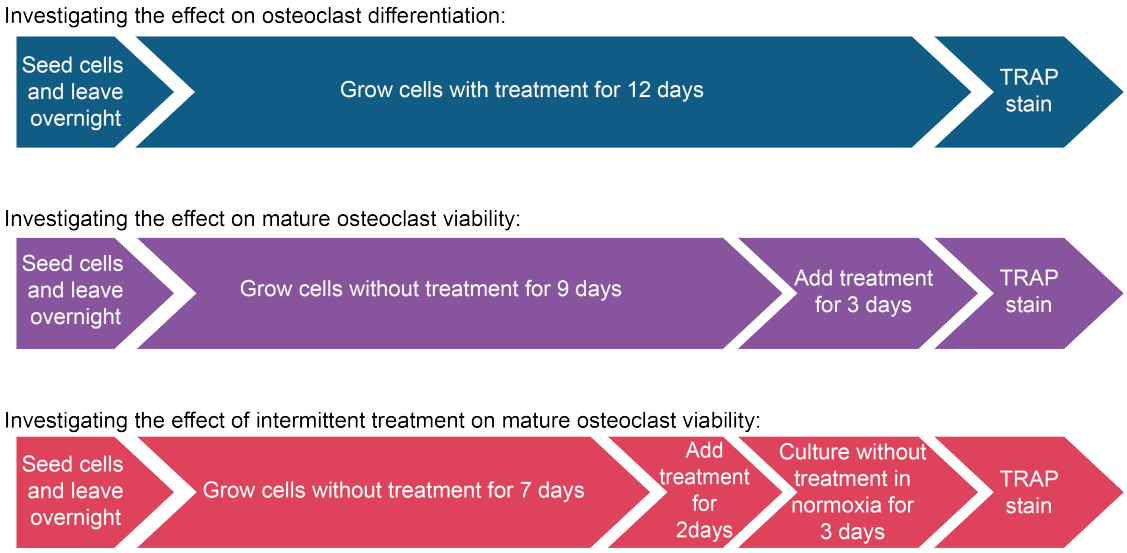

Figure 5.1: Hypoxia and nanodroplet exposure regimens used throughout this chapter. The 12-day exposure (blue) was chosen to demonstrate continuous exposure, the 3-day exposure (purple) demonstrates any effects on mature osteoclasts and the 2-day intermittent culture (pink) focuses on late-stage differentiation. This colour scheme is consistent throughout this chapter.

5.3 | Results

5.3.1 | Effect of Nanodroplets on Osteoclasts in Normoxia

Peripheral blood mononuclear cells (PBMCs) were isolated from leukocyte cones supplied by the NHS blood and transplant non-clinical issue service. Following CD14 selection, cells were seeded and cultured for a total of 12 days. At approximately day 5, small pre-osteoclasts start to form. between day 7 and 9 (patient dependent) larger osteoclasts start to form. All patients had osteoclasts present in normoxic, no-treatment groups by day 9 (Figure 5.2). For quantitative purposes, osteoclasts were defined as TRAP-positive cells with three or more nuclei.

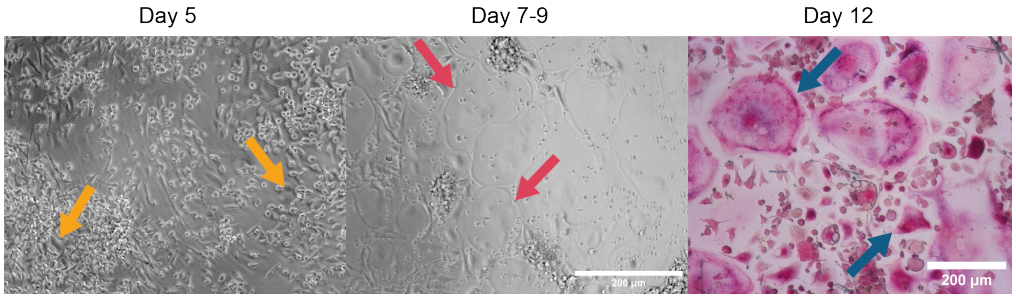

Figure 5.2: Images taken at 20x objective at day 5 and day 7 of osteoclast culture and at 10x objective for day 12 TRAP stained osteoclasts. The start of the formation of pre-osteoclasts is highlighted by the yellow arrows in the day 5 image. Examples of mature osteoclasts are highlighted by the pink arrows in the day 7-9 image. Examples of mature, TRAP-stained osteoclasts have been highlighted by the blue arrows in the day 12 image.

To investigate the effect of nanodroplets on early-stage metabolism, an Alamar Blue assay was performed. MCSF directs the monocytes down a macrophage lineage. With RANKL, the monocytes will be directed down an osteoclast lineage. There was no significant difference between nanodroplet treatment and the no treatment control in either MCSF or MCSF and RANKL supplemented media at either 24 hours or 72 hours (Figure 5.3).

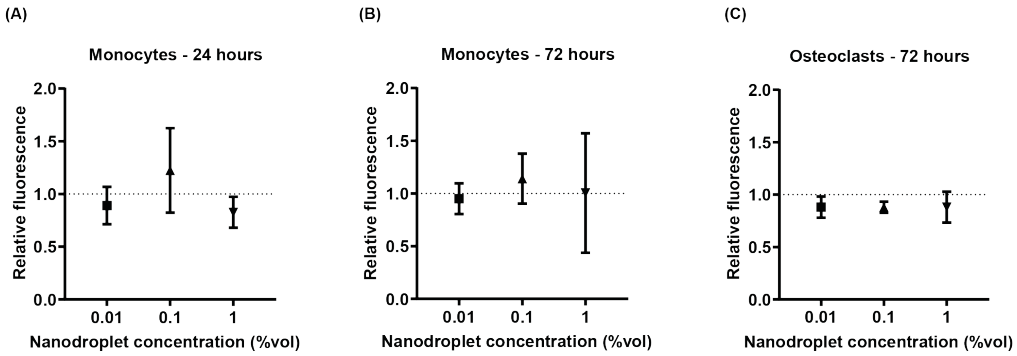

Figure 5.3: Nanodroplet treatment did not significantly affect monocyte and pre-osteoclast metabolic activity. Metabolism in PBMC-derived monocytes cultured in the presence of MCSF following (A) 24 hours and (B) 72 hours and (C) PBMCs cultured in the presence of MCSF and RANKL with nanodroplet treatment for 72 hours as measured using Alamar Blue (N=3, n=6). Fluorescence is given relative to the no treatment control, represented in each case by the dashed line. Error bars represent one standard deviation.

At day 12, the osteoclasts were TRAP stained. The osteoclasts were manually drawn around to quantify the average osteoclast number as well as average osteoclast surface area. The osteoclast area was assumed to be associated with the osteoclast fusion rate. Additionally, a significant increase in osteoclast area may also correspond to a reduced number of visible cells, due to fewer but larger multinucleated osteoclasts in an image with the same field of view. The resulting apparent decrease in cell number would be an imaging artefact rather than a true reflection of the cell culture. Measuring osteoclast area helps identify when this might be the case. It was found that osteoclast number decreased with 12 days of nanodroplet with significant decreases observed at 0.1 and 1 %vol ($P<0.0001$ in both cases, Figure 5.4B). Significant differences were observed in average osteoclast area for all three nanodroplet concentrations (0.01%: $P=0.0007$, 0.1%: $P=0.0003$, 1%: $P=0.0011$, Figure 5.4E). Nanodroplet treatment on day 9-12 of culture displayed a decrease in osteoclast number with nanodroplet treatment but not average nanodroplet size, although no statistically significant differences were observed (Figures 5.4C,F). A similar trend was observed in day 7-9 treatment, although was only found to be statistically significant in 1% vol day 7-9 treatment ($P=0.0268$, Figures 5.4D and G). Although average osteoclast surface area was also found to decrease with 12 days of nanodroplet treatment with significant differences at each nanodroplet concentration (Figure 5.4E), this same effect was not observed in the day 9-12 and day 7-9 treatment (Figure 5.4F and G).

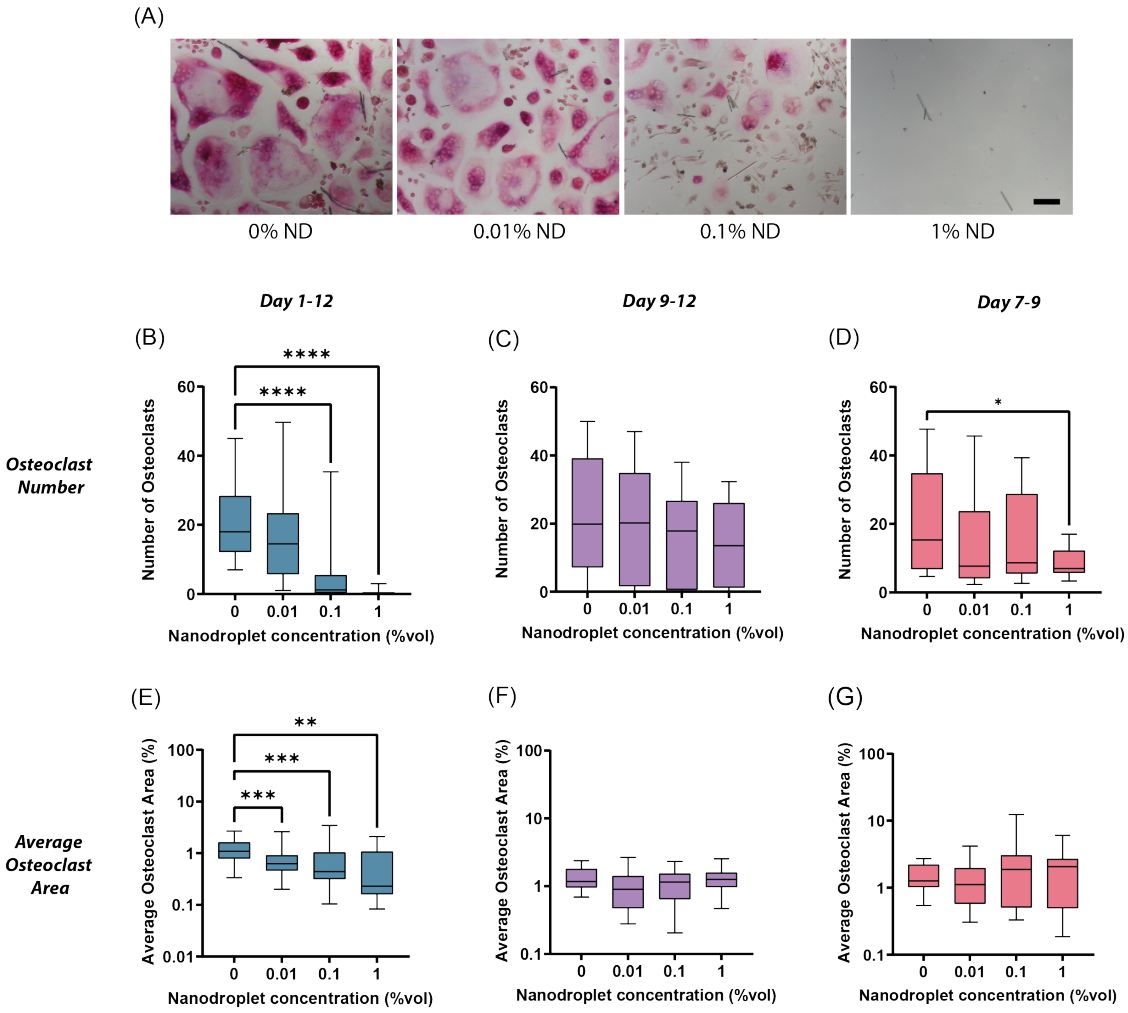

Figure 5.4: Osteoclast number and area was significantly decreased by nanodroplet treatment in normoxia. Osteoclast number and average area with nanodroplet exposure. (A) Representative images from the images used for quantification Scale bar: 100 μm. Average osteoclast number and average percentage area per osteoclast at day 12 of culture are given for 12 days of nanodroplet treatment (B and E respectively, N=3, n=6), nanodroplet treatment on days 9-12 (C and F respectively, N=5, n=6) and nanodroplet treatment of days 7-9 (D and G respectively, N=3, n=6).Central line represents the median, the box represent the interquartile range and the error bars represent the maximum and minimum value. *p<0.05, **p<0.01, ***p<0.001, ****p<0.0001

5.3.2 | Effect of Nanodroplet Constituents on Osteoclasts

To test the hypothesis that the effects were due to the nanodroplets themselves and not their components (DSPC and PEG(40)s), the impact of these components on early-

stage metabolism, osteoclast number and osteoclast size was investigated. A 9:1 ratio of the two was also investigated as the boiling point of PFP makes investigation of PFP alone impossible. These were all performed at 0.1% vol. As was the case with the different nanodroplet concentrations in Figure 5.3, the lipid components were also found not to have a statistically significant effect on cell metabolism as measured using Alamar Blue, although it is noted that all three constituent controls had a higher average metabolism than the 0.1% nanodroplet treatment (Figure 5.5).

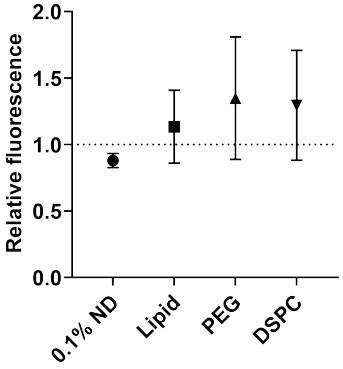

Figure 5.5: Monocyte metabolism was not significantly affected by nanodroplet treatment or their constituents. PBMC metabolism as measured using Alamar Blue following 72 hours of culture with MCSF and RANKL (osteoclast 72 hour) with nanodroplet constituent exposure throughout. Error bars represent one standard deviation and the dashed line represents the no treatment control. (N=3, n=6)

The lipid constituents caused a slight decrease in the number of osteoclasts following 12-day exposure, although DSPC was the only group to display any statistical significance compared to the no treatment control (P=0.029; Figure 5.6A). The 0.1% nanodroplet treatment group demonstrated a significant decrease in the number of osteoclasts over 12 days compared to each of the constituents and the no treatment control (Lipid: P<0.0001, PEG: P<0.0001, DSPC: P=0.0003 and 0% ND: P<0.0001). For osteoclast surface area, a similar trend was observed for 12 days of treatment with significant differences between the 0.1% vol group and the PEG and 0% vol groups (P<0.001 and P=0.0001, respectively). However, both the DSPC and lipid group were significantly different from the no treatment control (P=0.0250 and 0.0064 respectively, Figure 5.6D). For treatment on day 9-12, no significant differences were observed, although the no treatment control was again the largest value (Figure 5.6B,E). For day 7-9 treatment, osteoclast number was again greatest with no treatment, with a signif-

icant difference only observed between the no treatment control and the DSPC group (P=0.0320, Figure 5.6C). The surface area, however, was larger with nanodroplet treatment under these conditions (Figure 5.6F). A significant difference, however, was only observed between 0.1% nanodroplet treatment and PEG (P=0.0371). In general, this suggests the individual lipid components have a slight long-term cytotoxicity but not as significant as the the effect observed in the nanodroplets suggesting an additional mechanism.

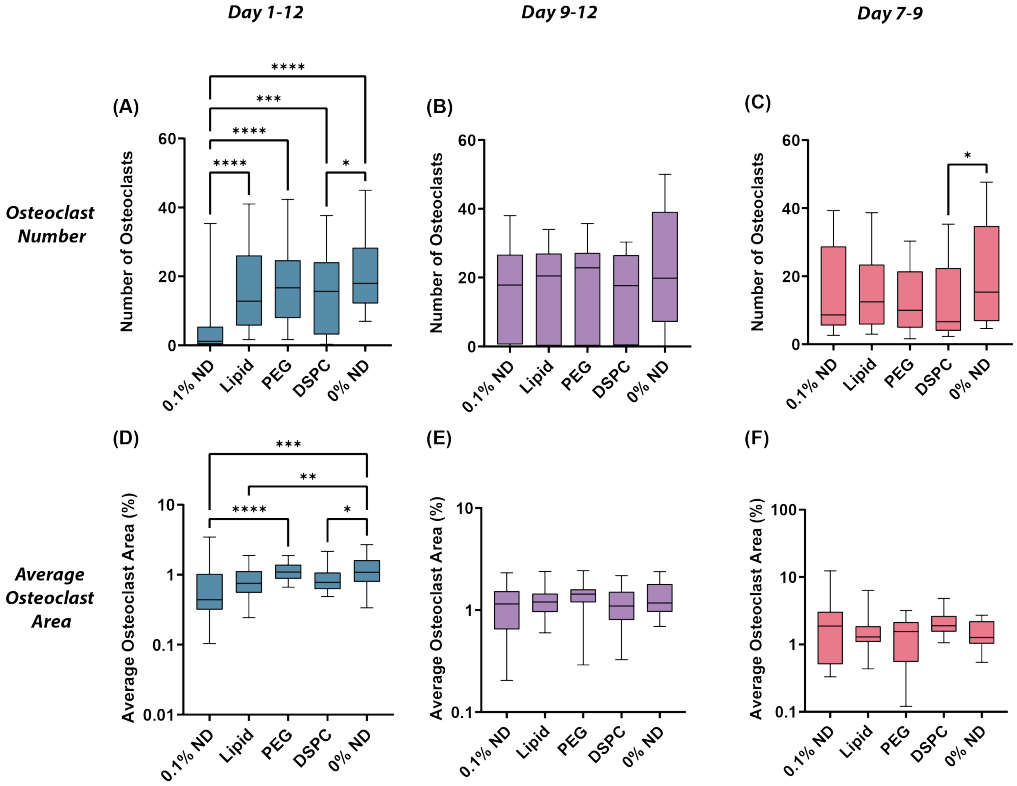

Figure 5.6: Nanodroplet dependent decrease in osteoclast number and size is more significant than the decrease caused by nanodroplet constituents. Osteoclast number (A-C) and average area (D-F) with nanodroplet constituent exposure for the full 12 days of culture (A, D), on days 9-12 only (B, E) and days 7-9 only (C, F). Central line represents the median, the box represent the interquartile range and the error bars represent the maximum and minimum value. *p<0.05, **p<0.01, ***p<0.001, ****p<0.0001 (N=3, n=6)

5.3.3 | Effect of Hypoxia on Osteoclasts

To evaluate the effect of hypoxia on early-stage PBMC metabolism in the presence of MCSF or MCSF and RANKL, PBMCs were cultured in both normoxia (air with 5% CO_2) and hypoxia (2% O_2) and metabolism was quantified using Alamar Blue. A paired t-test found no significant difference between the metabolism in normoxia and hypoxia (Figure 5.7).

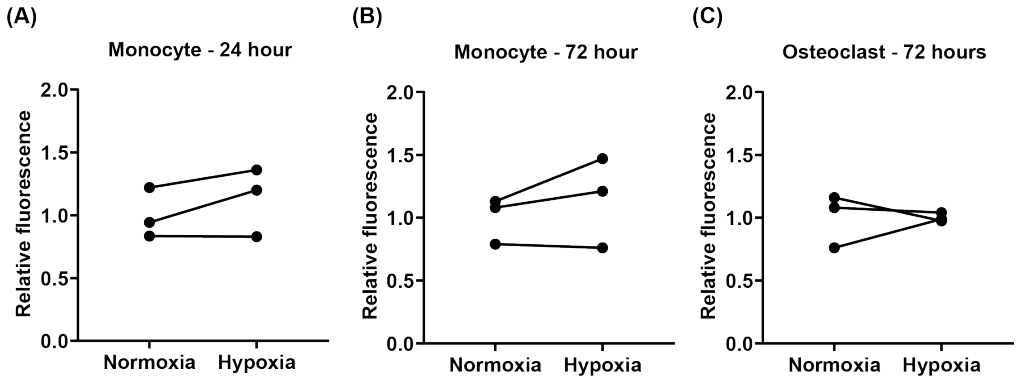

Figure 5.7: Monocyte and pre-osteoclastic metabolic activity is not affected by hypoxia. Metabolism as measured using Alamar Blue PBMCs from three separate patients cultured with MCSF in normoxia or 2% oxygen for 24 hours (A) and 72 hours (B). Metabolism was also measured in PBMCs cultured with both MCSF and RANKL in normoxia and 2% oxygen for 72 hours (C). (N=3, n=6)

Visibly, under microscope examination, hypoxia had a very significant effect on osteoclast number and behaviour at day 12 (Figure 5.8). 5% oxygen for the whole culture reduced the number of osteoclasts; however, more macrophage-like cells can be observed. 2% oxygen led to a substantial decrease in the number of all cells. 2% oxygen for day 9-12 has significantly affected the osteoclast culture, however, the macrophage-like cells have persisted. In the intermittent 2% oxygen culture (hypoxic conditions days 7-9), osteoclasts have persisted but less than in normoxic conditions.

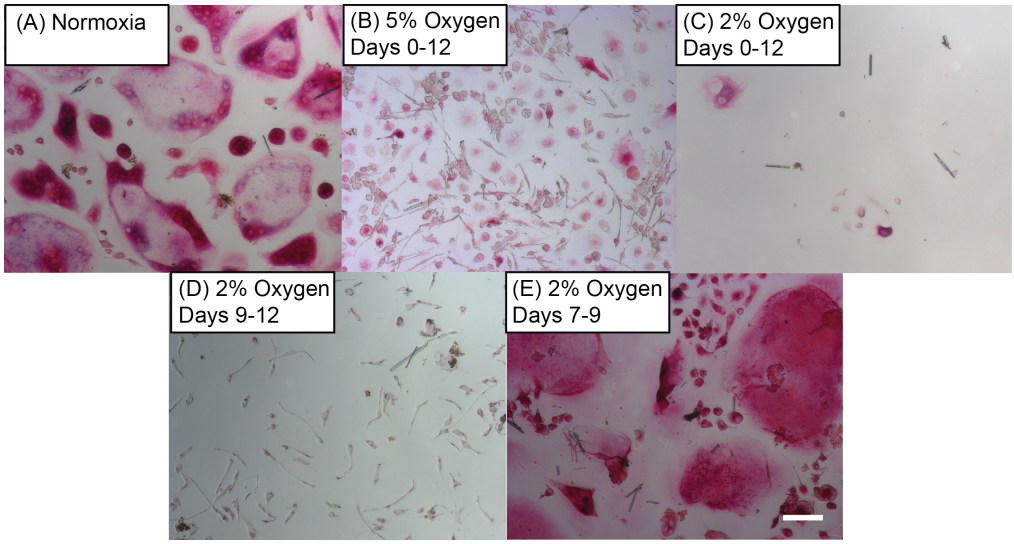

Figure 5.8: There are visibly fewer osteoclasts in culture following hypoxic exposure with a clear change in morphology. TRAP stained osteoclasts following 12 days of culture in (A) normoxia, (B) 5% oxygen, (C) 2% oxygen, (D) normoxia for 9 days then 2% oxygen for 3 days and (E) normoxia for 7 days, then 2% oxygen for 2 days and then normoxia for 3 days. Scale bar: 100 μm.

After manually drawing around each osteoclast, the osteoclast number and average osteoclast area were measured. Decreasing oxygen concentration for the full 12 days led to a decrease in osteoclast number with significant differences observed between normoxia and both 5% and 2% oxygen (P=0.0001 and P<0.0001, respectively) as well as statistical differences between 5% and 2% oxygen (P=0.0235). Despite this, there was no effect on osteoclast size (Figures 5.9A,D). When the culture was only exposed to 2% hypoxia after mature osteoclasts had formed, the number of osteoclasts still significantly decreased (P<0.0001, Figure 5.9B), however the osteoclast size also significantly decrease by a small margin under this oxygen regimen (P=0.0371, Figure 5.9E). In the intermittent hypoxia regimen, where osteoclasts were exposed to 2% oxygen for days 7-9 before being reintroduced to normoxia until day 12, the number again decreased but the average osteoclast area increased (P<0.0001 and P=0.0449 respectively, Figure 5.9C,F).

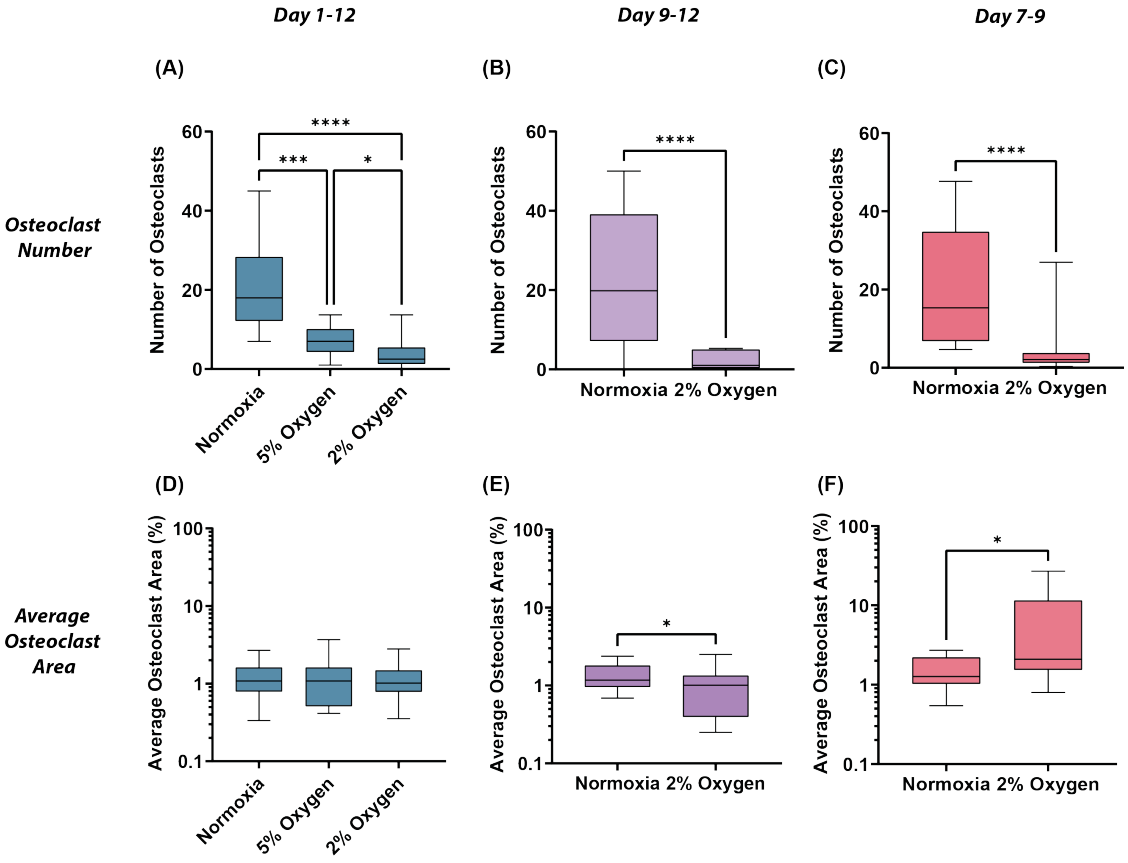

Figure 5.9: Hypoxia results in a decrease of osteoclast number but has a regimen dependent effect of osteoclast size. Osteoclast number (A-C) and average area (D-F) with hypoxic culture for the full 12 days of culture (A, D), on days 9-12 only (B, E) and days 7-9 only (C, F). Central line represents the median, the box represent the interquartile range and the error bars represent the maximum and minimum value. *p<0.05, ***p<0.001, ****p<0.0001 (N=3, n=6)

5.3.4 | Effect of Nanodroplets on Hypoxic Osteoclasts

In section 5.3.1 it was found that nanodroplet treatment had no measurable effect on early-stage cell metabolism in normoxia. To test the hypothesis that this is also true in hypoxia, an Alamar Blue assay was performed. Nanodroplet treatment was found to have no effect on PBMC metabolism at any time point when cultured with MCSF or MCSF and RANKL in 2% oxygen.

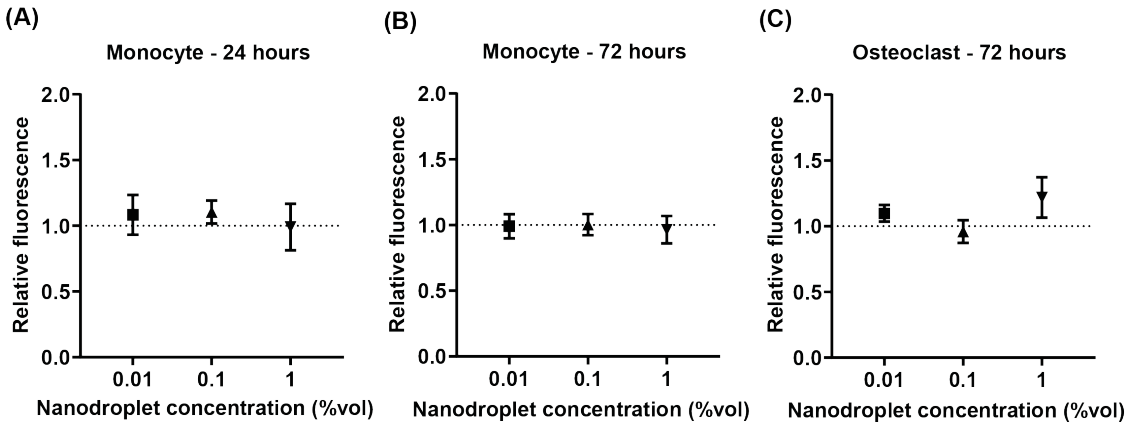

Figure 5.10: Nanodroplet treatment does not affect monocyte metabolic activity in hypoxia. Metabolism in PBMC derived monocytes cultured in 2% oxygen in the presence of MCSF following (A) 24 hours and (B) 72 hours and (C) PBMCs cultured in the presence of MCSF and RANKL with nanodroplet treatment for 72 hours as measured using Alamar Blue. Fluorescence is given relative to the no treatment control, represented in each case by the dashed line. Error bars represent one standard deviation. (N=3, n=6).

Nanodroplets were added to hypoxic osteoclast cultures to investigate whether they were capable of relieving the hypoxic stress. 12 days of nanodroplet exposure followed the same trend as in normoxia with increasing nanodroplet concentration leading to a decrease in osteoclast number with significant differences at 0.1 and 1% vol ($P<0.0001$ in both cases, Figure 5.11A,B). It is difficult to conclude much about the osteoclast size in this culture as the range of sizes increased with increasing nanodroplet concentration although a statistically significant decrease was observed at 1% vol ($P= 0.0227$ Figure 5.11). In mature osteoclasts (nanodroplet treatment day 9-12), nanodroplet treatment did not seem to affect the number of size of the osteoclasts (Figure 5.11C,F). However, in the intermittent (day 7-9) treatment, increasing nanodroplet concentration led to an increase osteoclast number with a statistically significant increase observed at 1% vol ($P=0.0198$), but has no effect on average osteoclast size (Figure 5.11D,G).

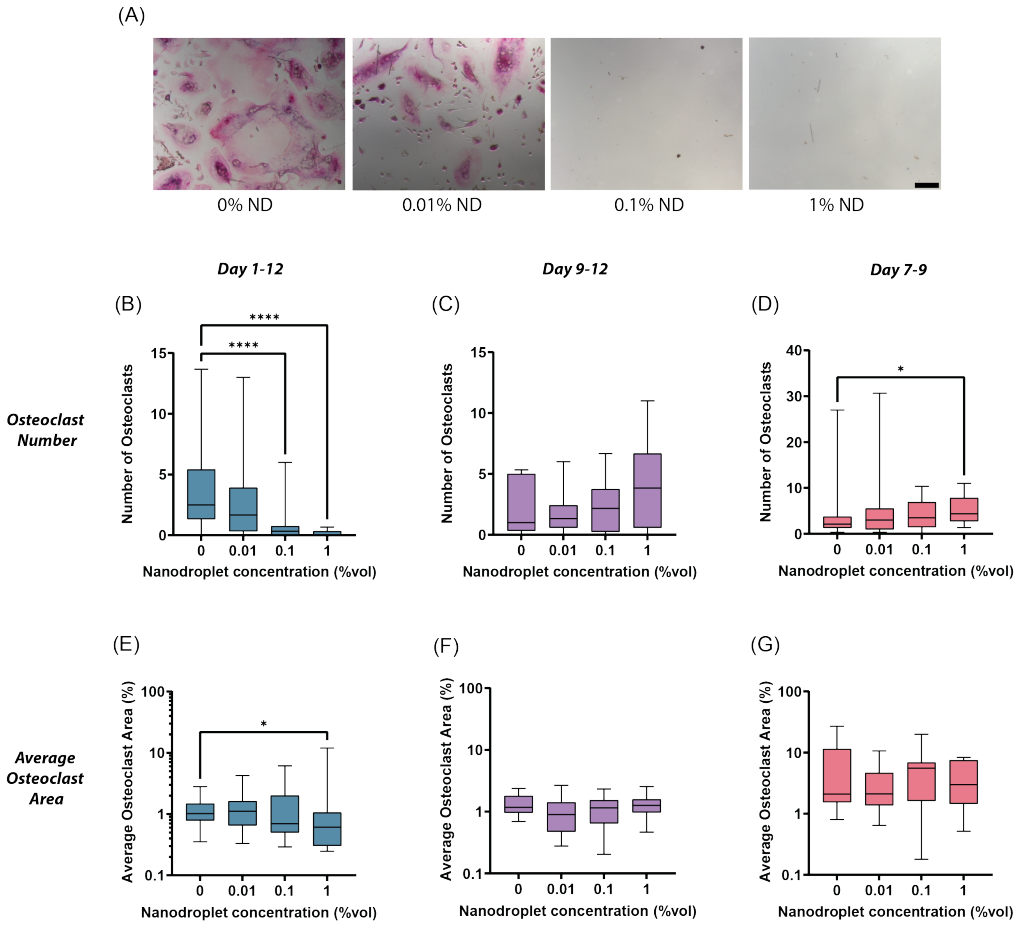

Figure 5.11: Osteoclast number and average area with nanodroplet exposure in 2% oxygen had a regimen dependent effect on osteoclast number. Hypoxic exposure was at the same time as nanodroplet treatment, and cells were cultured in normoxia at all other times. (A) Representative images from the images used for quantification Scale bar: 100 μm. Average osteoclast number and average percentage area per osteoclast at day 12 of culture are given for 12 days of nanodroplet treatment (B and E respectively, N=5, n=6), nanodroplet treatment on days 9-12 (C and F respectively, N=3, n=6) and nanodroplet treatment of days 7-9 (D and G respectively, N=3, n=6). Central line represents the median, the box represent the interquartile range and the error bars represent the maximum and minimum value. *p<0.05, **p<0.01, ***p<0.001, ****p<0.0001

To investigate the effect of loading the nanodroplets with oxygen and nitrogen on metabolism in PBMC-derived monocytes, cells were cultured for 72 hours with MCSF and RANKL supplemented media in the presence of varying concentrations of air, oxygen and nitrogen-saturated nanodroplets and the metabolism was measured us-

ing Alamar Blue. No statistically significant difference from the no treatment control were observed, although nitrogen-saturated nanodroplets consistently resulted in a higher average metabolism.

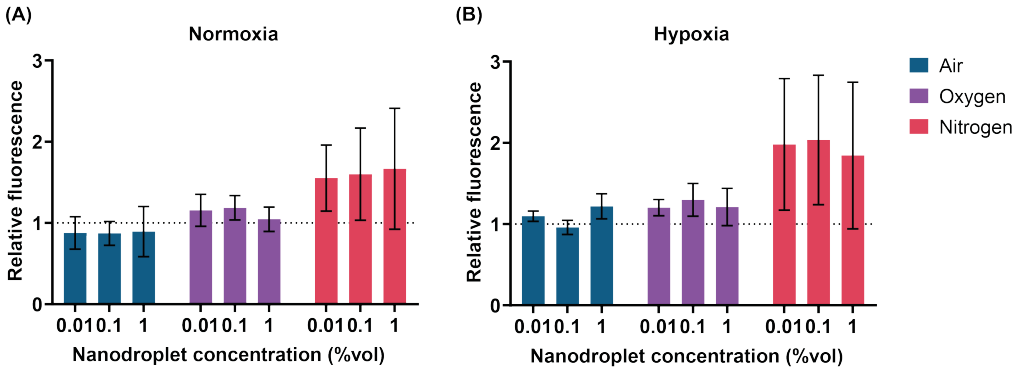

Figure 5.12: Gas-loaded nanodroplets did not lead to a statistically significant change in monocyte metabolism. Metabolic activity in PBMC-derived monocytes cultured at (A) 20% oxygen and (B) 2% oxygen treated with different concentrations of nanodroplets saturated with air, oxygen or nitrogen. Error bars represent one standard deviation.(N=3, n=6)

5.3.5 | Nanodroplet Cell Association in Cells of an Osteoclastic Lineage

To determine if the nanodroplets directly interact with the cells, the nanodroplet-treated, TRAP-stained cells were imaged using a microscope. During microscopic examination of TRAP-stained osteoblasts, it was noted that there was fluorescence signal at a wavelength of 647 nm under excitation at 633 nm. It can be seen in the imaged in Figure 5.13 that the more intense the fluorescence is associated with darker TRAP staining in the brightfield image using confocal microscopy. This supports the concept that it is the TRAP stain that is fluorescing.

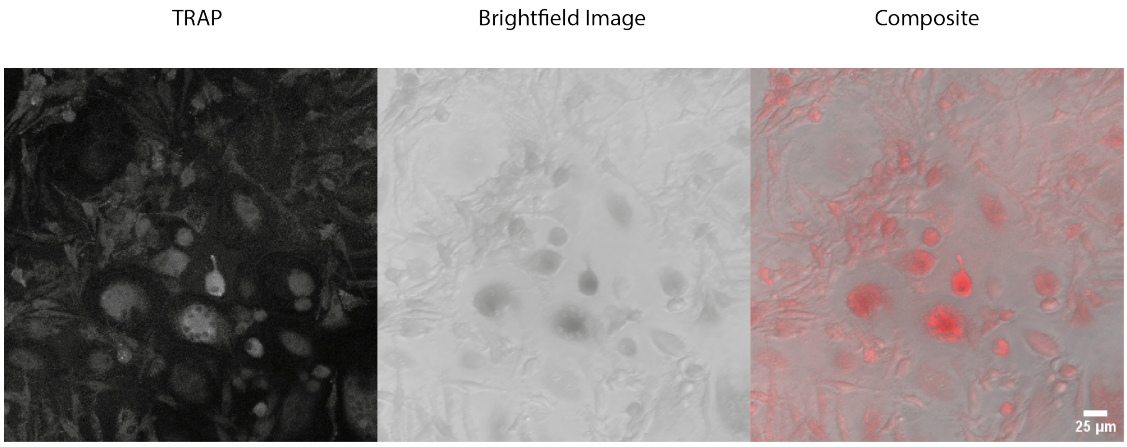

Figure 5.13: TRAP-stained cells fluoresce in the Cy5 channel. Osteoclast maximum projection image taken with a confocal microscope demonstrating TRAP staining fluorescence under the Cy5 excitation and emission (ex: 633 nm, em: 647 nm).

This fluorescent TRAP stain was used to detect potential association with the osteoclasts by treating mature osteoclasts with fluorescent, DiO-labelled nanodroplets for 72 hours (day 9-12 of osteoclast culture). It was found that the nanodroplets do not appear to strongly associate with osteoclasts (a TRAP positive cell with 3 or more nuclei) but did clearly associate with mononuclear cells present in the culture. Although the proportion of nanodroplets associating with the TRAP-positive mononuclear cells is not homogeneous.

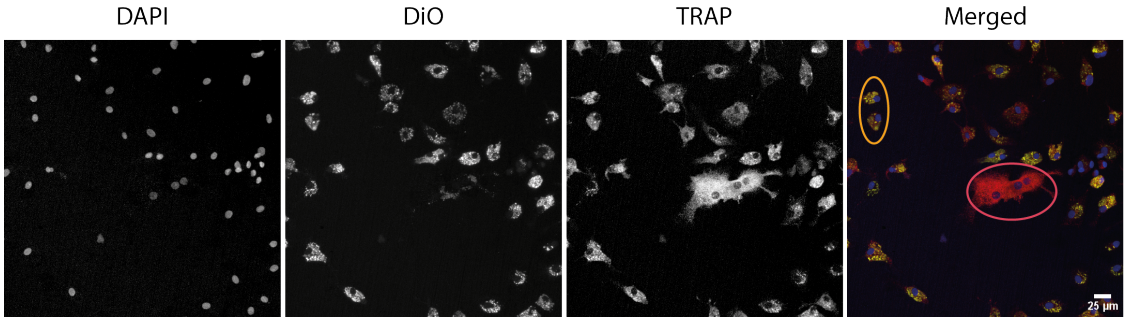

Figure 5.14: Nanodroplets strongly associate with mononuclear cells. Maximum projection images of TRAP-stained osteoclast cultures showing nanodroplets (green), TRAP (red) and nuclei (blue) following 2 day nanodroplet exposure. An example of an osteoclast (TRAP-positive cell with more than three nuclei) is circled in pink and two mononuclear cells are circled in yellow in the merged image.

A z-stack was performed and the z-profile intensity for the TRAP and the nanodroplets was analysed to try and establish whether this cell association is due to the nanodroplets being located on top of or within the cells. The TRAP and DiO fluorescence occur concurrently. As TRAP is an intracellular stain, this indicates that the DiO-labelled nanodroplets are intracellular.

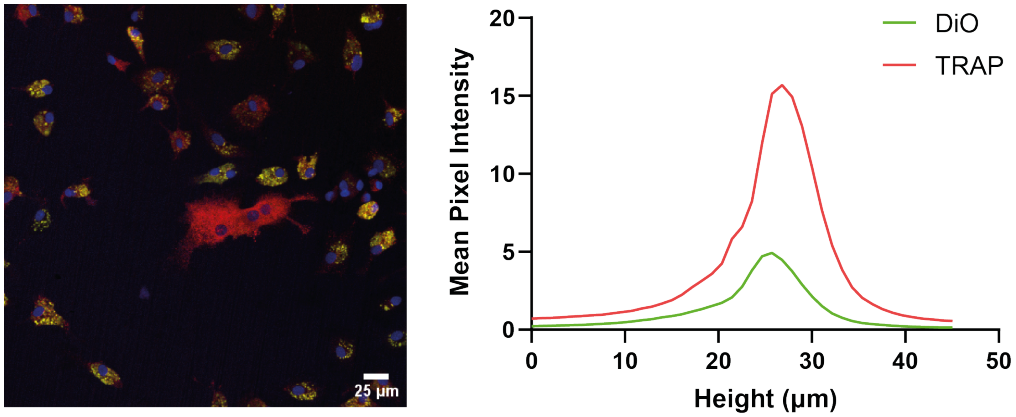

Figure 5.15: Concurrent DiO and TRAP fluorescence implies the fluorescent nanodroplets are intracellular. Maximum projection osteoclast confocal image and its z-profile of the DiO and TRAP fluorescence intensity.

5.3.6 | Effect of Nanodroplets on the Osteoclast-Macrophage Axis

To investigate whether nanodroplets affect macrophage behaviour, CD14+ PBMC-derived monocytes (the same cells used for osteoclast culture) were cultured for 6 days with MCSF supplemented media in the presence 0.1% vol lipid or nanodroplets or no additional treatment. The FSC (front scatter) against SSC (side scatter) plots showed a shift towards the SSC axis in the presence of nanodroplets (Figure 5.16), suggesting an increase in granularity. Increased granularity is indicative of nanoparticle-cell association.

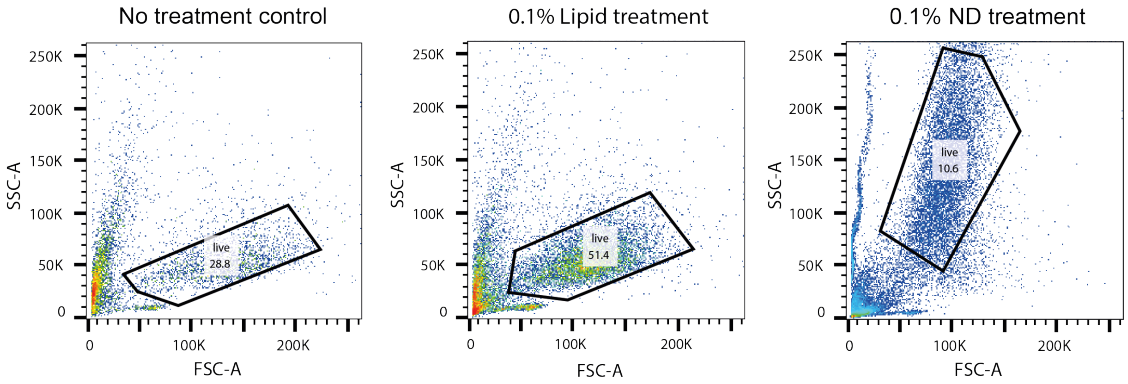

Figure 5.16: Nanodroplets cause increased side scatter in macrophages in flow cytometry implying nanodroplet-macrophage association. The front scatter vs side scatter plot from macrophages flowed through a flow cytometer following a 3 day nanodroplet exposure. SSC: side scatter, FSC: forward scatter.

Three days before the flow cytometry was performed, the M1 and M2 controls were supplemented with LPS and interferon γ, and IL-4 and IL-13 respectively. Three M0 (CD14, CD68 and HLADR), three M1 (CD38, CD40 and CD86) and three M2 markers (CD11b, CD206 and CD163) were selected for flow cytometry. The geometric mean fluorescence intensity (GMFI) of the individual cells was and the frequency of cells positive for each marker were analysed (Figure 5.17). There was a large amount of patient to patient variability in the GMFI. Despite this, the avergae GMFI appears to indicate a tendency towards M1 over M2 macrophages. The presence of nanodroplets also appears to have increased the frequency of M0 macrophages but not had much affect on the GMFI. The one exception to this is in patient 3 where a decrease in the GMFI in all markers was observed.

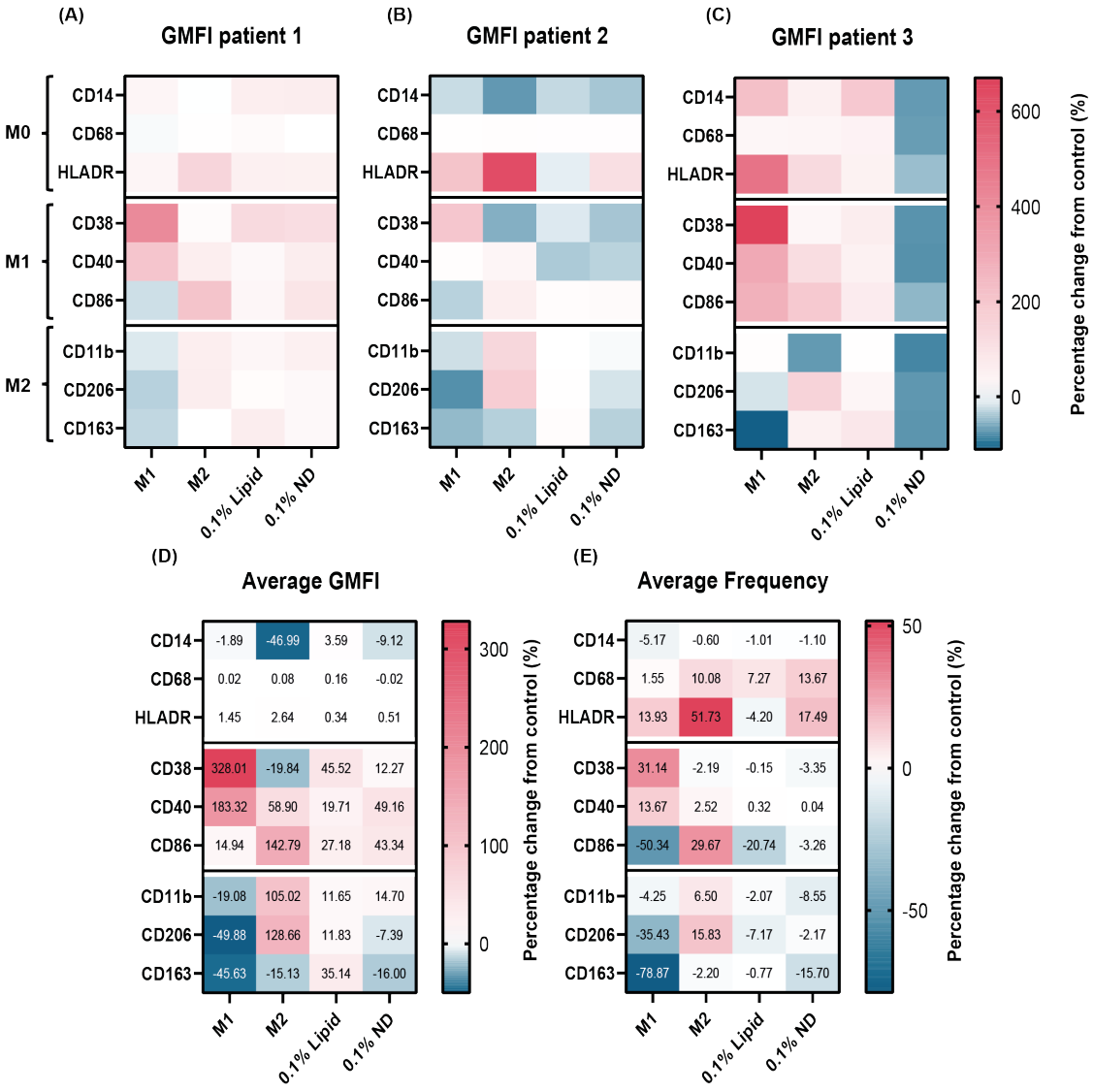

Figure 5.17: Nanodroplets do not cause significant macrophage M1/M2 polarisation. Results of flow cytometry on day 6 macrophages. Results are given as a percentage difference from the no treatment M0 control. The geometric mean fluorescence intensity (GMFI) is given for individual patients (A-C) and the average GMFI (D) and average frequency (E) for each macrophage marker (N=3).

5.4 | Discussion

This project aimed to develop nanodroplets capable of delivering oxygen to relieve the effects of hypoxia to aid with bone repair. Given that osteoclasts are responsible for the resorption of bone, a delivery mechanism capable of decreasing the number and activity of osteoclasts compared to the bone-forming osteoblasts are desirable. This chapter sought to establish whether nanodroplets were capable of this task by evaluating the effect of nanodroplet treatment on in vitro osteoclast culture from human donors.

These aims were addressed by experiments outlined in this chapter that demonstrated the following key findings:

- Nanodroplets and their constituents have no significant effect on monocyte metabolism;
- Nanodroplets consistently decrease osteoclast number in normoxia whether used to treat from the monocyte stage or on mature osteoclasts only;
- Osteoclast size was decreased by nanodroplet treatment when present during osteoclast fusion but not when treating mature osteoclasts;
- Hypoxia decreased osteoclast number for all oxygen regimens. The effect on osteoclast size was, however, regimen-dependent;
- Nanodroplet treatment may relieve the effects of hypoxia in mature osteoclasts and with intermittent hypoxia;
- Nanodroplets somewhat associated with osteoclasts but strongly associated with macrophage-like mononuclear cells.

Three different culture regimens were employed throughout this chapter (see Figure 5.1 where they are described in detail): a 12-day differentiation study, where hypoxia and/or nanodroplets were added for the full 12 days of culture to investigate the effect on the differentiation and fusion into osteoclasts; a mature osteoclast study, where hypoxia and/or nanodroplets were only applied at day 9 of culture for 3 days to determine the effect on mature osteoclasts; and an intermittent study, where hypoxia and/or nanodroplets were applied on days 7-9 of a 12-day study to investigate whether any effects are in fact being obscured by increased apoptosis.

5.4.1 | Nanodroplets Affect Osteoclast Size and Number but not Metabolism

In the previous chapter, it was found that nanodroplets had little to no effect on osteoblastic cell metabolism when measured using Alamar Blue. This was found to also be consistent with early-stage osteoclast culture (Figure 5.3). The nanodroplets do not, therefore, affect early-stage viability in monocytes. Metabolism was not used to measure later culture points due to the heterogeneity of the cell culture, and osteoclast number and size were measured instead. In the 12-day differentiation study, increasing nanodroplet concentration led to decreasing nanodroplet number and size. This implies that less osteoclast differentiation and fusion occurs in the presence of the nanodroplets. This effect can be said to be due to the presence of the nanodroplets rather than the lipid constituents that compose the shell as the lipid components themselves were found to significantly less effect on the osteoclast number and size than the nanodroplets of the same concentration (0.1% v/v) compared to the no treatment control (Figure 5.6).

In the mature osteoclast (days 9-12) and intermittent treatment (days 7-9) experiments, a non-significant trend of decreasing osteoclast number with increasing nanodroplet concentration was also observed, but osteoclast size remained fairly constant. This implies that osteoclasts are dying, but fusion is not being prevented, as the osteoclast size would also be expected to decrease if fusion was affected. In both cases, it is more difficult to rule out the lipid components as a possible cause of this cell death.

5.4.2 | Hypoxia Decreases Osteoclast Number

Before determining whether the nanodroplets are capable of relieving the effects of hypoxic stress, the effect of hypoxia needed to be established. The literature on the effect of hypoxia on osteoclasts is somewhat conflicting. In general, the literature seems to agree that osteoclast activity is increased in hypoxia (Arnett et al., 2003; Knowles, Athanasou, 2009; Murata et al., 2017; Muzylak et al., 2006; Nomura et al., 2014). This, however, is not necessarily correlated with cell number. In many cases, hypoxia has been shown to increase apoptosis and, therefore, decrease cell number (Gorissen et al., 2019; Knowles et al., 2010; Muzylak et al., 2006). This effect on cell number was clearly observed in the results in Figures 5.8 and 5.9 with a significant decrease in the num-

ber of osteoclasts in all hypoxic conditions compared to the normoxic control. The changes in the average individual osteoclast area can give more insight into whether this decrease is caused by an increase in osteoclast death or a decrease in fusion. Interestingly, the three different oxygen regimens investigated yielded different results for the average osteoclast area. Over 12 days of hypoxia, the average area of an individual osteoclast did not change. This implies fusion is not affected and so the decrease in osteoclast number is associated with apoptosis. The decrease in osteoclast size in mature osteoclasts exposed to 2% hypoxia (day 9-12) may suggest a decrease in fusion or that the larger osteoclasts are more sensitive. When the osteoclasts are treated for days 7-9 the average osteoclast area increased.

Both Nomura and Knowles suggested that the timing of the hypoxic conditions and any reoxygenation will affect the outcome of the hypoxia with earlier hypoxia resulting larger osteoclasts (Knowles, Athanasou, 2009; Nomura et al., 2014). Knowles suggests this is due to a balance between improved osteogenesis and increased apoptosis (Knowles, Athanasou, 2009). The result for the day 7-9 and day 9-12 hypoxic regimens would support this line of thought. Day 7-9 was typically the days over which the largest amount of fusion was observed (Figure 5.2). Hypoxic conditions over these days led to an increase in osteoclast area implying increased fusion (Figure 5.9C,F). Meanwhile, day 9-12 had existing osteoclasts and less differentiation occurring (Figure 5.9B,E). Hypoxic conditions over these days led to a marginal decrease in osteoclast area. This could either be due to a decrease in osteoclast fusion or larger osteoclasts being more susceptible to apoptosis. However, the lack of change in osteoclast area in the 12 day hypoxia contradicts the idea that hypoxia aids fusion, even with increased apoptosis (Figure 5.9A,D). This instead raises the idea that it is not the hypoxia that increases fusion observed in the day 7-9 experiment, in fact, the reoxygenation. Reoxygenation has been shown to increase both reactive oxygen species and NF-κB proteins both of which are associated with increased osteoclast differentiation (Boyce et al., 2015; Callaway, Jiang, 2015; Granger, Kvietys, 2015; Hulley et al., 2017; Rupec, Baeuerle, 1995).

Hypoxia had no effect on early-stage cell metabolism (Figure 5.7), implying the monocytes are not affected by the hypoxic conditions. Additionally, it can be seen visually that in 5% oxygen for the full culture and 2% in mature osteoclast culture, the culture still contains mostly macrophage-like cells left in the culture. This is consis-

tent with previous literature suggesting that both monocytes and macrophages survive well in hypoxia (Roiniotis et al., 2009).

5.4.3 | Nanodroplets Relieve the Effects of Hypoxia on Osteoclastic Cells

12-day exposure to the nanodroplets was previously shown to be toxic to osteoclasts in normoxia with a decrease in osteoclast number and area (Figure 5.4), this is consistent with the results in hypoxia (Figure 5.11). Additionally, the no significant change in osteoclast area with exposure to nanodroplets on days 7-9 or days 9-12 is consistent in normoxia and hypoxia. However, the non-significant decrease in osteoclast number that was observed in normoxia treated with nanodroplets either days 7-9 or day 9-12 is contrary to what was observed in hypoxia where an increasing number of osteoclasts with increasing nanodroplet concentration was observed (Figure 5.11). This suggests a competing mechanism. Whilst this is not the desired outcome in response to the nanodroplets if the objective is bone repair, it does provide evidence of the nanodroplets being capable of relieving hypoxic conditions. It is possible that the increased osteoclast number could be due to the nanodroplets successfully delivering oxygen that would relieve the hypoxia-induced apoptosis that was observed in Figure 5.9.

5.4.4 | Strong Cell Association was Observed in Mononuclear Cells

The nanodroplets strongly associated with macrophage-like cells. They had a slight but less obvious association with the osteoclasts (Figure 5.14). As TRAP staining is intracellular (Hayman, 2008); as a result, the concurrent nature of the DiO and TRAP fluorescence is indicative of nanodroplets endocytosing. This macrophage cell association was further evidenced by the increase in side scatter observed in flow cytometry performed on macrophages treated with nanodroplets. Increased side scatter implies an increase in granuality (Figure 5.16)(Haynes et al., 2009; Park et al., 2017). This increase in granularity further suggests that the nanodroplets are associated with the macrophages. This is consistent with the literature where an association between phagocytic cells, like macrophages and osteoclasts, with nanobubbles, a similar, al-

though not identical, submicron, lipid stablisised particle was observed (Knowles et al., 2024).

The geometric mean fluorescence intensity in patient 3 decreased in all groups when exposed to nanodroplets. This suggests that the nanodroplets interact with the antibodies' ability to bind with their surface markers on the macrophages. This is a key limitation of the flow cytometry technique. With this in mind, the M1 markers still seem slightly stronger than the M2 markers suggesting the macrophages may be leaning towards a pro-inflammatory lineage. It has been suggested that M1 is pro-osteoclastogenisis while M2 is anti-osteoclastogenesis which may have further implications for bone repair, although further experimentation is required to confirm this M1 polarisation as the flow cytometry is not neccessarily reliable due to limitations discussed above (Sun et al., 2021).

5.5 | Conclusion

To conclude, nanodroplets displayed a cytotoxic effect on the osteoclasts in normoxic conditions but less so in the monocytes. This was still seen in long-term culture in hypoxia, but in the shorter-term cultures, the opposite effect was observed. Although this is not desirable for the aim of aiding bone repair in hypoxic conditions, it provides notable evidence for the ability of nanodroplets to successfully relieve hypoxic conditions.

6

General Discussion and Conclusions

6.1 | Introduction

Bone fractures resulting in delayed or non-union fracture present a significant socio-economic burden. Despite this, there is currently no systemic therapy addressing the concern of bone regeneration. Low oxygen tension has been found to be associated with many bone diseases linked to delayed and non-union fracture (Hannah et al., 2021). The aim of this study was, therefore, to investigate the use of perfluorocarbon nanodroplets to relieve the effects of hypoxia on cells of an osteoblastic and osteoclastic lineage with the ultimate aim to aid bone repair.

6.1.1 | Key Findings

The thesis aims were achieved through experiments demonstrating the following achievements and findings:

- Development of an optimised protocol for nanodroplet formulation through probe sonication was established, allowing for better control over nanodroplet size and improved reproducibility;
- Nanodroplets, in general, have little to no effect on cell metabolism in cells of an early osteoblastic and osteoclastic lineage, suggesting low cytotoxicity;
- Nanodroplets had a dose-dependent effect on the proliferation of cells of an osteoblastic lineage but consistently decreased osteoclast number in normoxia;

- Hypoxia decreased both the proliferation and ALP expression in osteogenic MSCs. This effect was not found to be relieved by the presence of nanodroplets despite evidence from the HIF-1α expression that nanodroplets are successful in delivering oxygen;
- The effect of hypoxia of cells of an osteoclastic lineage has a time dependency and increased osteoclast fusion previously seen in the literature may be linked to reoxygenation rather than hypoxia. The effect of the nanodroplets on relieving the hypoxic effects was also time-dependent;
- Nanodroplets displayed a clear association with cells of an osteoclastic lineage, particularly mononuclear cells but not of an osteoblastic lineage. This is indicative of macrophagic behaviour and the nanodroplets were shown to associate with macrophages through flow cytometry.

6.2 | Summary

In chapter 3, the parameters involved with the formulation of nanodroplets were optimised with the specific aim to precisely control the size distribution and reproducibility. This was achieved by identifying the key parameters involved in the sonication process and how these parameters affected the nanodroplet suspension produced. The sonicator was characterised using calorimetry to allow a more direct comparison between this work and published literature. A suitable cooling mechanism and pulse regimen (ice/water bath, 2 seconds on, 15 seconds off) was developed to prevent the evaporation of PFP but also to prevent the freezing of the liquid. In order to keep the placement of the sonicator as reproducible as possible, a rig was designed and the desired tip-height from the bottom of the Eppendorf tube was determined. As the desired tip-height may have been associated with the placement of the tip in relation to the lipid-PFP boundary, which changes with PFP concentration, the tip height and PFP concentration were investigated together. It was found that a tip height of 12 mm and a PFP concentration of 4.67% produced the smallest nanodroplets with increasing tip-height leading to a more homogenous emulsion. Sonication time and amplitude were found to be less important to ensuring small nanodroplet size, except that a threshold of 60% amplitude was found to be necessary for nanodroplet production to take place. Overall, this chapter achieved a better understanding of the parameters

involved in the nanodroplet formulation process through sonication and their interaction with bone cells. The improved reproducibility and the ability to tailor the nanodroplet size more precisely allows not only for better stability and prediction of vaporisation threshold (Ferri et al., 2021), but also can help to improve the understanding of nanodroplet-cell interactions and there are fewer variables to consider.

With the nanodroplet manufacturing process optimised, Chapter 4 focused on the interactions of nanodroplets with the objective of addressing the hypothesis that nanodroplets increase osteoblastic cell activity in hypoxia by alleviating a hypoxia-induced reduction in osteogenesis. This was addressed by first establishing that the nanodroplets have a minimal cytotoxic effect on osteoblastic cells. This was done by measuring metabolism and proliferation in cell lines and primary cells of an osteoblastic lineage. Metabolism and proliferation of these cells in normoxia either increased or remained constant for all cell types at 0.1% v/v nanodroplets. Before investigating whether the nanodroplets could alleviate hypoxia-induced effects, the effect of hypoxia was confirmed. Hypoxia was found to increase the concentration of HIF-1α protein and decrease proliferation and ALP concentration in osteogenic MSCs. ALP concentration in more stem-like MSCs in basal media was less affected and proliferation was unaffected but increased metabolism. 0.1% v/v nanodroplets did temper the effects on HIF-1α concentration, mineralisation and proliferation, however they were found to decrease ALP concentration in all cases. Despite this, the overall effect of the 0.1% nanodroplets on hypoxic osteoblastic cells is such that it is likely to be beneficial for nascent bone formation.

To contrast with the effect of the osteoblastic cells, work in Chapter 5 explored the effects of nanodroplets on osteoclastic cells with the objective of testing the hypothesis that nanodroplets decrease osteoclastic cell activity in hypoxia by alleviating a hypoxia-induced increase in osteoclastogenesis. Where osteoblasts are essential for the formation of new bone material, osteoclasts are responsible for resorbing existing bone material. Whilst they are a necessary part of bone repair, too many of them could tip the balance towards net reduced or even reversed bone formation. Again, the cytotoxic effects of the nanodroplets were established by measuring metabolism and proliferation in normoxia. The nanodroplets were found to have a minimal effect on metabolism but decreased osteoclast number in both long-term and short-term cultures with the results implying a decrease in fusion as well as increased apopto-

sis of osteoclasts. The effect of hypoxic exposure was found to be far more complex than in osteoblastic culture. Hypoxia was found to increase osteoclast apoptosis but not affect cell fusion. In fact, hypoxic exposure on day 7-9 of the culture followed by normoxia led to an increase in osteoclast size implying reoxygenation may stimulate osteoclast fusion. Nanodroplets were found to reverse the effects of hypoxia (but not reoxygenation) in the short-term exposure experiments, resulting in an increase in osteoclast number in the day 7-9 and day 9-12 experiments. The full 12 day exposure still decrease osteoclast number and fusion suggesting that the cytotoxic effects of the nanodroplets overwhelmed the hypoxia-alleviating properties of the nanodroplets over this timescale. These results demonstrate that the nanodropets may be successful in relieving hypoxic conditions, however the effect of doing so was opposite to what was originally thought.

Overall, these results indicate that the effect of hypoxia on cells of an osteoblastic and osteoclastic lineage may not be as detrimental to the osteoblast-osteoclast balance (with the goal of new bone formation) as the literature would suggest. It was found that the decrease in osteoblastic activity when exposed to hypoxia *in vitro* was very slight, while there was a very significant decrease in osteoclast number, although the two cell types were not investigated in culture together and other factors *in vivo*, such as angiogenesis, may alter this effect.

The perfluorocarbon nanodroplets were formulated with the objective of reducing the effects of hypoxia. Significant evidence was provided in this thesis supporting the hypothesis that perfluorocarbon nanodroplets are capable of relieving hypoxic conditions. Firstly, the nanodroplets did reduce the concentration of HIF-1α protein. Additionally, short-term exposure of nanodroplets to osteoclasts in hypoxia increased osteoclast number, despite nanodroplets in normoxia reducing osteoclast number and hypoxia itself also decreasing osteoclast number.

Overall, it is difficult to conclude whether the nanodroplets would be beneficial towards bone repair. Whilst it has been demonstrated that the nanodroplets were capable of relieving hypoxic conditions, the evidence with regards to osteogenic activity was found to be conflicting. Mineralisation significantly increased with nanodroplet treatment although it is difficult to conclude that this is a result of the oxygen delivery as the same effect was observed in both normoxia and hypoxia. Additionally, ALP pro-

duction decreased with nanodroplet treatment. The osteoclast number increased with short-term nanodroplet exposure, this would be detrimental to bone repair.

6.3 | Limitations

Despite the achievements of this thesis, there are some limitations to this work. The first, very key limitation is what is considered normoxic. Generally, in the literature, including in this thesis, normoxic incubators are exposed to air with 5% carbon dioxide. This is not physiologically correct, especially once the difference over which the diffusion occurs is factored in (Wenger et al., 2015). It has been shown that the oxygen tension in bone is significantly less in the range of about 2-9% (Hannah et al., 2021; Mamalis, Cochran, 2011; Maurer et al., 2006). Therefore, what is normally considered normoxic in vitro may actually be hyperoxic. As previously discussed in section 1.3.5 of the literature review, hyperoxia may also have damaging effects on bone repair such as stimulating osteoclast activity.

The normoxic oxygen exposure is not the only limitation of *in vitro* cell culture. This work relies on a simplified *in vitro* 2D model. This model, although useful in understanding the direct effect on the individual cell types has many limitations. The first is that this model immediately removes any effect as a result of inter-cell interactions. Additionally, although media supplements aim to temper this loss, many organic and inorganic matrix characteristics are missing affecting a wide range of aspects such as mechanosensing and morphology (Ehnert et al., 2020).

Bone formation is by no means the only process affected by oxygen tension. Haematoma and cartilage formation and angiogenesis are essential for bone repair. Altering the local oxygen will likely affect these processes also, especially angiogenesis which is known to respond to hypoxia (Grosso et al., 2017; Lu et al., 2013; Schipani et al., 2009; Wang et al., 2007). The presence of nanoparticles is also likely to elicit an immune response, as demonstrated by the nanodroplet association with macrophages seen in chapter 5. The complex interplay between these different cells and functions was not examined in this thesis and is likely to have a significant effect on the in vivo outcome of the use of nanodroplets as a potential bone repair therapy.

In addition to the limitations due to the in vitro models employed, this work

also does not account for in vivo stability and perfusion. Especially if non-union has occurred due to poor vasculature, the ability although the literature on the use of nanodroplets in tumours demonstrates the nanodroplets' ability to perfuse through the leaky vasculature of the tumour, it has not been demonstrated to what extent this would be true in non-union fractures. Additionally, factors such as phagocytocis, lipid interactions in the blood and even the pressure in the blood may affect the stability of the nanodroplets allowing them to reach the fracture sight to begin with.

6.4 | Future Research Directions

The research in this thesis highlighted the potential of perfluorocarbon nanodroplets for potential oxygen carriers to aid with bone repair. The experiments in this report detailed changes in mineralisation in osteoblasts, macrophagic behaviour in PBMCs and changes in osteoclast number and size following nanodroplet exposure. The precise mechanism of these changes in behaviour could be better understood through examining gene expression to understand specifically how the nanodroplets affect bone cell differentiation. Additionally, future experiments could also aim to assess how nanodroplets affect bone cells in more complex systems such as in co-culture to elucidate the effect on inter-cell interactions or on dentine slices to investigate the effect on resorption or in vivo fracture models.

Further experimentation on the macrophagic behaviour of PBMCs could also help to answer many questions presented in this thesis. Macrophage phenotype has been shown to have a significant effect on the progression of bone repair (Mofarrah et al., 2023; Pajarinen et al., 2019). This thesis attempted to understand how the nanodroplet treatment affects macrophage differentiation through flow cytometry but encountered potential problems with nanodroplets interacting with the antibodies' ability to bind with the surface marker. Employing more methods to understand this relationship, such as RT-qPCR, western blotting and ELISAs could help to clarify the effect.

Another aspect potentially of interest for future study is to investigate the effect of lipids, specifically DSPC, on lipid deposition. Preliminary work on DSPC treatment on osteoblastic cells found increased mineralisation in the presence of DSPC. These results were not discussed in this thesis due to the controls not working, but the results obtained certainly suggest that DSPC would have an effect. In fact, it has previ-

ously been suggested that phosphatidylcholines (of which DSPC is just one type) are involved in inorganic phosphate liberation in bone formation (Dillon et al., 2019). This is a particularly interesting area of study as DSPC is commonly used in the pharmaceutical industry, even being used in the COVID-19 vaccine (Borgsteede et al., 2021).

Looking forward, assessing whether the nanodroplets retain their oxygen delivering abilities when activated by ultrasound would help to establish whether they could be used to deliver more than just oxygen. Given nanodroplets are capable of vaporising into microbubbles, it is possible that their oxygen delivery properties could be investigated alongside targeted microbubble therapies. Future experiments may look to investigate the effect of vaporised nanodroplets both in vitro and in vivo to establish whether nanodroplets retain their oxygen delivery properties in response to ultrasound stimulation.

6.5 | Concluding Remarks

This is the first reported investigation into the potential of nanodroplets as an oxygen carrier to aid with bone repair. The experiments described in this thesis demonstrate that precise control over sonication systems is required for repeatable and nanodroplet production, that nanodroplets are capable of delivering oxygen to cells and that they increase mineralisation with minimal cytotoxic effect on osteoblastic cells. Overall, although this work does not conclusively prove that oxygen-carrying nanodroplets are effective in aiding bone repair, it provides significant evidence of their ability to relieve hypoxic conditions in bone cells in vitro.

Supplementary Material

A note on Fick's Law

In it's purest form, Fick's first law ofdiffusion can be written as follows:

$$J = -D\frac{dC}{dx} \tag{1}$$

Where J is concentration flux, D is the diffusion coefficient, C is the concentration and x is the thickness of the membrane. In the interests of simplicity, in equation 1, the change in concentration across the phospholipid membrane has been assumed to decrease linearly. Additionally the concentration of oxygen within the perfluorocarbon is assumed to be uniform. A permeability constants, k_p was also employed to account for resistance to oxygen passing through the membrane.

Supplementary figures

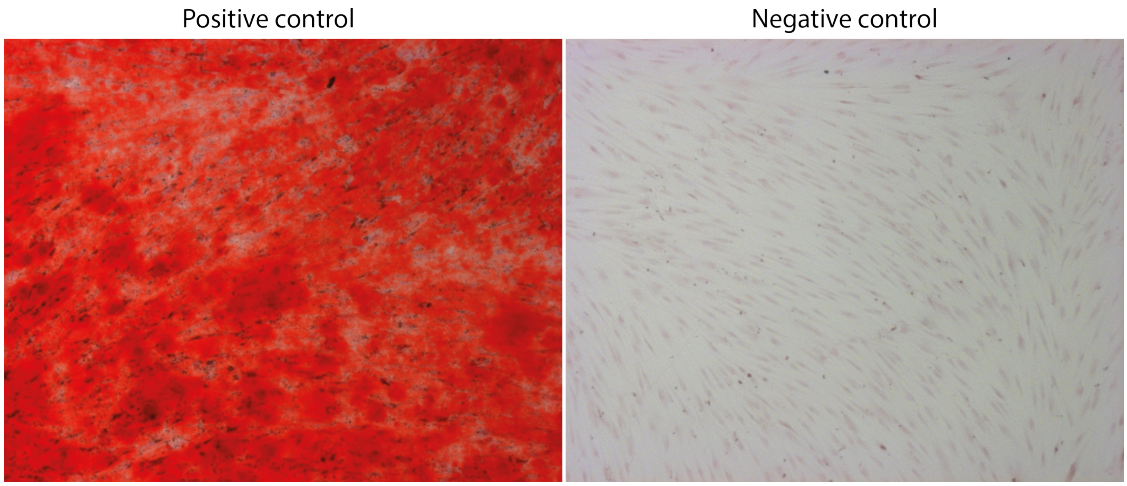

Figure S1: Example positive and negative control images used for CellProfiler alizarin red intensity

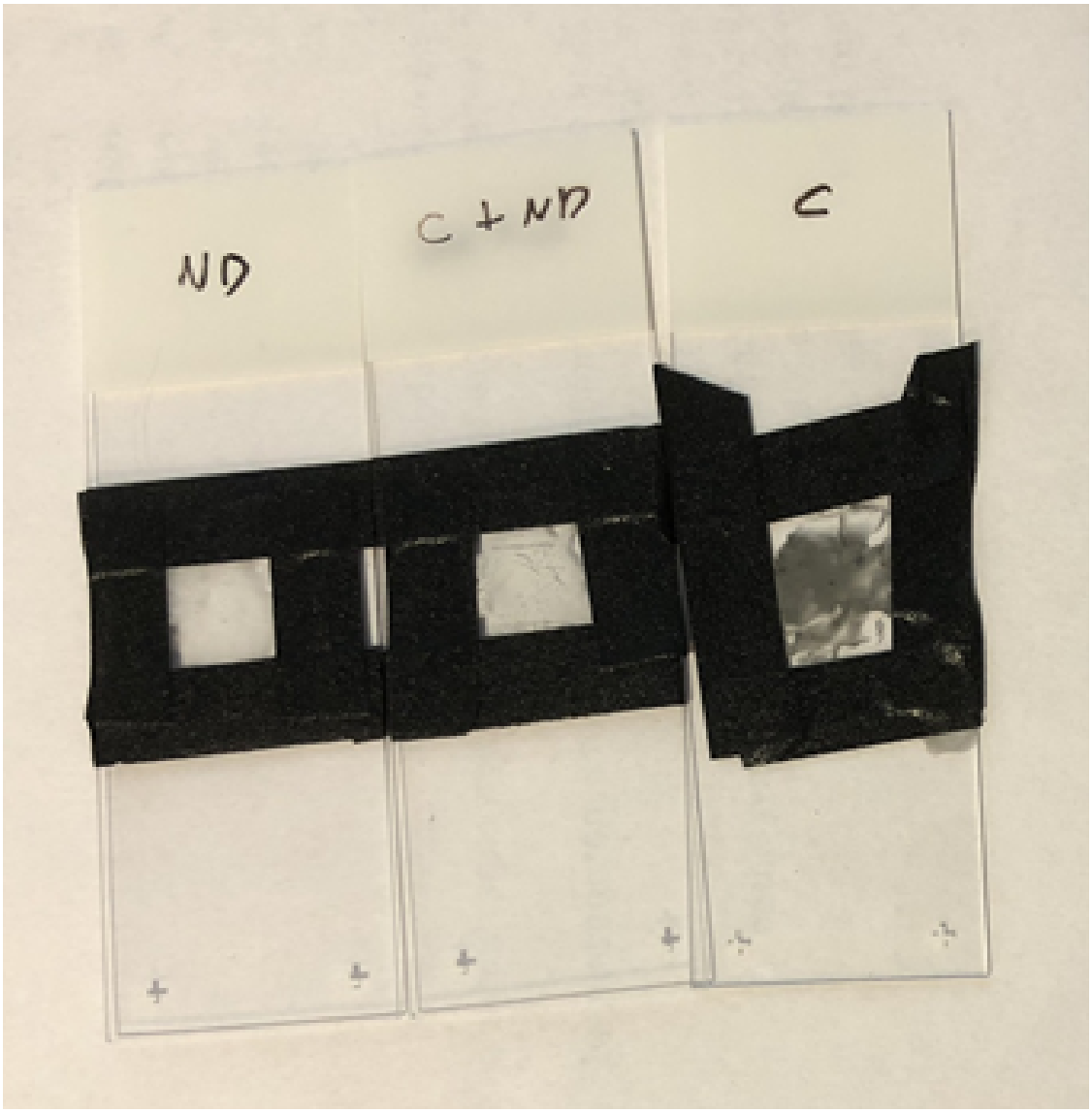

Figure S2: Image showing the samples used for SEM-EDX elemental analysis. ND was from a sample that was visually not grey. C+ND was a sample that was visibly grey. C was the grey contaminant material that was separated from the nanodroplets using centrifugation. The black tape is graphite tape.

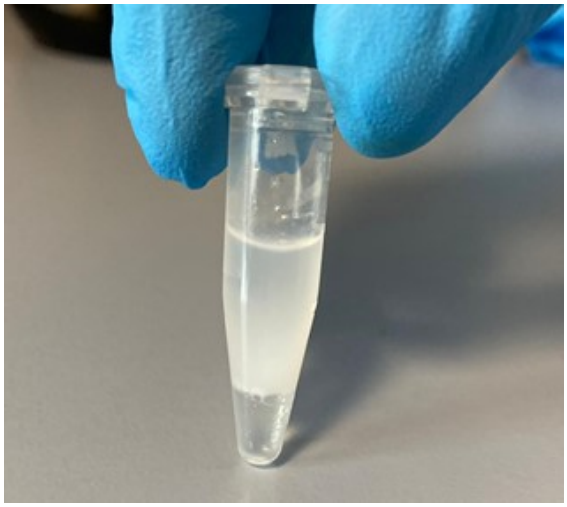

Figure S3: photo of a nanodroplet solution consisting of 20 %vol PFP after the second sonication at a tip height of 2mm. The separate phases of the PFP at the bottom and the lipid film above can be seen clearly

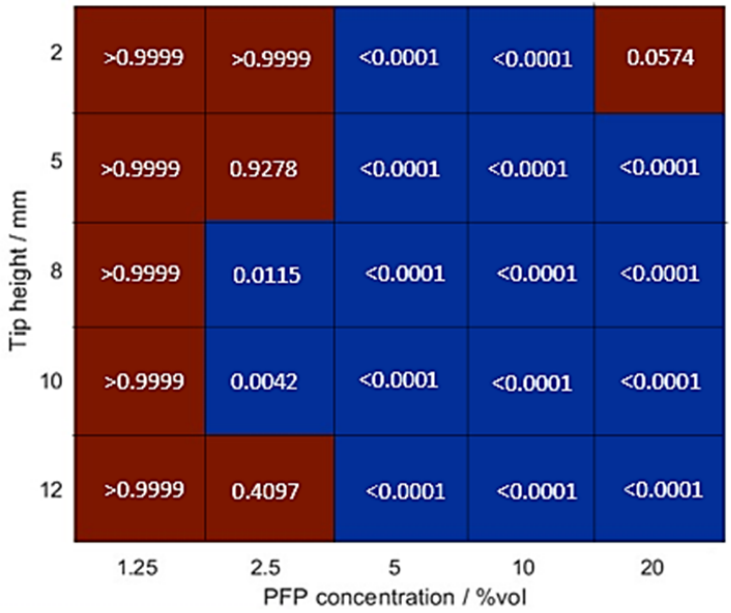

Figure S4: The P-values for the median value of the particle distribution in the tip height vs PFP concentration experiment for PFP concentration value at the given tip height compared to the 0% PFP control at the same tip height. (significance level: P=0.05)

Table S1: Qualitative analysis of the elemental composition of the nanodroplets and contaminated nanodroplets

	Glass Slide	Nanodroplets	Nanodroplets with Contaminant	Contaminant Only
Carbon	✓	✓	✓	✓
Oxygen	✓	✓	✓	✓
Sodium	✓	✓	✓	✓
Magnesium	✓	✓	✓	✓
Aluminium	✓	✓	✓	✓
Silicon	✓	✓	✓	✓
Potassium	✓	✓	✓	
Calcium	0.1%	✓	✓	0.1%
Tin	0.1%	0.1%	0.1%	
Phosphorus		✓	✓	✓
Chlorine		✓	✓	0.1%
Fluorine		✓	✓	
Rhodium		0.1%	0.1%	
Titanium		0.1%	0.1%	✓

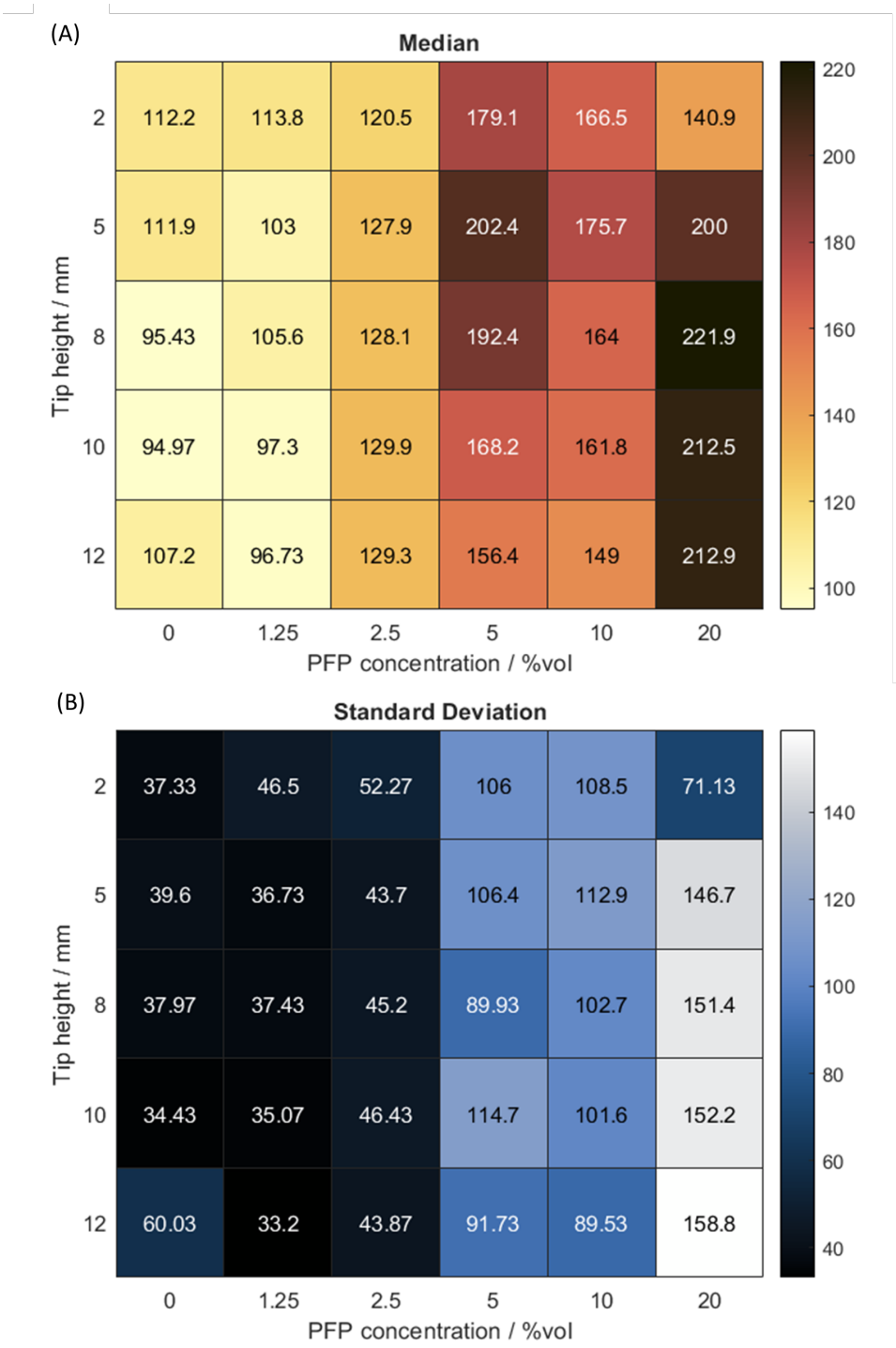

Figure S5: Results of varying the tip height against the PFP concentration. The colour varies with the value of the (A) median diameter of the resulting particle distribution and (B) the standard deviation of the resulting particle distribution to demonstrate the polydispersity of the system. Each value is the mean of n=3 values.

ImageJ macro for DAPI staining

```
//Macro written to count DAPI stained nuclei.
//Rohan Micklethwaite, University, December 2021.
    Modified from Kees Stratman 2008 'MAcro_Emre
requires("1.33n");
dir1 = getDirectory("Choose Source Directory ");
list = getFileList(dir1);
dir2 = dir1+"analysed"+File.separator;
File.makeDirectory(dir2);
run("Set Measurements...", "area area_fraction redirect=None decimal=0");
for (i=0; i<list.length; i++)
 {
 if (File.isDirectory(dir1+list[i])){}
 else{

  path = dir1+list[i];
  if (endsWith(path, ".db")){}
  else{
   open(path);
   if (bitDepth!=24){}  // Check the file is 24bit
   else {
    title1 = getTitle;
    run("Subtract Background...", "Rolling ball radius=8");
    run("8-bit");
    run("Sharpen");
    setAutoThreshold();
    setThreshold(13, 255);
    run("Convert to Mask");
    run("Watershed");
    run("Analyze Particles...", "size=5-Infinity circularity=0.50-1.00 show=Outlines
                summarize");
    saveAs("Jpeg", dir2+"Drawing "+title1+".jpg");
```

```
    close();
    close();


    }
   }
  }
 }
selectWindow("Summary");
saveAs("Results...",dir1+"Summary.csv");
run("Close");
```

Appendix B - Materials and Suppliers

Table S2: List of materials and suppliers

Supplier	Material	Catalogue Number
ATCC	SAOS-2 cell line	
	MC3T3E1 cell line	
Biolegend	CD14 APC antibody	367117
	CD163 PerCPCy5.5 antibody	333608
	HLA-DR PB antibody	307624
	CD38 PE antibody	356604
	CD40 PECy7 antibody	334322
	CD86 APC antibody	374208
	CD11b PerCPCy5.5 antibody	982610
	CD206 PE antibody	321106

Continued on next page

Table S2: List of materials and suppliers (Continued)

Supplier	Material	Catalogue Number
Corning	Dulbecco's phosphate buffered saline without calcium and magnesium (DPBS)	21-031-LB
Malvern Panalytical	NanoSight NS300	
	Zetasizer Ultra	
Promega	Herring sperm DNA	D1811
R&D Systems	Macrophage Colony Stimulating Factor recombinant human (E. coli-derived) (rhM-CSF)	216-MC
	Recombinant RANK L (E. coli-expressed)	6449-TEC-CF
Sigma-Aldrich/Merck	Acetic Acid	695092
	Acetone	650501
	Ascorbic acid-2-Phosphate (AA2P)	A8960
	Beta-glycerophosphate disodium hydrate salt	G5422
	Cellytic M	C2978
	Chloroform	288306
	Dexamethasone	D4902

Continued on next page

Table S2: List of materials and suppliers (Continued)

Supplier	Material	Catalogue Number
	18:0 PC (DSPC) in chloroform	850365C
	Eppendorf Protein LoBind Microcentrifuge Tube (2.0 mL)	EP0030108132-100EA
	Ethylenediaminetetraacetic acid disodium salt dihydrate (EDTA)	E5134
	Ethylene glycol monoethyl ether (2-ethoyethanol)	128082
	Fast Red violet LB salt	F3381
	Igepal CA-630	13021
	4-Nitrophenol solution 10nM	N7660
	Parafilm	P7793
	Polyoxyethylene (40) Stearate (PEG(40)s)	P3440
SLS	Dulbecco's modified Eagle's medium	12-604F
	Penicilin/Streptomycin	BE17512F
	Naphthol AS-MX phosphate, powder	N4875
	α-mem	M6074
Stem Chemicals	Perfluoro-n-pentane	N4875

Continued on next page

Table S2: List of materials and suppliers (Continued)

Supplier	Material	Catalogue Number
Thermofisher Scientific	AlamarBlue Cell viability Reagent	DAL1100
	Bovine Serum Albumin (BSA)	BP1600-100
	CD68 FITC antibody	11-0689-42
	70 μm cell strainer	22363548
	DiO′	D275
	Fetal bovine serum (FBS)	10270098
	Human IL-4 Recombinant Protein	200-04
	Human IL-13 Recombinant Protein	200-13
	Human Iterferon-gamma Recombinant Protein	300-02
	L-Glutamine	25030081
	Model 120 Sonic Dismembrator	
	Paraformaldehyde Solution, 4% in PBS	15670799
	Phenol red free Dulbecco's modified Eagle's medium	11594416
	Quanti-iT Picogreen ds DNA Reagent	P7581

Continued on next page

Table S2: List of materials and suppliers (Continued)

Supplier	Material	Catalogue Number
	Sodium Acetate Anhydrous	011554-30
	Sodium Hydroxide	1310-73-2
	SuperSignal West Pico PLUS substrate	34580
	T175 cell culture flask (corning)	10296861
	T75 cell culture flask (corning)	
	L(+)-Tartaric acid	388280010
	CellTracker Deep red	C34565
Thorlabs	25.0 mm Translation Stage with Standard Micrometer	PT1/M
VWR	Ethanol absolute	20821.467

Glossary

A

adipocyte Fat forming cell.

angiogenesis New blood vessel formation.

apoptosis Programmed cell death.

autologous Self donation.

C

chondrocyte Cartilage forming cell.

cortical Dense outer surface of bone.

cytokine Proteins produced as part of the immune system.

D

diffusion Natural movement of particles from a higher concentration to a lower.

E

endochondral Occurring within the cartilage.

endothelium Single layer of cells liningthe blood vessels.

erythrocyte Red blood cell.

H

haematoma Blood clot formation consisting of inflammatory cells, cytokines and growth factors.

haematopoietic Of blood lineage.

hyperoxia High oxygen tension.

hypertrophic (non-union fractures) Inadequate stability but sufficient biology.

hypoxia Low oxygen tension.

I

intramembranous Bone is formed directly without a cartilage intermediary step.

ischaemic no or significantly low blood supply.

M

multipotent Potential to become multiple mature cell types.

myoblast Muscle forming cell.

N

normoxia Normal oxygen tension.

O

osteoblast Bone forming cell.

osteoblastogenesis Differentiation into an osteoblast.

osteochondral Relating to bone or cartilage.

osteoclast Bone resorbing cell.

osteoclastogenesis Differntiation into an osteoclast.

osteoconductive Bone able to grow on the surface.

osteocyte Former osteoblast, lies witin the fully formed bone.

osteoinductive Induces osteogenesis through recruitment and stimulation of immature cells.

osteoporosis Disease that makes bone fragile and easy to break.

P

perfluorocarbon Molecule made up of entirely fluorine and carbon.

perfusion Ability of a fluid to pass through the circulatory system to tissue.

periosteal Relating to the periosteum, the thin layer of tissue that surrounds bones.

progenitor Precursor.

R

resorption The absorption into the circulation of cells or tissue.

S

sonication The act of disrupting a system using high pressure soundwaves.

T

thermolabile Easily destroyed by heat.

trabecular bone Porous bone structure that makes up most of bone's volume.

V

vasoconstriction narrowing of the blood vessels.

References

Abdalkader Rodi, Unga Johan, Maruyama Kazuo, Yamashita Fumiyoshi, Hashida Mitsuru. The Application of the in-Situ Hyperthermia Emission from Acoustic Nanodroplets for Theranostic Dual-Imaging and Antitumor Modalities // Biological and Pharmaceutical Bulletin. 7 2020. 43, 7. 1141–1145.

Al-Sebaei Maisa O., Daukss Dana M., Belkina Anna C., Kakar Sanjeev, Wigner Nathan A., Cusher Daniel, Graves Dana, Einhorn Thomas, Morgan Elise, Gerstenfeld Louis C. Role of Fas and Treg Cells in Fracture Healing as Characterized in the Fas-Deficient (lpr) Mouse Model of Lupus // Journal of Bone and Mineral Research. 6 2014. 29, 6. 1478–1491.

Alayash Abdu I. Hemoglobin-based blood substitutes: oxygen carriers, pressor agents, or oxidants? // Nature Biotechnology 1999 17:6. 6 1999. 17, 6. 545–549.

Alayash Abdu I. Blood substitutes: why haven't we been more successful? // Trends in Biotechnology. 4 2014. 32, 4. 177–185.

Anton Nicolas, Hallouard François, Attia Mohamed F., Vandamme Thierry F. Nano-emulsions for Drug Delivery and Biomedical Imaging // Fundamental Biomedical Technologies. 2016. 8. 273–300.

Arnett Timothy R., Gibbons Daniel C., Utting Jennifer C., Orriss Isabel R., Hoebertz Astrid, Rosendaal Martin, Meghji Sajeda. Hypoxia is a major stimulator of osteoclast formation and bone resorption // Journal of Cellular Physiology. 7 2003. 196, 1. 2–8.

Avery Steven James, Ayre Wayne Nishio, Sloan Alastair James, Waddington Rachel Jane. Interrogating the Osteogenic Potential of Implant Surfaces In Vitro: A Review of Current Assays // Tissue engineering. Part B, Reviews. 6 2020. 26, 3. 217–229.

Bai Xiao Chun, Lu Di, Bai Jie, Zheng Hang, Ke Zi Yong, Li Xiao Ming, Luo Shen Qiu. Oxidative stress inhibits osteoblastic differentiation of bone cells by ERK and NF-κB // Biochemical and Biophysical Research Communications. 1 2004. 314, 1. 197–207.

Bampouli Ariana, Goris Quinten, Hussain Mohammed Noorul, Louisnard Olivier, Stefanidis Georgios D., Van Gerven Tom. Importance of design and operating parameters in a sonication system for viscous solutions: effects of input power, horn tip diameter and reactor capacity // Chemical Engineering and Processing - Process Intensification. 4 2024. 198. 109715.

Barker Nick. The canonical wnt/β-catenin signalling pathway // Methods in Molecular Biology. 2008. 468. 5–15.

Baron Roland, Kneissel Michaela. WNT signaling in bone homeostasis and disease: from human mutations to treatments // Nature Medicine 2013 19:2. 2 2013. 19, 2. 179–192.

Berniakovich Ina, Giorgio Marco. Low Oxygen Tension Maintains Multipotency, Whereas Normoxia Increases Differentiation of Mouse Bone Marrow Stromal Cells // International Journal of Molecular Sciences 2013, Vol. 14, Pages 2119-2134. 1 2013. 14, 1. 2119–2134.

Bhavsar Mit Balvantray, Han Zhihua, DeCoster Thomas, Leppik Liudmila, Costa Oliveira Karla Mychellyne, Barker John H. Electrical stimulation-based bone fracture treatment, if it works so well why do not more surgeons use it? // European Journal of Trauma and Emergency Surgery 2019 46:2. 4 2019. 46, 2. 245–264.

Blume Gabriele, Cevc Gregor. Liposomes for the sustained drug release in vivo // Biochimica et Biophysica Acta (BBA) - Biomembranes. 11 1990. 1029, 1. 91–97.

Bonewald Lynda F. Cell–Cell and Cell–Matrix Interactions in Bone // Handbook of Cell Signaling, 2/e. 1 2010. 3. 2647–2662.

Bonewald Lynda F. The amazing osteocyte // Journal of Bone and Mineral Research. 2 2011. 26, 2. 229–238.

Borgsteede Sander D., Geersing Tjerk H., Tempels-Pavlica Žana. Other excipients than PEG might cause serious hypersensitivity reactions in COVID-19 vaccines // Allergy. 6 2021. 76, 6. 1941.

Bouakaz Ayache, Zeghimi Aya, Doinikov Alexander A. Sonoporation: Concept and mechanisms // Advances in Experimental Medicine and Biology. 1 2016. 880. 175–189.

Boyce Brendan F., Xiu Yan, Li Jinbo, Xing Lianping, Yao Zhenqiang. NF-κB-mediated regulation of osteoclastogenesis // Endocrinology and Metabolism. 2015. 30, 1. 35–44.

Boyle William J., Simonet W. Scott, Lacey David L. Osteoclast differentiation and activation // Nature 2003 423:6937. 5 2003. 423, 6937. 337–342.

Bray Christopher C., Walker Clark M., Spence David D. Orthobiologics in Pediatric Sports Medicine // Orthopedic Clinics of North America. 7 2017. 48, 3. 333–342.

Callaway Danielle A., Jiang Jean X. Reactive oxygen species and oxidative stress in osteoclastogenesis, skeletal aging and bone diseases // Journal of Bone and Mineral Metabolism. 7 2015. 33, 4. 359–370.

Cao Min, Wang Guoqing, He Hongli, Yue Ruiming, Zhao Yong, Pan Lingai, Huang Weiwei, Guo Yang, Yin Tao, Ma Lina, Zhang Dingding, Huang Xiaobo. Hemoglobin-Based Oxygen Carriers: Potential Applications in Solid Organ Preservation // Frontiers in Pharmacology. 11 2021. 12. 3423.

Carpenter Anne E., Jones Thouis R., Lamprecht Michael R., Clarke Colin, Kang In Han, Friman Ola, Guertin David A., Chang Joo Han, Lindquist Robert A., Moffat Jason, Golland Polina, Sabatini David M. CellProfiler: Image analysis software for identifying and quantifying cell phenotypes // Genome Biology. 10 2006. 7, 10. 1–11.

Castro Camila Irene, Briceno Juan Carlos. Perfluorocarbon-Based Oxygen Carriers: Review of Products and Trials // Artificial Organs. 8 2010. 34, 8. 622–634.

Center for Musculoskeletal Research . TRAP stain for Paraffin Sections. 2020.

Chen Jiin Yu, Scerbo Michelle, Kramer George. A Review of Blood Substitutes: Examining The History, Clinical Trial Results, and Ethics of Hemoglobin-Based Oxygen Carriers // Clinics. 8 2009. 64, 8. 803–813.

Chen Xiao-Wei, Chen Ya-Jun, Wang Jin-Mei, Guo Jian, Yin Shou-Wei, Yang Xiao-Quan. Phytosterol structured algae oil nanoemulsions and powders: improving antioxidant and flavor properties // Food & Function. 9 2016. 7, 9. 3694–3702.

Chung Dai Jung, Hayashi Kei, Toupadakis Chrisoula A., Wong Alice, Yellowley Clare E. Osteogenic proliferation and differentiation of canine bone marrow and adipose tissue derived mesenchymal stromal cells and the influence of hypoxia // Research in Veterinary Science. 2 2012. 92, 1. 66–75.

Clanton Thomas L. Hypoxia-induced reactive oxygen species formation in skeletal muscle // Journal of Applied Physiology. 6 2007. 102, 6. 2379–2388.

Colnot Céline. Skeletal Cell Fate Decisions Within Periosteum and Bone Marrow During Bone Regeneration // Journal od Bone and Mineral Research. 12 2009. 24, 2. 274–282.

Cunningham Brian P., Brazina Sloane, Morshed Saam, Miclau Theodore. Fracture healing: A review of clinical, imaging and laboratory diagnostic options // Injury. 6 2017. 48. S69–S75.

Dallas Sarah L., Prideaux Matthew, Bonewald Lynda F. The Osteocyte: An Endocrine Cell ... and More // Endocrine Reviews. 10 2013. 34, 5. 658–690.

Dauba Ambre, Delalande Anthony, Kamimura Hermes A.S., Conti Allegra, Larrat Benoit, Tsapis Nicolas, Novell Anthony. Recent Advances on Ultrasound Contrast Agents for Blood-Brain Barrier Opening with Focused Ultrasound // Pharmaceutics. 11 2020. 12, 11. 1–30.

De Bari Cosimo, Dell'Accio Francesco, Vanlauwe Johan, Eyckmans Jeroen, Khan Ilyas M., Archer Charles W., Jones Elena A., McGonagle Dennis, Mitsiadis Thimios A., Pitzalis Costantino, Luyten Frank P. Mesenchymal multipotency of adult human periosteal cells demonstrated by single-cell lineage analysis // Arthritis & Rheumatism. 4 2006. 54, 4. 1209–1221.

Deregowski Valerie, Gazzerro Elisabetta, Priest Leah, Rydziel Sheila, Canalis Ernesto. Notch 1 Overexpression Inhibits Osteoblastogenesis by Suppressing Wnt/β-Catenin but Not Bone Morphogenetic Protein Signaling * // Journal of Biological Chemistry. 3 2006. 281, 10. 6203–6210.

Di Mattia Miriam, Mauro Annunziata, Citeroni Maria Rita, Dufrusine Beatrice, Peserico Alessia, Russo Valentina, Berardinelli Paolo, Dainese Enrico, Cimini Annamaria, Barboni Barbara. Insight into Hypoxia Stemness Control // Cells. 8 2021. 10, 8. 2161.

Dijkman Bernadette G., Sprague Sheila, Bhandari Mohit. Low-intensity pulsed ultrasound: Nonunions // Indian Journal of Orthopaedics. 4 2009. 43, 2. 141.

Dillon Scott, Staines Katherine A., Millán José Luis, Farquharson Colin. How To Build a Bone: PHOSPHO1, Biomineralization, and Beyond // JBMR Plus. 7 2019. 3, 7.

Drager Justin, Harvey Edward J., Barralet Jake. Hypoxia signalling manipulation for bone regeneration // Expert Reviews in Molecular Medicine. 1 2015. 17.

Ehnert Sabrina, Rinderknecht Helen, Aspera-Werz Romina H., Häussling Victor, Nussler Andreas K. Use of in vitro bone models to screen for altered bone metabolism, osteopathies, and fracture healing: challenges of complex models // Archives of Toxicology 2020 94:12. 9 2020. 94, 12. 3937–3958.

Einhorn Thomas A., Gerstenfeld Louis C. Fracture healing: mechanisms and interventions // Nature reviews. Rheumatology. 1 2015. 11, 1. 45.

Ekegren Christina L., Edwards Elton R., Steiger Richard de, Gabbe Belinda J. Incidence, Costs and Predictors of Non-Union, Delayed Union and Mal-Union Following Long Bone Fracture // International Journal of Environmental Research and Public Health 2018, Vol. 15, Page 2845. 12 2018. 15, 12. 2845.

Farris Ashley L., Lambrechts Dennis, Zhou Yuxiao, Zhang Nicholas Y., Sarkar Naboneeta, Moorer Megan C., Rindone Alexandra N., Nyberg Ethan L., Perdomo-Pantoja Alexander, Burris S. J., Free Kendall, Witham Timothy F., Riddle Ryan C., Grayson Warren L. 3D-printed oxygen-releasing scaffolds improve bone regeneration in mice // Biomaterials. 2022. 280.

Feng Jianguo, Shi Yali, Yu Qianyao, Sun Chencheng, Yang Guantian. Effect of emulsifying process on stability of pesticide nanoemulsions // Colloids and Surfaces A: Physicochemical and Engineering Aspects. 5 2016. 497. 286–292.

Fernando P. L.N., Abeygunawardane Aravinda, Wijesinghe P. C.I., Dharmaratne Parakrama, Silva Pujitha. An engineering review of external fixators // Medical Engineering & Physics. 12 2021. 98. 91.

Ferri Sara, Wu Qiang, De Grazia Antonio, Polydorou Anastasia, May Jonathan P., Stride Eleanor, Evans Nicholas D., Carugo Dario. Tailoring the size of ultrasound responsive lipid-shelled nanodroplets by varying production parameters and environmental conditions // Ultrasonics Sonochemistry. 5 2021. 73. 105482.

Filipe Vasco, Hawe Andrea, Jiskoot Wim. Critical Evaluation of Nanoparticle Tracking Analysis (NTA) by NanoSight for the Measurement of Nanoparticles and Protein Aggregates // Pharmaceutical Research. 5 2010. 27, 5. 796.

Franz-Odendaal Tamara A., Hall Brian K., Witten P. Eckhard. Buried alive: How osteoblasts become osteocytes // Developmental Dynamics. 1 2006. 235, 1. 176–190.

Fraser J. H.E., Helfrich M. H., Wallace H. M., Ralston Stuart H. Hydrogen peroxide, but not superoxide, stimulates bone resorption in mouse calvariae // Bone. 9 1996. 19, 3. 223–226.

Gao Zhonggao, Kennedy Anne M., Christensen Douglas A., Rapoport Natalya Y. Drug-loaded nano/microbubbles for combining ultrasonography and targeted chemotherapy // Ultrasonics. 8 2008. 48, 4. 260–270.

Garrett Ross, Boyce Brendan F, Oreffo Richard O C, Bonewald Lynda, Poser James, Mundy Gregory R. Oxygen-derived free radicals stimulate osteoclastic bone resorption in rodent bone in vitro and in vivo. // The American Society for Clinical Investigation. 1990. 85. 632–639.

Gerber Frédéric, Waton Gilles, Krafft Marie Pierre, Vandamme Thierry F. Long Lived Microbubbles for Oxygen Delivery // https://doi.org/10.1080/10731190600974939. 1 2009. 35, 1. 119–124.

Giannoudis Peter V., Einhorn Thomas A., Marsh David. Fracture healing: The diamond concept // Injury. 9 2007. 38, 4 SUPPL.

Osteogenesis: The Development of Bones. // . 2000.

Glass Graeme E., Chan James K., Freidin Andrew, Feldmann Marc, Horwood Nicole J., Nanchahal Jagdeep. TNF-alpha promotes fracture repair by augmenting the recruitment and differentiation of muscle-derived stromal cells // Proceedings of the National Academy of Sciences of the United States of America. 1 2011. 108, 4. 1585–1590.

Gorissen Ben, Bruin Alain de, Miranda-Bedate Alberto, Korthagen Nicoline, Wolschrijn Claudia, Vries Teun J. de, Weeren René van, Tryfonidou Marianna A. Hypoxia negatively affects senescence in osteoclasts and delays osteoclastogenesis // Journal of Cellular Physiology. 1 2019. 234, 1. 414–426.

Granger D. Neil, Kvietys Peter R. Reperfusion injury and reactive oxygen species: The evolution of a concept // Redox Biology. 12 2015. 6. 524–551.

Grosso Andrea, Burger Maximilian G., Lunger Alexander, Schaefer Dirk J., Banfi Andrea, Di Maggio Nunzia. It Takes Two to Tango: Coupling of Angiogenesis and Osteogenesis for Bone Regeneration // Frontiers in Bioengineering and Biotechnology. 11 2017. 0, NOV. 68.

Halleen Jussi M., Räisänen Seija R., Alatalo Sari L., Väänänen H. Kalervo. Potential Function for the ROS-Generating Activity of TRACP // Journal of Bone and Mineral Research. 10 2003. 18, 10. 1908–1911.

Hannah Scott S., McFadden Sonyia, McNeilly Andrea, McClean Conor. "Take My Bone Away?" Hypoxia and bone: A narrative review // Journal of Cellular Physiology. 2 2021. 236, 2. 721–740.

Hannouche D, Petite H, Sedel L. Current Trends in the Enhancement of Fracture Healing. 83, 2. 2001. 157–64.

Hayman Alison. Tartrate-resistant acid phosphatase (TRAP) and the osteoclast/immune cell dichotomy // Autoimmunity. 5 2008. 41, 3. 218–223.

Haynes Mark K., Strouse J. Jacob, Waller Anna, Leitao Andrei, Curpan Ramona F., Bologa Cristian, Oprea Tudor I., Prossnitz Eric R., Edwards Bruce S., Sklar Larry A., Thompson Todd A. Detection of Intracellular Granularity Induction in Prostate Cancer Cell Lines by Small Molecules Using the HyperCyt® High-Throughput Flow Cytometry System // SLAS Discovery. 6 2009. 14, 6. 596–609.

Heyboer Marvin, Sharma Deepali, Santiago William, Mcculloch Norman. Hyperbaric Oxygen Therapy: Side Effects Defined and Quantified // Advances in Wound Care. 2017. 6, 6. 210–224.

Huang Biying, Chen Sijie, Pei Wenjing, Xu Yan, Jiang Zichao, Niu Chengcheng, Wang Long. Oxygen-Sufficient Nanoplatform for Chemo-Sonodynamic Therapy of Hypoxic Tumors // Frontiers in Chemistry. 4 2020. 8. 358.

Hulley Philippa A., Bishop Tammie, Vernet Aude, Schneider Jurgen E., Edwards James R., Athanasou Nick A., Knowles Helen J. Hypoxia-inducible factor 1-alpha does not regulate osteoclastogenesis but enhances bone resorption activity via prolyl-4-hydroxylase 2 // The Journal of Pathology. 7 2017. 242, 3. 322–333.

Hung Shih Chieh, Pochampally Radhika R., Hsu Shu Ching, Sanchez Cecelia C., Chen Sy Chi, Spees Jeffrey, Prockop Darwin J. Short-Term Exposure of Multipotent Stromal Cells to Low Oxygen Increases Their Expression of CX3CR1 and CXCR4 and Their Engraftment In Vivo // PLOS ONE. 5 2007. 2, 5. e416.

Jaakkola Panu, Mole David R., Tian Ya-Min, Wilson Michael I., Gielbert Janine, Gaskell Simon J., Kriegsheim Alexander von, Hebestreit Holger F., Mukherji Mridul, Schofield Christopher J., Maxwell Patrick H., Pugh ‡ Christopher W., Ratcliffe ‡ Peter J. Targeting of HIF-α to the von Hippel-Lindau Ubiquitylation Complex by O2-Regulated Prolyl Hydroxylation // Science. 4 2001. 292, 5516. 468–472.

Jafari Seid Mahdi, McClements David Julian. Nanoemulsions : formulation, applications, and characterization. 2018. IV.

Jägers Johannes, Wrobeln Anna, Ferenz Katja B. Perfluorocarbon-based oxygen carriers: from physics to physiology // Pflügers Archiv - European Journal of Physiology 2020 473:2. 11 2020. 473, 2. 139–150.

Jahr Jonathan S., Guinn Nicole R., Lowery David R., Shore-Lesserson Linda, Shander Aryeh. Blood Substitutes and Oxygen Therapeutics: A Review // Anesthesia and Analgesia. 1 2021. 132, 1. 119–129.

Jahr Jonathan S., Nesargi Susmita B., Lewis Kenneth, Johnson Calvin. Blood substitutes and oxygen therapeutics: an overview and current status. 2002.

Jennison T., Brinsden M. Fracture admission trends in England over a ten-year period // Annals of the Royal college of Surgeons of England. 2019. 101. 208–214.

Johnstone A. H. CRC Handbook of Chemistry and Physics,ISBN 0-8493-0369-5. 50, 2. Boca Raton, Florida: CRC Press Inc., 2007. 69. 294–295.

Kalogeris Theodore, Baines Christopher P., Krenz Maike, Korthuis Ronald J. Cell Biology of Ischemia/Reperfusion Injury // International Review of Cell and Molecular Biology. 1 2012. 298. 229–317.

Katagiri T., Takahashi N. Regulatory mechanisms of osteoblast and osteoclast differentiation // Oral Diseases. 5 2002. 8, 3. 147–159.

Khan Fahad, Singh Kunwar, Friedman Mark T. Artificial Blood: The History and Current Perspectives of Blood Substitutes // Discoveries. 3 2020. 8, 1. e104.

Kim Dae Seong, Ko Young Jong, Lee Myoung Woo, Park Hyun Jin, Park Yoo Jin, Kim Dong-Ik, Sung Ki Woong, Koo Hong Hoe, Yoo Keon Hee. Effect of low oxygen tension on the biological characteristics of human bone marrow mesenchymal stem cells // Cell Stress and Chaperones 2016 21:6. 8 2016. 21, 6. 1089–1099.

Kim Ho Yong, Kim So Young, Lee Hye Young, Lee Jin Ho, Rho Gyu Jin, Lee Hyeon Jeong, Lee Hee Chun, Byun June Ho, Oh Se Heang. Oxygen-Releasing Microparticles for Cell Survival and Differentiation Ability under Hypoxia for Effective Bone Regeneration // Biomacromolecules. 2019.

Kim Jinwook, DeRuiter Ryan M., Goel Leela, Xu Zhen, Jiang Xiaoning, Dayton Paul A. A Comparison of Sonothrombolysis in Aged Clots Between Low-Boiling-Point Phase-Change Nanodoplets and Microbubbles of the Same Composition // Ultrasound in medicine & biology. 11 2020. 46, 11. 3059.

Kim Yang Hee, Kanczler Janos M., Lanham Stuart, Rawlings Andrew, Roldo Marta, Tozzi Gianluca, Dawson Jonathan I., Cidonio Gianluca, Oreffo Richard O.C. Biofabrication of nanocomposite-based scaffolds containing human bone extracellular matrix for the differentiation of skeletal stem and progenitor cells // Bio-Design and Manufacturing. 3 2024. 7, 2. 121–136.

Kinsler Lawrence, Frey Austin, Coppens Alan, Sanders James. Fundamentals of Acoustics. 1982.

Klang Victoria, Matsko Nadejda B., Valenta Claudia, Hofer Ferdinand. Electron microscopy of nanoemulsions: An essential tool for characterisation and stability assessment // Micron. 2 2012. 43, 2-3. 85–103.

Knowles Helen J., Athanasou Nicholas A. Acute hypoxia and osteoclast activity: a balance between enhanced resorption and increased apoptosis // The Journal of Pathology. 6 2009. 218, 2. 256–264.

Knowles Helen J., Schaefer Karl Ludwig, Dirksen Uta, Athanasou Nicholas A. Hypoxia and hypoglycaemia in Ewing's sarcoma and osteosarcoma: Regulation and phenotypic effects of Hypoxia-Inducible Factor // BMC Cancer. 7 2010. 10, 1. 1–10.

Knowles Helen J., Vasilyeva Alexandra, Sheth Mihir, Pattinson Oliver, May Jonathan, Rumney Robin M.H., Hulley Philippa A., Richards Duncan B., Carugo Dario, Evans Nicholas D., Stride Eleanor. Use of oxygen-loaded nanobubbles to improve tissue oxygenation: Bone-relevant mechanisms of action and effects on osteoclast differentiation // Biomaterials. 3 2024. 305. 122448.

Komori Toshihisa. Regulation of osteoblast differentiation by transcription factors // Journal of Cellular Biochemistry. 12 2006. 99, 5. 1233–1239.

Krafft Marie Pierre. Alleviating tumor hypoxia with perfluorocarbon-based oxygen carriers // Current Opinion in Pharmacology. 8 2020. 53. 117–125.

Krafft Marie Pierre, Riess Jean G. Therapeutic oxygen delivery by perfluorocarbon-based colloids // Advances in Colloid and Interface Science. 2021. 294. 102407.

Kumar A, Sadiq S. Non-union of the humeral shaft treated by internal fixation // International Orthopaedics. 2002. 26, 4. 214–216.

Kwon Se Yun, Chun So Young, Ha Yun Sok, Kim Dae Hwan, Kim Jeongshik, Song Phil Hyun, Kim Hyun Tae, Yoo Eun Sang, Kim Bum Soo, Kwon Tae Gyun. Hypoxia Enhances Cell Properties of Human Mesenchymal Stem Cells // Tissue Engineering and Regenerative Medicine. 10 2017. 14, 5. 595–604.

Langenbach Fabian, Handschel Jörg. Effects of dexamethasone, ascorbic acid and β-glycerophosphate on the osteogenic differentiation of stem cells in vitro // Stem Cell Research and Therapy. 9 2013. 4, 5. 1–7.

Latson Gary W. Perftoran (Vidaphor)-Introduction to Western medicine // Shock. 10 2019. 52, 1S. 65–69.

Lea-Banks H., O'Reilly M. A., Hynynen K. Ultrasound-responsive droplets for therapy: A review // Journal of Controlled Release. 1 2019. 293. 144–154.

Lea-banks Harriet, Meng Ying, Wu Sheng-kai, Belhadjhamida Rania. Ultrasound-sensitive nanodroplets achieve targeted neuromodulation // Journal of Controlled Release. 2021. 332, January. 30–39.

Lee Pearl, Chandel Navdeep S., Simon M. Celeste. Cellular adaptation to hypoxia through hypoxia inducible factors and beyond // Nature Reviews Molecular Cell Biology 2020 21:5. 3 2020. 21, 5. 268–283.

Lee Sun Young, Park Ka Hyon, Yu Hyung Gu, Kook Eunbyul, Song Won Hyun, Lee Gyuseok, Koh Jeong Tae, Shin Hong In, Choi Je Yong, Huh Yun Hyun, Ryu Je Hwang. Controlling hypoxia-inducible factor-2α is critical for maintaining bone homeostasis in mice // Bone Research 2019 7:1. 5 2019. 7, 1. 1–14.

Li Ji, Sarosi Ildiko, Yan Xiao-Qiang, Morony Sean, Capparelli Casey, Tan Hong-Lin, Mccabe Susan, Elliott Robin, Scully Sheila, Van Gwyneth, Kaufman Stephen, Juan Shao-Chieh, Sun Yu, Tarpley John, Martin Laura, Christensen Kathleen, Mccabe James, Kostenuik Paul, Hsu Hailing, Fletcher Frederick, Dunstan Colin R, Lacey David L, Boyle William J. RANK is the intrinsic hematopoietic cell surface receptor that controls osteoclastogenesis and regulation of bone mass and calcium metabolism // PNAS February. 2000. 15, 4. 1566–1571.

Li Wei, Hu Zhen Fu, Chen Bin, Ni Guo Xin. Response of C2C12 Myoblasts to Hypoxia: The Relative Roles of Glucose and Oxygen in Adaptive Cellular Metabolism // BioMed Research International. 1 2013. 2013, 1. 326346.

Little Nick, Rogers Benedict, Flannery Mark. Bone formation, remodelling and healing // Surgery. 4 2011. 29, 4. 141–145.

Lu Chuanyong, Saless Neema, Wang Xiaodong, Sinha Arjun, Decker Sebastian, Kazakia Galateia, Hou Huagang, Williams Benjamin, Swartz Harold M., Hunt Thomas K., Miclau Theodore, Marcucio Ralph S. The role of oxygen during fracture healing // Bone. 2013. 52, 1. 220–229.

Mak Tak W., Saunders Mary E. The Immune Response. 2006. 463–516.

Mamalis Anastasios A., Cochran David L. The therapeutic potential of oxygen tension manipulation via hypoxia inducible factors and mimicking agents in guided bone regeneration. A review // Archives of Oral Biology. 12 2011. 56, 12. 1466–1475.

Mannaris Christophoros, Bau Luca, Grundy Megan, Gray Michael, Lea-Banks Harriet, Seth Anjali, Teo Boon, Carlisle Robert, Stride Eleanor, Coussios Constantin C. Microbubbles, Nanodroplets and Gas-Stabilizing Solid Particles for Ultrasound-Mediated Extravasation of Unencapsulated Drugs: An Exposure Parameter Optimization Study // Ultrasound in Medicine & Biology. 4 2019. 45, 4. 954–967.

Marshall Karen M., McLaren Jane S., Wojciechowski Jonathan P., Callens Sebastien J. P., Echalier Cécile, Kanczler Janos M., Rose Felicity R. A. J., Stevens Molly M., Dawson Jonathan I., Oreffo Richard O.C. Bioactive coatings on 3D printed scaffolds for bone regeneration: Use of Laponite® to deliver BMP-2 in an ovine femoral condyle defect model // bioRxiv. 2 2024. 2024.02.25.581921.

Martz Thomas D., Bardin David, Sheeran Paul S., Lee Abraham P., Dayton Paul A. Microfluidic Generation of Acoustically Active Nanodroplets // Small. 6 2012. 8, 12. 1876–1879.

Matsuura Naomi, Williams Ross, Gorelikov Ivan, Chaudhuri Joydeep, Rowlands John, Hynynen Kullervo, Foster Stuart, Burns Peter, Resnik Nikita. Nanoparticle-loaded perfluorocarbon droplets for imaging and therapy // 2009 IEEE International Ultrasonics Symposium. 2009.

Maurer Peter, Meyer L., Eckert A. W., Berginski M., Schubert J. Measurement of oxygen partial pressure in the mandibular bone using a polarographic fine needle probe // International Journal of Oral and Maxillofacial Surgery. 3 2006. 35, 3. 231–236.

McGarry Trudy, Biniecka Monika, Veale Douglas J., Fearon Ursula. Hypoxia, oxidative stress and inflammation // Free Radical Biology and Medicine. 9 2018. 125. 15–24.

McKinley Todd. Principles of Fracture Healing // Surgery (Oxford). 9 2003. 21, 9. 209–212.

Menendi Umman, Nusran Gürdal, Kaymaz Burak, Tıskaoğlu Ramazan, Yılmaz Onur, Goret Ceren Canbey. The effects of carbogen and hyperbaric oxygen treatment on fracture healing in rats // Ulusal Travma ve Acil Cerrahi Dergisi. 2022. 28, 4.

Menger Maximilian M., Laschke Matthias W., Nussler Andreas K., Menger Michael D., Histing Tina. The vascularization paradox of non-union formation // Angiogenesis 2022 25:3. 2 2022. 25, 3. 279–290.

Millar Ian L., Lind Folke G., Jansson Karl Åke, Hájek Michal, Smart David R., Fernandes Tiago D., McGinnes Rosemary A., Williamson Owen D., Miller Russell K., Martin Catherine A., Gabbe Belinda J., Myles Paul S., Cameron Peter A. Hyperbaric Oxygen for Lower Limb Trauma (HOLLT): an international multi-centre randomised clinical trial // Diving and hyperbaric medicine. 9 2022. 52, 3. 164–174.

Millar Ian L, McGinnes Rosemary A, Williamson Owen, Lind Folke, Jansson Karl-Åke, Hajek Michal, Smart David, Fernandes Tiago, Miller Russell, Myles Paul, Cameron Peter. Hyperbaric Oxygen in Lower Limb Trauma (HOLLT); protocol for a randomised controlled trial // BMJ Open. 6 2015. 5, 6. e008381.

Mills Leanora A., Aitken Stuart A., Simpson A. Hamish R.W. The risk of non-union per fracture: current myths and revised figures from a population of over 4 million adults // Acta Orthopaedica. 7 2017. 88, 4. 434.

Mizoguchi Toshihide, Ono Noriaki. The diverse origin of bone-forming osteoblasts // Journal of Bone and Mineral Research. 8 2021. 36, 8. 1432–1447.

Mofarrah Mohsen, Jafari-Gharabaghlou Davoud, Farhoudi-Sefidan-Jadid Mahdi, Zarghami Nosratollah. Potential application of inorganic nano-materials in modulation of macrophage function: Possible application in bone tissue engineering // Heliyon. 6 2023. 9, 6. e16309.

Møller Peter, Loft Steffen, Lundby Carsten, Olsen Niels Vidienal. Acute hypoxia and hypoxic exercise induce DNA strand breaks and oxidative DNA damage in humans // The FASEB Journal. 5 2001. 15, 7. 1181–1186.

Montesi Monica, Jähn Katharina, Bonewald Lynda, Stea Susanna, Bordini Barbara, Beraudi Alina. Hypoxia mediates osteocyte ORP150 expression and cell death in vitro // Molecular Medicine Reports. 11 2016. 14, 5. 4248–4254.

Mountford Paul A., Borden Mark A. On the thermodynamics and kinetics of superheated fluorocarbon phase-change agents // Advances in Colloid and Interface Science. 11 2016. 237. 15–27.

Murata Koichi, Fang Celestia, Terao Chikashi, Giannopoulou Eugenia G., Lee Ye Ji, Lee Min Joon, Mun Se Hwan, Bae Seyeon, Qiao Yu, Yuan Ruoxi, Furu Moritoshi, Ito Hiromu, Ohmura Koichiro, Matsuda Shuichi, Mimori Tsuneyo, Matsuda Fumihiko, Park-Min Kyung Hyun, Ivashkiv Lionel B. Hypoxia-Sensitive COMMD1 Integrates Signaling and Cellular Metabolism in Human Macrophages and Suppresses Osteoclastogenesis // Immunity. 7 2017. 47, 1. 66–79.

Muz Barbara, De La Puente Pilar, Azab Feda, Azab Abdel Kareem. The role of hypoxia in cancer progression, angiogenesis, metastasis, and resistance to therapy // Hypoxia. 12 2015. 83.

Muzylak M., Price J. S., Horton M. A. Hypoxia induces giant osteoclast formation and extensive bone resorption in the cat // Calcified Tissue International. 11 2006. 79, 5. 301–309.

Nakashima Tomoki, Hayashi Mikihito, Fukunaga Takanobu, Kurata Kosaku, Oh-Hora Masatsugu, Feng Jian Q., Bonewald Lynda F., Kodama Tatsuhiko, Wutz Anton, Wagner Erwin F., Penninger Josef M., Takayanagi Hiroshi. Evidence for osteocyte regulation of bone homeostasis through RANKL expression // Nature Medicine 2011 17:10. 9 2011. 17, 10. 1231–1234.

National Institute for Health and Care Excellence (NICE) . EXOGEN ultrasound bone healing system for long bone fractures with non-union or delayed healing | Guidance. 2013.

Nicolaije Claudia, Koedam Marijke, Leeuwen Johannes P.T.M. van. Decreased oxygen tension lowers reactive oxygen species and apoptosis and inhibits osteoblast matrix mineralization through changes in early osteoblast differentiation // Journal of Cellular Physiology. 4 2012. 227, 4. 1309–1318.

Nomura Takayuki, Aoyama Mineyoshi, Waguri-Nagaya Yuko, Goto Yoh, Suzuki Mieko, Miyazawa Ken, Asai Kiyofumi, Goto Shigemi. Tumor necrosis factor stimulates osteoclastogenesis from human bone marrow cells under hypoxic conditions // Experimental Cell Research. 2 2014. 321, 2. 167–177.

O'Brien John, Wilson Ian, Orton Terry, Pognan François. Investigation of the Alamar Blue (resazurin) fluorescent dye for the assessment of mammalian cell cytotoxicity // European Journal of Biochemistry. 9 2000. 267, 17. 5421–5426.

Okamoto Kazuo, Nakashima Tomoki, Shinohara Masahiro, Negishi-Koga Takako, Komatsu Noriko, Terashima Asuka, Sawa Shinichiro, Nitta Takeshi, Takayanagi Hiroshi. Osteoimmunology: The conceptual framework unifying the immune and skeletal systems // Physiological Reviews. 10 2017. 97, 4. 1295–1349.

Olson John S., Foley Erin W., Rogge Corina, Tsai Ah Lim, Doyle Michael P., Lemon Douglas D. No scavenging and the hypertensive effect of hemoglobin-based blood substitutes // Free Radical Biology and Medicine. 3 2004. 36, 6. 685–697.

Ontiveros Christopher, Irwin Regina, Wiseman Robert W., McCabe Laura R. Hypoxia suppresses runx2 independent of modeled microgravity // Journal of Cellular Physiology. 8 2004. 200, 2. 169–176.

Padhye Kedar P., Kulkarni Vidhisha S., Kulkarni G. S., Kulkarni Milind G., Kulkarni Sunil, Kulkarni Ruta, Patil Mayur D., Ravi Priyanka Y. Plating, nailing, external fixation, and fibular strut grafting for non-union of humeral shaft fractures // Journal of orthopaedic surgery (Hong Kong). 2013. 21, 3. 327–331.

Pajarinen Jukka, Lin Tzuhua, Gibon Emmanuel, Kohno Yusuke, Maruyama Masahiro, Nathan Karthik, Lu Laura, Yao Zhenyu, Goodman Stuart B. Mesenchymal stem cell-macrophage crosstalk and bone healing // Biomaterials. 3 2019. 196. 80–89.

Parhizkar M., Edirisinghe M., Stride E. The effect of surfactant type and concentration on the size and stability of microbubbles produced in a capillary embedded T-junction device // RSC Advances. 1 2015. 5, 14. 10751–10762.

Park Jonghoon, Ha My Kieu, Yang Nuri, Yoon Tae Hyun. Flow Cytometry-Based Quantification of Cellular Au Nanoparticles // Analytical Chemistry. 2 2017. 89, 4. 2449–2456.

Perevedentseva E. V., Zaritskiy A. R., Fok M. V., Kuznetsova I. N. Perfluorocarbon Emulsions Increase Transfer of Oxygen in Plasma from Erythrocyte to Tissues // http://dx.doi.org/10.3109/10731199809119780. 2009. 26, 2. 223–229.

Phillips A. M. Overview of the fracture healing cascade // Injury. 11 2005. 36, 3. S5–S7.

Pina Sandra, Ferreira José M.F. Bioresorbable plates and screws for clinical applications: A review // Journal of Healthcare Engineering. 2012. 3, 2. 243–260.

Pittman Roland N. Oxygen Transport // Regulation of Tissue Oxygenation. 2011.

Raheja Leah Forquer, Genetos Damian C., Yellowley Clare E. Hypoxic osteocytes recruit human MSCs through an OPN/CD44-mediated pathway // Biochemical and Biophysical Research Communications. 2 2008. 366, 4. 1061–1066.

Rankin Erinn B., Biju Mangatt P., Liu Qingdu, Unger Travis L., Rha Jennifer, Johnson Randall S., Simon M. Celeste, Keith Brian, Haase Volker H. Hypoxia-inducible factor–2 (HIF-2) regulates hepatic erythropoietin in vivo // The Journal of Clinical Investigation. 4 2007. 117, 4. 1068–1077.

Rapoport Natalya. Drug-loaded perfluorocarbon nanodroplets for ultrasound-mediated drug delivery // Advances in Experimental Medicine and Biology. 2016.

Ren Hongying, Cao Ying, Zhao Qinjun, Li Jing, Zhou Cixiang, Liao Lianming, Jia Mingyue, Zhao Qian, Cai Huiguo, Han Zhong Chao, Yang Renchi, Chen Guoqiang, Zhao Robert Chunhua. Proliferation and differentiation of bone marrow stromal cells under hypoxic conditions // Biochemical and Biophysical Research Communications. 8 2006. 347, 1. 12–21.

Riess Jean G. Understanding the fundamentals of perfluorocarbons and perfluorocarbon emulsions relevant to in vivo oxygen delivery // Artificial Cells, Blood Substitutes, and Immobilization Biotechnology. 2005. 33, 1. 47–63.

Roberts Timothy T., Rosenbaum Andrew J. Bone grafts, bone substitutes and orthobiologics: The bridge between basic science and clinical advancements in fracture healing // Organogenesis. 10 2012. 8, 4. 114.

Rocha Flaviana Soares, Gomes Moura Camilla Christian, Rocha Rodrigues Denise Betulucci, Zanetta-Barbosa Darceny, Nakamura Hiraki Karen Renata, Dechichi Paula. Influence of hyperbaric oxygen on the initial stages of bone healing // Oral Surgery, Oral Medicine, Oral Pathology and Oral Radiology. 11 2015. 120, 5. 581–587.

Roiniotis John, Dinh Hang, Masendycz Paul, Turner Amanda, Elsegood Caryn L., Scholz Glen M., Hamilton John A. Hypoxia Prolongs Monocyte/Macrophage Survival and Enhanced Glycolysis Is Associated with Their Maturation under Aerobic Conditions // The Journal of Immunology. 6 2009. 182, 12. 7974–7981.

Rupec Rudolf A., Baeuerle Patrick A. The Genomic Response of Tumor Cells to Hypoxia and Reoxygenation // European Journal of Biochemistry. 12 1995. 234, 2. 632–640.

Rutkovskiy Arkady, Stensløkken Kåre-Olav, Vaage Ingvar Jarle. Osteoblast Differentiation at a Glance // Medical Science Monitor Basic Research. 9 2016. 22. 95.

Sakkas Andreas, Wilde Frank, Heufelder Marcus, Winter Karsten, Schramm Alexander. Autogenous bone grafts in oral implantology—is it still a "gold standard"? A consecutive review of 279 patients with 456 clinical procedures // International Journal of Implant Dentistry. 12 2017. 3, 1. 1–17.

Salim Ali, Nacamuli Randall P., Morgan Elise F., Giaccia Amato J., Longaker Michael T. Transient Changes in Oxygen Tension Inhibit Osteogenic Differentiation and Runx2 Expression in Osteoblasts * // Journal of Biological Chemistry. 9 2004. 279, 38. 40007–40016.

Schindeler Aaron, McDonald Michelle M., Bokko Paul, Little David G. Bone remodeling during fracture repair: The cellular picture // Seminars in Cell & Developmental Biology. 10 2008. 19, 5. 459–466.

Schipani Ernestina, Maes Christa, Carmeliet Geert, Semenza Gregg L. Regulation of Osteogenesis-Angiogenesis Coupling by HIFs and VEGF // Journal of Bone and Mineral Research. 8 2009. 24, 8. 1347–1353.

Schipani Ernestina, Ryan Heather E., Didrickson Susanna, Kobayashi Tatsuya, Knight Melissa, Johnson Randall S. Hypoxia in cartilage: HIF-1α is essential for chondrocyte growth arrest and survival // Genes & Development. 11 2001. 15, 21. 2865–2876.

Schmidt Andrew H. Autologous bone graft: Is it still the gold standard? // Injury. 6 2021. 52. S18–S22.

Sen M. K., Miclau T. Autologous iliac crest bone graft: should it still be the gold standard for treating nonunions? // Injury. 3 2007. 38 Suppl 1, SUPPL. 1.

Sheen Jonathon R., Garla Vishnu V. Fracture Healing Overview // StatPearls. 5 2022.

Sheeran Paul S., Dayton Paul A. Phase-Change Contrast Agents for Imaging and Therapy // Current pharmaceutical design. 4 2012. 18, 15. 2152.

Sheeran Paul S., Luois Samantha, Dayton Paul A., Matsunaga Terry O. Formulation and Acoustic Studies of a New Phase-Shift Agent for Diagnostic and Therapeutic Ultrasound // Langmuir. 9 2011a. 27, 17. 10412–10420.

Sheeran Paul S., Matsuura Naomi, Borden Mark A., Williams Ross, Matsunaga Terry O., Burns Peter N., Dayton Paul A. Methods of Generating Submicrometer Phase-Shift Perfluorocarbon Droplets for Applications in Medical Ultrasonography // IEEE transactions on ultrasonics, ferroelectrics, and frequency control. 1 2017. 64, 1. 252.

Sheeran Paul S., Wong Vincent P., Luois Samantha, McFarland Ryan J., Ross William D., Feingold Steven, Matsunaga Terry O., Dayton Paul A. Decafluorobutane as a Phase-Change Contrast Agent for Low-Energy Extravascular Ultrasonic Imaging // Ultrasound in Medicine & Biology. 9 2011b. 37, 9. 1518–1530.

Shirakura Maya, Tanimoto Keiji, Eguchi Hidetaka, Miyauchi Mutsumi, Nakamura Hideaki, Hiyama Keiko, Tanimoto Kotaro, Tanaka Eiji, Takata Takashi, Tanne Kazuo. Activation of the hypoxia-inducible factor-1 in overloaded temporomandibular joint, and induction of osteoclastogenesis // Biochemical and Biophysical Research Communications. 3 2010. 393, 4. 800–805.

Shykoff Barbara E., Lee Rees L. Risks from Breathing Elevated Oxygen // Aerospace Medicine and Human Performance. 2019. 90, 12. 1041–1049.

Silva Hélder Daniel, Cerqueira Miguel Ângelo, Vicente António A. Nanoemulsions for Food Applications: Development and Characterization // Food and Bioprocess Technology 2011 5:3. 9 2011. 5, 3. 854–867.

Sohn Hoon Sang, Oh Jong Keon. Review of bone graft and bone substitutes with an emphasis on fracture surgeries // Biomaterials Research. 3 2019. 23, 1. 9.

Song Renjie, Zhang Chunbing, Teng Fengmeng, Tu Juan, Guo Xiasheng, Fan Zheng, Zheng Yinfei, Zhang Dong. Cavitation-facilitated transmembrane permeability enhancement induced by acoustically vaporized nanodroplets // Ultrasonics Sonochemistry. 11 2021. 79. 105790.

Song Xuejiao, Feng Liangzhu, Liang Chao, Yang Kai, Liu Zhuang. Ultrasound Triggered Tumor Oxygenation with Oxygen-Shuttle Nanoperfluorocarbon to Overcome Hypoxia-Associated Resistance in Cancer Therapies // Nano Letters. 2016.

Spiess Bruce D. Basic mechanisms of gas transport and past research using perfluorocarbons // Diving and Hyperbaric Medicine. 2010. 40, 1. 23–28.

Srinivasan Satish, Avadhani Narayan G. Hypoxia-Mediated Mitochondrial Stress in RAW264.7 Cells Induces Osteoclast-Like TRAP-Positive Cells // Annals of the New York Academy of Sciences. 2007. 1117. 51.

Srinivasan Satish, Koenigstein Alexander, Joseph Joy, Sun Li, Kalyanaraman B., Zaidi Mone, Avadhani Narayan G. Role of Mitochondrial Reactive Oxygen Species in Osteoclast Differentiation // Annals of the New York Academy of Sciences. 2010. 1192, 1. 245.

Stetefeld Jörg, McKenna Sean A., Patel Trushar R. Dynamic light scattering: a practical guide and applications in biomedical sciences // Biophysical Reviews. 12 2016. 8, 4. 409.

Stewart Sarah K. Fracture Non-Union: A Review of Clinical Challenges and Future Research Needs // Malaysian Orthopaedic Journal. 7 2019. 13, 2. 1.

Sun Yang, Li Jiangbi, Xie Xiaoping, Gu Feng, Sui Zhenjiang, Zhang Ke, Yu Tiecheng. Macrophage-Osteoclast Associations: Origin, Polarization, and Subgroups // Frontiers in Immunology. 12 2021. 12. 778078.

Sutkar Vinayak S., Gogate Parag R. Design aspects of sonochemical reactors: Techniques for understanding cavitational activity distribution and effect of operating parameters // Chemical Engineering Journal. 12 2009. 155, 1-2. 26–36.

Swanson Edward J., Mohan Vickram, Kheir John, Borden Mark A. Phospholipid-stabilized microbubble foam for injectable oxygen delivery // Langmuir. 10 2010. 26, 20. 15726–15729.

Syed Usman Taqui, Dias Ana M.A., Crespo Joao, Brazinha Carla, Sousa Hermínio C. de. Studies on the formation and stability of perfluorodecalin nanoemulsions by ultrasound emulsification using novel surfactant systems // Colloids and Surfaces A: Physicochemical and Engineering Aspects. 5 2021. 616. 126315.

Talu Esra, Lozano Monica M., Powell Robert L., Dayton Paul A., Longo Marjorie L. Long-Term Stability by Lipid Coating Monodisperse Microbubbles Formed by a Flow-Focusing Device // Langmuir : the ACS journal of surfaces and colloids. 11 2006. 22, 23. 9487.

Tanaka Tetsuhiro, Wiesener Michael, Bernhardt Wanja, Eckardt Kai Uwe, Warnecke Christina. The human HIF (hypoxia-inducible factor)-3α gene is a HIF-1 target gene and may modulate hypoxic gene induction // Biochemical Journal. 11 2009. 424, 1. 143–151.

Taurozzi J.T., Hackley V, Wiesner M. Preparation of nanoparticle dispersions from powdered material using ultrasonic disruption // CEINT-NIST Protocol. 6 2012. 1200, 2. 1–14.

Teitelbaum Steven L. Bone Resorption by Osteoclasts // Science. 9 2000. 289, 5484. 1504–1508.

Terzi Rabia, Yılmaz Zahide. Bone mineral density and changes in bone metabolism in patients with obstructive sleep apnea syndrome // Journal of Bone and Mineral Metabolism. 7 2016. 34, 4. 475–481.

Teston E., Hingot V., Faugeras V., Errico C., Bezagu M., Tanter M., Couture O. A versatile and robust microfluidic device for capillary-sized simple or multiple emulsions production // Biomedical Microdevices. 12 2018. 20, 4. 1–12.

Torgersen Sissel, Gjerdet Nils Roar, Erichsen Egil S., Bang Gisle. Metal particles and tissue changes adjacent to miniplates a retrieval study // Acta Odontologica Scandinavica. 1995. 53, 2. 65–71.

Tuck Stephen Paul, Layfield Robert, Walker Julie, Mekkayil Babitha, Francis Roger. Adult Paget's disease of bone: a review // Rheumatology. 12 2017. 56, 12. 2050–2059.

Udagawa Nobuyuki, Takahashi Naoyuki, Yasuda Hisataka, Mizuno Atsuko, Itoh Kanami, Ueno Yutaka, Shinki Toshimasa, Gillespie Matthew T., Martin T. John, Higashio Kanji, Suda Tatsuo. Osteoprotegerin Produced by Osteoblasts Is an Important Regulator in Osteoclast Development and Function // Endocrinology. 9 2000. 141, 9. 3478–3484.

Unger Evan C., Porter Thomas, Culp William, Labell Rachel, Matsunaga Terry, Zutshi Reena. Therapeutic applications of lipid-coated microbubbles // Advanced Drug Delivery Reviews. 5 2004. 56, 9. 1291–1314.

Upadhyay Awaneesh, Dalvi Sameer V., Gupta Gaurav, Khanna Nitin. Effect of PEGylation on performance of protein microbubbles and its comparison with lipid microbubbles // Materials Science and Engineering: C. 2 2017. 71. 425–430.

Utting J. C., Robins S. P., Brandao-Burch A., Orriss I. R., Behar J., Arnett T. R. Hypoxia inhibits the growth, differentiation and bone-forming capacity of rat osteoblasts. 2006. 1693–1702.

Uveges Thomas E., Collin-Osdoby Patricia, Cabral Wayne A., Ledgard Felicia, Goldberg Leah, Bergwitz Clemens, Forlino Antonella, Osdoby Philip, Gronowicz Gloria A., Marini Joan C. Cellular Mechanism of Decreased Bone in Brtl Mouse Model of OI: Imbalance of Decreased Osteoblast Function and Increased Osteoclasts and Their Precursors // Journal of Bone and Mineral Research. 12 2008. 23, 12. 1983–1994.

Valderrábano Rodrigo J., Lui Li Yung, Lee Jennifer, Cummings Steven R., Orwoll Eric S., Hoffman Andrew R., Wu Joy Y. Bone Density Loss Is Associated With Blood Cell Counts // Journal of Bone and Mineral Research. 2 2017. 32, 2. 212–220.

Valenti Maria Teresa, Serafini Paola, Innamorati Giulio, Gili Anna, Cheri Samuele, Bassi Claudio, Carbonare Luca Dalle. Runx2 expression: A mesenchymal stem marker for cancer // Oncology Letters. 11 2016. 12, 5. 4167.

Vanderkarr Mari F., Ruppenkamp Jill W., Vanderkarr Mollie, Holy Chantal E., Blauth Michael. Risk factors and healthcare costs associated with long bone fracture non-union: a retrospective US claims database analysis // Journal of Orthopaedic Surgery and Research. 12 2023. 18, 1. 1–10.

Victoria Galkowski, Petrisor Brad, Drew Brian, Dick David. Bone stimulation for fracture healing: What's all the fuss? // Indian Journal of Orthopaedics. 4 2009. 43, 2. 117.

Voggenreiter Gregor, Leiting Stefan, Brauer Holger, Leiting Peter, Majetschak Matthias, Bardenheuer Mark, Obertacke Udo. Immuno-inflammatory tissue reaction to stainless-steel and titanium plates used for internal fixation of long bones // Biomaterials. 1 2003. 24, 2. 247–254.

Waddington Rachel J., Sloan Alastair J. Tissue Engineering and Regeneration in Dentistry: Current Strategies. 11 2016. 69–88.

Wan Chao, Shao Jin, Gilbert Shawn R., Riddle Ryan C., Long Fanxin, Johnson Randall S., Schipani Ernestina, Clemens Thomas L. Role of HIF-1α in skeletal development // Annals of the New York Academy of Sciences. 4 2010. 1192, 1. 322–326.

Wang Bo, Dong Yutong, Tian Zhansong, Chen Yueqi, Dong Shiwu. The role of dendritic cells derived osteoclasts in bone destruction diseases // Genes & Diseases. 7 2020. 8, 4. 401.

Wang Xuelin, Li Pan, Ning Rongsheng, Ratul Rehman, Zhang Xianren, Ma Jun. Mechanisms on stability of bulk nanobubble and relevant applications: A review // Journal of Cleaner Production. 11 2023. 426. 139153.

Wang Ying, Wan Chao, Deng Lianfu, Liu Ximeng, Cao Xuemei, Gilbert Shawn R., Bouxsein Mary L., Faugere Marie Claude, Guldberg Robert E., Gerstenfeld Louis C., Haase Volker H., Johnson Randall S., Schipani Ernestina, Clemens Thomas L. The hypoxia-inducible factor α pathway couples angiogenesis to osteogenesis during skeletal development // The Journal of Clinical Investigation. 6 2007. 117, 6. 1616–1626.

Wenger Roland H, Kurtcuoglu Vartan, Scholz Carsten C, Marti Hugo H, Hoogewijs David. Frequently asked questions in hypoxia research // Hypoxia. 9 2015. 3. 35.

Wesseler Eugene P., Iltis Ronald, Clark Leland C. The solubility of oxygen in highly fluorinated liquids // Journal of Fluorine Chemistry. 1977. 9, 2. 137–146.

Williams Ross, Wright Cameron, Cherin Emmanuel, Reznik Nikita, Lee Mike, Gorelikov Ivan, Foster F. Stuart, Matsuura Naomi, Burns Peter N. Characterization of Submicron Phase-change Perfluorocarbon Droplets for Extravascular Ultrasound Imaging of Cancer // Ultrasound in Medicine & Biology. 3 2013. 39, 3. 475–489.

Wu Qiang, Mannaris Christophoros, May Jonathan P., Bau Luca, Polydorou Anastasia, Ferri Sara, Carugo Dario, Evans Nicholas D., Stride Eleanor. Investigation of the Acoustic Vaporization Threshold of Lipid-Coated Perfluorobutane Nanodroplets Using Both High-Speed Optical Imaging and Acoustic Methods // Ultrasound in Medicine and Biology. 2021. 00, 00.

Xiang Yun, Bernards Nicholas, Hoang Bryan, Zheng Jinzi, Matsuura Naomi. Perfluorocarbon nanodroplets can reoxygenate hypoxic tumors in vivo without carbogen breathing // Nanotheranostics. 2019. 3, 2. 135–144.

Yamaoka Hitoshi, Matsuoka Hideki, Kago Keitaro, Endo Hitoshi, Eckelt John, Yoshitome Ryuji. Monolayer X-ray reflectometry at the air–water interface // Chemical Physics Letters. 10 1998. 295, 3. 245–248.

Yamasaki Naomi, Tsuboi Hideki, Hirao Makoto, Nampei Akihide, Yoshikawa Hideki, Hashimoto Jun. High oxygen tension prolongs the survival of osteoclast precursors via macrophage colony-stimulating factor // Bone. 1 2009. 44, 1. 71–79.

Yang K. H., Parvizi J., Wang S. J., Lewallen D. G., Kinnick R. R., Greenleaf J. F., Bolander M. E. Exposure to low-intensity ultrasound increases aggrecan gene expression in a rat femur fracture model // Journal of Orthopaedic Research. 1996. 14, 5. 802–809.

Yang Xu, Ricciardi Benjamin F., Hernandez-Soria Alexia, Shi Yuexian, Pleshko Camacho Nancy, Bostrom Mathias P.G. Callus mineralization and maturation are delayed during fracture healing in interleukin-6 knockout mice // Bone. 12 2007. 41, 6. 928–936.

Yarmoska Steven K., Yoon Heechul, Emelianov Stanislav Y. Lipid Shell Composition Plays a Critical Role in the Stable Size Reduction of Perfluorocarbon Nanodroplets // Ultrasound in Medicine & Biology. 6 2019. 45, 6. 1489–1499.

Yellowley Clare E., Genetos Damian C. Hypoxia Signaling in the Skeleton: Implications for Bone Health // Current Osteoporosis Reports 2019 17:1. 2 2019. 17, 1. 26–35.

Yilmaz Erol, Borchert Hans-Hubert. Effect of lipid-containing, positively charged nanoemulsions on skin hydration, elasticity and erythema–an in vivo study // International journal of pharmaceutics. 1 2006. 307, 2. 232–238.

Yu Xi Jiao, Xiao Chang Jie, Du Yan Mei, Liu Shuang, Du Yi, Li Shu. Effect of hypoxia on the expression of RANKL/OPG in human periodontal ligament cells in vitro // International Journal of Clinical and Experimental Pathology. 2015. 8, 10. 12929.

Yuan Zheng, Demith Alec, Stoffel Ryan, Zhang Zhe, Park Yoonjee C. Light-activated doxorubicin-encapsulated perfluorocarbon nanodroplets for on-demand drug delivery in an in vitro angiogenesis model: Comparison between perfluoropentane and perfluorohexane // Colloids and Surfaces B: Biointerfaces. 12 2019. 184. 110484.

Zeng Qiang, Qiao Lijuan, Cheng Lili, Li Chao, Cao Zhong, Chen Zhiyi, Wang Yi, Liu Jie. Perfluorohexane-Loaded Polymeric Nanovesicles with Oxygen Supply for Enhanced Sonodynamic Therapy // ACS Biomaterials Science and Engineering. 5 2020. 6, 5. 2956–2969.

Zhang Peng, Ha Nayoung, Dai Qinggang, Zhou Siru, Yu Chuangqi, Jiang Lingyong. Hypoxia suppresses osteogenesis of bone mesenchymal stem cells via the extracellular signal-regulated 1/2 and p38-mitogen activated protein kinase signaling pathways // Molecular Medicine Reports. 10 2017. 16, 4. 5515–5522.

Zhang Peng, Porter Tyrone. An in vitro Study of a Phase-Shift Nanoemulsion: A Potential Nucleation Agent for Bubble-Enhanced HIFU Tumor Ablation // Ultrasound in Medicine & Biology. 11 2010. 36, 11. 1856–1866.

Zhang Weiqi, Shi Yuhong, Abd Shukor Shazwan, Vijayakumaran Aaran, Vlatakis Stavros, Wright Michael, Thanou Maya. Phase-shift nanodroplets as an emerging sonoresponsive nanomaterial for imaging and drug delivery applications // Nanoscale. 2 2022. 14, 8. 2943–2965.

Zhao Weijie, Qian Jiale, Li Ji, Su Tian, Deng Xiaozhong, Fu Yonghua, Liang Xuelong, Cui Hongwang. From death to birth: how osteocyte death promotes osteoclast formation // Frontiers in Immunology. 3 2025. 16. 1551542.

Zhou Yufeng. Application of acoustic droplet vaporization in ultrasound therapy // Journal of Therapeutic Ultrasound. 11 2015. 3, 1.

Ziello Jennifer E., Jovin Ion S., Huang Yan. Hypoxia-Inducible Factor (HIF)-1 Regulatory Pathway and its Potential for Therapeutic Intervention in Malignancy and Ischemia // The Yale Journal of Biology and Medicine. 6 2007. 80, 2. 51.

Zura Robert, Della Rocca Gregory J., Mehta Samir, Harrison Andrew, Brodie Chris, Jones John, Steen R. Grant. Treatment of chronic (>1 year) fracture nonunion: Heal rate in a cohort of 767 patients treated with low-intensity pulsed ultrasound (LIPUS) // Injury. 10 2015. 46, 10. 2036–2041.